

**The Hawaii Infrared Parallax Program.  
II. Young Ultracool Field Dwarfs<sup>1,2</sup>**

Michael C. Liu,<sup>3,4</sup>

mliu@ifh.hawaii.edu

Trent J. Dupuy,<sup>5</sup> Katelyn N. Allers<sup>4,6</sup>

**ABSTRACT**

We present a large, uniform analysis of young ( $\approx 10$ – $150$  Myr) ultracool dwarfs, based on new high-precision infrared (IR) parallaxes for 68 objects. We find that low-gravity (VL-G) late-M and L dwarfs form a continuous sequence in IR color-magnitude diagrams, separate from the field population and from current theoretical models. These VL-G objects also appear distinct from young substellar (brown dwarf and exoplanet) companions, suggesting the two populations may have a different range of physical properties. In contrast, at the L/T transition, young, old, and spectrally peculiar objects all span a relatively narrow range in near-IR absolute magnitudes. At a given spectral type, the IR absolute magnitudes of young objects can be offset from ordinary field dwarfs, with the largest offsets occurring in the  $Y$  and  $J$  bands for late-M dwarfs (brighter than the field) and mid/late-L dwarfs (fainter than the field). Overall, low-gravity (VL-G) objects have the most uniform photometric behavior while intermediate-gravity (INT-G) objects are more diverse, suggesting a third governing parameter beyond spectral type

---

<sup>1</sup>This work is largely based on observations obtained with WIRCam, a joint project of CFHT, Taiwan, Korea, Canada, France, and the Canada-France-Hawaii Telescope (CFHT) which is operated by the National Research Council (NRC) of Canada, the Institut National des Sciences de l'Univers of the Centre National de la Recherche Scientifique of France, and the University of Hawaii.

<sup>2</sup>Some of the data presented herein were obtained at the W.M. Keck Observatory, which is operated as a scientific partnership among the California Institute of Technology, the University of California, and the National Aeronautics and Space Administration. The Observatory was made possible by the generous financial support of the W.M. Keck Foundation.

<sup>3</sup>Institute for Astronomy, University of Hawaii, 2680 Woodlawn Drive, Honolulu HI 96822

<sup>4</sup>Visiting Astronomer at the Infrared Telescope Facility, which is operated by the University of Hawaii under Cooperative Agreement no. NNX-08AE38A with the National Aeronautics and Space Administration, Science Mission Directorate, Planetary Astronomy Program.

<sup>5</sup>The University of Texas at Austin, Department of Astronomy, 2515 Speedway C1400, Austin, TX 78712, USA

<sup>6</sup>Department of Physics and Astronomy, Bucknell University, Lewisburg, PA 17837

and gravity class. We examine the moving group membership for all young ultracool dwarfs with parallaxes, changing the status of 23 objects (including 8 previously identified planetary-mass candidates) and fortifying the status of another 28 objects. We use our resulting age-calibrated sample to establish empirical young isochrones and show a declining frequency of VL-G objects relative to INT-G objects with increasing age. Notable individual objects in our sample include high-velocity ( $\gtrsim 100 \text{ km s}^{-1}$ ) INT-G objects; very red late-L dwarfs with high surface gravities; candidate disk-bearing members of the MBM20 cloud and  $\beta$  Pic moving group; and very young distant interlopers. Finally, we provide a comprehensive summary of the absolute magnitudes and spectral classifications of young ultracool dwarfs, using a combined sample of 102 objects found in the field and as substellar companions to young stars.

*Subject headings:* brown dwarfs — proper motions — parallaxes — solar neighborhood

## 1. Introduction

Observational studies of brown dwarfs have been inspired by two complementary perspectives. One has been the desire to expand the parameter space of classical stellar astrophysics. Brown dwarfs are the lowest mass products of the star formation process and thus represent the terminus of the mass function that has been well-mapped for hydrogen-burning stars (e.g. Chabrier 2005). Similarly, the ultracool temperatures of field brown dwarfs extend spectral classification from the late-M dwarfs into the new regimes of the L, T, and Y dwarfs ( $T_{\text{eff}} \approx 2500$  to 300 K; e.g., Kirkpatrick 2005, Cushing et al. 2011). There has been sustained progress over the last  $\approx 15$  years in exploring ever lower masses and temperatures, in large part thanks to wide-area digital sky surveys sensitive to such cool objects (e.g. Delfosse et al. 1999; Kirkpatrick et al. 1999; Chiu et al. 2006; Burningham et al. 2010; Reyl e et al. 2010; Liu et al. 2011b; Kirkpatrick et al. 2011; Best et al. 2015).

The second perspective has been the connection between brown dwarfs and gas-giant planets, both planets in our own solar system and around other stars. This has been an equally powerful inspiration — indeed, the interpretation of the first unambiguous brown dwarf Gl 229B (Nakajima et al. 1995) was guided by its spectral similarity to the planet Jupiter (Oppenheimer et al. 1995). However, in contrast to the numerous connections with stellar astronomy, observations in common between the brown dwarf and exoplanet populations have been far more limited. The underlying cause is that magnitudes, colors, and spectra are the most accessible measurements for brown dwarfs but the least accessible ones for exoplanets. In addition, for the case of planets in our own solar system, the gap between them and brown dwarfs is substantial. Jupiter (124 K; Hanel et al. 1981) is much cooler than the coldest known brown dwarf WISE J085510.83–071442.5 ( $\approx 250$  K; Luhman 2014), which is itself much cooler than the next coolest known brown dwarfs at  $\approx 350$ –400 K (Luhman et al. 2012; Dupuy & Kraus 2013). This range of effective temperature

corresponds to a factor of  $\sim 100$  in luminosity.

Direct detection of young gas-giant exoplanets is now strengthening the link between the exoplanet and brown dwarf populations, enriching our understanding of both classes of objects. Young ( $\lesssim 100$  Myr) planetary-mass ( $\lesssim 13 M_{\text{Jup}}$ ) companions have been discovered over a wide range of separations, luminosities, and mass ratios with respect to the host star (Chauvin et al. 2005b; Luhman et al. 2006; Lafrenière et al. 2008; Lagrange et al. 2009, 2010; Ireland et al. 2011; Janson et al. 2012; Carson et al. 2013; Kuzuhara et al. 2013; Rameau et al. 2013; Bailey et al. 2014; Macintosh et al. 2015; Gauza et al. 2015), possibly suggesting a range of origins for these systems. The inferred temperatures for these objects amply overlap the known brown dwarf census, but the young ages mean these companions have significantly lower surface gravities. The HR 8799 system has been particularly illuminating as it is the only directly imaged multi-planet system (Marois et al. 2008; Marois et al. 2010), and the planets possess extreme photospheric properties compared to previously known substellar objects. Their absolute magnitudes and inferred effective temperatures ( $T_{\text{eff}} \approx 1000$  K) overlap field T dwarfs, which are cloud-poor and methane-rich. But the planets’ infrared photometry and spectra indicate the presence of very cloudy photospheres and weak methane, stemming from the lower surface gravity (Marois et al. 2008; Hinz et al. 2010; Bowler et al. 2010; Currie et al. 2011; Barman et al. 2011a; Skemer et al. 2012, 2014). Theoretical work (e.g., Barman et al. 2011b; Madhusudhan et al. 2011; Marley et al. 2012; Lee et al. 2013; Zahnle & Marley 2014) has helped provide physical context for direct imaging observations. But we are still faced with the conundrum of how to integrate young gas-giant planets and field brown dwarfs into a common understanding of substellar evolution.

A promising approach to understanding such low-gravity ultracool atmospheres is to identify the analogs of young exoplanets among the field brown dwarf census. The initial mass functions in the young star-forming clusters appear to go down to a few Jupiter masses (e.g. Lodieu et al. 2008), and thus such low-mass objects should be found in the field after departing their birth sites. For objects of spectral type L ( $T_{\text{eff}} \approx 1300 - 2300$  K; Golimowski et al. 2004; Stephens et al. 2009), a field object of typical age ( $\approx 1-5$  Gyr) has a mass of  $\approx 40-80 M_{\text{Jup}}$  according to evolutionary models (Chabrier et al. 2000; Saumon & Marley 2008). But for the same temperature, an age of 10–100 Myr corresponds to an object of 6–40  $M_{\text{Jup}}$ , encompassing the planetary-mass regime ( $\lesssim 13 M_{\text{Jup}}$ ). Such young field objects will have larger radii and, combined with their lower masses, this means a reduction in surface gravity by a factor of  $\sim 10$  compared to older field objects. Evolutionary models predict that brown dwarf radii become nearly constant at ages of  $\gtrsim 300$  Myr, which sets an approximate upper age limit for field objects displaying signatures of low gravity.

Young objects are expected to be a small minority population in the field and can be identified primarily in three ways. (1) The first young field L dwarf, G196-3B, was found in seeing-limited imaging as a wide companion to a star (Rebolo et al. 1998). Such imaging surveys have now uncovered  $\approx 20$  brown dwarfs as bound companions to young ( $\approx 10-300$  Myr) field stars in seeing-limited data (Kirkpatrick et al. 2001; Reid & Walkowicz 2006; Goldman et al. 2010; Huélamo et al. 2010; Naud et al. 2014; Gauza et al. 2015), space-based imaging (Lowrance et al. 1999, 2000; Luhman et al.

2007), and ground-based adaptive optics imaging (Metchev & Hillenbrand 2004; Chauvin et al. 2005b,a; Metchev & Hillenbrand 2006; Biller et al. 2010; Wahhaj et al. 2011; Nielsen et al. 2012; Delorme et al. 2013; Bowler et al. 2013; Carson et al. 2013; Meshkat et al. 2015). (2) Young objects can be distinguished from older objects as their lower surface gravities are manifested as differences in their optical and near-infrared (IR) spectra compared to field objects (e.g. Martín et al. 1999b; Lucas et al. 2001). Among the spectroscopic studies of hundreds of ultracool dwarfs from wide-field surveys, a small fraction of young late-M and L dwarfs have been identified in this fashion (e.g. Reid et al. 2008; Kirkpatrick et al. 2008; Cruz et al. 2009; Allers & Liu 2013a; Liu et al. 2013b; Best et al. 2015), with implied masses down to  $\approx 7 M_{\text{Jup}}$ . (3) Finally, there have been significant recent efforts to find young ultracool dwarfs in the nearest young moving groups through kinematic and stellar-activity criteria (e.g., Shkolnik et al. 2009, 2011, 2012; Rodriguez et al. 2011; Schlieder et al. 2012; Malo et al. 2013; Gagné et al. 2014b; Kraus et al. 2014; Gagné et al. 2015b; Aller et al. 2016). For such objects, their ages can be assigned using the ages of the higher mass stellar members derived from theoretical isochrones and/or lithium depletion boundaries.

Parallaxic distances for young brown dwarfs are critical for directly establishing basic properties like absolute magnitudes and bolometric magnitudes. Given their younger ages, it may not be appropriate to derive photometric distances using relations between absolute magnitude and spectral type established for field objects (e.g. Vrba et al. 2004; Dupuy & Liu 2012).<sup>1</sup> In addition, high-quality parallaxes and proper motions allow for more stringent assessments of membership in young moving groups than possible with spectrophotometric distances alone. Previous work has produced parallaxes for relatively small samples of low-gravity ultracool dwarfs (Faherty et al. 2012; Liu et al. 2013a; Zapatero Osorio et al. 2014). This work has resulted in discordant conclusions regarding spectrophotometric trends, such as whether young L dwarfs are brighter, fainter, or similar to field objects at *JHK* bands. To date, with the exception of late-M dwarfs in the TW Hydrae Association (TWA), only a handful of free-floating ultracool dwarfs have membership in a young moving group validated by a measured parallax and radial velocity (Faherty et al. 2013; Liu et al. 2013a,b; Gizis et al. 2015; Gagné et al. 2015). Furthermore, the codification of near-IR spectral types and gravity indicators for M and L dwarfs by Allers & Liu (2013a) enables a rigorous investigation of the spectrophotometric properties of low-gravity ultracool dwarfs using a uniform classification system.

We present here a large sample of high-precision parallaxes for young ultracool field dwarfs, based on our ongoing astrometric monitoring program at the Canada-France-Hawaii Telescope (CFHT). The immediate aims of this effort are to provide distances for these objects and to compare their spectrophotometric properties to the field population. Preliminary results from this work for a smaller set of objects were presented in Liu et al. (2013a), where we showed for the first time

---

<sup>1</sup>In principle, spectroscopic distance estimates can be computed from fitting model atmospheres to the observed spectra and assuming a radius (Bowler et al. 2009), though current models have not yet been validated for this purpose, even for old (high-gravity) field objects (Liu et al. 2011a; Cushing et al. 2011).

that young field objects form a separate sequence on the near-IR color-magnitude diagram, residing redder and/or brighter than the field population. We revisit this work with a much larger sample of parallaxes, supplemented with a uniform analysis of near-IR spectral type and gravity classifications using the methods of Allers & Liu (2013a). We also perform a uniform assessment of membership in canonical young moving groups for the entire known sample of young ultracool dwarfs with parallaxes. The broader goal of our work is to critically examine this intriguing class of brown dwarfs as empirical analogs for directly imaged exoplanets.

## 2. Observations

Since 2007, we have been carrying out a high-precision parallax program at the 3.6-meter Canada-France-Hawaii Telescope (CFHT) using the facility wide-field IR camera WIRCcam (Puget et al. 2004). CFHT offers an excellent platform for parallax work, given its combination of large aperture, excellent seeing, and queue scheduling, though to our knowledge it had not been used to measure IR parallaxes prior to our program. Our initial motivation was to determine accurate distances to ultracool binaries, which can be used to directly measure dynamical masses when parallaxes are combined with visual orbit determinations (e.g. Liu et al. 2008; Dupuy et al. 2009, 2011; Dupuy et al. 2015). This goal compelled us to establish observing protocols and data reduction methods to achieve the best possible accuracy, since the total dynamical mass scales with the cube of the binary distance via Kepler’s Third Law.

After a few seasons of observations, it became apparent that the CFHT/WIRCcam was incredibly effective for IR parallaxes. Thus, we expanded the scope of our program to other interesting classes of ultracool dwarfs. As described in Dupuy & Liu (2012), our measurements are as good as have ever been achieved in the near-IR, producing parallaxes with typical uncertainties of 1.3 mas and as good as 0.7 mas, but for objects  $\approx 2\text{--}3$  mags fainter than have been measured by previous parallax programs. This combination of faint limiting magnitudes and high precision naturally lends itself to two broad classes of targets: (1) extremely low-luminosity late-type brown dwarfs, as illustrated by our IR parallax to the  $J = 19.7$  mag T9 binary CFBDS J1458+1013AB (Liu et al. 2011a and updated in Dupuy & Liu 2012), and (2) more distant objects, where the same small uncertainties needed for nearby binaries can benefit science cases that need only moderate S/N distances. The latter is relevant for studying young field brown dwarfs. Since such objects are a small minority population (e.g., Kirkpatrick et al. 2008 find that  $8\% \pm 2\%$  of field L dwarf are younger than  $\approx 100$  Myr), their typical distances will be larger than those of older field objects. Furthermore, the known stellar members of even the youngest and nearest moving groups can extended to distances of  $\approx 60$  pc (e.g. Torres et al. 2008). This is quite distant compared to previous brown dwarf parallax programs — in comparison, among  $\geq L4$  dwarfs, no objects had high precision ( $\leq 3\%$ ) parallaxes beyond 13 pc prior to our CFHT effort.

## 2.1. Sample

Our ongoing CFHT program is monitoring candidate young field objects with spectral types of M6 and later that have been identified from a variety of sources. This paper presents results for a sample of 67 such objects (and 1 object with a spectral type of M4.5), chosen for publication solely based on a sufficient number of observing epochs and time baseline to determine a robust parallax and proper motion. These objects fall into four subsets (Table 1):

- *Low-gravity objects (44 objects)*: We selected targets noted as having lower surface gravity than typical field objects based on their optical and/or near-IR spectra. Most of these objects were originally identified by 2MASS-based searches for ultracool dwarfs in the solar neighborhood (e.g., Cruz et al. 2003, 2007; Reid et al. 2008; Kirkpatrick et al. 2008), with low-gravity signatures identified in their discovery spectra or followup studies (e.g. Cruz et al. 2009; Allers & Liu 2013a). We included the young L dwarf binary SDSS J2249+0044AB, which has signs of low gravity in the near-IR spectrum presented by Nakajima et al. (2004) and has been resolved into a tight binary by Allers et al. (2010). We also included the extremely red young L dwarf PSO J318.5–22 discovered from our ultracool dwarf search using Pan-STARRS; this parallax has already been published in Liu et al. (2013b), and a slightly revised parallax and proper motion based on a larger dataset are presented here.

Also, we added two L dwarf companions to young stars, G 196-3B (Rebolo et al. 1998) and LP 261-75B (Reid & Walkowicz 2006). The former was included for its known low-gravity spectrum (e.g. Rebolo et al. 1998; McGovern et al. 2004). The latter was included as its primary star (LP 261-75A, NLTT 22741) is young ( $\approx 100$ -200 Myr [Reid & Walkowicz 2006],  $\approx 40$ -300 Myr [Shkolnik et al. 2009]), though in the end we classified the near-IR spectrum of LP 261-7B as field gravity (see Appendix). In fact, the M4.5 primary LP 261-75A was the target of our CFHT observations, so we used a narrow-band filter to observe this system. The same data also yielded a parallax for LP 261-75B, albeit with  $2\times$  larger uncertainties than for the primary.

In total, our 44 young field objects in 42 systems represent a  $4\times$  larger sample than targeted by previous parallax studies of such objects (Faherty et al. 2012; Zapatero Osorio et al. 2014).

- *Candidate stellar association members (12 objects)*: We targeted a smaller sample of ultracool dwarfs proposed as members of open clusters and moving groups, for the purpose of assessing their membership and/or establishing them as age-calibrated benchmark objects. These candidates have been identified based on their common kinematics with the stellar members of these groups. As these were drawn from different sources, the candidacy criteria differs in construction and stringency.

The two sources from the TW Hya Association (TWA;  $\approx 10$  Myr [e.g., Weinberger et al. 2013; Ducourant et al. 2014]) had already been strongly confirmed as members based on their kinematics (Mamajek 2005; Teixeira et al. 2008) and corroborated to be young based

on their low-gravity spectra. We included one T dwarf candidate in the Hyades cluster ( $\approx 600$ – $800$  Myr; Perryman et al. 1998; Brandt & Huang 2015) identified in a proper motion search by Bouvier et al. (2008).

Our remaining objects were flagged by Seifahrt et al. (2010) as candidates of the nearby moving groups studied by Montes et al. (2001): the Pleiades (1 object;  $130 \pm 20$  Myr [Barrado y Navascués et al. 2004]), Ursa Majoris (2 objects;  $\approx 400$ – $500$  Myr [King et al. 2003; Jones et al. 2015]), and Hyades (4 objects;  $\approx 600$ – $800$  Myr) moving groups. Note that these are not the open clusters themselves, but rather more dispersed stars claimed to be coeval with the clusters.

This sample contains 12 objects in 10 systems, with DENIS J1441–0945AB and DENIS J2200–3038AB being binaries. For the latter, we were able to measure parallaxes to each individual component (see Appendix).

- *Extremely red ultracool dwarfs (8 objects)*: A small number of field objects have extremely red near-IR colors and peculiar near-IR spectra. The original archetype for this genre is 2MASS J2244+2043, which has an ordinary L6.5-type optical spectrum but a very unusual near-IR spectrum, distinguished by its much redder color, stronger CO, and more peaked  $H$ -band continuum shape compared to other field objects (Kirkpatrick et al. 2000; McLean et al. 2003). Kirkpatrick et al. (2008) and Allers & Liu (2013a) have concluded this is in fact a young field object, as opposed to being a ordinary (high gravity) object with extreme cloud properties. However, since its discovery, about a dozen similarly red objects have been identified that do not appear to be low gravity (Looper et al. 2008b [though see Appendix for discussion of 2MASS J2148+4003]; Kirkpatrick et al. 2010, 2011; Mace et al. 2013; Thompson et al. 2013; Marocco et al. 2014). Instead their extreme colors are thought to be due to high gravity (i.e., old age) and/or metallicity. Parallaxes for eight of these objects are presented here, as these objects are valuable laboratories for understanding the extrema of ultracool atmospheres.
- *Strong  $H\alpha$  emitters (3+1 objects)*: Strong line emission from L dwarfs is uncommon. Unlike for earlier M-type objects,  $H\alpha$  emission is not necessarily a diagnostic of youth (e.g. Schmidt et al. 2015). Nevertheless we included three objects with strong  $H\alpha$  emission in our program to help better diagnose these objects, including one object with a close T7.5 companion (2MASS J1315–2649AB; Burgasser et al. 2011). Note that a fourth object known to have strong and variable  $H\alpha$  emission, 2MASS J1022+5825 (Schmidt et al. 2007), was already included in our low-gravity sample ( $\beta$  in the optical but FLD-G in the near-IR).

Table 1 details the full sample of 67 ultracool objects in 63 systems, including youth properties. All but one of our targets have near-IR spectra, mostly from published work and a few obtained by us (Section 2.3). (The exception is the young M4.5 primary LP 261-75A, whose early spectral type removes it from our subsequent analysis.) This complete spectroscopic dataset allows the entire sample analyzed in this paper, both objects with parallaxes from our CFHT program and those

from the literature (Section 2.5), to be spectrally classified in a homogeneous fashion using the Allers & Liu (2013a) system (Section 2.3).

## 2.2. CFHT Parallaxes

Our analysis methods for obtaining high-precision astrometry from CFHT/WIRCam images are described in detail in Section 2 of Dupuy & Liu (2012). Briefly, we obtain many dithered images (average of 21) at each observing epoch, thereby achieving a median standard error per epoch of 3.6 mas for targets presented here. Targets are observed on each WIRCam run if they fulfill strict airmass constraints, needed to reduce differential chromatic refraction to a level below the astrometric noise. We began observing the majority of the sample presented here in mid-2009, except for SDSS J2249+0044AB which was started in mid-2008 and several objects that we added to our program during 2010–2013.

Images were obtained in  $J$  band for most of our targets, while brighter targets at risk of saturating in the WIRCam minimum integration time (5 s) were observed in a narrow  $K$ -band filter ( $K_{H2}$ ) centered at  $2.122 \mu\text{m}$ . Table 1 summarizes our target list and the details of our observations for each target such as the seeing (median of  $0.63''$ , full range of  $0.50$ – $0.85''$ ), number of epochs, time baseline, number of reference stars ( $S/N > 10$ ), and the mean parallax for the reference stars determined from the Besançon model of the Galaxy (Robin et al. 2003) as described in Section 2.4.2 of Dupuy & Liu (2012). In addition, we now derive proper motion corrections also from the Besançon model of the Galaxy in a similar manner as the parallax correction, using the median proper motion of modeled stars as the correction and computing the uncertainty in this correction through a Monte Carlo simulation of sampling variance given our finite number of reference stars. These proper motion corrections are small, with a median amplitude of  $2.5 \text{ mas yr}^{-1}$ , but necessary for accurately computing space motions.

We derived astrometric parameters and their uncertainties from our data using a Markov Chain Monte Carlo fit. Figure 1 plots the results, and the parallax and proper motion values are given in Table 2, along with the  $\chi^2$  of the best-fit solutions. In all cases  $\chi^2$  is commensurate with the degrees of freedom and thus validates the accuracy of the astrometric errors used in our analysis, which are simply the standard error of the position measured across multiple dithers at a given epoch. We report parallaxes and proper motions both as relative values (i.e., the direct output of our MCMC analysis) and absolute values (i.e., corrected for the parallax and proper motion of our reference grid). The median absolute parallax uncertainty for the sample presented here is 1.4 mas (5.0% uncertainty in distance), with a best precision of 0.8 mas (1.0%) and 90% have errors of 1.0–2.1 mas. Figure 2 summarizes all parallaxes measured to date for ultracool dwarfs by us and other programs, illustrating CFHT’s excellent combination of small parallax errors and faint limiting magnitudes.

Our astrometry pipeline automatically detects any object in the field with a significant parallax



by comparing the  $\chi^2$  of astrometric solutions where the parallax was fixed to zero or freely fitted. Normally this simply allows for easy identification of our targets, but occasionally we find other objects in the field with significant parallaxes. We found two such objects in the sample presented here, LP 415-22<sup>2</sup> ( $\pi_{\text{abs}} = 13.0 \pm 1.6$  mas,  $M_K = 6.49 \pm 0.26$  mag) and 2MASS J07521548+1614237 ( $\pi_{\text{abs}} = 13.2 \pm 1.4$  mas,  $M_K = 8.76 \pm 0.23$  mag), and their astrometric solutions are included in Table 2. Based on the photometric relationship with spectral type from Kraus & Hillenbrand (2007), we estimate spectral types of M3 for LP 415-22 and M6 for 2MASS J07521548+1614237.

### 2.3. Near-IR Spectroscopy and Classification

#### 2.3.1. New Near-IR Spectroscopy

We obtained near-IR spectra for a few of our targets in order to assign spectral types and assess surface gravity. CFHT-Hy-20 and DENIS J1441–0945AB did not have any previous comparable spectra. 2MASS J0619–2903, 2MASS J2140+3655, and WISE J2335+4511 have spectra published in Allers & Liu (2013a), Kirkpatrick et al. (2010) and Thompson et al. (2013), respectively, but with only modest S/N, so we re-observed these objects to better classify them.

We obtained high S/N spectra of these five objects using the NASA Infrared Telescope Facility on the summit of Mauna Kea, Hawaii. We used the facility spectrograph SpeX (Rayner et al. 2003) in prism mode with the 0.5'' slit, which provided an average spectral resolution ( $R \equiv \Delta\lambda/\lambda$ ) of  $\approx 150$ . We dithered in an ABBA pattern on the science target to enable sky subtraction during the reduction process. We obtained calibration frames (arcs and flats) and observed an A0 V star contemporaneously for telluric calibration of each object. All spectra were reduced using version 4.0 of the SpeXtool software package (Vacca et al. 2003; Cushing et al. 2004). Table 3 summarizes our observations.

#### 2.3.2. Spectral Typing and Gravity Classification

For consistency, we classify the near-IR spectra of all M5–L7 dwarfs in our sample using the system developed by Allers & Liu (2013a, hereinafter AL13). The AL13 classification system includes a gravity-independent determination of spectral type, followed by a classification of the surface gravity of the object. First, a combination of visual comparison to field standards as well as spectral indices is used to determine the near-IR spectral type. These generally agree with optical spectral types to better than 1 subtype. Then given an object’s near-IR spectral type, indices and equivalent widths for gravity-sensitive features (VO, FeH, K I, Na I, and the *H*-band continuum

---

<sup>2</sup>LP 415-22 is listed in SIMBAD as a Hyades member, but our proper motion and parallax rule out this association for any assumed radial velocity, in agreement with previous work using only the proper motion (van Altena 1969).

shape) are used to classify the gravity of the object as VL-G (very low), INT-G (intermediate), or FLD-G (field). As noted in AL13, the gravity classifications of VL-G, INT-G, and FLD-G roughly correspond to ages of  $\lesssim 30$  Myr,  $\sim 30\text{--}200$  Myr, and  $\gtrsim 200$  Myr, respectively. The near-IR gravity classifications of VL-G, INT-G, and FLD-G are designed to agree with the Cruz et al. (2009) optical classifications of  $\gamma$ ,  $\beta$ , and  $\alpha$ , respectively. The majority of our sample have classifications already published in the AL13 system. For the remaining objects, we determine the spectral type and gravity (Table 4). Table 1 gives the near-IR spectral types and gravity classifications on the AL13 system for our entire sample of M5–L7 objects. Unless stated otherwise, these types and classifications are used throughout the paper.

The AL13 method of spectral typing is only valid for objects with spectral types of L7 and earlier. To determine near-IR spectral types for the three late-L and early-T dwarfs in our sample (WISE J0206+2640, CFHT-Hy-20 and WISE J0754+7909), we compute the set of flux indices defined by Burgasser et al. (2006) and assign spectral types to each resulting index based on the Burgasser (2007) polynomial fits (Table 5). Each object has four of the indices with values suitable for this purpose. We average the spectral types from the four usable indices and compute an overall index-based type, with the RMS of the spectral types quoted as the uncertainty. We also visually compared these objects to spectral standards from Burgasser et al. (2006). (For the T3 subclass, the original standard 2MASS J1209–10 has since been found to be a binary with estimated component types of T2+T7.5, so we also compared with the T3 dwarf SDSS J1206+28 [Liu et al. 2010].) There is no established system for identifying low-gravity features for late-L and early-T dwarfs,<sup>3</sup> so this information is not available for such objects in our sample. The Appendix discusses the typing results for each of these three objects.

## 2.4. Keck Laser Guide Star Adaptive Optics Imaging

We obtained resolved imaging of DENIS J1441.6–0945AB on 2014 March 14 UT using the facility camera NIRC2 in concert with the laser guide star adaptive optics (LGS AO) system on the Keck II telescope (Bouchez et al. 2004; Wizinowich et al. 2006; van Dam et al. 2006). We used the wide camera mode of NIRC2, with a pixel scale of  $39.686 \pm 0.008$  mas pixel<sup>-1</sup> (H. Fu, priv. comm.), and standard Mauna Kea Observatories (MKO) filters *J*, *H*, and *K* (Simons & Tokunaga 2002; Tokunaga et al. 2002) in addition to the NIRC2 *Y*-band filter (see Appendix of Liu et al. 2012). Our procedure for reducing and analyzing NIRC2 imaging data of binaries is described in detail in our previous work (e.g. Liu et al. 2008; Dupuy et al. 2009; Dupuy et al. 2009; Dupuy et al. 2010). In brief, we measure binary parameters using a three-component Gaussian representation of the point-spread function and use the RMS of the dithered images to determine our measurement

---

<sup>3</sup>For mid/late-T dwarfs, the ratios of the near-IR continuum flux peaks are known to be sensitive to metallicity and gravity (e.g. Liu et al. 2007; Burningham et al. 2009), and Naud et al. (2014) suggest a similar effect for the young T3.5 companion GU Psc b.

uncertainties. We measured flux ratios of  $\Delta Y_{\text{NIRC2}} = 0.32 \pm 0.06$  mag,  $\Delta J_{\text{MKO}} = 0.250 \pm 0.016$  mag,  $\Delta H_{\text{MKO}} = 0.232 \pm 0.014$  mag, and  $\Delta K_{\text{MKO}} = 0.200 \pm 0.010$  mag. Given the nearly equal magnitudes and colors of the components, we assume that within the measurement errors here  $\Delta Y_{\text{NIRC2}} = \Delta Y_{\text{MKO}}$ ,  $\Delta J_{\text{MKO}} = \Delta J_{2\text{MASS}}$ ,  $\Delta H_{\text{MKO}} = \Delta H_{2\text{MASS}}$ , and  $\Delta K_{\text{MKO}} = \Delta K_{S;2\text{MASS}}$ . The astrometry we measured was consistent between filters, and after correcting for distortion<sup>4</sup> the weighted averages are  $314.2 \pm 1.1$  mas for the separation and  $328^\circ.12 \pm 0^\circ.13$  for the PA.

The vast majority of our field ultracool sample (both our CFHT targets and the literature objects described in Section 2.5.2) have been imaged at high angular resolution, either with *HST* (e.g. Bouy et al. 2003; Gizis et al. 2003) or with Keck LGS AO by us. Also, young companion objects included in our study have largely been identified with AO imaging. For the objects lacking high angular resolution imaging, the low intrinsic binary frequency among field ultracool dwarfs (e.g. Duchêne & Kraus 2013) suggests few undetected binaries, especially when accounting for the decline in binary frequency with stellar mass. (The young ages of our targets mean they are lower mass than old field objects of similar spectral type.) Overall, unresolved binarity is unlikely to be an important factor in our analysis.

## 2.5. Photometry

### 2.5.1. Our CFHT Sample

The vast majority of our targets have photometry in the 2MASS Point Source Catalog (Cutri et al. 2003), and several have published photometry on the Mauna Kea Observatories filter system (Simons & Tokunaga 2002; Tokunaga et al. 2002), primarily from Data Release 10 (DR10) of the UKIRT Infrared Deep Sky Survey (UKIDSS; Lawrence et al. 2007). All targets also have photometry in the AllWISE Source Catalog that merges the cryogenic *WISE* mission survey data (Wright et al. 2010) with the post-cryogenic NEOWISE survey (Mainzer et al. 2011). Only LP 261-75B is not resolved from its primary in the *WISE* data. In order to create a homogeneous collection of near-infrared photometry, we have supplemented these published results with synthesized photometry. All of our targets have spectra published either here or elsewhere, and we use these to compute 2MASS–MKO photometric conversions for each object as well as synthetic  $Y - J$  colors. As described in Dupuy & Liu (2012), we assume the synthesized colors within a given bandpass (e.g.,  $J_{2\text{MASS}} - J_{\text{MKO}}$ ) are errorless and assume an error of 0.05 mag for the synthesized  $Y - J$  colors. The young binary SDSS J2249+0044AB has published  $K$ -band flux ratios in both 2MASS and MKO systems but  $J$ - and  $H$ -band flux ratios reported only in the MKO system ( $\Delta J_{\text{MKO}} = 1.024 \pm 0.016$  mag and  $\Delta H_{\text{MKO}} = 0.953 \pm 0.009$  mag; Allers et al. 2010). We used the spectral decomposition method of Dupuy & Liu (2012) to derive 2MASS flux ratios of  $\Delta J_{2\text{MASS}} = 1.04 \pm 0.03$  mag and  $\Delta H_{2\text{MASS}} = 0.95 \pm 0.04$  mag.

---

<sup>4</sup>NIRC2 wide camera distortion solution computed by H. Fu: <http://herschel.uci.edu/fu/id1/nirc2wide/>.

### 2.5.2. Other Objects from the Literature

We have also compiled photometry for all field objects with published parallaxes that have possible evidence for low-gravity spectra, youth ( $\approx 10\text{--}200$  Myr), or being unusual redness. This compilation of objects from the literature includes 11 field objects and 20 systems with (one or more) ultracool companions.<sup>5</sup> We do not include objects in star-forming regions such as Taurus and Sco-Cen, as they are younger than the sample being considered here. Combined with our parallax sample of 67 ultracool objects in 63 systems (excluding the young M4.5 primary LP 261-75A), our compilation includes a total of 102 ultracool dwarfs in 93 systems. (For objects with parallaxes from multiple sources, we choose the one with the lowest uncertainty.) We supplemented the published photometry for this extended sample in the same way as our main sample, using published spectra to compute synthesized photometry when available. For objects without published spectra, we estimated 2MASS–MKO photometric conversions from other objects with similar spectral types or absolute magnitudes. We expect these estimates to be reasonably accurate as, e.g., over our entire sample the differences in these corrections vary by  $\pm 0.06$  mag or less in any one band. These estimates allow us to have an almost complete collection of *JHK* photometry for our combined sample, only lacking *J*-band photometry for HD 948B and HR 8799e and *K*-band photometry for 51 Eri b.

Table 6 gives the 2MASS (*JHK<sub>S</sub>*), MKO (*YJHK*), and AllWISE (*W1* and *W2*) photometry for our combined sample along with the parallax we use for each object. Table 7 gives the resulting absolute magnitudes.

### 2.5.3. Objects Not Included in Our Analysis

We discuss other potential young objects with parallaxes in the literature that we excluded from our analysis for the various reasons given here. EROS-MP J0032–4405 (L0 $\gamma$  optical/L0 INT-G near-IR; Cruz et al. 2009; Allers & Liu 2013a) has two published parallaxes that are highly discrepant ( $1.9\sigma$ , 78% different),  $38.4 \pm 4.8$  mas from Faherty et al. (2012) and  $21.6 \pm 7.2$  mas from Marocco et al. (2013). These gives absolute magnitudes that are 1.25 mag different, and rather than perform our analysis contingent on both scenarios we simply exclude this object. 2MASSW J0103320+193536 (L6 $\beta$ ; Kirkpatrick et al. 2000; Faherty et al. 2012) has a parallax from Faherty et al. (2012). However, its near-IR gravity status is uncertain, as Allers & Liu (2013a) type this object as L6 INT-G but Gagné et al. (2015a) typed it as L6p with no clear sign of low gravity. TVLM831-154910 has a parallax from Tinney et al. (1995) and has recently been typed as M7: $\beta$  VL-G and identified

---

<sup>5</sup>Four well-known young ultracool companions are not included in our compilation as their primary stars lack parallaxes: GSC 08047–00232 B (M9.5 $\pm 1$ , Tuc-Hor member; Chauvin et al. 2003; Neuhäuser & Guenther 2004; Chauvin et al. 2005a), 1RXS J235133.3+312720 (L0 $_{-1}^{+2}$ , probable AB Dor member; Bowler et al. 2012), 2MASS J01225093–2439505 B (L3.7 $\pm 1.0$ , probable AB Dor member; Bowler et al. 2013; Hinkley et al. 2015), and GU Psc b (T3.5 $\pm 1$ , probable AB Dor member; Naud et al. 2014).

as a  $\beta$  Pic moving group candidate member by Gagné et al. (2015a). An updated parallax from Pan-STARRS-1 (E. Magnier 2015, priv. comm.) is highly discrepant with the published value, making the distance and membership indeterminate. NLTT 13728, 2MASS J19303829–1335083, and G44-9 are M6 dwarfs that have parallaxes from Shkolnik et al. (2012) but lack infrared spectra. 2MASS J06524851–5741376AB is a binary discovered by Chauvin et al. (2012) with a S/N = 10 parallax from Faherty et al. (2012) who also typed it as M8 $\beta$ . This binary lacks resolved spectral information for the individual components, though the  $JK_S L'$  flux ratios for the system are modest ( $\approx 0.3$  mag) suggesting comparable spectral types. If they were late-M dwarfs, both components would be  $\sim 1$  mag fainter than any such objects in our sample, suggesting this is an atypical system or else the parallax has a significant systematic error. 2MASS J07123786–6155528 (L1 $\beta$ ; Cruz et al. 2009) has a S/N = 2.5 parallax from Faherty et al. (2012). The primary star of the VHS 1256–12AB binary (M7.5 INT-G + L7 VL-G; Gauza et al. 2015) has been found to be a binary by Stone et al. (2016), who note that the resolved components would be extremely faint compared to any other known M7.5 objects if the parallax from Gauza et al. (2015) is correct. Also, a preliminary parallax from Pan-STARRS1 (E. Magnier 2015, priv. comm.) disagrees substantially with the published parallax. So we exclude all three components of this system from our sample. LSPM J1314+1320AB has a parallax and optical spectral type of M7 from Lépine et al. (2009) and was discovered to be a binary by Law et al. (2006). Schlieder et al. (2014) present resolved photometry and integrated-light near-infrared spectral evidence of low gravity. Gravity classifications are lacking for the individual components, so this object is not included in our work here. A detailed analysis of this system, including its component dynamical masses, is in Dupuy et al. (2016a). SIPS J2045–6332 (M9/L1; Schmidt et al. 2007; Marocco et al. 2013) has a parallax from Dieterich et al. (2014), but the only published youth signatures are a triangular  $H$ -band spectrum from Marocco et al. (2013) and lithium from Gálvez-Ortiz et al. (2014). 2MASS J21011544+1756586AB is a binary with a parallax from Vrba et al. (2004) that has been noted to have a triangular  $H$ -band spectrum and red colors (Gagné et al. 2014b). It has no resolved spectra or near-infrared photometry. We classify the integrated-light near-IR spectrum from Burgasser et al. (2010) as L7 and lacking any strong indication of youth, though the spectral resolution ( $R \sim 120$ ) of the data is not particularly sensitive to gravity for such a late-type object (Figure 3). CFBDSIR J214947.2–040308.9 (T7) was discovered by Delorme et al. (2012) as a potential low-gravity object in the AB Dor moving group. However, a recent parallax measurement rejects this membership (P. Delorme et al., submitted), and thus the interpretation of its unusual near-IR spectrum as low gravity is now uncertain.

### 3. Comparison to Published Distances

#### 3.1. Parallax Distances

A number of objects in our sample have independent measurements of their parallaxes in the literature. Comparing these published values to each other and to our CFHT results allows us to vet the quality of all of these measurements. There are two programs that have produced parallaxes

for significant subsets of our sample. Faherty et al. (2012, 2013) have published parallaxes for 10 of our targets based on SMARTS/ANDICAM and CTIO Blanco/ISPI observations. In addition, our sample includes all 10 parallaxes from Zapatero Osorio et al. (2014), which are based on combining astrometry from Calar Alto/OMEGA2000, NOT/NOTCam and WHT/LIRIS. Finally, 14 objects in our sample have published parallaxes in several other papers (Dahn et al. 2002; Vrba et al. 2004; Costa et al. 2006; Teixeira et al. 2008; Gatewood & Coban 2009; Andrei et al. 2011; Shkolnik et al. 2012; Weinberger et al. 2013; Ducourant et al. 2014; Gizis et al. 2015). Given that there is some overlap among these various literature sources, the total number of objects in our sample with some published parallax is 26.

Figure 4 shows our new parallaxes compared to published values. Our results broadly agree with published values as most of our parallaxes are consistent at  $\leq 1\sigma$  with previous results, and 90% are consistent at  $\leq 2.5\sigma$ . However, there are a number of more extreme ( $\approx 4-6\sigma$ ) outliers. As can be seen from the histograms of parallaxes differences in  $\sigma$  in Figure 4, all of the most extreme outliers are from the programs of Faherty et al. (2012) and Zapatero Osorio et al. (2014). We now consider all of the  $>2\sigma$  outliers individually,<sup>6</sup> and in the end we decide to use our parallaxes for all these cases (except for 2MASS J1139–3159).

*2MASSW J0033239–152131.* Zapatero Osorio et al. (2014) report an absolute parallax of  $24.8 \pm 2.5$  mas, and we find a value  $5.8\sigma$  different,  $42.8 \pm 1.8$  mas. The total proper motion of this object is  $300.6 \pm 2.3$  mas yr<sup>-1</sup>, and our RA and Dec proper motions both agree to better than 4 mas yr<sup>-1</sup> with those reported by Zapatero Osorio et al. (2014). In this case, our parallax seems to resolve an anomaly that Zapatero Osorio et al. (2014) found when placing 2MASSW J0033–1521 on their H-R diagram that used a spectral type-based  $T_{\text{eff}}$  and parallax-based luminosity. They found that this object appeared to have an age of  $<10$  Myr and thereby a mass well below the lithium fusion limit, but it has a clear non-detection of lithium absorption ( $<1$  Å; Cruz et al. 2009). It also does not display evidence of very low surface gravity (i.e.,  $\gamma$ ,  $\delta$ , or VL-G) as might be expected for such a young object, rather it is classified as L4 $\beta$  (Cruz et al. 2009) in the optical and L1 FLD-G (Allers & Liu 2013a) in the near-infrared (see Appendix). Zapatero Osorio et al. (2014) note that their parallax could be the cause of the problem, as a closer distance would reconcile the H-R diagram position and lack of lithium, and our parallax does indicate a much closer distance. We therefore use our parallax for this object.

*2MASSW J0045214+163445.* Zapatero Osorio et al. (2014) report an absolute parallax of  $57.3 \pm 2.0$  mas, and we find a value  $3.6\sigma$  different,  $65.9 \pm 1.3$  mas. Our proper motions agree reasonably well within their quoted errors ( $\approx 16$  mas yr<sup>-1</sup> or  $1.5\sigma$ ). Our correction from relative to absolute parallax is only  $1.56 \pm 0.20$  mas and thus not sufficient to explain why our parallax is 8.6 mas larger. We share all 10 objects from Zapatero Osorio et al. (2014) in common with our program, and as

---

<sup>6</sup>Note that we consider proper motion discrepancies in units of mas yr<sup>-1</sup> rather than  $\sigma$  since most authors do not report absolute proper motions, and even absolute proper motions may contain systematic errors associated with imperfect knowledge of the reference frame.

noted above there is at least one other case (2MASS J0033–1521) where the Zapatero Osorio et al. (2014) parallax is likely to be in error. In contrast, the 15 parallax measurements we have in common with programs other than Faherty et al. (2012) and Zapatero Osorio et al. (2014) have no  $>2\sigma$  outliers. We therefore use our own parallax for 2MASSW J0045+1634.

*GJ 3276 (a.k.a. 2MASS J04221413+1530525)*. Faherty et al. (2012) report an absolute parallax of  $24.8 \pm 3.1$  mas and a relative proper motion of  $(-17.2 \pm 2.7, 7.4 \pm 2.6)$  mas yr $^{-1}$ . However, we find only a marginally significant relative parallax detection of  $2.6 \pm 1.0$  mas, from which we compute an absolute parallax of  $3.9 \pm 1.0$  mas. We also do not detect a significant relative proper motion, finding  $(1.4 \pm 1.5, 1.8 \pm 1.4)$  mas yr $^{-1}$ . Thus our parallax is  $6.4\sigma$  discrepant from Faherty et al. (2012), and the total proper motion is different by  $16$  mas yr $^{-1}$ . We believe this is unlikely to be a case of mistaken identity, as we observe no other stars near GJ 3276 in our CFHT imaging with  $\approx 0''.5$  seeing, and there are no other objects in the field with a similar parallax or proper motion. We automatically detect any sources with significant parallaxes in each field, and this field did have one such detection (LP 415-22,  $4''.1$  away from GJ 3276), but its parallax ( $13.2 \pm 1.5$  mas) and total proper motion ( $112.5 \pm 1.7$  mas yr $^{-1}$ ) are also inconsistent with Faherty et al. (2012). Allers & Liu (2013a) note that this the spectrum of GJ 3276 is particularly red for its spectral type and report a reddening of  $A_V = 4.6$  mag. They also note that it is only  $\sim 10^\circ$  from the Taurus star-forming region on the sky and thus may be behind or embedded in interstellar material. Either of these scenarios is consistent with our parallax, which places it at or behind the distance of Taurus within  $2\sigma$ . Such reddening would be more challenging to explain using the Faherty et al. (2012) parallactic distance of  $\approx 40$  pc. Thus, we favor our parallax for this object, but given its low S/N we do not end up including it in the analysis that follows.

*2MASS J05012406–0010452*. Faherty et al. (2012) report an absolute parallax of  $76.4 \pm 4.8$  mas, and we find a value  $5.6\sigma$  different,  $48.4 \pm 1.4$  mas. Like GJ 3276 above, our value is  $\approx 20$  mas smaller than the Faherty et al. (2012) value. Our two proper motions agree reasonably well ( $<10$  mas yr $^{-1}$ ) for this object that has a total motion of  $236$  mas yr $^{-1}$ . Zapatero Osorio et al. (2014) also report a parallax for this object,  $51.0 \pm 3.7$  mas, which agrees with ours at  $0.7\sigma$ , and proper motions that also agree well ( $\lesssim 1$  mas yr $^{-1}$ ). Zapatero Osorio et al. (2014) note this parallax discrepancy and show that 2MASS J0501–0010 would be unique among objects of its spectral type, i.e., much fainter than the field sequence or other low-gravity objects, if the Faherty et al. (2012) parallax is used. Therefore, we use our parallax, consistent with but more precise than that of Zapatero Osorio et al. (2014).

*LP261-75B (2MASS J09510549+3558021)*. Vrba et al. (2004) reported a preliminary absolute parallax of  $16.1 \pm 7.4$  mas, and we find a value  $2.1\sigma$  different,  $31.6 \pm 1.3$  mas. Our proper motions agree well ( $3\text{--}6$  mas yr $^{-1}$ ) for this object with a total motion of  $189$  mas yr $^{-1}$ . An updated parallax distance of  $33.0_{-2.4}^{+2.8}$  pc from Vrba et al. is reported in Bowler et al. (2013), which is in excellent agreement with our parallax distance. Therefore, we do not consider this object a  $>2\sigma$  outlier in the end, and we use our parallax in the following analysis.

*2MASSW J1139511–315921 (a.k.a. TWA 26)*. Faherty et al. (2012) report an absolute parallax of  $35.1 \pm 4.3$  mas, and we find a value  $2.5\sigma$  different,  $23.7 \pm 1.6$  mas. Our proper motions are also somewhat discrepant at  $10\text{--}20$  mas yr<sup>−1</sup>. Weinberger et al. (2013) and Ducourant et al. (2014) also report parallaxes for this object of  $23.8 \pm 2.6$  mas and  $26.2 \pm 1.1$  mas, respectively, which agree with ours at  $0.1\sigma$  and  $1.3\sigma$  (as does the Mamajek 2005 kinematic parallax of  $25.0 \pm 2.5$  mas). Their proper motions also agree with ours at  $6$  mas yr<sup>−1</sup>. We use the Ducourant et al. result, given its somewhat higher precision than our CFHT result and the fact that this group has measured parallaxes for several other TWA members using the same methods.

*2MASSW J2208136+292121*. Zapatero Osorio et al. (2014) report an absolute parallax of  $21.2 \pm 0.7$  mas, and we find a value  $2.2\sigma$  different,  $25.1 \pm 1.6$  mas. This marginal discrepancy is largely driven by the very small quoted parallax error of Zapatero Osorio et al. (2014). Our proper motions agree reasonably well ( $<10$  mas yr<sup>−1</sup>) for this object with a total motion of  $96$  mas yr<sup>−1</sup>. Our correction from relative to absolute parallax is  $0.85 \pm 0.04$  mas, which is slightly larger than the quoted parallax error from Zapatero Osorio et al. (2014) and slightly smaller than their adopted correction of  $1.0$  mas. Given that 2 of 10 objects from Zapatero Osorio et al. (2014) are  $\approx 4\text{--}6\sigma$  ( $\approx 10\text{--}20$  mas) outliers, we are reluctant to take their very small quoted parallax uncertainty of  $0.7$  mas for 2MASS J2208+2921 at face value. Therefore, we use our own parallax value in the following analysis.

To summarize, our parallax sample overlaps with 10 out of 15 young objects from Faherty et al. (2012, 2013),<sup>7</sup> the entire sample of 10 objects from Zapatero Osorio et al. (2014), and 15 measurements from various other programs (Table 8). The only  $>2\sigma$  outliers in this sample come from Faherty et al. (2012) and Zapatero Osorio et al. (2014), and for the three largest discrepancies ( $>5\sigma$ ) our new parallaxes seem to resolve standing problems with the interpretation of those objects. One of the other  $>2\sigma$  discrepant objects, 2MASS J1139–3159, has two independent parallaxes in the literature that agree with ours. For all of these overlapping cases except 2MASS J1139–3159, in the end we choose to use our CFHT parallaxes, which has the added benefit of internal consistency for the handling of systematic effects such as the correction from relative to absolute parallax and proper motion.

### 3.2. Kinematic Distances

Given prior knowledge of the expected space motions of stars, such as membership in co-moving associations, distance estimates are possible for objects that have some kinematic information (proper motion and/or radial velocity). Such kinematic distance estimates exist in the literature for a number of our targets, either because they have been proposed as members of young moving

---

<sup>7</sup>Of the 5 non-overlapping Faherty et al. (2012) objects, we use two in our analysis (2MASS J02212859–6831400 and DENIS J205754.1–025229), as their near-IR absolute magnitudes are consistent with the objects from our CFHT sample. The remaining 3 parallaxes appear to be problematic (Section 2.5.3) and thus are excluded from our analysis.



groups or through a kinematic model of the solar neighborhood. The most homogeneous and complete collection of such kinematic distances for our ultracool dwarf sample comes from the BANYAN II analysis (Malo et al. 2013; Gagné et al. 2014b). (Note that subsequent BANYAN II analysis in Gagné et al. 2015a does not publish independent kinematic distances.) We now compare our trigonometric parallax distances to these kinematic distance estimates. We also compare our TWA parallaxes to the kinematic distances from Mamajek (2005). Table 9 presents the complete list of overlapping objects.

Overall, the kinematic distances are reasonably consistent with parallax distances within the quoted uncertainties, with 50% of BANYAN II distances agreeing within  $1.2\sigma$  and 90% agreeing within  $2.3\sigma$ . In terms of absolute fractional difference, 50% of BANYAN II kinematic distances are within 20% of the parallax distance, with the other half being more discrepant. (Note that the typical parallax error is much smaller than this: the median fractional error for the CFHT sample is 6%.) In fact, for the best studied groups (TWA,  $\beta$  Pic, AB Dor, Tuc-Hor), there are no  $>2\sigma$  outliers out of a sample of 11 objects. However, outliers are present in the larger sample, and we find that SIMP J2154–1055 is significantly more distant ( $2.9\sigma$ , 28%) than predicted from its kinematic distance based on Argus membership (Gagné et al. 2014a). Other candidate group members with  $>2\sigma$  or  $>50\%$  discrepancies are 2MASS J0045+1634 (Argus) and 2MASS J0619–2903 (Columba). All four TWA and Tuc-Hor proposed members that have CFHT parallaxes are consistent at  $<1\sigma$  and 5%–10% with kinematic distances from Mamajek (2005) and Gagné et al. (2014b).

For objects identified to belong to the “young field” population by Gagné et al. (2014b), there is a significant preference for kinematic distances to be larger than parallax distances (Figure 5). The median offset is +11% with a dispersion of  $\pm 37\%$ . In terms of the absolute value of the fractional difference, the median offset for the young field sample is 25%. The rate of highly discrepant BANYAN II kinematic distances ( $>2.5\sigma$ ,  $>60\%$  fractional offset) is 10% for the whole sample. The largest of these discrepancies seem to only occur for the young field population. For example, we find that 2MASS J0435–1414 is at  $88_{-12}^{+9}$  pc while Gagné et al. (2014b) report  $10.5 \pm 1.6$  pc. Another large difference in the opposite direction is for 2MASS J1711+2326 that we place at  $32.7_{-1.9}^{+1.7}$  pc but for which Gagné et al. (2014b) estimate to be at  $53_{-6}^{+7}$  pc.

In summary, we find that BANYAN II kinematic distances are generally not as accurate as their quoted precision of 8% (Gagné et al. 2014b), with 50% of kinematic distances being  $\geq 20\%$  different from parallactic distances. Kinematic distances for young field objects seem to be systematically overestimated by 11%, with an RMS dispersion of 37% with respect to the parallactic distances, and have a failure rate (i.e., values that are  $>2.5\sigma$ ,  $>60\%$  discrepant) of  $\approx 10\%$ .

## 4. Results

### 4.1. Absolute Magnitudes

Figures 6, 7, and 8 show the absolute magnitudes of our sample in the standard 2MASS, MKO, and *WISE* infrared bandpasses as a function of Allers & Liu (2013a) near-IR spectral type and gravity classifications, applicable for objects down to L7. (Later-type objects are discussion in Section 4.7.) While there are many possible criteria for partitioning our sample, near-IR spectral type and gravity classification are the only spectroscopic properties available for all our CFHT targets. Also, surface gravity is the key defining characteristic of this young sample, so it is natural to examine how reduced gravity impacts the photometry of ultracool dwarfs.

The figures also show the loci of field ultracool dwarfs for comparison. Because our sample is predominantly composed of late-M and L dwarfs, which change monotonically in absolute magnitude with spectral type, we derive new linear relations to represent the M6–L8 field population, instead of using the higher-order polynomials from Dupuy & Liu (2012) which were derived for a much larger range in spectral type. (In particular, the near-IR magnitudes become non-monotonic in the L/T transition. This leads to curvature in the polynomial fits, and thus the higher-order fits do not track the behavior of the earlier L dwarfs as well as linear fits.) Also, our complete young sample has near-IR spectral types, and thus we would like to compare with a field relation based solely on near-IR types (unlike the relations of Dupuy & Liu 2012, which used optical types for M and L dwarfs when available, though the effect of their inclusion is small). For our field data, we used the IDL structure posted at the Database of Ultracool Parallaxes,<sup>8</sup> which includes the comprehensive summary of Dupuy & Liu (2012) along with more recent published parallaxes and photometry for ultracool dwarfs (M6 and later). In order to use only normal field objects with high-quality absolute magnitudes, we excluded anything without `nu11` in the IDL structure’s `flag` tag (which excludes, e.g., subdwarfs and young objects), with a peculiar optical or infrared spectral type noted in the `osptstr` or `isptstr` tags, or with a  $S/N < 10$  parallax. We then used the least absolute deviation method (`LADFIT` in IDL) to compute robust linear fits of absolute magnitude as a function of infrared spectral type for objects having spectral types of M6 to L8. Table 10 reports the coefficients of these fits along with the RMS about the fit. Note that the RMS does vary with spectral type range so a single number is not fully representative (e.g., Figure 27 of Dupuy & Liu 2012 and discussion below.)

#### 4.1.1. General Trends in Absolute Magnitudes with Spectral Type and Gravity

Our data reveal three main trends in the behavior of the near-IR (*YJHK*) absolute magnitudes.

---

<sup>8</sup><http://www.as.utexas.edu/~tdupuy/plx>, maintained by T. Dupuy and last updated 2013 September 9.

1. In a given bandpass, the loci of young objects relative to the field follows a consistent pattern, with young late-M dwarfs being brighter than the field, young early-L ( $\approx$ L0-L2) dwarfs being comparable, and young mid/late-L ( $\gtrsim$ L3) dwarfs being fainter than the field sequence. This is in accord with the preliminary  $J$ -band results presented in Liu et al. (2013a).
2. The offset of the young objects relative to the field sequence (brighter at earlier types, fainter at later types) is more dramatic at bluer wavelengths. At  $Y$  and  $J$  bands, the young late-M's and late-L's can be  $\approx 2$  magnitudes offset from the field sequence, whereas at  $K$  band most L dwarfs are comparable to the field.
3. The low-gravity (VL-G) population is more distinct from the field objects than the intermediate-gravity (INT-G) population, especially for the late-L dwarfs, though individual young objects of both gravity classifications do overlap. To highlight the differences between each other and the field, Figures 6, 7, and 8 include robust linear fits to the VL-G and INT-G samples, and Table 10 gives the fitted coefficients.

The first two trends have been noted in earlier studies of young ultracool dwarfs using smaller samples and more heterogenous spectra classifications, though not as conclusively. (1) Based on the companions to young ( $\approx 10$ –500 Myr) stars known at the time, Wahhaj et al. (2011) showed that young late-L dwarfs were always fainter than the field sequence, but that young early/mid-L dwarfs could be brighter or fainter, broadly consistent with our results presented here. The spectral types available for their companion sample was of variable quality, perhaps enhancing the scatter in the absolute-magnitude relations. (2) Faherty et al. (2013) found that most young L dwarfs are fainter than the field sequence in  $J$  band, by up to 1 mag, based on their own IR parallaxes for a comparable sample of young field objects. This result is not confirmed with our CFHT sample: while some of the young L dwarfs show such a large offset, many are comparable to the field sequence.<sup>9</sup> (3) Finally, Zapatero Osorio et al. (2014) found most of the young early/mid L dwarfs in their IR parallax sample are comparable or brighter than the field sequence (i.e., the opposite of Faherty et al.), whereas our CFHT results do not find brighter objects except among the earliest L dwarfs. To summarize, while young late-L dwarfs have long been recognized as being fainter at  $J$  band than the field, previous studies of young early/mid-L dwarfs have been inconsistent. The large sample and high precision of our CFHT sample now affords a clear view of the spectrophotometric trends.

Recently, Filippazzo et al. (2015) reported a similar trend in the  $J$ -band magnitudes of young late-M to late-L dwarfs as seen in our CFHT sample. (Note that a significant fraction of their sample relied on kinematic distances, rather than parallaxes.) They found that their young sequence and field sequence cross at a spectral type of L0, whereas our VL-G and field sequences cross at a spectral

---

<sup>9</sup>Note that the summary plots in Wahhaj et al. and Faherty et al. both show the young L0 companion AB Pic b (Chauvin et al. 2005b) as being significantly fainter in  $J$  band than the field sequence. However, improved photometry by Biller et al. (2013) produces a brighter flux for AB Pic b, leading to a less anomalous appearance.

type of L2. This small discrepancy may be due to our separate analysis of VL-G and INT-G samples whereas Filippazzo et al. consider all young objects as a single sample, or due to slightly different definitions of the field sequence (see below). In addition, Filippazzo et al. find young objects have brighter *W2* magnitudes than the field sequence at all spectral types, in accord with our results.

In the *WISE* mid-IR bandpasses, the young targets appear generally to be brighter than the field sequence in Figure 8, especially among the young early/mid-L dwarfs. There may be a more clear distinction between the loci of INT-G and VL-G L dwarfs than seen at shorter wavelengths, with the VL-G objects being systematically brighter in the mid-IR than INT-G, and similarly between INT-G and FLD-G.

Many of our objects have optical spectra, so Figure 9 shows the absolute-magnitude trends using optical spectral types from the literature. Many of the objects also have optical gravity classifications, or at least reported signatures of youth in the literature (e.g. Reid et al. 2008; Kirkpatrick et al. 2008; Cruz et al. 2009; Shkolnik et al. 2009; Kirkpatrick et al. 2010). The overall behavior of the young objects relative to the field sequence is the same for optical and near-IR spectral types. (Note that optical types for L dwarfs only go down to L8, while near-IR types include L9.) The scatter in the young L dwarf sequence is smaller for optical types, likely reflecting the greater spectral heterogeneity of L dwarfs in the near-IR (e.g., see discussion in Kirkpatrick 2005 and Allers & Liu 2013a).

#### 4.1.2. Dispersion in Absolute Magnitudes

In conjunction with the aforementioned general trends, there is significant scatter in the absolute magnitudes of young objects. This phenomenon is real and not simply due to parallax uncertainties. Among the late-M dwarfs, the VL-G objects show relatively uniform magnitudes, perhaps in part because 5 out of 7 of them are TWA members, and thus have common ages. (The six TWA objects in our sample are all the brightest VL-G objects in *J*-band for their spectral type, ranging from M6 [TWA 8B] to L0 [2MASS J1245–4429 a.k.a. TWA 29].) The scatter is far more notable for the INT-G late-M dwarfs, where objects can be comparable to the field locus or up to  $\approx 2$  magnitudes brighter at *YJHK*.

In fact, while the sample is small, the INT-G late-M’s seem to bifurcate in the magnitude-vs-spectral type plots and near-IR color-magnitude diagrams (Section 4.2), into a pair of M8’s brighter than field objects (2MASS J1411–2119 and 2MASSI J0019+4614) and a fainter pair of M7.5’s comparable to field objects (SO J0253+1652 [a.k.a. Teegarden’s Star] and 2MASS J0714+3702). Furthermore, this bifurcation is also reflected in the lithium abundances, with the two brighter objects having lithium absorption in their optical spectra (Reiners & Basri 2009) while the one fainter object with an optical spectrum does not show lithium (SO J0253+1652; Henry et al. 2004). And thus the bifurcation of our INT-G late-M sample may reflect the conflation of a younger population (e.g., 2MASSI J0019+4614 is a member of the  $\approx 125$  Myr AB Dor group) and an older

one. An additional consideration is that the M7–M8 range is where Dobbie et al. (2002) have suggested the mass-luminosity relation changes due to the onset of dust formation, as inferred from the luminosity function of young clusters (see also Pinfield et al. 2003; Chappelle et al. 2005). So the INT-G bifurcation may also reflect dust opacity variations. (Intriguingly, the VL-G objects seem to show the largest dispersion right at the M/L transition.) Altogether, more INT-G late-M objects with parallaxes are needed to refine our view of this sub-population.

For young L dwarfs, the scatter relative to the field population is less than for the late-M’s, though young L’s can still be brighter or fainter than the field. The notable outlier is the companion 2MASS J1207–3932b (L3 VL-G), which may reflect the difficulties of assigning a single number, namely spectral type, to this spectrally extreme object (e.g., see Figure 2 of Liu et al. 2013b). In this vein, it is worth remembering that differences between the young and old populations also reflect the challenges of near-IR spectral typing for dusty ultracool dwarfs (e.g., see Section 4.1 of Allers & Liu 2013a). Some of the scatter may be due to spectral type uncertainties, rather than the intrinsic dispersion of absolute magnitudes in objects of the same spectral type.

While the VL-G and INT-G populations show clear trends, perhaps a comparably interesting result is how the near-IR absolute magnitudes are only partly influenced by surface gravity. A sizeable number of young objects do *not* have significantly different absolute magnitudes than the field sample. Similarly, for objects of comparable near-IR spectral type, the offsets from the field sequence only partly correlate with gravity classification. Some INT-G objects can be just as faint or bright relative to the field as VL-G objects, except for the late-L dwarfs, where the VL-G objects can achieve fainter magnitudes. Spectral type (a proxy for temperature) and gravity (a proxy for age) do not seem to be the only factors driving the absolute magnitudes, at least given our current ability to assign types and gravities. (Note this is not the case for the color-magnitude diagram, where VL-G objects show a clearly defined sequence, as discussed in Section 4.2.)

#### 4.1.3. Absolute Magnitudes of Unusually Red Field-Gravity Objects

Figures 6, 7, and 8 also show the behavior of field objects with unusually red colors but FLD-G gravities, such as 2MASS J1821+1414 and 2MASS J2148+4003. Interestingly, such objects mostly fall within the absolute magnitude range seen in field objects. Thus while these objects have absolute magnitudes and colors that overlap low-gravity objects (see also Section 4.2), they are not unusually bright (for the case of the late-M dwarfs) or faint (for the case of the mid/late-L dwarfs) compared to objects of similar spectral type, unlike the low-gravity objects. In this respect, absolute magnitudes for late-M and late-L dwarfs may help to distinguish dusty objects from low-gravity ones, in cases where the spectra are insufficient or unavailable to assess surface gravity.

Figure 10 shows the FLD-G objects and objects having strong H $\alpha$  emission from our CFHT sample. For the most part, the FLD-G objects appear similar to the field locus, including the young companion LP 261-75B and peculiar object SDSS J1025+3212. The most discrepant FLD-G object

compared to the field locus is 2MASSW J0033–1521, which is L4 $\beta$  in optical but L1 FLD-G in NIR. This is 0.8 mag fainter at  $J$ -band than the field locus, making it notably fainter than even the low-gravity L1 dwarfs, though its absolute magnitudes would be field-like if it were classified as L4. Among the H $\alpha$  emitters, the two objects brighter than the field locus both have low-gravity signatures: 2MASS J0335+2342 is a VL-G object, and LP 423-31 is classified as FLD-G in the near-IR but has signs of low gravity in its optical spectrum (Shkolnik et al. 2009). The two H $\alpha$  emitters without any low-gravity signatures (2MASS J0407+15464 and 2MASS J1707+4301) have comparable magnitudes to the field.

#### 4.1.4. Polynomial Relations

A common use of absolute magnitude-spectral type relations is to estimate photometric distances. As seen in our plots, the field and young sequences differ depending on bandpass, spectral type, and gravity, but there are some regimes where they overlap. For instance, the  $H$ -band absolute magnitudes of early-L dwarfs ( $\approx$ L0–L2) are comparable for field and young objects, likewise for  $K$  band with mid-L dwarfs ( $\approx$ L3–L6), and for  $W1$  band with late-L dwarfs ( $\approx$ L5–L8), though there still exist young outliers. Such trends may be useful for estimating distances for ultracool dwarfs where spectral types are available but gravity information is not, e.g., typing from modest S/N spectra or purely photometric estimates. Unfortunately, for the late-M dwarfs, the young and field sequences are distinct so they are not amenable to this approach. Similarly, if gravity information is known, then specific choices of bandpasses for certain spectral types may be quite useful for photometric distance estimates, e.g., the low-gravity L dwarfs show remarkably small scatter in their  $W1$ -band magnitudes, more so than it would appear from simply quoting the RMS about the robust linear fit in Table 10.

Figure 11 compares polynomial fits for absolute magnitude versus near-IR spectral type for the field sequence from Dupuy & Liu (2012); for field late-M and L dwarfs from this paper, Gagné et al. (2015a), and Filippazzo et al. (2015); for the INT-G and VL-G samples from this paper; and for the young field sample from Gagné et al. (2015a). We caution that the Gagne et al. relations are derived from a sample that has some objects with parallactic distances but most with kinematic distances derived from their Bayesian classification method (described here in Section 4.4). Overall, the differences between the polynomial relations can be very significant between our low-gravity relations and those of Gagne et al., depending on the spectral types and filters of interest.

## 4.2. Color-Magnitude Diagrams

As another comparison of our sample to the field population, we examine several infrared color–magnitude diagrams (CMDs) based on near-IR ( $YJHK$ ) and mid-IR ( $W1$  and  $W2$ ) data with objects distinguished by their gravity classifications (Figures 12 and 13). For the field population,

we use the same data described in the previous section. Note that our CMDs contain more objects than the plots of absolute magnitude versus spectral type in the previous section, since some objects have measured photometry but have not been classified spectroscopically. For brevity, we plot near-IR photometry on the MKO system only, though our compilation is complete for both 2MASS and MKO systems. All CMD plots span 9.5 mag in absolute magnitude for ready comparison.

#### 4.2.1. General CMD Trends with Gravity

The most obvious feature of all the CMDs is that VL-G objects are displaced from the field sequence, being brighter and/or redder than field objects. In fact, the distinction between the respective VL-G and field sequences is remarkable, with only a very small fraction of interlopers. The Appendix discusses the individual interlopers in detail. In short, four of them (2MASS J0407+1546, LP 423-31, 2MASS J0835–0819, and 2MASS J2208+2921) appear to have CMD positions that are discrepant with their gravity classifications, though three of these have hints of low-gravity spectral signatures (all except 2MASS J2208+2921). One interloper (2MASS J1935–2846) appears to have a mid-IR excess.

In contrast, objects classified as INT-G share CMD positions with both the field and VL-G objects. There seems to be a slight preference for the early-type INT-G objects, brighter than  $M_{J,\text{MKO}} \sim 12$  mag, to sit on the field sequence (in accord with Saumon & Marley 2008 models which show surface gravity has a minimal influence on the CMD positions of the hottest ultracool dwarfs), while fainter INT-G objects are redder and intermediate between the field and VL-G sequences. However, there are also counterexamples of this trend, with a few bright INT-G objects being closer to the VL-G sequence or faint INT-G objects being consistent with the field population.

Figure 14 provides a master summary of our low-gravity sequences, the field population, the unusually red field objects, and the locus of young ultracool companions of stars, with many individual objects labeled. We plot  $J$ -band absolute magnitude versus  $J - K$  color because we have nearly complete data in these bands, and this captures more dynamic range in the observed properties than other CMDs. We have also plotted linear fits to the three sequences shown here (VL-G, INT-G, and the field). We used the same least absolute deviation method (LADFIT in IDL) as in Section 4.1 to fit  $(J - K)_{\text{MKO}}$  color as a function of absolute magnitude, since absolute magnitude is the more precisely measured quantity and has the larger dynamic range. We exclude 2MASS J1207–3932 from the fits given its extreme position. These linear fits quantify the behavior discussed above for the three sequences, and the coefficients and RMS about the fits are in Table 10.

Figure 15 examines how the CMD behavior described above relates to spectral type, plotting our VL-G sample and the field population, as well as the linear fits between color and absolute magnitude. We also show the mean absolute magnitude at each spectral type from M7 to L7 using the linear relations derived in Section 4.1 for both the VL-G and field samples, thereby indicating the direction in which objects of the same spectral type but different gravity classifications move on

the CMD. Late-M dwarfs are much brighter at nearly the same color at lower gravity. This behavior gradually changes from late-M to early-L such that low gravity objects of the same spectral become more similar in absolute magnitude but increasingly redder in  $J - K$ . At spectral type L3 and beyond, low-gravity counterparts are on average fainter in  $J$  band and even redder in  $J - K$ . At the latest L types, low gravity objects are fainter in both  $J$  band (by  $\sim 1.6$  mag) and  $K$  band (by  $\sim 0.8$  mag) and correspondingly  $\sim 0.8$  mag redder in  $J - K$ . Thus, the overall effect of decreasing surface gravity on the CMD positions of ultracool dwarfs follows a complex pattern, with the changes in the absolute magnitudes and colors depending on the spectral type

#### 4.2.2. *Young Companions versus Young Field Objects*

One of the prime motivations for studying young ultracool dwarfs is to use these objects as analogs for young gas-giant exoplanets. The overlapping temperatures, ages, and masses of young ultracool dwarfs and young imaged companions make this analogy appealing. At the same time, we expect that field objects and companions typically form via different mechanisms, e.g., gravitational collapse of a gas cloud as compared to formation within a circumstellar disk., respectively, which could result in different thermal evolution, metallicities, elemental mixtures, etc. High-quality data enables an empirically driven comparison of free-floating objects with substellar companions. In this aspect, our CMD plots reveal the following:

1. At the bright end, the young companion and young field samples overlap on the CMD. The brightest companions (HR 7329B, PZ Tel B, and TWA 5B) are consistent with the VL-G sequence, mainly because they are brighter than anything of similar spectral type and/or color.
2. Most of the fainter young companions are more consistent with the old field sequence than the VL-G sequence. There are exceptions among the early/mid-L companions, as CD-35 2722B (INT-G), AB Pic b (VL-G), and G 196-3B (VL-G) all coincide with the VL-G sequence, and 2MASS J0103–5515 b might as well given its (larger) photometric uncertainties. In addition, as is well known, the extreme companions HR 8799b and 2MASS J1207–3932 fall off the field sequence.

Overall, the late-M to late-L companions appear to be bluer and/or fainter than the young field sample, which suggests that the companions and the field objects span a different range in physical properties. These two samples cover similar age ranges and spectral types, including objects in the same moving groups (Section 4.4), and thus should have similar masses and temperatures given their similar absolute magnitudes. Thus, difference in other physical properties, e.g., formation history or composition, may be relevant here.

Figure 17 highlights the difference between the VL-G sequence and the young companions, using a robust linear fit as in our other CMD plots. The construction of the two samples are



heterogeneous, which deters a more rigorous comparison between the two. But the overall pattern is intriguing — the VL-G sequence is notably offset from the young companion sequence. Note that most of the free-floating objects were identified as low-gravity in *optical* spectra (Section 2.1), and thus their redder colors are not due to a selection effect. Given the large number of young field objects with parallaxes, the next significant step in such a comparison will likely rely on more discoveries to grow the companion sample.<sup>10</sup>

3. Companions in the L/T transition are beyond the spectral type and color range where we have defined our linear fits, but the companions broadly appear to be consistent with the field population on the CMD. Finally, the late-T companions Ross 458C and Gl 504b are notably redder than the field T dwarf CMD sequence, likely due to the gravity dependence of collisionally induced H<sub>2</sub> absorption (e.g. Burningham et al. 2011).

#### 4.2.3. Unusually Red Field-Gravity Objects

The eight FLD-G objects identified as unusually red behave in a way distinct from either of the field or low-gravity samples (Figure 16). The four earlier-type red objects (M9–L5) are indistinguishable from the field sequence on all our CMDs. 2MASS J2224–0158 (L3 FLD-G) is the reddest of these, but it is only marginally inconsistent with the field sequence within its color errors. In contrast, the late-type red objects 2MASS J2148+4003 (L6 FLD-G) and WISE J2335+4511 (L7p FLD-G) intermingle with the bottom of our VL-G sequence on CMDs where the color includes *K* band, having colors and magnitudes similar to such objects as 2MASS J0355+1133 (L3 VL-G), 2MASS J2244+2043 (L6 VL-G), and WISE J0047+6803 (L7 INT-G). This intermingling is surprising, given that work to date on late-L dwarfs has focused on low-gravity being the prime mover to generate extremely red colors and faint magnitudes (see Section 4.7). Perhaps these two red FLD-G late-L dwarfs have enhanced metallicity compared to most objects in the field, a possibility that could be examined in the future with higher-resolution spectra.

In the mid-infrared  $W1 - W2$  versus  $M_{W2}$  plot, the red FLD-G objects both appear to be intermediate between the field and VL-G sequence. Only in  $Y - J$  or  $Y - H$  CMDs do they distinguish themselves, with 2MASS J2148+4003 sitting with the VL-G sequence and WISE J2335+4511 being consistent with the field. Finally, the latest-type unusually red objects WISE J0206+2640 (L8 (red)) and WISE J0754+7909 (T2p (red)) appear in locations on all CMDs that seem to be consistent with the field sequence, which we discuss further in Section 4.7.

---

<sup>10</sup>The paucity of young companions with  $M(J) \approx 13 - 15$  mag on the CMDs is interesting, though we note that the young mid-L dwarf companion 2MASS J0122–2439 B (Bowler et al. 2013) has  $M(J_{\text{MKO}}) = 14.0 \pm 0.3$  mag based on a photometric distance. Its  $(J - K)_{\text{MKO}}$  color is  $2.28 \pm 0.15$  mag, placing it in the VL-G sequence.

### 4.3. Tangential Velocities

Given our measured parallaxes and proper motions, we can readily compute the projected tangential velocities ( $V_{\text{tan}}$ ) for all of our targets. Objects that have not acquired significant velocities relative to their natal material should have small tangential velocities with respect to the local standard of rest (LSR) and overall a small velocity dispersion as a sample. This allows for an interesting probe of our low-gravity sample, since we do not expect our objects to be old enough to have acquired large space motions. While tangential velocities cannot be used to rule out large space motions, if an object does have a large space motion we might detect it through  $V_{\text{tan}}$ .

While it is common practice to quote directly observed tangential velocities ( $V_{\text{tan}} \equiv \mu/\pi$ ), we also compute here tangential velocities corrected for the Sun’s space motion with respect to the LSR, adopting the recent determination of  $(U, V, W)_{\odot} = (-11.10, 12.24, 7.25) \text{ km s}^{-1}$  from Schönrich et al. (2010). For a given position on the sky it is straightforward to convert  $(U, V, W)_{\odot}$  into projected component velocities in RA and Dec, and with a parallactic distance these can be converted into proper motion in angular units. Table 11 reports our uncorrected tangential velocities, our derived corrections to proper motion in RA and Dec, and the final tangential velocities of our objects in the LSR frame ( $V'_{\text{tan}}$ ). We compute all of these quantities in a Monte Carlo fashion, accounting for the uncertainties in parallax and proper motion.

Two objects with signatures of low gravity display raw (i.e., not LSR corrected) tangential velocities of  $\gtrsim 90 \text{ km s}^{-1}$ . 2MASS J1022+5825 (L1 $\beta$ /L1 FLD-G) is an object from our parallax program for which we measure  $\mu_{\text{abs}} = 1''.0775 \pm 0''.0031 \text{ yr}^{-1}$  and  $\pi_{\text{abs}} = 0''.0526 \pm 0''.0031$ , resulting in  $V_{\text{tan}} = 97 \pm 6 \text{ km s}^{-1}$  ( $V'_{\text{tan}} = 82 \pm 6 \text{ km s}^{-1}$ ). SO J0253+1652 (M7.5 INT-G; a.k.a., Teegarden’s Star) has a parallax of  $\pi_{\text{abs}} = 0''.2593 \pm 0''.0009$  from Gatewood & Coban (2009) and proper motion of  $\mu_{\text{abs}} = 5''.129 \pm 0''.029 \text{ yr}^{-1}$  from Roeser et al. (2010), resulting in  $V_{\text{tan}} = 93.8 \pm 0.6 \text{ km s}^{-1}$  ( $V'_{\text{tan}} = 79.2 \pm 0.6 \text{ km s}^{-1}$ ). In fact, both of these objects have radial velocities (Table 12) showing that 2MASS J1022+5825 and SO J0253+1652 have total space motions of  $99 \pm 4 \text{ km s}^{-1}$  and  $116.0 \pm 0.5 \text{ km s}^{-1}$ , respectively (not LSR corrected). Such velocities are inconsistent with young stars, e.g., the high probability (>75%) moving group members from Torres et al. (2008) have a median of  $24 \text{ km s}^{-1}$  and a 95% confidence limit of 18–34  $\text{km s}^{-1}$ . The existence of these two objects demonstrates that one of two possibilities must be true: (1) objects with low gravity spectral signatures are indeed young but are sometimes born with, or quickly acquire, large space motions; or (2) the optical/near-IR spectral signatures being used to identify low-gravity objects are sometimes manifested by much older objects. If the former is true, then high velocity cannot be used to distinguish between objects that are red because they are dusty and those that are red because they are low gravity, as has been suggested previously (e.g., see discussion of 2MASS J2148+4003 in the Appendix). We note that these kinematic outliers only occur among objects with intermediate gravities, not the VL-G objects, which thus might prefer the latter possibility, namely that other effects besides lower gravity can lead to an INT-G spectrum. However, visual inspection of the near-IR SpeX prism spectra for our two high-velocity objects (Allers & Liu 2013a; Burgasser et al. 2008) do not reveal any obvious discrepancies compared to other INT-G objects of similar spectral

type but lower tangential velocity.

Figure 18 shows all of the tangential velocity measurements for objects with signatures of low gravity as noted in Table 7, including those without formal gravity classifications, along with the unusually red FLD-G objects. With the exception of the two highest velocity objects discussed above, the low-gravity objects have a median  $V'_{\text{tan}}$  of  $10 \text{ km s}^{-1}$  and standard deviation of  $8 \text{ km s}^{-1}$ . This distribution is a somewhat tighter than has been noted previously in the literature for low-gravity objects (e.g., Faherty et al. 2012; Thompson et al. 2013). It is also tighter than standard deviations typically quoted for normal field dwarfs of similar spectral type ( $\approx 20 \text{ km s}^{-1}$ ; e.g., Schmidt et al. 2007; Schmidt et al. 2010; Faherty et al. 2009; Faherty et al. 2012). These results are consistent with the notion that low-gravity objects have younger ages.<sup>11</sup>

Unusually red FLD-G objects tend to have higher tangential velocities, with a median  $V'_{\text{tan}}$  of  $29 \text{ km s}^{-1}$  and a standard deviation of  $15 \text{ km s}^{-1}$ . We caution however that these objects have sometimes been discovered in proper motion searches (e.g., Looper et al. 2008b; Kirkpatrick et al. 2010) and thus could harbor a selection bias toward higher velocities.<sup>12</sup> The unusually red objects with the highest velocities are the two earliest-type ones (2MASS J2224–0158 [L4.5/L3 FLD-G] and 2MASS J1331+3407 [L0/L0 FLD-G] with  $V'_{\text{tan}} = 41.4 \pm 0.7 \text{ km s}^{-1}$  and  $40.1 \pm 2.4 \text{ km s}^{-1}$ , respectively) and the latest-type one (WISE J0754+7909 [T2p (red)] with  $56.0 \pm 1.0 \text{ km s}^{-1}$ ). As noted in Section 4.2, all three of these red objects are consistent with the field sequence on CMDs. In contrast, the two unusually red objects that seem to follow the VL-G sequence on CMDs have velocities marginally consistent with the low-gravity sample ( $V'_{\text{tan}} = 25.1 \pm 0.5 \text{ km s}^{-1}$  for 2MASS J2148+4003 and  $V'_{\text{tan}} = 24.8 \pm 0.4 \text{ km s}^{-1}$  for WISE J2335+4511).

## 4.4. Membership

### 4.4.1. Young Moving Groups

Assessing the membership of our young sample in nearby young moving groups (YMGs) is a prime result from our new parallaxes. Placing young brown dwarfs in such groups allows their ages to be established, by tying to the stellar YMG members. Establishing membership also allows a more complete census of the low-mass population in YMGs. We consider several approaches.

---

<sup>11</sup>Note that our text and the references cited here refer to the standard deviation of the tangential velocities. As highlighted by Reiners & Basri (2009) and Seifahrt et al. (2010), this is distinct from the velocity dispersion, a term which commonly refers to the quadrature sum of the standard deviations in the three components of space velocity ( $U$ ,  $V$ , and  $W$ ).

<sup>12</sup>We note that one red object, 2MASS J21481633+4003594 (L6/L6 FLD-G), was previously thought to have a relatively high tangential velocity ( $V_{\text{tan}} = 62 \text{ km s}^{-1}$ ; Looper et al. 2008b), but our parallax and proper motion give a lower velocity ( $34.4 \pm 0.5 \text{ km s}^{-1}$ ; see Appendix), consistent with the bulk of the low-gravity objects.

1. *Kinematic BANYAN II analysis:* We used the BANYAN II online tool (Malo et al. 2013; Gagné et al. 2014b), which relies on a model of the kinematic and spatial distribution of the solar neighborhood, assumed to be composed of seven YMGs (Argus [ARG], Columba [COL],  $\beta$  Pic [BPMG], AB Dor [ABDMG], Carina [CAR], TW Hyd [TWA], and Tuc-Hor [THA]) and two components of the field population (old [O.FLD] and young [Y.FLD]). Each of these nine components is represented by triaxial gaussians in their space motions ( $UVW$ ) and positions ( $XYZ$ ), where the gaussians’ principal axes are not necessarily aligned with the  $UVWXYZ$  coordinate axes, and then weighted by the expected number of objects, based on a log-normal initial mass function that has been scaled to the number of known stellar members in these YMGs.

Given the observed proper motion, parallax, and (when available) radial velocity for an ultracool dwarf, this online tool uses Bayesian classification to compute the probability for membership in each of the nine components. (See Gagné et al. 2014b and Gagné et al. 2015b for an in-depth discussion about the classification and resulting probabilities.) Note that the BANYAN model only contains groups within 100 pc and the field population only extends to 200 pc, so the model is not appropriate for analysis of our most distant objects (GJ 3276, 2MASS J0557–1359, and 2MASS J0619–2903).

For objects with clear spectroscopic signatures of youth, we use the online tool’s “Young Field” option, which removes the old field component from consideration, leaving just the young field population to represent field objects <1 Gyr old. Note that for objects with discrepant information between their optical and near-IR gravity classifications,<sup>13</sup> we run the tool both with the Young Field option and without. The resulting probabilities for field membership are unchanged, though the objects are assigned to young field or old field depending on the age assumed.

Table 13 shows the resulting Bayesian probabilities for all the field objects, computed using the astrometry compiled in Table 7, and supplemented with radial velocities from the literature given in Table 12. As discussed in Gagné et al. (2014b), bona fide YMG members within  $1\sigma$  of their group’s six-dimensional  $UVWXYZ$  location have membership probabilities of  $\gtrsim 95\%$ , and more peripheral members ( $\approx 1.0\text{--}2.5\sigma$ ) have probabilities of  $\approx 10\text{--}95\%$ , based on a full Bayesian analysis using kinematic and photometric information (described below). Using this as a benchmark, we report all membership outcomes with a probability  $>10\%$  from our kinematics-only BANYAN II analysis. Most objects are uniquely matched to a single YMG or the field population.

2. *Kinematic+SED BANYAN II analysis:* For most of our objects, membership results are avail-

---

<sup>13</sup>For all objects with discrepant optical and near-IR gravity classifications (2MASS J0033–1521 [L4 $\beta$ /L1 FLD-G], 2MASS J0253+3206 [M7 low- $g$ /M6 FLD-G], LP 423-31 [M7 low- $g$ /M6 FLD-G], 2MASS J1022+0200 [M9 $\beta$ /M9 FLD-G], and 2MASS J1022+5825 [L1 $\beta$ /L1 FLD-G], the optical spectrum is low gravity while the IR spectrum is classified as FLD-G. This suggests that optical spectra are somewhat more discriminating for gravity.

able from the full BANYAN II modeling by Gagné et al. (2014b) and Gagné et al. (2015a). While the BANYAN II online tool uses only kinematics, the full BANYAN II model evaluates YMG membership for ultracool dwarfs using both kinematic and spectrophotometric information, the latter based on the 2MASS and *WISE* colors and absolute magnitudes of old and young ultracool dwarfs. For this reason, the probabilities that compute from the BANYAN II online tool cannot be directly compared to those from the full BANYAN II analysis of Gagne et al.. The full BANYAN II model evaluates 4 kinematic criteria and 2 photometric ones, and thus kinematics still plays a large role in the membership calculation but not an exclusive one.

While BANYAN II can efficiently identify low-gravity ultracool dwarfs (Gagné et al. 2015a), there are known deficiencies that deter us from relying solely on its results. The first is its kinematic model of the solar neighborhood may not be complete as there may be (1) stellar YMG members that are currently unidentified, which would alter the triaxial gaussians used by BANYAN II, (2) uncertainties in the reality of all seven adopted YMGs, e.g., the exact nature of Argus is disputed (Bell et al. 2015), and (3) new YMGs in the solar neighborhood that remain to be discovered. The second important deficiency is the photometric aspect of BANYAN II, which relies on the census of young ultracool dwarfs known at the time of its construction. Our CFHT work has expanded this census by a factor of  $\gtrsim 4$ , most notably growing the L dwarf sample, and has significantly revised parallaxes for some objects used by BANYAN II. Thus, the definition of the sequence used by the full BANYAN II analysis may need to be updated. Finally, Gagne et al. require objects to show low-gravity features to be considered YMG members. However, we consider this to be too strict, given the diversity of gravity classifications seen in YMG brown dwarfs and the lack of firm constraints on the upper age at which gravity signatures persist (Allers & Liu 2013a; Aller et al. 2016) — this is especially relevant for 2MASS J2351+3010 discussed below.

In short, while the full BANYAN II analysis provides a powerful tool for assessing membership, we do not consider it to be a complete representation of the nearby young ultracool population.

3. *Comparison to known stellar members:* As a simple check, we compare our objects' *UVWXYZ* position with the nearby young groups, using reduced chi-squared ( $\tilde{\chi}^2$ ) as a metric, namely in velocity position:

$$\tilde{\chi}_{UVW}^2 = \frac{1}{3} \left( \frac{(U_{obj} - U_{ymg})^2}{\sigma_U^2} + \frac{(V_{obj} - V_{ymg})^2}{\sigma_V^2} + \frac{(W_{obj} - W_{ymg})^2}{\sigma_W^2} \right) \quad (1)$$

where  $\sigma$  is the quadrature sum of the measurement uncertainty for an individual object and uncertainties in the group kinematics (both centroid uncertainty and group dispersion).  $\tilde{\chi}_{XYZ}^2$  is calculated similarly. We adopt a cutoff value of 4 in  $\tilde{\chi}_{XYZ}^2$  and  $\tilde{\chi}_{UVW}^2$ , as this encompasses most ( $\approx 95\%$ ) of the known members.

Thus,  $\tilde{\chi}^2$  values provides a simple assessment of whether an object's membership proposed by BANYAN II is plausible. Obviously, this is an incomplete view since it does not consider

false positives, namely that an object from the young field population happens to have a very similar  $UVW$  and/or  $XYZ$  with the YMGs being considered (and likewise for intermixing of members from different YMGs). For this reason, we chiefly use  $\tilde{\chi}^2$  to rule out cases of marginal membership.

We calculate the  $UVW$  velocities for our sample in a right-handed coordinate system. Given the uncertainty for the parallax, proper motion and radial velocity of each object, we track uncertainties using a Monte Carlo approach. Table 12 lists literature radial velocities as well as our calculated  $UVW$  velocities and total velocity for the subset of our sample having measured radial velocities. For this  $\tilde{\chi}^2$  consideration, we exclude our targets with RV uncertainties of  $>3 \text{ km s}^{-1}$ , as these will have unsuitably small  $\tilde{\chi}_{UVW}^2$  values.

For objects without RVs, we calculate the radial velocity that gives the smallest velocity offset to each group and the accompanying minimum possible  $\tilde{\chi}_{UVW}^2$  value, as a plausibility check on membership. Objects that never reach a small enough velocity distance, or corresponding have minimum possible  $\tilde{\chi}_{UVW}^2$  values that are large, can be refuted as members even in the absence of RV information.

For the YMG properties, we use Torres et al. (2008) as a starting point and incorporate more recent updates as appropriate. Table 14 summarizes our adopted groups. Note that BANYAN II uses rotated ellipses to define the galactic position and velocity of each group, thus we cannot directly compare their group definitions to ours. As a check, we computed the mean and standard deviation of  $UVWXYZ$  for group members from the BANYAN II lists (Gagné et al. 2014b). With the exception of the Argus group, we find that our adopted group  $UVWXYZ$  agree with those determined from BANYAN II members to within the uncertainties. For Argus, our adopted  $Y$  for the group ( $-115.1 \pm 35.5 \text{ pc}$ ) does not agree with the mean  $Y$  value for objects in the BANYAN II Argus membership list ( $-21.7 \pm 26.7 \text{ pc}$ ). This discrepancy could be due to contamination of the membership lists for Argus, as recently noted by Bell et al. (2015).

In the end, we adopt a holistic approach in assessing the membership of our young sample. At one extreme, for objects with complete spatial-kinematic data (both parallaxes and radial velocities) as well as full agreement among our three membership methods (kinematics-only BANYAN II, full kinematics+SED BANYAN II, and  $\tilde{\chi}^2$  confirmation), there is no ambiguity in the result. Similarly, objects with parallaxes only, without RVs, but with agreement between BANYAN II analyses are also considered highly probable members, especially if the minimum RV distance between the object and the known members is plausible (equivalently, the minimum possible  $\tilde{\chi}_{UVW}^2$  value is less than our nominal cutoff of  $\lesssim 4$ ). And likewise, some objects flagged by Gagne et al. as strong members from their full BANYAN II analysis but that lacked parallactic distances now have measured parallaxes from our work, thereby strengthening the case for membership.

Where the three membership methods disagree, we scrutinize the differing results along with the available data to make an assessment. For instance, when our kinematic BANYAN II analysis

has a different outcome than the Gagne et al. full BANYAN II analysis, we examine the observations and the Bayesian calculations. Our new parallaxes often help to resolve the disagreement. The full (kinematic+SED) BANYAN II analyses for many objects were done without parallaxes, producing membership assignments along with statistical estimates of the distances. These statistical distances, and thus the associated membership claims, can be evaluated in light of our CFHT parallactic distances. (Likewise, some objects’ parallaxes have changed significantly from published work to our CFHT measurements; see Section 3.1.) Similarly, new CFHT distances for objects can establish their *UVWXYZ* positions as being highly discrepant with known stellar members based on  $\tilde{\chi}^2$ , even if the BANYAN II analyses (either our kinematics-only one or the published kinematics+SED one) points to membership.

Table 13 provides our membership results. Young companions are not included here, as their membership is assessed in their discovery papers. Individual objects that warrant discussion are given in the Appendix, primarily those where the different membership methods give discrepant results or where our CFHT parallaxes lead to a revision in the membership assigned by previous work. A few particularly notable findings are:

- *Argus FLD-G members:* we identify two possible Argus members with FLD-G near-IR gravities (2MASS J0030–1450 and 2MASS J2351+3010), suggesting an older age than previously claimed ( $\approx 40$  Myr; Torres et al. 2008), if the group actually a physical one (see Bell et al. 2015). Another Argus candidate found by Gagné et al. (2014a), SIMP J2154–1055, is refuted as a member based on our new parallax.
- *Disk-bearing brown dwarfs in the  $\beta$  Pic moving group:* we support the membership of the accreting object 2MASS J0335+2342 proposed by Shkolnik et al. (2012), and we identify 2MASS J1935–2846 as a potential member with a mid-IR excess indicative of a disk. These are the two longest-lived (24 Myr; Bell et al. 2015) brown dwarf disks known to date.
- *Distant young ultracool dwarfs with disks:* Four M5–M7 dwarfs originally thought to be nearby young objects turn out to be very young ( $\sim$ Myr) objects at distances of  $\approx 100$ –300 pc: GJ 3276 (a.k.a. 2MASS J0422+1530), 2MASS J0435–1414, 2MASS J0557–1359, and 2MASS J0619–2903. All of them have signatures of having circumstellar disks, most notably 2MASS J0435–1414 which is detected at far-IR, sub-millimeter, and millimeter wavelengths. Based on their spectral types, they straddle the stellar/substellar mass boundary.
- *An intermediate-age very red L dwarf:* 2MASS J2148+4003 is a notable very red L6 FLD-G object claimed to be an old object by Looper et al. (2008b) based on its  $V_{\text{tan}}$ . As discussed in the Appendix, we find its  $V_{\text{tan}}$  value is actually only half the Looper et al. value, and a BANYAN II-based analysis suggests it may be a young field object. When combined with its FLD-G gravity, these results suggest this may be an intermediate-age object.
- *Refuted planetary-mass members of YMGs:* A number of candidate planetary-mass ( $\lesssim 13 M_{\text{Jup}}$ ) objects in young moving groups have been identified by the BANYAN II searches: 2MASS J0033–1521

(9–11  $M_{\text{Jup}}$ ), 2MASS J0253+3206 (13–15  $M_{\text{Jup}}$ ), 2MASS J2148+4003 (6–7  $M_{\text{Jup}}$ ), and 2MASS J2351+3010 (9–11  $M_{\text{Jup}}$ ) from Gagné et al. (2014b); 2MASS J0030–1450 ( $10.8_{-0.6}^{+0.4} M_{\text{Jup}}$ ), 2MASS J0501–0010 ( $10.2_{-1.0}^{+0.8} M_{\text{Jup}}$ ), and 2MASS J2213–2136 ( $13.5 \pm 0.3 M_{\text{Jup}}$ ) from Gagné et al. (2015a); and SIMP J2154–1055 ( $10.3_{-0.3}^{+0.7} M_{\text{Jup}}$ ) from Gagné et al. (2014a). In all these cases, we weaken or eliminate the case for planetary-mass status, either by assigning field membership or finding the near-IR spectra are not low-gravity. Our analysis does preserve one young planetary-mass candidate from Gagné et al. (2014b), the  $\beta$  Pic candidate 2MASS J2208+2921 ( $12.9_{-0.1}^{+0.3} M_{\text{Jup}}$ ). These are all discussed individually in the Appendix.

Table 15 provides a concise summary of our membership results relative to the published BANYAN II analyses. We adopt two simple categories: (1) 23 objects for which our results have changed the membership assignments, and (2) 28 objects for which our results have improved/fortified the existing assignments. For the former, we include all objects identified as YMG member candidates which end up with changed memberships. This count includes objects previously identified as only marginal candidates based on their low BANYAN II membership probabilities and/or high contamination rates, under the rationale that such candidates would still warrant followup observations whereas we conclude they are unlikely to be worth pursuing. For the latter, most are objects with BANYAN II membership determinations done without parallaxes where our CFHT results reinforce the BANYAN II assignments. There is inevitable ambiguity for a handful of objects when using this simple 2-bin categorization, so those interested in the details of specific objects should consult the Appendix and Table 13.

Broadly speaking, objects with  $\gtrsim 80\%$  BANYAN II probabilities to reside in a YMG are confirmed by our work, except for the Argus (1 object) and Columba (1 object) candidates, which we refute and assign to the field. Objects with  $\lesssim 60\%$  probabilities are usually refuted as members and assigned to the field. These numbers are a very rough summary — the reasons for the membership changes depend on the individual objects and their specific datasets.

For several objects, our parallaxes improve/fortify the previous YMG membership claims based on BANYAN II analyses without parallaxes (Gagné et al. 2014b; Gagné et al. 2015b). These are 2MASS J0019+4614 (ABDMG), 2MASS J0045+1634 (ARG), WISE J0047+6803 (ABDMG; see also Gizis et al. 2015), 2MASS J0117–3403 (THA), 2MASS J0241–0326 (THA), SDSS J0443+0002 (BPMG), 2MASS J0518–2756 (COL), 2MASS J0536–1920 (COL), and 2MASS J2244+2043 (ABDMG).

Similarly, our parallaxes have added three objects for which YMG memberships are now secured based on both parallax and RV data: 2MASSI J0019+4614 (ABDMG), 2MASS J0045+1634 (ARG), and SDSS 0443+0002 (BPMG). (These had previously been noted as members based on BANYAN II statistical distances and RVs, and hence are also listed in the previous paragraph.) We have also tentatively added a fourth YMG member with both parallax and RV data, 2MASS J0608–2753 (COL). This object was previously considered a marginal candidate by BANYAN II, and our improvement in the parallax has strengthened the case (see Appendix).



Finally, Figures 19 and 20 present the color-magnitude diagrams again, this time with the YMG memberships indicated. These results provide empirical isochrones for substellar evolution as a function of age and spectral type. We use these in Section 4.6 to test current theoretical isochrones.

#### 4.4.2. Older Stellar Kinematic Groups

Several field L dwarfs from Seifahrt et al. (2010) were included in our sample, as they were reported to be candidate members of older ( $\gtrsim 100$  Myr) moving groups, namely the Hyades, Pleiades, Ursa Major streams (e.g. Montes et al. 2001; Zuckerman & Song 2004). These are more kinematically distributed than the aforementioned young moving groups and lack a definite spatial concentration. Accordingly Seifahrt et al. (2010) adopted a rather large velocity dispersion (7–10 km s<sup>-1</sup>) combined with photometric distances (and an unrealistically small uncertainty of 1 pc) to select candidates.

With our CFHT parallaxes, the  $UVW$  values of these candidates is consistent with group membership, as judged by  $\tilde{\chi}_{UVW}^2$  and using the updated group definitions from Klutsch et al. (2014) (Table 14). However, the large velocity extent of these older groups means that a given object can overlap more than one group. Moreover, the reality of these groups and the purity of their membership lists are still being debated (e.g. Bovy & Hogg 2010; Tabernero et al. 2012). In the absence of a quantitative method to assign membership and the lack of any matches to younger groups, we simply assign these objects to the general field population and propagate their original assignments from Seifahrt et al. (2010).

### 4.5. Age Calibration of the Ultracool Gravity Sequence

Low-gravity spectral signatures in optical and near-IR spectra of ultracool dwarfs have been valuable for distilling the rare subset of young field brown dwarfs from the general field population. Theory predicts that the radii of substellar objects cease contracting by  $\sim 300$  Myr (e.g. Burrows et al. 2001), but accurate predictions about the time-evolution of gravity-sensitive features leading up to this cessation are beyond current models. Thus, empirical calibration of the spectral evolution is needed, based on ultracool dwarfs in stellar associations/groups and as companions to stars. Such a calibration would also be prized for diagnosing ages of field ultracool objects unaffiliated with any stellar group as well as ultracool companions around host star with uncertain ages.

For late-M and L dwarfs, evidence to date supports the expected  $\sim 300$  Myr timescale disappearance of low-gravity features (e.g. Kirkpatrick et al. 2008; Allers & Liu 2013a; Smith et al. 2015), with ample evidence that objects at  $\sim 100$  Myr still have distinct gravity signatures (e.g. Martín et al. 1999b; McGovern et al. 2004; Aller et al. 2016). At optical wavelengths, Kirkpatrick et al.

(2008) also showed that low-gravity signatures for late-M dwarfs are distinct between  $\sim 10$  Myr and  $\sim 100$  Myr objects, and Cruz et al. (2009) speculated that a similar distinction for young L dwarfs was possible for their  $\beta/\gamma$  gravity classifications. At near-IR wavelengths, Allers & Liu (2013a) used a sparse sample of YMG members and candidates to estimate VL-G and INT-G classifications occur for  $\sim 10$ – $30$  Myr and  $\sim 50$ – $200$  Myr, respectively. At the youngest ages ( $\approx 10$  Myr), they found VL-G gravity classifications are ubiquitous, but intermediate ages could display objects with both VL-G and INT-G classifications (see also Allers & Liu 2013b), in accord with evolutionary models (e.g., Figures 4 and 5 of Saumon & Marley 2008). Surprisingly, they also found that brown dwarfs of the same age and spectral type could have differing gravity classifications, as demonstrated by the AB Dor members CD-35 2722B (L3 INT-G) and 2MASS J0355+1133 (L3 VL-G). Finally, Gagné et al. (2015a) found that the strength of gravity-sensitive near-IR spectral features do generally correlate with age, but with too much scatter to diagnose individual objects.

Our membership assignments and uniform near-IR gravity classifications afford an opportunity to revisit this issue. Figure 21 shows the distribution of VL-G and INT-G objects in different young moving groups, as a function of group age. While the number of objects and age sampling is still rather sparse, the data do indicate a decline in VL-G objects with age, with INT-G objects becoming prevalent by  $\approx 150$  Myr. However, the transition from low to high gravity (i.e., VL-G to INT-G to FLD-G) does not purely depend on age, nor simply depend on spectral type, as might be expected. This is highlighted in the AB Dor group, where L dwarfs are both VL-G (2MASS J0355+1133 [L3] and 2MASS J2244+2043 [L6]) and INT-G (CD-35 2722B [L3] and DENISJ1425–3650 [L4]). The one AB Dor late-M dwarf has INT-G, but one cannot reach conclusions based on one object. (See also Aller et al. 2016.) Finally, the Argus group may be the best illustration of the diverse spectral behavior, where the one secure group member is VL-G (2MASS J0045+1634 [L2]) while the two other possible members are FLD-G (2MASS J0030–1450 [L6] and 2MASS J2351+3010 [L5]).<sup>14</sup>

#### 4.6. Comparison to Theoretical Models

We now examine whether current model atmospheres can reproduce the locus of low-gravity ultracool dwarfs on the CMD. This has previously been addressed primarily for planetary-mass companions like HR 8799b (e.g., Barman et al. 2011a; Marley et al. 2012) and 2MASS J1207–3932b (e.g., Barman et al. 2011b), and our new large sample of low-gravity objects spans a much wider range in mass and temperature. Here we consider two sets of models. Saumon & Marley (2008) provide a model atmosphere grid over a wide range of  $T_{\text{eff}}$ ,  $\log(g)$ , and cloud properties based on the cloud treatment of Ackerman & Marley (2001), which is parameterized by the sedimentation

---

<sup>14</sup>Dupuy et al. (2016a) have recently determined the individual component dynamical masses for the ultracool binary LSPM J1314+1320AB, which has an integrated-light spectrum on the borderline of FLD-G and INT-G. The measured masses and luminosities combined with evolutionary models yield an age estimate of  $81 \pm 3$  Myr, rather young compared to its spectroscopic gravity.

efficiency  $f_{\text{sed}}$ . (Larger values of  $f_{\text{sed}}$  mean more efficient sedimentation, leading to faster particle growth, larger particle sizes, and thinner clouds.) This grid predicts the range of colors and magnitudes that objects would have, regardless of the particular prescription for cloud evolution as objects cool. We also examine BT-Settl evolutionary model isochrones (Baraffe et al. 2015; Allard et al. 2015, in preparation) that adopt a particular prescription for the formation and sedimentation of clouds as objects age (Allard et al. 2012).

Figure 22 shows our VL-G CMD sequence, along with the field population and HR 8799bcd. (HR 8799e is lacking  $J$ -band photometry.) We have overplotted Saumon & Marley (2008) model atmospheres of different gravities and cloud thicknesses, from very thick ( $f_{\text{sed}} = 1$ ) and red in  $J-K$  to thin ( $f_{\text{sed}} = 3$ ) and bluer. We plot models for  $T_{\text{eff}} = 1100\text{--}2400$  K at  $\log(g) = 4.5$  dex and 5.5 dex, while for the lowest gravity  $\log(g) = 4.0$  dex models are only complete over  $T_{\text{eff}} = 1100\text{--}1500$  K.<sup>15</sup>

We find that the vast majority of our VL-G objects do not overlap with the Saumon & Marley (2008) model atmosphere locus. This is because the models do not reach sufficiently red colors at a given absolute magnitude (or equivalently are too faint at a given color). The discrepancy is especially severe for the earlier type objects, the late-M and early-L dwarfs. and also occurs when using  $K$ -band absolute magnitude for the CMD. While the Saumon & Marley models are similarly too blue (and/or faint) compared to the field population given the expected field gravities of  $\log(g) \approx 5$  (e.g., also see Figure 10 of Saumon & Marley 2008), the discrepancy is more severe for the VL-G sample. Finally, a similar discrepancy with the data is seen when considering the Marley et al. (2012) evolutionary models, which adopt a gravity dependence to the L/T transition (Figure 23).

The cloud treatment is perhaps the most ready explanation for the discrepancy on the CMD between the VL-G sequence and the models. Since Figure 22 shows that reducing  $f_{\text{sed}}$  at fixed temperature and gravity moves the models redder, one natural explanation is that more extreme  $f_{\text{sed}}$  values are needed for young objects than currently modeled, namely even smaller  $f_{\text{sed}}$  and thus smaller particles and thicker clouds. Another alternative is unphysically large radii (i.e., lower gravities) to boost the absolute magnitudes at a given temperature.

A more speculative idea is that the cloud particle size distribution differs in low-gravity objects compared to higher-gravity field objects, the latter of which have served as the notional references for model developments. For instance, Ackerman & Marley (2001) assume the size distribution is always log-normal, as detailed computations over the range of parameter space are prohibitive. In addition, brown dwarf radii decrease by a factor of  $\approx 2\text{--}3$  from 10–100 Myr (e.g. Burrows et al.

---

<sup>15</sup>Previous comparison of these models by Faherty et al. (2012) for a sample of four low-gravity L dwarfs seemed to show (1) the model locus overlapping with the data, and (2) the low-gravity models being too red relative to their data (see their Figure 12). Their two results are the opposite of our results, likely due to issues with their plotted sample. Two out of the four have problematic parallaxes (2MASS J0032–4405 and 2MASS J0501–0010; see Sections 2.5.3 and 3.1, respectively); another is only intermediate gravity [2MASS J2322–3133]; and the fourth has either intermediate or field gravity (2MASS J0103+1935; see Section 2.5.3).

2001), so perhaps the correspondingly longer rotation periods of young brown dwarfs change the dynamics of condensate formation and sedimentation. Note that there is a large spread in natal brown dwarf rotation rates (e.g., factor of  $\approx 10$ ; Scholz et al. 2015), which might lead to differences in the cloud properties. These could manifest as differences in colors, magnitudes, and spectra for objects of similar mass, age, and metallicity (e.g., Sections 4.1 and 4.5). However, the fact that the VL-G sequence is rather tight and distinct from the field sequence on the CMD hints that evolutionary changes play a larger role than initial conditions.

Figure 24 shows our VL-G CMD sequence alongside BT-Settl isochrones ranging from 1 Myr to 10 Gyr. We also show the confirmed and probable members of young moving groups compared to isochrones encompassing the age ranges for these groups from Bell et al. (2015). Overall, isochrones tend to have bluer colors (or equivalently fainter  $J$ -band absolute magnitudes) than the empirical sequences, and faint red L dwarfs are not reproduced at all as the models begin to turn to the blue due to cloud clearing at relatively bright magnitudes. Notable exceptions to these trends are  $\beta$  Pic b (L1), which is bluer than the 20–30 Myr isochrones (albeit with a large  $J - K$  uncertainty), and the AB Dor member DENIS J1425–3650 (L4 INT-G), which aligns well with the 120–200 Myr isochrone.

#### 4.7. The L/T Transition at Low Gravity

Our sample contains mostly M6–L7 dwarfs and thus well covers the earlier spectral types of the L/T transition (which we loosely consider as spectral types L6–T5 here). In this arena, the mid/late-L dwarfs have been the focus on much attention, in light of the relevance to young directly imaged planets such as 2MASS J1207–3932b and HR 8799bcde, which have redder and fainter IR fluxes than field objects. Similarly, studies of benchmark brown dwarfs (those with known masses and/or ages) show the L/T transition occurs at lower effective temperatures for younger objects (e.g. Metchev & Hillenbrand 2006; Dupuy et al. 2009; Bowler et al. 2013; Liu et al. 2013b). Initial attempts to model the full evolution of the transition from Saumon & Marley (2008) indicated that the absolute magnitudes of the transition (where the near-IR CMD locus crosses from red L dwarfs to blue T dwarfs) should be brighter for young ages. However, with the addition of a gravity-dependent recipe for the transition, chosen to match the HR 8799 planets, more recent evolutionary models by Marley et al. (2012) point to fainter absolute magnitudes for the transition at young ages.

Our combined sample also contains a handful of young objects at later types and thus begins to probe the impact of reduced surface gravity across the entire L/T transition. Figure 25 again shows behavior of the absolute magnitude versus spectral type, but with a larger range in spectral types than previous plots to highlight the L/T objects. The most straightforward result comes from the T2.5 Hyades member CFHT-Hy-20, which at all IR bandpasses is consistent with field objects. This is not surprising since evolutionary models indicate that brown dwarf contraction has largely completed by the  $\approx 600$ –800 Myr age of the Hyades. Similarly, the young ( $\approx 100$ –500 Myr) wide

L/T companions known to date — HD 203030B (L7.5; Metchev & Hillenbrand 2006), HN Peg B (T2.5; Luhman et al. 2007), and GU Psc b (T3.5, which only has a BANYAN statistical distance; Naud et al. 2014) — have positions on the IR color-magnitude diagrams consistent with the field locus (e.g., Figure 14). Finally, the AB Dor member SDSS J1110+0116 (T5.5; Gagné et al. 2015) also coincides with the field locus. Thus, for L/T objects as young as  $\approx 100$  Myr, while the temperatures for a given spectral type may be age-dependent, the IR absolute magnitudes across the L/T transition do not seem to strongly depend on age.

The two latest-type red objects in our sample, WISE J0206+2640 (L9 (red)) and WISE J0754+7909 (T2p (red)), may be illuminating landmarks for the transition. Their spectra are unusual compared to most field objects of similar type, especially WISE J0754+7909 (see details in Appendix). And yet their absolute magnitudes are largely consistent with field objects, with the largest discrepancy being WISE J0206+2640 having  $\approx 0.5$  mag fainter magnitudes at  $Y$  and  $J$  bands compared to the field. Even given its very peculiar spectrum, WISE J0754+7909 has absolute magnitudes and color-magnitude positions in accord with the field. Thus, while the spectral peculiarities of these two objects may not be due to low gravity (indeed both have old field kinematics; Table 15), their consistency with field objects may be circumstantial evidence that the IR magnitudes of the L/T transition are robust over a range of physical properties.

One interesting question that we can address is whether the  $J$ -band flux reversal that is a hallmark of L/T transition binaries in the field population (e.g. Liu et al. 2006) would appear different at lower gravities. The most extreme such flux reversal binaries known are 2MASS J1404–3159AB ( $\Delta J = -0.54 \pm 0.08$  mag,  $\Delta K = 1.33 \pm 0.05$  mag; Looper et al. 2008a) and SDSS J1052+4422AB ( $\Delta J = -0.45 \pm 0.09$  mag,  $\Delta K = 0.52 \pm 0.05$  mag; Dupuy et al. 2015). SDSS J1052+4422AB has a very precise evolutionary model-based age derived from its dynamical masses and luminosities, clearly demonstrating that it is field age and gravity ( $1.11^{+0.17}_{-0.20}$  Gyr and  $\log(g) = 5.0$ – $5.2$  dex; Dupuy et al. 2015). Now that we have parallaxes for members of young moving groups that span the L/T transition, we can imagine hypothetical L/T transition binaries composed of these coeval objects. For example, if the AB Dor members WISEP J0047+6803 (L7 INT-G) and SDSS J1110+0116 (T5.5) were paired together in a binary, they would have  $\Delta J = -0.37 \pm 0.11$  mag,  $\Delta K = 2.04 \pm 0.09$  mag. If the primary were instead 2MASS J2244+2043 (L6 VL-G), the flux ratios would be  $\Delta J = -0.47 \pm 0.09$  mag,  $\Delta K = 1.89 \pm 0.09$  mag.

Thus, it seems plausible that young  $J$ -band flux-reversal binaries have comparable  $J$ -band flux ratios as field systems, with the caveat that the current sample of young objects for such hypothetical pairings is very small. However, the “bump” relative to  $K$  band in these binaries would be somewhat larger, i.e., their  $K$ -band ratios may be larger, as low gravity late-L dwarfs are both fainter at  $K$  and redder in  $J - K$  than field objects of comparable spectral type, while the young mid-T dwarf SDSS J111010.01+011613 seems to lie close to or perhaps only slightly below the field CMD sequence. Although little work has been done on field  $J$ -band flux-reversal binaries at bandpasses bluer than  $J$ , we note that the  $Y$ -band bump of a hypothetical AB Dor L/T transition binary composed of 2MASS J2244+2043 and SDSS J1110+0116 would be even larger

than at  $J$ -band ( $\Delta Y = -0.71 \pm 0.09$  mag), while SDSS  $z$ -band photometry of these sources indicates no significant  $z$ -band bump ( $\Delta z = 0.18 \pm 0.14$  mag).

## 5. Conclusions

We have completed a large, uniform analysis of the spectrophotometric properties of young ultracool dwarfs in the field, based on a populous new sample of high precision distances from the Hawaii Infrared Parallax Program combined with a uniform analysis of near-IR spectral types and gravity classifications. Our parallax sample is a factor of  $4\times$  larger than previous studies of young field objects and with significantly higher parallax precision. Objects with already published parallaxes from other groups mostly agree with our (typically higher precision) CFHT results, though we note that at least 6 out of the 15 parallaxes for young objects measured by Faherty et al. (2012) appear to be problematic. A few young objects previously thought to have odd/extraordinary properties in fact are unremarkable when considering our new distances.

Combined with previously published measurements (mostly substellar companions to young stars), we have assembled a sample of 102 ultracool objects with parallaxes that allows us to clearly delineate the spectrophotometric behavior of young ultracool dwarfs as a function of spectral type, gravity, and age. The absolute magnitudes of young field objects as a function of near-IR spectral type differ from those of old field objects, with young late-M objects being brighter and mid/late-L dwarfs being fainter in the near-IR ( $YJHK$ ) bandpasses. The brightness differences relative to the field are more dramatic for bluer bandpasses. In contrast, in the *WISE* mid-IR bandpasses, young targets generally appear brighter than the field sequence.

As delineated by the Allers & Liu (2013a) gravity classifications, the VL-G and INT-G populations have differing spectrophotometric behavior. The VL-G population forms a well-defined sequence, both in its absolute magnitudes as a function of spectral type and in near-IR color-magnitude diagrams. For the latter, the VL-G sequences now extended smoothly from late-M to the late-L spectral types, offset from the field sequence to both redder colors and brighter absolute magnitudes. Our work reveals that the effect of decreasing surface gravity from field to VL-G follows an evolving pattern with spectral type, making the IR absolute magnitudes of late-M and early-L dwarfs brighter, then making the colors of mid-L dwarfs redder while not affecting their IR absolute magnitudes, and then making the late-L dwarfs both redder and fainter.

In contrast, the INT-G population is more heterogeneous. Its absolute magnitudes as a function of spectral type have more scatter, especially among the late-M dwarfs. Limited data, based on the presence of lithium, suggests this scatter may be age-related. The INT-G sample is also notable for having two kinematic outliers, with tangential velocities of  $>99$  km s $^{-1}$ , far exceeding known young stars. Two natural explanations are that some young objects experience early dynamical interactions that lead to significant acceleration (e.g., ejection from their birth clouds; Reipurth & Clarke 2001) or old (high-gravity) objects can display spectra that mimic low gravity. We note that the

absence of any high-velocity VL-G objects disfavors the former possibility. Though the current sample sizes and selection effects limit firm conclusions, we notionally propose that older high-gravity objects can show near-IR spectra that appear to be intermediate in gravity (INT-G) between typical young and old field objects.

Along with these trends, there is notable dispersion among the population as a whole that is not well-correlated with spectral type or gravity classification, at least given current ability to diagnose these two properties. There appears to be (at least) a third physical parameter that governs the spectral energy distributions of young ultracool dwarfs. Metallicity is unlikely to be such a parameter, given the metallicity of local high-mass stars (Nieva & Przybilla 2012) and YMG stars (Biazzo et al. 2012; Barenfeld et al. 2013; McCarthy & Wilhelm 2014) appear to be basically solar ( $\sigma \lesssim 0.1$  dex in metallicity). Other possibilities might be early formation history, rotation, or inclination.

We included some objects in our study with unusual properties possibly connected to youthfulness. Very red objects with field gravities turn out to have IR absolute magnitudes similar to ordinary field objects, as do ultracool field dwarfs with strong H $\alpha$  emission. The latest-type red FLD-G objects do overlap the color-magnitude positions of the young late-L dwarfs, meaning they might provide an interesting case study for extreme cloud formation. The extreme redness of young field L dwarfs is believed to be due to extreme clouds, which in turn are believed to be the consequence of reduced surface gravity. But we find two field-gravity objects (2MASS J2148+4003 and WISE J2335+4511) also demonstrate such extreme near-IR properties. *Thus, the current theoretical framework for the extreme red and faint magnitudes of late-L dwarfs is incomplete.*

Young field brown dwarfs are appealing in large part given their potential utility as analogs for brown dwarf and planetary companions around stars, given the observational difficulties of studying the latter. We find the photometric properties of the free-floating and companion populations are quite similar. However, the young field population may inhabit more extreme parameter space, as seen by the brighter and/or redder locations of the young late-M and L dwarfs in the near-IR color magnitude diagrams relative to known young companions. With the young field population now well-mapped, progress on this issue will rely on discovery of more substellar companions to determine whether the two populations do in fact differ in their physical range, which might reflect differences in formation history, photospheric processes, and/or composition. In a similar vein, theoretical models for ultracool objects roughly coincide with the data, but the observational properties are more extreme than the models, with the young objects being redder and/or brighter than the models especially among the young late-M and early-L dwarfs (contrary to the results of Faherty et al. 2012).

We have conducted a comprehensive membership analysis of all young field objects with parallaxes. We establish several new members of young moving groups, as well as strengthen, revise, or refute previously published memberships of many others. Altogether, memberships assigned by BANYAN II for young field objects appear to be reliable when group membership probabilities

are  $\gtrsim 80\%$  (except for the less-certain Columba and Argus groups), whereas objects with lower group membership probabilities appear in fact to be field objects. Similarly, objects with high membership probabilities in well-established groups have BANYAN II kinematic distances that are comparable to actual parallactic distances ( $\lesssim 10\%$  errors). For the remaining objects, either with lower membership probabilities or assignments to the field population, the BANYAN II statistical distances have significantly larger errors than reported. (We caution that our comparison with BANYAN II is based on our specific sample of objects, which does not uniformly sample the full range of spectral types, photometric properties, and moving groups.) Out of the nine planetary-mass ( $\lesssim 13 M_{\text{Jup}}$ ) objects from the BANYAN II searches (e.g. Gagné et al. 2015a) that coincide with our sample, we weaken or eliminate the case for planetary-mass status for eight of them.

With a robust sample of objects in young moving groups, our work provides age-calibrated benchmarks for ultracool dwarfs. We find clear evolution in the mix of IR gravity classifications, with  $\lesssim 20$  Myr objects being entirely composed of VL-G objects and by  $\sim 100$  Myr most objects being INT-G. At the older ages, we note that objects of the same spectral type can have different gravity classifications even within the same moving group, as first suggested by Allers & Liu (2013). Our benchmark sample defines empirical color-magnitude isochrones for substellar evolution from 10–150 Myr, and shows that current BT-Settl evolutionary models are not a good match to the data. The few young age-benchmarks in the L/T transition regime (late-L to mid-T) suggest that the *J*-band brightening may be slightly enhanced for young objects compared to the field. But the evolutionary locus in the near-IR CMD does not appear to be significantly different, namely young early/mid-T dwarfs, appear to have similar IR absolute magnitudes as the field sequence and even spectrally peculiar objects. Overall, the L/T transition on the CMD is relatively narrow in near-IR absolute magnitudes ( $\lesssim 1$  mag).

As a by-product of such a large parallax sample, we have identified a number of individual objects that warrant specialized followup. Four objects appear to be very young ( $\lesssim \text{Myr}$ ), distant ( $\gtrsim 200$  pc) brown dwarfs (GJ 3276, 2MASS J0435–1414, 2MASS J0557–1359, and 2MASS J0619–2903), at least one of which has a well-detected circumstellar disk. Another candidate disk-bearing object might be a member of the  $\beta$  Pic moving group (2MASS J1935–2846), which would make it the oldest disk found to date around a brown dwarf. The two aforementioned high-velocity INT-G objects would benefit from high resolution spectroscopy to assess their gravity and abundances.

Our work enables several future lines of inquiry. A larger sample of parallaxes at later types than covered by our sample would help delineate the L/T transition at low gravities. A larger sample of directly imaged substellar companions would help to clarify if the companion population and young field populations have different photometric properties, perhaps reflecting different origins. Memberships for strong YMG candidates with parallaxes should be further secured by measuring radial velocities. Expanding the stellar census in these groups will be an important complementary effort, energized by the upcoming high-precision astrometric catalogs from *Gaia*. The culmination of such work will establish the full membership census from the highest mass stars to the planetary-mass regime, creating a rich empirical grid of stellar and substellar evolution to



test our understanding of how low-mass self-gravitating objects form and evolve.

We greatly appreciate the CFHT staff for their constant observing support and dedication to delivering the highest-quality data. We thank Will Best and Kimberly Aller for assistance with the IRTF near-IR spectroscopy. We thank Didier Saumon, Mark Marley, Adam Burrows, Bruce Macintosh, Jonathan Fortney, Michael Line, Caroline Morley, and Ruth Murray-Clay for insightful comments on this work. We thank Jonathan Gagné for helpful discussions and for making published data and the BANYAN II model tools publicly available. M. Liu thanks the University of California Observatories; the University of California, Santa Cruz; and the Other Worlds Laboratory for supporting a sabbatical to help complete this work. This publication makes use of data products from the Wide-Field Infrared Survey Explorer, which is a joint project of the University of California, Los Angeles, and the Jet Propulsion Laboratory/California Institute of Technology, funded by the National Aeronautics and Space Administration. Our research has employed the 2MASS data products; NASA’s Astrophysical Data System; the SIMBAD database operated at CDS, Strasbourg, France; the M, L, T, and Y dwarf compendium housed at [DwarfArchives.org](http://DwarfArchives.org); the Spex Prism Spectral Libraries maintained by Adam Burgasser; the Montreal Brown Dwarf and Exoplanet Spectral Library maintained by Jonathan Gagné; and the Database of Ultracool Parallaxes maintained by Trent Dupuy. This research was supported by NSF grants AST-0507833, AST-0909222, and AST-1518339 awarded to M. Liu. Finally, the authors wish to recognize and acknowledge the very significant cultural role and reverence that the summit of Mauna Kea has always had within the indigenous hawaiian community. We are most fortunate to have the opportunity to conduct observations from this mountain.

*Facilities:* CFHT (WIRCAM), IRTF (SpeX), Keck-2 (LGS/NIRC2)

### A. Notes on Individual Objects

For each object, the optical and near-IR spectral types are listed in parentheses, along with gravity classifications when available. Objects noted in the literature as having low gravity but without a formal gravity classification are indicated by “low- $g$ ” (also see Table 1).

**2MASSW J0030300–145033 (L7/L6 FLD-G):** Gagné et al. (2015a) classify 2MASS J0030–1450 as L4–L6  $\beta$  based on the published near-IR spectrum of Burgasser et al. (2010).<sup>16</sup> Using the same spectrum, we assign a spectral type of L6 in the AL13 system to 2MASS J0030–1450 (Table 4). We note that our spectral type is close to the optical L7 spectral type of this object (Kirkpatrick et al.

---

<sup>16</sup>The spectral classification system of Gagné et al. (2015a) uses visual comparison to spectral templates to assign near-IR spectral types and gravities, whereas the AL13 system uses a combination of visual comparison and spectral indices. Gagné et al. (2015a) use gravity designations of  $\beta/\gamma/\delta$  for near-IR spectra (the same notation as the Cruz et al. 2009 optical gravity classification), which are similar to (but not the same as) the near-IR INT-G and VL-G gravity classifications of the AL13 system.

2000). At low spectral resolution, the AL13 system can not classify the gravities of objects with spectral types later than L5. We can visually compare the spectrum of 2MASS J0030–1450 to VL-G and INT-G L6 objects (Figure 26). 2MASS J0030–1450 has deeper FeH and alkali features relative to the L6 INT-G standard, indicating that it likely has higher gravity. Overall, the features of 2MASS J0030–1450 better match the field dwarf standard, so we adopt a spectral type of L6 FLD-G. Oddly, our calculated indices agree with those of Gagné et al. (2015a), but the overall classification does not. We note that Gagné et al. (2015a) use their own (template-based) spectral type when determining the AL13 gravity classification of 2MASS J0030–1450, but the AL13 gravity classification is designed to incorporate AL13 spectral type classifications which are derived from both index-based and visual typing (as described in Section 2.3.2). This likely explains the discrepant gravity classifications.

Gagné et al. (2015a) find that 2MASS J0030–1450 is a possible ARG member, with 26% probability and 3% contamination, based on a parallactic distance of  $27 \pm 3$  pc from Vrba et al. (2004). Their resulting mass estimate is  $10.8_{-0.6}^{+0.4} M_{\text{Jup}}$ , based on an age of 30–50 Myr. While we do not provide a new parallax for this object, our reclassification of the spectrum as field gravity would have led Gagné et al. to remove this object from YMG consideration. However, we retain it given (1) the uncertain diversity of gravity classifications within young groups (Section 4.5) and (2) the ambiguous age/nature of the Argus moving group (Bell et al. 2015). Both of these aspects suggest a substantially higher mass for this object.

Removing the assumption of youth used by Gagné et al., our kinematics-only BANYAN II analysis gives 16% ARG, 20% Y.FLD, and 64% O.FLD. We note that the membership lists of Argus differ substantially between BANYAN II and Torres et al. (2008), with the former having a much larger  $UVWXYZ$  extent. Using the Torres et al. list, we find  $\tilde{\chi}_{UVW}^2=1.0$  and  $\tilde{\chi}_{XYZ}^2=4.1$ , making 2MASS J0030–1450 only a marginal candidate. A radial velocity of  $2.5 \text{ km s}^{-1}$  would place the object at its minimum velocity distance from the Argus group (based on Torres et al.) of  $4.9 \text{ km s}^{-1}$ . We consider this a possible Argus member for now, but a radial velocity for this object and a renewed evaluation of the Argus group are needed to clarify the situation.

**2MASSW J0033239–152131 (L4 $\beta$ /L1 FLD-G):** Kirkpatrick et al. (2008) characterized this as low gravity based on relatively weak K I, CaH, and FeH in its optical spectrum compared to field objects. However, they caution that its atypically weak VO compared to other young L dwarfs (which show enhanced VO absorption) may indicate that its age is near the  $\sim 100$  Myr limit where low-gravity indications are present. Allers & Liu (2013a) find that this object has near-IR FeH, VO, K I and  $H$ -band continuum features consistent with field dwarfs and classify 2MASS J0033–1521 as L1 FLD-G. Our parallax shows that the  $JHK$  absolute magnitudes of this object are comparable to other field objects.

Based on a parallax-free analysis, Gagné et al. (2014b) found this is a modest probability ARG member, with 32% probability, 22% contamination, and a statistical distance of  $17.3_{-2.0}^{+1.6}$  pc. Their associated mass estimate is 9–11  $M_{\text{Jup}}$ , based on an age of 30–50 Myr. Our new parallactic distance of  $23.4_{-1.0}^{+0.9}$  pc disfavors this possibility, agreeing instead with their  $28.1_{-4.8}^{+4.4}$  pc statistical distance for Y.FLD. If we assume youthfulness ( $< 1$  Gyr), our kinematics-only BANYAN II analysis reports

99% Y.FLD. Thus we categorize this as a young field object. If we do not assume youthfulness, then BANYAN II gives membership probabilities of O.FLD(82%) and Y.FLD(18%).

**2MASSW J0058425–065123 (L0/L1 INT-G):** Gagné et al. (2014b) identify this as a possible ABDMG (64%) or BPMG (32%) member, based on a parallax from Marocco et al. (2013). Our kinematics-only BANYAN II analysis finds a similar bifurcation in membership probability using the same published parallax, with ABDMG(75%) and BPMG(22%).

**2MASS J01262109+1428057 (L0/L1 INT-G):** Based on a parallax-free analysis, Gagné et al. (2014b) indicate this is a low probability BPMG member, with 3% probability, 77% contamination, and a statistical distance of  $38.6_{-4.8}^{+6}$  pc. Our new parallactic distance of  $58.5_{-3.8}^{+4.4}$  pc disfavors this possibility, agreeing instead with their  $62.6_{-14}^{+18}$  pc statistical distance for Y.FLD. Our kinematics-only BANYAN II analysis reports 97% Y.FLD with a small residual probability BPMG (1.3%) and COL (1.2%). The minimum  $UVW$  distance from these groups are modest,  $4.1 \text{ km s}^{-1}$  and  $2.9 \text{ km s}^{-1}$  for RVs of  $4.5 \text{ km s}^{-1}$  and  $0.4 \text{ km s}^{-1}$ , respectively, and the object seems to be at the spatial periphery of the known members ( $\tilde{\chi}_{XYZ}^2=5.5$  and  $2.2$ , respectively). Young field membership seems preferred, but an RV measurement would be useful.

**WISEP J020625.26+264023.6 (—/L8 (red)):** This was discovered and classified as “L9p (red)” by Kirkpatrick et al. (2011). We derive a spectral type of L8 based on visual comparison with spectral standards and the index measurements given in Table 5. The spectrum is slightly redder than a normal L8, so we assign a spectral type of L8 (red).

**2MASS J02212859–6831400 (M8 $\beta$ /—):** Gagné et al. (2014b) find this is a young field object based on a parallax from Faherty et al. (2012), as does our kinematics-only BANYAN II analysis. We note that its position is consistent with the known BPMG members ( $\tilde{\chi}_{XYZ}^2=1.3$ ). A radial velocity of  $14.2 \text{ km s}^{-1}$  would yield the smallest possible velocity distance from BPMG,  $6.0 \text{ km s}^{-1}$ , with a corresponding  $\tilde{\chi}_{UVW}^2=2.6$ . Thus, BPMG membership seems marginal at best given the velocity distance.

**2MASSI J0253597+320637 (M7 low- $g$ /M6 FLD-G):** Based on a parallax-free analysis, Gagné et al. (2014b) indicate this is a modest probability BPMG member, with 26% probability, 30% contamination and a statistical distance of  $35.8_{-2.4}^{+2.8}$  pc. (Their tables report both a 21% and 26% membership probability. We take the larger value as it is the one reported alongside the contamination rate.) Their associated mass estimate is 13–15  $M_{\text{Jup}}$ , based on an age of 12–22 Myr. Our new parallactic distance of  $47.0_{-2.3}^{+2.1}$  pc disfavors this possibility, agreeing instead with their  $60.6_{-11.2}^{+12.8}$  pc statistical distance for Y.FLD. Using an RV of  $-36.3 \pm 0.8 \text{ km s}^{-1}$  (E. Shkolnik, priv. comm.), the  $UVW$  position is inconsistent with any known young group. Assuming youthfulness, our kinematics-only BANYAN II analysis reports >99.9% Y.FLD. Thus we categorize this as a young field object.

Cruz et al. (2003) identify this as a young object based on its optical spectrum, which upon examination may show weak CaH, K I, and Na I though not conclusively so. Allers & Liu (2013a) classify the near-IR spectrum as FLD-G. If we do not assume youthfulness in the BANYAN II analysis, the result is 99.3% O.FLD probability.

**2MASS J03140344+1603056 (L0/L0 FLD-G):** Seifahrt et al. (2010) identify this object as a candidate member of the Ursa Majoris moving group. Its location on the sky, however, does not coincide with the core of UMa nucleus members. As discussed in Allers & Liu (2013a), its near-IR spectrum does not show any signs of low gravity (Allers & Liu 2013a), which would not be unexpected at the age of UMa ( $500 \pm 100$  Myr; King & Schuler 2005).

**2MASSI J0335020+234235 (M8.5 low- $g$ /M7 VL-G):** This object was first proposed to be a  $\beta$  Pic member by Shkolnik et al. (2012), using a parallax ( $23.6 \pm 1.3$  mas) that agrees well with ours ( $21.8 \pm 1.8$  mas). Reid et al. (2002) detected Li I absorption in this object, and Shkolnik et al. (2009) noted it as a low-gravity accreting source. This makes it the oldest known accreting brown dwarf.

**LP 944-20, a.k.a. 2MASS J03393521–3525440 (M9/L0 FLD-G):** As discussed in Gagné et al. (2014b), BANYAN II analysis indicates that ARG membership may be an option for this object, which is also found from our kinematics-only analysis, but this object most likely belongs to the Castor moving group, which is not included in the standard BANYAN II model.

**2MASS J03552337+1133437 (L5 $\gamma$ /L3 VL-G):** This object has the reddest  $J - K$  color in our sample, and both Cruz et al. (2009) and Allers & Liu (2013a) characterize it as very low gravity. We find that this object is faint for its spectral type at  $J$  band, but its  $H$  and  $K$ -band absolute magnitudes are comparable to the field population.

At a distance of only  $9.10 \pm 0.10$  pc, this object is the nearest known young brown dwarf. In addition, it is one of the very closest known young moving group members, with only the M2 dwarf BD+01 2447 ( $7.07 \pm 0.02$  pc; van Leeuwen 2007) in the AB Dor moving group being closer (Torres et al. 2008) and the young M dwarfs AT Mic ( $10.7 \pm 0.4$  pc) and AU Mic ( $9.91 \pm 0.10$  pc) in the  $\beta$  Pic moving group (Zuckerman et al. 2001) being comparable.

**2MASS J04070752+1546457 (L3.5/L3 FLD-G):** This is a strong ( $EW \sim 60 \text{ \AA}$ ) H $\alpha$  emitting L3.5 dwarf (Reid et al. 2008), classified as FLD-G by Allers & Liu (2013a). It has normal  $J$ -band absolute magnitudes for its near-IR spectral type but slightly brighter in  $K$  and  $W2$  than the field sequence (Figure 10). On both near- and mid-IR CMDs, this makes it a clear FLD-G interloper in the VL-G sequence, being unusually red in  $J - K$ ,  $H - W1$ , and  $W1 - W2$  given its absolute magnitude.

Gagné et al. (2015a) note some marginal visual signs of low gravity but do not associate it with any YMG. Our kinematics-only BANYAN analysis finds 49% Y.FLD and 40% O.FLD, perhaps in accord with possible mild youth seen in the near-IR spectrum. For these spectral subclasses, the IR absolute magnitudes of the young and field populations are very similar, so they provide no age discrimination. We assign a generic “field” membership to this object, as we cannot distinguish between the young and old possibilities.

**GJ 3276, a.k.a. 2MASS J04221413+1530525 (M6 $\gamma$ /M6 VL-G):** Allers & Liu (2013a) note that its near-IR spectrum appears reddened and that it has a mid-IR excess indicative of a circumstellar disk, which combined with its sky position points to possible membership with the Taurus

star formation region  $\sim 10^\circ$  away. Our CFHT parallax puts this at a distance ( $240^{+70}_{-40}$  pc) that is marginally consistent with the young stars in Taurus (130–160 pc; Torres et al. 2009). (See Section 3 for a discussion of the highly discrepant parallax from Faherty et al. 2012.) The absolute magnitudes of this object derived from our CFHT parallax are  $\approx 5$  mag brighter than the field dwarf sequence and comparable to very young ( $\lesssim 3$  Myr old) mid-M dwarfs in the Taurus star-forming region (e.g. Luhman et al. 2003).

**CFHT-Hy-20 (—/T2.5):** The depth of this object’s *JH* and *HK* water absorption bands are well-matched to the T2 standard SDSSp J1254–0122, though its *H*-band and *K*-band methane absorption and *YJ* water absorption are slightly deeper and would suggest a type of T2.5 (Figure 27). Our visual and index-based types are in good agreement, and we assign a final near-IR spectral type of T2.5. This agrees well with the T2 assigned by Bouvier et al. (2008), based on their very low resolution ( $R = 50$ ) near-IR spectrum of CFHT-Hy-20 compared to field T dwarfs observed with their same instrument.

CFHT-Hy-20 lies  $3^\circ$  from the center of the Hyades (e.g., Figure 1 in Bouvier et al. 2008). No radial velocity is available, but it has a minimum *UVW* distance of  $2.5 \text{ km s}^{-1}$  from the Hyades. We measure a parallactic distance of  $32.5^{+1.5}_{-1.7}$  pc, which agrees well with the *Hipparcos* distance of  $46.34 \pm 0.27$  pc given the cluster tidal radius of 10 pc (Perryman et al. 1998). We therefore confirm this object as a Hyades member.

**2MASS J0435145–141446 (M6 $\delta$ /M7 VL-G):** A parallax-free analysis by Gagné et al. (2014b) indicates this is a young field object ( $>99.9\%$  probability) with a statistical distance of  $10.5 \pm 1.6$  pc. We measure a parallactic distance of  $87.7^{+9.4}_{-11.8}$  pc, with a kinematics-only BANYAN II analysis still indicating  $>99.9\%$  Y.FLD. Cruz et al. (2003) noted that the object lies in the direction of the high-galactic latitude MBM20 (LDN 1642) cloud, which has an estimated distance of  $124 \pm 19$  pc (Schlafly et al. 2014). Our parallax is  $1.7\sigma$  different than the cloud, placing the object in front of or plausibly within the cloud. The radial velocity for the object (E. Shkolnik, priv. comm.) is notably different than the cloud’s CO emission at  $\approx 0\text{--}1 \text{ km s}^{-1}$  (Liljestrom 1991; Russeil et al. 2003), perhaps due to spectroscopic binarity or unusual kinematics. Our proper motion measurement of  $(\mu_\alpha, \mu_\delta) = (-0.6 \pm 1.9, +9.3 \pm 2.0) \text{ mas/yr}$  is consistent with that of the *IRAS*-excess star EW Eri associated with the cloud (Sandell et al. 1987), which has a proper motion of  $(-5.3 \pm 5.6, +7.1 \pm 5.5) \text{ mas/yr}$  from UCAC4 (Zacharias et al. 2013).

Allers & Liu (2013a) noted that this object’s *WISE* photometry (3.6–22  $\mu\text{m}$ ) shows no sign of a disk, while Malinen et al. (2014) associate this object with a source detected in far-IR, sub-millimeter, and millimeter data (100–1100  $\mu\text{m}$ ). The overall (1.2–1100  $\mu\text{m}$ ) spectral energy distribution points to a Class III source, namely one without a substantial circumstellar disk but still possessing residual material at large separations. A modified blackbody fit finds a dust color temperature of only  $\approx 15$  K. Malinen et al. (2014) remark that the object is clearly extended at 160  $\mu\text{m}$  and overall conclude 2MASS J0435–14 is an embedded young object, consistent with the very bright absolute magnitudes derived from our parallax.

Allers & Liu (2013a) also noted that the spectrum of this M7 VL-G dwarf appears to be highly

reddened, with a rough estimate of  $A_V \sim 7.4$  based on its observed  $J - K$  color ( $1.93 \pm 0.04$  mag in 2MASS) compared other young objects of similar spectral type. Similarly, we also found that young late-M dwarfs in Taurus from Allers et al. (2009) are a reasonable match to the near-IR spectrum assuming a modest reddening ( $A_V \sim 4.5$ ). However, we note that the Cruz et al. (2003) optical spectrum shows a normal continuum shape, which is inconsistent with reddening as is the overall Class III SED. Instead, we suggest that the unusual near-IR spectrum and very red  $J - K$  color may be manifestations of very low surface gravity, more extreme than young field objects (Figure 28). Low surface gravity is also consistent with the very bright absolute magnitudes and its optical gravity classification of  $\delta$ , the only such object in our entire sample. Given the low effective temperature, relatively large bolometric luminosity ( $\approx 0.05 L_\odot$ , from scaling the Malinen et al. results to our parallax), and very low surface gravity, this object appears to be a very young ( $\lesssim 1$  Myr) brown dwarf with a residual circumstellar disk.

**SDSS J044337.60+000205.2 (M9 low- $g$ /L0 VL-G):** Cruz et al. (2007) identified this object as having low-gravity based on optical spectroscopy. It also shows strong signatures of low-gravity in its near-IR spectrum (Allers & Liu 2013a). Based on a radial velocity of  $17.1 \pm 2.0$  km s $^{-1}$  from Reiners & Basri (2009) and a SUPERBLINK proper motion of  $(+48, -122)$  mas yr $^{-1}$ , Schlieder et al. (2012) reported SDSS J0443+0002 as a likely member of the AB Dor moving group. Using the same RV but a proper motion of  $(+36 \pm 8, -98 \pm 8)$  mas yr $^{-1}$  from Faherty et al. (2009), Gagné et al. (2014b) instead concluded that SDSS J0443+0002 is a strong  $\beta$  Pic moving group candidate (99.8%) and predicted a statistical distance of  $25.7_{-2.4}^{+3.2}$  pc, with Gagné et al. (2015a) providing a mass estimate of  $20.6_{-3.8}^{+5.9} M_{\text{Jup}}$ . Our work now provides a parallax distance of  $21.1_{-0.5}^{+0.4}$  pc and a refined proper motion of  $(+53.6 \pm 1.3, -104.6 \pm 1.5)$  mas yr $^{-1}$ . With this new information we confirm SDSS J0443+0002 as a member of  $\beta$  Pic (99.8% probability from our kinematics-only BANYAN II analysis).

**2MASS J05012406–0010452 (L4 $\gamma$ /L3 VL-G):** Gagné et al. (2015a) identify this as a possible COL (49%) or CAR (17%) member, based on a parallactic distance of  $13.1 \pm 0.8$  pc from Faherty et al. (2012), with an associated mass estimate of  $10.2_{-1.0}^{+0.8} M_{\text{Jup}}$ . As discussed in Section 3.1 and shown in Figure 4, their parallax is the among the most discrepant of all the results with our CFHT measurements ( $20.7 \pm 0.6$  pc) and also disagrees with Zapatero Osorio et al. (2014). Our CFHT distance leads to brighter absolute magnitudes, and our kinematics-only BANYAN II analysis gives  $>99.9\%$  probability of young field membership. So our new parallax weakens the case for 2MASS J0501–0010 being a planetary-mass object.

We note that the membership lists of Columba and Carina differ substantially between BANYAN II and Torres et al. (2008), with the BANYAN II lists having larger  $UVWXYZ$  extents. Using our CFHT parallax and the BANYAN II membership lists, radial velocities of 19.2 and 18.4 km s $^{-1}$  would would place the object at minimum velocity distances of 8.5 and 8.2 km s $^{-1}$  from the Columba and Carina group cores, respectively, which is rather far given the dispersions of the known members. We conclude that 2MASS J0501–0010 is a young field object.

Cruz et al. (2007) originally identified this as a giant during a search for nearby ultracool

dwarfs, Shkolnik et al. (2009) found this object is actually a M7.0 dwarf and estimated a photometric distance of 60 pc assuming an age of 10 Myr based on its strong lithium absorption, low-gravity features in the optical, and possible H $\alpha$  accretion. The Allers & Liu (2013) near-IR classification of VL-G is in accord with this young age. Its 2MASS *JHK* colors are consistent with late-type dwarfs, rather than giants.

Our parallax measurement is very marginal ( $S/N = 2.8$ ) and places the object at  $\approx 300$  pc. Our result agrees with a similarly poor parallactic distance by Shkolnik et al. (2012) of  $526 \pm 277$  pc. Based on the evolutionary models of Chabrier et al. (2000), such a high luminosity implies that this is a very young ( $\sim 1$  Myr old) brown dwarf. Similarly, its *K*-band absolute magnitude of  $4.4 \pm 0.8$  mag is  $\approx 1.5$  mag brighter than the individual components of the very young ( $\sim 1$  Myr) M6.5 eclipsing binary 2MASS J05352184–0546085 in Orion (Stassun et al. 2006). A comparison of the near-IR spectrum of 2MASS J0557–1359 with the aforementioned 2MASS J0435–1414 shows the two have a comparable surface gravities, both more extreme than young field objects (Figure 28).

A parallax-free analysis by Gagné et al. (2014b) indicated that 2MASS J0557–1359 is a young field member (99.7%) with a statistical distance of  $45_{-8}^{+12}$  pc. Our parallactic distance of  $290_{-110}^{+80}$  pc suggests that 2MASS J0557–1359 is beyond the 200-pc spatial extent of the BANYAN II field model.

**2MASSI J0608528–275358 (M8.5 $\gamma$ /L0 VL-G):** Rice et al. (2010b) proposed this is a  $\beta$  Pic moving group member based on their radial velocity measurement ( $24.0 \pm 1.0$  km s $^{-1}$ ) and an ad hoc photometric distance of  $30 \pm 10$  pc. Based on a parallactic distance of  $31.3 \pm 3.5$  pc and proper motion of  $(+8.9 \pm 3.5, +10.7 \pm 3.5)$  mas yr $^{-1}$  from Faherty et al. (2012), Malo et al. (2013) determined 2MASS J0608–2753 as a *bona fide* member of BPMG. In the analysis of Gagné et al. (2014b), 2MASS J0608–2753 was excluded from the list of *bona fide* members based on their proper motion significance criterion ( $S/N > 5\sigma$ ). Gagné et al. (2014b) then indicated 2MASS J0608–2753 as a peripheral COL candidate, with 4% probability and 2% contamination, finding that BPMG membership is not viable in their model due to the RV measurement. Our new parallactic distance of  $40.0_{-2.2}^{+2.3}$  pc and proper motion of  $(+12.4 \pm 0.6, +7.3 \pm 0.8)$  mas yr $^{-1}$  strengthens the case for COL membership, with our kinematics-only BANYAN II analysis giving a 33% membership probability. The BANYAN II membership list for COL has a significantly larger *UVWXYZ* extent than that of Torres et al. (2008), but even the latter suggests COL is viable, with  $\tilde{\chi}_{UVW}^2=2.7$ ,  $\tilde{\chi}_{XYZ}^2=1.1$ , and a velocity distance of 3.2 km s $^{-1}$ . Thus Columba membership seems plausible but not definitive yet.

We note that the Mamajek & Bell (2014) group membership suggests that  $\beta$  Pic membership is still a marginal option, with  $\tilde{\chi}_{UVW}^2=3.2$ ,  $\tilde{\chi}_{XYZ}^2=1.2$ , and a velocity distance of 5.2 km s $^{-1}$ .

**2MASSI J0619526–290359 (M6 low-*g*/M5 low-*g*):** Cruz et al. (2007) identified this object as having low-gravity in the optical. Allers & Liu (2013a) classify 2MASS J0619–2903 as M5 and therefore outside the spectral type range of their gravity classification scheme. They deredden the spectrum ( $A_V = 6.5$ ) and note that it appears low in gravity (Figure 29), and that its mid-IR

photometry suggests a circumstellar disk. A parallax-free analysis by Gagné et al. (2014b) indicate this object is a modest probability COL member, with a 81% membership, 22% contamination, a statistical distance of  $55.8_{-6}^{+5.6}$  pc, and a mass of 15–23  $M_{\text{Jup}}$  based on an age of 20–40 Myr. We measure a parallactic distance of  $270_{-100}^{+270}$  pc making 2MASS J0619–2903 likely beyond the 200-pc extent of the BANYAN II field model. The very bright absolute magnitudes derived from our CFHT parallax support the notion that this is a very young low-mass star.

Comparing our new 2015 spectrum with the 2008 one from Allers & Liu (2013a) shows that the object appears to be spectrally variable (Figure 30). We classify the new spectrum as M6 VL-G, slightly later than the published M5 type. (The published classification did not include a gravity class, since the object was too early-type, but the first-epoch spectrum was visually identified as low gravity.) The individual H<sub>2</sub>O spectral indices suggest a slightly later type in the second-epoch spectrum (Table 4).

**2MASS J07140394+3702459 (M8/M7.5 INT-G):** Gagné et al. (2015a) classify this as M7.5 $\beta$  and assign this to ARG with 88.9% probability and 0.6% contamination rate, based on a parallax from Dittmann et al. (2014) and no radial velocity information. Gagné et al. (2015b) estimate a mass of  $20.6_{-1.7}^{+2.5}$   $M_{\text{Jup}}$  based on an age of 30–50 Myr. Using the published parallax and an RV from Deshpande et al. (2013), our kinematics-only BANYAN II analysis robustly places the object in the young field population (>99.9%). In *UVWXYZ*, this object barely overlaps the spatial positions of the most distant members of Argus ( $\tilde{\chi}_{XYZ}^2 = 4.8$ ) and is 120 pc from the group core. Also its *UVW* position is  $22.2 \pm 0.4$  km s<sup>-1</sup> from the mean group velocity, placing it far beyond the  $\approx 1$  km s<sup>-1</sup> dispersion of the known members ( $\tilde{\chi}_{UVW}^2 = 299$ ). Thus we categorize this as a young field object and hence expect a more uncertain (and likely higher) mass than originally reported.

**LP 423-31 (M7 low-g/M6 FLD-G):** This object is relatively bright for its spectral type, and on *YJHK* CMDs is a marginal case of a FLD-G interloper in the VL-G sequence. LP 423-31 is classified as FLD-G in the near-IR (Allers & Liu 2013a) but has signs of low gravity in its optical spectrum (Shkolnik et al. 2009). Our BANYAN II analysis gives >99.9% Y.FLD or 89% O.FLD membership depending on whether youthfulness is assumed or not, respectively.

**WISE J075430.95+790957.8 (—/T2p (red)):** Mace et al. (2013) discovered and classified this object as “extremely red,” noting that its extremely unusual near-IR spectrum made classification very difficult with available methods. We visually compared this object to spectral standards, finding a spectral type of T2 in the *J*-band and T1.5 in the *K*-band. The *H*-band spectrum, however, is very unusual, with the central continuum plateau resembling an L8–L9 spectrum but the surrounding water absorption bands being closer to T2. The spectral indices in Table 5 indicate a spectral type of  $T1.7 \pm 1.5$ , while WISE J0754+7909 is much redder than a typical T2. Thus, we assign a spectral type of T2p (red) to WISE J0754+7909, with the caveat that it warrants more detailed examination.

**2MASS J08354256–0819237 (L5/—):** This object is not in our CFHT sample, but it is in the sample of parallaxes that we plot for the field population (Sections 4.1 and 4.2). It has a parallax



from Andrei et al. (2011) and is one of the nearest objects of its spectral type ( $8.5_{-0.7}^{+0.9}$  pc). It is also one of the reddest with  $(J - K)_{\text{MKO}} = 1.97 \pm 0.03$  mag (and  $M(J) = 13.42 \pm 21$ ). Thus, in our  $YJHK$  CMDs it appears as a possible VL-G sequence interloper. To our knowledge, this object has no properties associated with low gravity or youth. Examination by us of its near-IR SpeX prism spectrum (Burgasser et al. 2010) suggests the object’s gravity is on the borderline between FLD-G and INT-G.

**LP 261-75B, a.k.a. 2MASSW J09510549+35580021 (L6/L6 FLD-G):** Bowler et al. (2013) classified the low resolution infrared spectrum of LP 261-75B as L4.5 FLD-G. Using the same spectrum, we determine a later spectral type of L6 in AL13 system, in agreement with its optical spectral type of L6 (Kirkpatrick et al. 2000). At low spectral resolution, the AL13 system can not classify the gravity of an L6 object, so we use visual comparison. Figure 26 compares the spectrum of LP 261-75B to VL-G, INT-G, and FLD-G L6 standards as well as the aforementioned 2MASS J0030–1450. Overall, the spectrum of LP 261-75B is very similar to that of 2MASS J0030–1450 but has deeper FeH and alkali features indicating likely higher gravity. The spectral features of LP 261-75B are better matched to the FLD-G template than the INT-G template, and thus we classify LP 261-75B as L6 FLD-G.

Based on a parallax-free analysis and no assumption of youth, Gagné et al. (2015a) indicated this as a possible ABDMG member, with 19% probability, 31% contamination, and a statistical distance of  $32.5_{-2.0}^{+1.6}$  pc. While our new parallactic distance for LP 261-75A ( $31.6_{-1.4}^{+1.2}$  pc) agrees well, our kinematics-only BANYAN II analysis reports >99.9% Y.FLD membership. The  $XYZ$  is broadly consistent with known AB Dor members ( $\tilde{\chi}_{XYZ}^2 = 1.9$ ), but the  $UVW$  is off by  $15.2 \pm 1.1$  km s<sup>-1</sup>, much larger than the group dispersion ( $\tilde{\chi}_{UVW}^2 = 64$ ). Thus we categorize this as a young field object.

**G 196-3B, a.k.a. 2MASS J10042066+5022596 (L3 $\beta$ /L3 VL-G):** As a well studied companion to a young M3 star that lacks a parallax measurement, the age of G 196-3B has been estimated to be anywhere from 20–300 Myr (Rebolo et al. 1998; Kirkpatrick et al. 2001; Shkolnik et al. 2009). Based on a parallax-free analysis, Gagné et al. (2014b) placed this either in ABDMG or CAR, depending on the adopted radial velocity. Considering our new parallax, the  $UVW$  agrees much better with CAR than ABDMG, but the reverse is true for  $XYZ$ . Our kinematics-only BANYAN II analysis favors young field, which we adopt as the outcome.

**2MASS J10220489+0200477 (M9 $\beta$ /M9 FLD-G):** Based on a low S/N parallax of  $38 \pm 16$  pc from Faherty et al. (2012) and a radial velocity of  $-7.9 \pm 4.8$  km s<sup>-1</sup> derived from the literature, Gagné et al. (2015a) indicated this is a peripheral ABDMG candidate, with a 3% probability and 6% contamination. Using our new parallactic distance of  $28.9_{-1.8}^{+1.6}$  pc and a radial velocity of  $-8.4 \pm 5.0$  km s<sup>-1</sup> from West et al. (2008), our kinematics-only BANYAN II analysis reports >99.9% Y.FLD membership assuming youthfulness or >99.9% O.FLD membership without this assumption.

**SDSS J102552.43+321234.0 (—/L7 FLD-G):** Upon its discovery, Chiu et al. (2006) reported

that SDSS J1025+3212 has an unusual L7.5 spectrum, with scattered spectral indices indicating a spectral type of L4.5–T2 and hints of variability based on two epochs of spectra. Kirkpatrick et al. (2008) listed SDSS J1025+3212 as a potential young object on the basis of weak K I and H<sub>2</sub>O features. AL13 determined a spectral type of L7 for this object, but could not reliably determine its gravity, as the AL13 system only provides gravity classification for low-resolution spectra with spectral types earlier than L6. Recently, two bona-fide young L7 objects have been discovered, PSO J318.5–22 (L7 VL-G; Liu et al. 2013b) and WISE J0047+6803 (L7 INT-G; Gizis et al. 2015), which allows for a visual assessment of the gravity of SDSS J1025+3212 (Figure 31). We do not find evidence of low gravity, as the FeH absorption bands, alkali lines, and *H*-band continuum shape are all consistent with FLD-G. The *H*-cont index from AL13 also yields a score of “0”, which corresponds to FLD-G. We assign a spectral type of L7 FLD-G.

Based on a parallax-free analysis and adopting the Kirkpatrick et al. (2008) interpretation of the near-IR spectrum as being low gravity, Gagné et al. (2014b) assign young field membership (>99.9%) with a statistical distance of  $19.7_{-2.4}^{+2.8}$  pc. Using our FLD-G gravity classification and CFHT parallax ( $26.8_{-0.8}^{+0.9}$  pc), a kinematics-only BANYAN II analysis finds a probability of 99.8% of belonging to the old field population. (If youth is assumed based on the optical spectrum, then the result is >99.9% membership for young field.) Its *UVW* position is far from any known young group. We also note that our parallax gives absolute magnitudes for SDSS J1025+3212 (e.g.,  $M_J = 14.75 \pm 0.09$  mag) that are more consistent with field objects of the same spectral type ( $M_J = 14.7$  mag; Dupuy & Liu 2012) than with the low-gravity L7 dwarfs PSO J318.5–22 ( $M_J = 15.42 \pm 0.09$  mag) and WISE J0047+6803 ( $M_J = 15.07 \pm 0.08$  mag) Thus, this appears to be an old field object.

**2MASSW J1139511–315921, a.k.a. TWA 26 (M9 low-*g*/M9 VL-G):** Gizis (2002) identified this young brown dwarf as a candidate TWA member based on its proximity to previously known members and its low-gravity optical spectral features. Mohanty et al. (2003) found a radial velocity consistent with the other TWA members, while Reid (2003) suggested that this object is not a TWA member based on the (low-quality) proper motion available at the time. As discussed in Section 3, our parallactic distance of  $42.2_{-3.0}^{+2.6}$  pc agrees well with parallaxes from Weinberger et al. (2013) and Ducourant et al. (2014) as well as the Mamajek (2005) kinematic distance. (All of these disagree with the Faherty et al. 2012 parallax.) Thus, our membership analysis is also in accord with this previous work, showing unambiguous TWA membership. It is clearly overluminous in *JHK* relative to field objects, consistent with its young age.

**2MASS J13153094–2649513AB (L5.5/L6 FLD-G):** 2MASS J1315–2649 was first identified as a mid-L dwarf with strong, variable H $\alpha$  emission by Hall (2002b). Based on a high-quality composite optical spectrum, Kirkpatrick et al. (2008) assigned a spectral type of L5.5. Burgasser et al. (2011) resolved 2MASS J1315–2649 into binary and determined component spectral types of  $L3.5 \pm 2.5$  and  $T7 \pm 0.6$  from *H*-band spectra. Using the composite near-IR spectrum of Burgasser et al. (2011), we classify 2MASS J1315–2649AB as L6 FLD-G on the Allers & Liu (2013a) system. The composite near-IR spectrum shows subtle peculiarities, but these do not appear low-gravity in nature, and

the  $H$ -cont index is consistent with field gravity. As discussed by Burgasser et al., the peculiar spectrum is well-explained by unresolved L+T binarity.

**2MASS J13313310+3407583 (L0/L0<sub>FLD-G</sub>):** Based on comparison to field dwarf standards, Kirkpatrick et al. (2010) classify 2MASS J1331+3407 as L0 from its optical spectrum and an “L1 pec (red)” based on its near-IR spectrum. Using the near-IR spectrum of Kirkpatrick et al. (2010), we classify 2MASS J1331+3407 as L0<sub>FLD-G</sub>. The  $(J-K_S)_{2MASS}$  color of 2MASS J1331+3407 ( $1.448 \pm 0.035$  mag) is slightly redder than the  $J-K_S$  color of L0 field dwarfs (median color = 1.24 mag, RMS = 0.18 mag; Schmidt et al. 2010). Likewise, the near-IR spectrum of 2MASS J1331+3407 is slightly redder than a field L0 standard (e.g., Figure 10 of Allers & Liu), but otherwise shows no spectral peculiarities.

**2MASS J14112131–2119503 (M9/M8<sub>INT-G</sub>):** A kinematics-only BANYAN analysis using our new CFHT parallax favors the young field population, as does the full BANYAN II analysis by Gagné et al. (2014b) done with a radial velocity from Reiners & Basri (2009) but without a parallax. We note that the  $UVWXYZ$  position of this object is close to TWA, with  $\tilde{\chi}_{UVW}^2 = 2.0$  and  $\tilde{\chi}_{XYZ}^2 = 2.0$ . However, the known members of TWA have a filamentary  $XYZ$  distribution (e.g. Weinberger et al. 2013), and 2MASS J1411–2119 is not well aligned with this. Thus we favor assignment to the young field population.

**2MASSI J1615425+495321 (L4 $\gamma$ /L3<sub>VL-G</sub>):** Cruz et al. (2007) first noted low gravity features in the optical spectrum of 2MASS J1615+4953. Kirkpatrick et al. (2008) tentatively concluded this object is low gravity, but caution that the modest S/N of their optical spectra cannot discount the possibility that the object is a very dusty, old field L dwarf. Faherty et al. (2013) assigned an optical gravity classification of  $\gamma$  to this L4 dwarf. Allers & Liu (2013a) determined that the near-IR spectrum of this source is indicative of a very low surface gravity (VL-G classification), not merely being dusty. Its  $J$ -band absolute magnitude is notably fainter than field objects, supporting its low-gravity classification.

**DENIS J170548.3–051645 (L0.5/L1<sub>FLD-G</sub>):** This was identified as a candidate member of the Ursa Major moving group by Seifahrt et al. (2010), which agrees with our kinematic determination. This object is far removed on the sky from the core Ursa Major members, being one of many group candidates from Montes et al. (2001) that are widely distributed. Allers & Liu (2013a) find this object’s near-IR spectrum is consistent in gravity with field objects. King et al. (2003) and Jones et al. (2015) estimate ages for the Ursa Major core members of  $500 \pm 100$  Myr and  $414 \pm 23$  Myr, respectively, consistent with the spectroscopic gravity. The absolute magnitudes of DENIS J1705–0516 are also consistent with field objects, so its spectrophotometry and kinematics are in accord.

Reid et al. (2006) identified a possible companion to this object in *HST*/NICMOS imaging from 2005 June 24 UT at a separation of  $1''.36$ , PA of  $355^\circ$ , and  $\Delta J \approx 4.1$  mag. At a recent CFHT epoch with good seeing (JD 2455988.17) we measured a source with  $\Delta J = 3.82 \pm 0.06$  mag at separation of  $2''.445 \pm 0''.007$  and PA of  $332^\circ.71 \pm 0^\circ.15$ . Accounting for the proper motion of DENIS J1705–0516,

this source would have been at a separation of  $1''.413 \pm 0''.011$  and PA of  $346^\circ.1 \pm 0^\circ.4$  at the NICMOS epoch. (Note that our quoted errors do not account for the uncertainty in the proper motion of the faint source.) We therefore conclude that this possible companion is a background object, which is seemingly at odds with a recent note by Dieterich et al. (2014) that they observe orbital motion in their astrometry of DENIS J1705–0516.

**2MASS J18212815+1414010 (L4.5/L5p<sub>FLD-G</sub>):** Looper et al. (2008b) flag this as a potential young object, based on its slightly red color (2MASS  $J - K_S = 1.78 \pm 0.05$  mag), peculiar near-IR spectrum (including somewhat triangular  $H$ -band peak and strong CO), and low tangential velocity of  $10 \text{ km s}^{-1}$  (based on a photometric distance of  $9.8 \pm 1.3$  pc). Using the low resolution near-IR spectrum of Looper et al. (2008b), we determine a near-IR spectral type of L5 FLD-G and similarly assign a peculiar designation to denote its red color and triangular  $H$ -band continuum shape.

Our astrometry gives a tangential velocity of  $15.20 \pm 0.17 \text{ km s}^{-1}$  and a parallactic distance of  $9.56 \pm 0.09$  pc. The photometric and parallactic distances agree well because 2MASS J1821+1414 has normal absolute magnitudes compared to the field sequence. Also its position in the near-IR CMDs resides among the field L dwarfs. Similar to 2MASS J0314+1603 and DENIS J1705–0516, this object has kinematics consistent with the Ursa Major moving group but resides far from the core members on the sky. The  $\approx 400$ – $500$  Myr age of the group would be consistent with the near-IR gravity classification. Thus, we conclude that 2MASS J1821+1414 is likely to be an older dusty object, as opposed to a young one as suggested by Looper et al. (2008b). This is consistent with the notion that objects with triangular  $H$ -band spectra are not necessarily young, as found by Allers & Liu (2013a).

Based on a parallax-free analysis using an radial velocity of  $9.8 \pm 0.8 \text{ km s}^{-1}$  (Blake et al. 2010; Kirkpatrick et al. 2010) and an assumption of low gravity, Gagné et al. (2014b) assign this young field membership ( $>99.9\%$ ) with a statistical distance of  $13.3 \pm 2.8$  pc. With our new CFHT parallax and no assumption of youth, a kinematics-only BANYAN II analysis reports 82% old field population and 18% young field population. Its  $UVW$  places it far from any known young group. Altogether we assign it to the old field population.

**2MASS J19355595–2846343 (M9 low- $g$ /M9<sub>VL-G</sub>):** A parallax-free BANYAN II analysis of 2MASS J1935–2846 by Gagné et al. (2014b) found a slim possibility for BPMG membership (9%), with a statistical distance of  $57 \pm 5$  pc and favoring the hypothesis that the system is a binary. (Keck laser guide star adaptive optics imaging by us finds the source to be single at  $0.07''$  resolution at  $K$  band.) For young field membership, they derive a statistical distance of  $62^{+12}_{-10}$  pc. Our new CFHT parallax ( $70.4^{+6.5}_{-5.5}$  pc) yields a smaller BPMG possibility (1.1%) from the kinematics-only BANYAN II analysis, but shows that the  $XYZ$  position of this object is quite compatible with known BPMG members ( $\tilde{\chi}^2_{XYZ} = 2.0$ ). This BPMG probability increases modestly if the radial velocity for the system (E. Shkolnik 2015, priv. comm.) is included in the analysis but is still small. We note that this object lies beyond the  $\approx 50$ -pc limiting distance of the original Zuckerman et al. (2001) search that identified the  $\beta$  Pic moving group, and it is also farther than 42 out of the 48 members identified by Torres et al. (2008). Thus the relatively low BPMG probability assigned

by the BANYAN II model may simply reflect the incomplete membership census for more distant stars. A radial velocity of  $-9.3 \text{ km s}^{-1}$  would bring the object to  $3.2 \text{ km s}^{-1}$  from the group core. Altogether, we consider BPMG membership to be unlikely but still viable — further investigation is warranted. More precise *UVWXYZ* data for this object as well as a more expansive census of the  $\beta$  Pic stellar members would help refine the membership.

Martín et al. (2010) noted that 2MASS J1935–2846 is near the R CrA star forming region on the sky, but our proper motion of  $(+27.3 \pm 0.9, -61.6 \pm 1.1) \text{ mas yr}^{-1}$  is inconsistent with the mean of known members,  $(+5.5, -27.0) \text{ mas yr}^{-1}$  (Neuhäuser et al. 2000), and our parallax distance of  $70.4_{-5.5}^{+6.5} \text{ pc}$  is much closer than the region’s best distance estimate of 130 pc (Neuhäuser & Forbrich 2008).

2MASS J1935–2846 also possesses a mid-IR excess, standing out in Figure 13 as being both bright in *W2* and red in *W1 – W2*. Only two other objects are redder at this absolute magnitude: 2MASS J1207–3932 (TWA 27) and SSSPM J1102–3431 (TWA 28). Both of these are noted by Riaz & Gizis (2008) to have excess thermal emission as short as  $5 \mu\text{m}$  due to circumstellar disks that likely explains their red colors on this plot. The similar mid-infrared photometry of 2MASS J1935–2846 suggests that it too possesses circumstellar material. We note that the mid-IR excess of 2MASS J1935–2846 lends circumstantial support to the possibility of  $\beta$  Pic membership, since an older age would make a circumstellar disk more implausible. If confirmed, this would join the  $\beta$  Pic member 2MASS J0335+2342 as the oldest disks found to date around brown dwarfs.

**2MASS J20135152–2806020 (M9 low-*g*/L0 VL-G):** Reid et al. (2008) classify this object as a low-gravity M9 dwarf, while Kirkpatrick et al. (2008) indicate an optical spectral type of M8–M9 III. Our parallax detection and the resulting absolute magnitudes show that it is a dwarf. Near-IR spectra of the object from Allers & Liu (2013a) also show that it is a low-gravity dwarf and not a giant.

A parallax-free BANYAN II analysis by Gagné et al. (2014b) identified this as a low probability BPMG member, with a 43% probability, a 71% contamination rate, and a statistical distance of  $44_{-4}^{+5} \text{ pc}$ , as well as an estimated mass of  $15.7_{-0.6}^{+1.5} M_{\text{Jup}}$  from Gagné et al. (2015a). Our new CFHT parallax ( $48 \pm 3 \text{ pc}$ ) also suggests BPMG membership (70% probability) and places the object comfortably among the known members ( $\tilde{\chi}_{XYZ}^2 = 1.0$ ). The velocity offset between 2MASS J2013–2806 and the group would be only  $2.2 \text{ km s}^{-1}$  for a radial velocity of  $-8.1 \text{ km s}^{-1}$ . Like 2MASS J1935–2806, we thus consider this a promising  $\beta$  Pic member, with radial velocity followup and a more complete group census needed.

**2MASS J21403907+3655563 (—/M8p FLD-G):** Kirkpatrick et al. (2010) originally typed the near-IR spectrum of 2MASS J2140+3655 as “M8 pec” and noted that it appears to be redder than vB 10, the dwarf field M8 standard. We obtained a higher S/N spectrum of 2MASS J2140+3655 suitable for gravity classification on 2015 July 23 UT (Figure 32). The *H*-cont index of Allers & Liu (2013) indicates intermediate gravity, but the FeH<sub>z</sub> and K I indices are consistent with FLD-G. We type 2MASS J2140+3655 as M8 FLD-G but also assign a “p” designation to its spectral classification, to denote the peculiarity of having a triangular *H*-band continuum shape while lacking any other

low-gravity indications. Its IR absolute magnitudes are consistent with field objects.

In contrast to Kirkpatrick et al., our new spectrum does not appear redder than vB 10 but instead is slightly bluer. To check for possible spectral variability, we obtained an additional spectrum of 2MASS J2140+3655 on 2015 September 25 UT (Figure 33). Our two spectra from 2015 are consistent with each other, making the Kirkpatrick et al. (2010) spectrum the discrepant one. In addition, the 2MASS  $J - K_S$  color of this object ( $0.94 \pm 0.13$  mag) agrees with the synthetic 2MASS  $J - K_S$  colors from our spectra (1.01 mag and 0.93 mag for our July and September spectra, respectively) and is bluer than vB 10 ( $1.14 \pm 0.03$  mag). Thus, 2MASS J2140+3655 does not appear to be systematically red for its spectral type. Assessing its potential variability would benefit from more observations.

**2MASS J21481633+4003594 (L6/L6 FLD-G):** Looper et al. (2008b) discovered this object, noting that its red color, peculiar near-IR spectrum, and field-gravity optical spectrum indicate an unusually dusty photosphere. From their measured proper motion ( $1''.33 \pm 0''.24$ ,  $75^\circ 6' \pm 0^\circ 3'$ ), and estimated distance of  $9.9 \pm 1.3$  pc, they estimated  $V_{\text{tan}} = 62 \text{ km s}^{-1}$  and suggested that such a value implied this object is not young but rather possibly high metallicity. Our proper motion of ( $0''.9041 \pm 0''.0018$ ,  $59^\circ 63' \pm 0^\circ 13'$ ) is 50% ( $1.8\sigma$ ) smaller than theirs, and our parallax distance of  $8.03^{+0.11}_{-0.12}$  pc is 10% ( $0.6\sigma$ ) smaller. (The Looper et al. 2008b photometric distance turns out to be an overestimate, because this object is faint at  $J$  band compared to field objects.) Thus, we find a significantly smaller  $V_{\text{tan}} = 34.4 \pm 0.5 \text{ km s}^{-1}$ , which is in fact consistent with the high end of tangential velocities for our low-gravity sample (Section 4.3).

A parallax-free BANYAN II analysis by Gagné et al. (2014b) identified this as a modest ARG candidate, with a probability of 48%, a contamination rate of 37%, a statistical distance of  $4.9^{+0.4}_{-0.4}$  pc, and an estimated mass of 6–7  $M_{\text{Jup}}$  based on an age of 30–50 Myr. They also derived a statistical distance of  $8.1^{+0.8}_{-1.2}$  pc, under the assumption that the object is young. However, Allers & Liu (2013a) classify the gravity as FLD-G. Our new CFHT parallactic distance ( $8.03^{+0.11}_{-0.08}$  pc) greatly favors field membership, 67% young field and 33% old field based on no prior assumption about the object’s youth. The  $UVW$  are incompatible with any known young group. Thus, 2MASS J2148+4003 might have an intermediate age, old enough that spectroscopic signatures of gravity have receded but whose kinematics are still indicative of youth. Its mass is more uncertain and likely higher than estimated by Gagné et al.

**SIMP J215434.5–105530.8 (—/L4 INT-G):** Based on a parallax-free analysis, Gagné et al. (2014a) identify this as a ARG candidate, with Gagné et al. (2015b) reporting a revised 59% membership probability, 34% contamination rate, a statistical distance of  $22.5 \pm 2.4$  pc, and an estimated mass of  $10.3^{+0.7}_{-0.3}$   $M_{\text{Jup}}$  based on an age of 30–50 Myr. We had independently identified this object as a low-gravity L dwarf during a search for nearby ultracool dwarfs using Pan-STARRS1 (e.g. Liu et al. 2013b) and had begun parallax observations prior to its published discovery. Using our resulting CFHT parallax ( $30.7^{+1.0}_{-0.9}$  pc), a kinematics-only BANYAN II analysis leads to ARG membership probability of 23% and a spatial position that is just beyond the known members ( $\tilde{\chi}^2_{XYZ} = 4.6$ ). Its smallest velocity offset from ARG would be  $6.0 \text{ km s}^{-1}$  for a radial velocity of

$-14.5 \text{ km s}^{-1}$ , using the Torres et al. (2008) group properties. Radial velocity is needed for better assessment, but given the available data we favor young field membership and thus likely a higher mass than originally estimated.

**DENIS J220002.0–303832AB (M9/M9 FLD-G and L0/L0 FLD-G):** Resolved photometry and spectra are available for both components from Burgasser & McElwain (2006). Allers & Liu (2013a) analyzed only the A component, assigning M9 FLD-G. We find the B component is L0 FLD-G. Reid et al. (2008) report component optical spectral types of M9 and L0, respectively.

In our CFHT images we typically cleanly resolve this  $1''.09$  binary. Any images in which two sources were not detected by SExtractor were not used in our astrometric analysis. We report the individual solutions in Table 2. The individual parallaxes are  $41 \pm 4 \text{ mas}$  and  $35 \pm 4 \text{ mas}$ , among the worst precision of our sample due to the difficulty in obtaining centroids for such a close pair. We adopt a common parallax of  $38 \pm 4 \text{ mas}$  for the system.

**2MASSW J2208136+292121 (L3 $\gamma$ /L3 VL-G):** Kirkpatrick et al. (2008) estimated an age of  $\sim 100 \text{ Myr}$  for this object, based on the similarity of its optical spectrum to the young L-type companion G 196-3B, whose primary star has an estimated age of 20–300 Myr.

This object is the only case where something classified as VL-G lies closer to the field CMD sequence than the VL-G CMD sequence, although given the photometric and parallax uncertainties this is only a marginally significant discrepancy ( $\approx 2\sigma$ ). Given a sample of 28 VL-G objects on our CMD plots, such a  $\approx 2\sigma$  outlier is not unexpected. In fact, if we use the spectrum of this object to synthesize its  $(J - K_S)_{2\text{MASS}}$  color, we get a value 0.12 mag redder than the catalog value of  $1.65 \pm 0.11 \text{ mag}$ , which would reduce the discrepancy to an  $\approx 1\sigma$ . Therefore, we determine that this object is not unusual for its gravity classification.

Based on a parallax-free analysis, Gagné et al. (2014a) identify this as a modest BPMG candidate, with 10% membership probability,<sup>17</sup> a 54% contamination rate, and a statistical distance of  $35.4_{-3.2}^{+3.6} \text{ pc}$ , along with an estimated mass of  $12.9_{-0.1}^{+0.3} M_{\text{Jup}}$  from Gagné et al. (2015a) based on an age of 20–26 Myr. The young field hypothesis gives a statistical distance of  $55_{-10}^{+9} \text{ pc}$ . Using our new CFHT parallax ( $39.8_{-2.7}^{+2.4} \text{ pc}$ ), a kinematics-only BANYAN II analysis leads to a BPMG membership probability of 18% and a spatial position that is at the outskirts of the known members ( $\tilde{\chi}_{XYZ}^2 = 2.4$ ). A radial velocity of  $-12.4 \text{ km s}^{-1}$  would give this object an offset of only  $0.7 \text{ km s}^{-1}$  from the group core. We consider this a promising  $\beta$  Pic member but not definitive. Similar to 2MASS J1935–2846 and 2MASS J2013–2806, a radial velocity measurement and a more complete group census are needed.

**2MASS J22134491–2136079 (L0 $\gamma$ /L0 VL-G):** Kirkpatrick et al. (2008) estimate an age significantly younger than the Pleiades ( $\approx 125 \text{ Myr}$ ), based on this object’s spectral similarity to the very young field L dwarf 2MASS J01415823–4633574, for which they estimate an age of 1–50 Myr. They also noted the proximity of this object on the sky to members of the  $\beta$  Pic moving group. Based

---

<sup>17</sup>Their text and tables report both a 7% and 10% probability. We take the larger value as it is the one reported alongside the contamination rate.

on a parallax-free analysis, Gagné et al. (2014b) identify this as a marginal BPMG candidate, with 3% membership probability, a 80% contamination rate, and a statistical distance of  $45 \pm 3.6$  pc, along with an estimated mass of  $13.5 \pm 0.3 M_{\text{Jup}}$  from Gagné et al. (2015a) based on an age of 20–26 Myr. Their young field hypothesis gives a statistical distance of  $63_{-8}^{+7}$  pc.

Using our new CFHT parallax ( $47.8_{-4.0}^{+4.8}$  pc), its spatial position is at the outskirts of the known  $\beta$  Pic members ( $\tilde{\chi}_{XYZ}^2 = 3.1$ ), and a kinematics-only BANYAN II analysis gives 88% probability of young field. Its smallest possible velocity offset from BPMG would be a relatively large value of  $6.0 \text{ km s}^{-1}$ , for a radial velocity of  $-3.1 \text{ km s}^{-1}$ . Altogether, we favor young field membership and thus the mass is more uncertain and likely to be higher than reported by Gagné et al.

**2MASSW J2224438–015852 (L4.5/L3p<sub>FLD-G</sub>):** Using the low resolution near-IR spectrum of (Burgasser et al. 2010), we classify 2MASS J2224–0158 as L3 FLD-G. Cushing et al. (2005) first noted that 2MASS J2224–0158 has abnormally red colors for its spectral type ( $(J - K_S)_{2\text{MASS}} = 2.03 \pm 0.04 \text{ mag}$ ), thus we assign a “p” designation to denote this spectral peculiarity.

**2MASSW J2244316+204343 (L6.5/L6<sub>VL-G</sub>):** This object serves as the archetype for extremely red L dwarfs, with an ordinary optical spectrum but a very peculiar near-IR one (Kirkpatrick et al. 2000; McLean et al. 2003). The very red near-IR colors, weak FeH and alkali features in the  $J$ -band, and triangular  $H$ -band spectra indicate this a low-gravity object (Allers & Liu 2013a) as opposed to an ordinary (high-gravity) object with extreme cloud properties. Kirkpatrick et al. (2008) suggest that the bland optical spectrum arises from a fortuitous degeneracy of photospheric chemistry, whereby the weakened alkali lines and stronger oxides due to reduced surface gravity act to mimic an earlier type L dwarf of higher gravity. As noted in Section 4.2, its near-IR absolute magnitudes are among the faintest in our sample (exceeded only by SDSS J2249+0044B), and on the CMD it appears to be an extension of the L dwarf sequence towards the very red planetary-mass objects 2MASS J1207–3932b and HR 8799b.

**SDSS J224953.46+004404.6AB (—/L3<sub>INT-G</sub> and —/L5<sub>INT-G</sub>):** Allers et al. (2010) identified this as possible young object by examining the near-IR spectrum from Nakajima et al. (2004) as well as their own low-resolution spectrum. They then resolved this object into a  $0.32''$  binary with component spectral types of L3 and L5. This agrees with the integrated-light optical spectrum typed as L3 by Hawley et al. (2002).

The secondary component of the binary has the faintest near-IR absolute magnitudes of our entire sample. Allers et al. estimated a photometric distance of  $54 \pm 16$  pc by comparing to other young objects with distances, which was also consistent with the photometric distance to a wide-separation early-M dwarf comoving with the binary. We find that the object is closer, with a parallactic distance of  $39.2_{-2.1}^{+2.3}$  pc.

The closer parallax distance also means that SDSS J2249+0044A and B are less luminous than assumed by Allers et al. (2010). As a result, the estimated masses of the components are also smaller. For possible ages of 20–300 Myr, we estimate masses of  $0.007\text{--}0.027 M_{\odot}$  and  $0.005\text{--}0.019 M_{\odot}$  for the A and B components, respectively, based on the Saumon & Marley (2008)  $f_{\text{sed}} = 2$  models.



**WISE J233527.07+451140.9 (—/L7p<sub>FLD-G</sub>):** WISE J2335+4511 was discovered and classified as “L9 pec (v.red)” by Thompson et al. (2013), based on a fairly low S/N spectrum. Using our higher S/N spectrum (Figure 31), we determine a spectral type of L7 for WISE J2335+4511, based on visual classification (L9±2 in the *J*-band and L7±1 in the *K*-band) and the H<sub>2</sub>OD index (L6.9±0.9). The only index in the Allers & Liu (2013) system applicable to low-resolution L7 spectra is the *H*-cont index. The *H*-cont index value for WISE J2335+4511 yields a gravity score of “0”, indicating FLD-G. The gravity of this object can be assessed by visual comparison to L7 VL-G and INT-G spectra (Figure 31). Overall, the spectrum of WISE J2335+4511 appears intermediate between that of WISE J0047+6803 (L7 INT-G) and the L7 field standard, showing subtle hints of low gravity in its FeH and alkali features but not distinct enough from the field standard to warrant an INT-G classification. Thus, we assign a final spectral type of L7p<sub>FLD-G</sub> to WISE J2335+4511, where the “p” derives from its red color and subtle spectral peculiarities.

As discussed in Section 4.2, WISE J2335+4511 also displays the unusual behavior of appearing with the VL-G sequence on CMDs where the color involves *K*-band but appearing with the field sequence on *Y – J* and *Y – H* CMDs. Thus, this object (along with the aforementioned 2MASS J2148+4003) demonstrates that *high gravity L dwarfs can reside in the extremely red, faint portion of the CMD previously ascribed solely to low-gravity objects.*

Based on a parallax-free analysis and no assumption of youth, Gagné et al. (2014b) identify this as an old field candidate (97% probability) with statistical distance of  $23.3_{-7.6}^{+9.6}$  pc, with a slim probability (3%) of being young field with a statistical distance of  $14.9_{-4.4}^{+4.8}$  pc. Our new CFHT parallax ( $22.7_{-0.7}^{+0.7}$  pc) yields old field membership at 73% with a kinematics-only BANYAN II analysis, and young field at 27%. Thus we assign this to the general field population.

**2MASS J23512200+3010540 (L5.5/L5<sub>FLD-G</sub>):** Kirkpatrick et al. (2010) assign a near-IR type of L5 pec (red), while we assign a type of L5<sub>FLD-G</sub> to their spectrum without a peculiar flag. Using a parallax-free analysis and no assumption of youth, Gagné et al. (2014b) identify this as a modest ARG candidate, with 47% membership probability, a 63% contamination rate, a statistical distance of  $20.9_{-2.4}^{+2.0}$  pc, and a mass of 9–11  $M_{\text{Jup}}$  based on an age of 30–50 Myr. The corresponding statistical distances for young and old field are  $32.5 \pm 6$  pc and  $47.8_{-9.2}^{+8.8}$  pc, respectively. Based on its near-IR spectrum having only weak evidence for low gravity (consistent with our classification as FLD-G), Gagné et al. (2015a) place this in the field population, with 93% probability and a 6% contamination rate. Using our new CFHT parallax ( $24.3_{-0.9}^{+0.8}$  pc), its spatial position is at the outskirts of the known members ( $\tilde{\chi}_{XYZ}^2 = 5.0$ ), and a kinematics-only BANYAN II analysis gives 89% probability for ARG membership. Its smallest velocity offset from the group would be  $3.2 \text{ km s}^{-1}$  for a radial velocity of  $-3.4 \text{ km s}^{-1}$ . Given the uncertain state of this group’s membership and thus its age (Bell et al. 2015), the presence of low-gravity spectral features seems to be an inappropriate selection criterion at this point. Thus we consider Argus membership to be viable despite the absence of low-gravity spectra, with more data needed both for this object and the group as whole.

## REFERENCES

- Ackerman, A. S., & Marley, M. S. 2001, *ApJ*, 556, 872
- Allard, F., Homeier, D., & Freytag, B. 2012, *Philosophical Transactions of the Royal Society of London Series A*, 370, 2765
- Aller, K. M., et al. 2016, *ApJ*, 821, 120
- Allers, K. N., et al. 2007, *ApJ*, 657, 511
- Allers, K. N., & Liu, M. C. 2013a, *ApJ*, 772, 79
- . 2013b, *Mem. Soc. Astron. Italiana*, 84, 1089
- Allers, K. N., Liu, M. C., Dupuy, T. J., & Cushing, M. C. 2010, *ApJ*, 715, 561
- Allers, K. N., et al. 2009, *ApJ*, 697, 824
- Andrei, A. H., et al. 2011, *AJ*, 141, 54
- Bailey, V., et al. 2014, *ApJ*, 780, L4
- Baraffe, I., Homeier, D., Allard, F., & Chabrier, G. 2015, *A&A*, 577, A42
- Barenfeld, S. A., Bubar, E. J., Mamajek, E. E., & Young, P. A. 2013, *ApJ*, 766, 6
- Barman, T. S., Macintosh, B., Konopacky, Q. M., & Marois, C. 2011a, *ApJ*, 733, 65
- . 2011b, *ApJ*, 735, L39
- Barrado y Navascués, D., Stauffer, J. R., & Jayawardhana, R. 2004, *ApJ*, 614, 386
- Basri, G., Mohanty, S., Allard, F., Hauschildt, P. H., Delfosse, X., Martín, E. L., Forveille, T., & Goldman, B. 2000, *ApJ*, 538, 363
- Bell, C. P. M., Mamajek, E. E., & Naylor, T. 2015, *MNRAS*, 454, 593
- . 2016, 314, 41
- Best, W. M. J., et al. 2015, *ApJ*, 814, 118
- Biazzo, K., D’Orazi, V., Desidera, S., Covino, E., Alcalá, J. M., & Zusi, M. 2012, *MNRAS*, 427, 2905
- Biller, B. A., et al. 2010, *ApJ*, 720, L82
- . 2013, *ApJ*, 777, 160
- Blake, C. H., Charbonneau, D., & White, R. J. 2010, *ApJ*, 723, 684

- Bonnefoy, M., Chauvin, G., Rojo, P., Allard, F., Lagrange, A.-M., Homeier, D., Dumas, C., & Beuzit, J.-L. 2010, *A&A*, 512, A52
- Bonnefoy, M., et al. 2014a, *A&A*, 562, A111
- . 2011, *A&A*, 528, L15
- . 2014b, *A&A*, 567, L9
- Bouchez, A. H., et al. 2004, in *Advancements in Adaptive Optics*. Edited by Domenico B. Calia, Brent L. Ellerbroek, and Roberto Ragazzoni. *Proc. of the SPIE.*, Vol. 5490, 321–330
- Bouvier, J., et al. 2008, *A&A*, 481, 661
- Bouy, H., Brandner, W., Martín, E. L., Delfosse, X., Allard, F., & Basri, G. 2003, *AJ*, 126, 1526
- Bovy, J., & Hogg, D. W. 2010, *ApJ*, 717, 617
- Bowler, B. P., Liu, M. C., & Cushing, M. C. 2009, *ApJ*, 706, 1114
- Bowler, B. P., Liu, M. C., Dupuy, T. J., & Cushing, M. C. 2010, *ApJ*, 723, 850
- Bowler, B. P., Liu, M. C., Shkolnik, E. L., & Dupuy, T. J. 2013, *ApJ*, 774, 55
- Bowler, B. P., Liu, M. C., Shkolnik, E. L., Dupuy, T. J., Cieza, L. A., Kraus, A. L., & Tamura, M. 2012, *ApJ*, 753, 142
- Brandt, T. D., & Huang, C. X. 2015, *ApJ*, 807, 58
- Burgasser, A. J. 2007, *ApJ*, 659, 655
- Burgasser, A. J., Cruz, K. L., Cushing, M., Gelino, C. R.,Looper, D. L., Faherty, J. K., Kirkpatrick, J. D., & Reid, I. N. 2010, *ApJ*, 710, 1142
- Burgasser, A. J., Geballe, T. R., Leggett, S. K., Kirkpatrick, J. D., & Golimowski, D. A. 2006, *ApJ*, 637, 1067
- Burgasser, A. J., Liu, M. C., Ireland, M. J., Cruz, K. L., & Dupuy, T. J. 2008, *ApJ*, 681, 579
- Burgasser, A. J., & McElwain, M. W. 2006, *AJ*, 131, 1007
- Burgasser, A. J., McElwain, M. W., Kirkpatrick, J. D., Cruz, K. L., Tinney, C. G., & Reid, I. N. 2004, *AJ*, 127, 2856
- Burgasser, A. J., Sitarski, B. N., Gelino, C. R., Logsdon, S. E., & Perrin, M. D. 2011, *ApJ*, 739, 49
- Burgasser, A. J., Vrba, F. J., Lépine, S., Munn, J. A., Luginbuhl, C. B., Henden, A. A., Guetter, H. H., & Canzian, B. C. 2008, *ApJ*, 672, 1159

- Burningham, B., et al. 2011, MNRAS, 414, 3590
- . 2010, MNRAS, 406, 1885
- . 2009, MNRAS, 395, 1237
- Burrows, A., Hubbard, W. B., Lunine, J. I., & Liebert, J. 2001, *Reviews of Modern Physics*, 73, 719
- Carson, J., et al. 2013, ApJ, 763, L32
- Chabrier, G. 2005, in *Astrophysics and Space Science Library*, Vol. 327, *The Initial Mass Function 50 Years Later*, ed. E. Corbelli, F. Palla, & H. Zinnecker, 41
- Chabrier, G., Baraffe, I., Allard, F., & Hauschildt, P. 2000, ApJ, 542, 464
- Chappelle, R. J., Pinfield, D. J., Steele, I. A., Dobbie, P. D., & Magazzù, A. 2005, MNRAS, 361, 1323
- Chauvin, G., et al. 2012, A&A, 548, A33
- Chauvin, G., Lagrange, A.-M., Dumas, C., Zuckerman, B., Mouillet, D., Song, I., Beuzit, J.-L., & Lowrance, P. 2004, A&A, 425, L29
- Chauvin, G., et al. 2005a, A&A, 430, 1027
- Chauvin, G., et al. 2003, A&A, 404, 157
- Chauvin, G., et al. 2005b, A&A, 438, L29
- Chiu, K., Fan, X., Leggett, S. K., Golimowski, D. A., Zheng, W., Geballe, T. R., Schneider, D. P., & Brinkmann, J. 2006, AJ, 131, 2722
- Costa, E., Méndez, R. A., Jao, W.-C., Henry, T. J., Subasavage, J. P., Brown, M. A., Ianna, P. A., & Bartlett, J. 2005, AJ, 130, 337
- Costa, E., Méndez, R. A., Jao, W.-C., Henry, T. J., Subasavage, J. P., & Ianna, P. A. 2006, AJ, 132, 1234
- Cruz, K. L., Kirkpatrick, J. D., & Burgasser, A. J. 2009, AJ, 137, 3345
- Cruz, K. L., et al. 2007, AJ, 133, 439
- Cruz, K. L., Reid, I. N., Liebert, J., Kirkpatrick, J. D., & Lowrance, P. J. 2003, AJ, 126, 2421
- Currie, T., et al. 2011, ApJ, 729, 128
- Currie, T., et al. 2013, ApJ, 776, 15

- Cushing, M. C., et al. 2011, *ApJ*, 743, 50
- Cushing, M. C., Rayner, J. T., & Vacca, W. D. 2005, *ApJ*, 623, 1115
- Cushing, M. C., Vacca, W. D., & Rayner, J. T. 2004, *PASP*, 116, 362
- Cutri, R. M., et al. 2003, 2MASS All Sky Catalog of Point Sources.
- Dahn, C. C., et al. 2008, *ApJ*, 686, 548
- Dahn, C. C., et al. 2002, *AJ*, 124, 1170
- Delfosse, X., Tinney, C. G., Forveille, T., Epchtein, N., Borsenberger, J., Fouqué, P., Kimeswenger, S., & Tiphène, D. 1999, *A&AS*, 135, 41
- Delorme, P., et al. 2013, *A&A*, 553, L5
- Delorme, P., et al. 2012, *A&A*, 548, A26
- Deshpande, R., et al. 2013, *AJ*, 146, 156
- . 2012, *AJ*, 144, 99
- Dieterich, S. B., Henry, T. J., Jao, W.-C., Winters, J. G., Hosey, A. D., Riedel, A. R., & Subasavage, J. P. 2014, *AJ*, 147, 94
- Dittmann, J. A., Irwin, J. M., Charbonneau, D., & Berta-Thompson, Z. K. 2014, *ApJ*, 784, 156
- Dobbie, P. D., Pinfield, D. J., Jameson, R. F., & Hodgkin, S. T. 2002, *MNRAS*, 335, L79
- Duchêne, G., & Kraus, A. 2013, *ARA&A*, 51, 269
- Ducourant, C., Teixeira, R., Chauvin, G., Daigne, G., Le Campion, J.-F., Song, I., & Zuckerman, B. 2008, *A&A*, 477, L1
- Ducourant, C., Teixeira, R., Galli, P. A. B., Le Campion, J. F., Krone-Martins, A., Zuckerman, B., Chauvin, G., & Song, I. 2014, *A&A*, 563, A121
- Dupuy, T. J., Forbrich, J., Rizzuto, A., Mann, A. W., Aller, K., Liu, M. C., Kraus, A. L., & Berger, E. 2016a, *ApJ*, 827, 23
- . 2016b, ArXiv e-prints
- Dupuy, T. J., & Kraus, A. L. 2013, *Science*, 341, 1492
- Dupuy, T. J., & Liu, M. C. 2012, *ApJS*, 201, 19
- Dupuy, T. J., Liu, M. C., Bowler, B. P., Cushing, M. C., Helling, C., Witte, S., & Hauschildt, P. 2010, *ApJ*, 721, 1725

- Dupuy, T. J., Liu, M. C., & Ireland, M. J. 2009, *ApJ*, 692, 729
- Dupuy, T. J., Liu, M. C., & Ireland, M. J. 2009, *ApJ*, 699, 168
- Dupuy, T. J., Liu, M. C., & Ireland, M. J. 2011, in *Astronomical Society of the Pacific Conference Series*, Vol. 448, 16th Cambridge Workshop on Cool Stars, Stellar Systems, and the Sun, ed. C. Johns-Krull, M. K. Browning, & A. A. West, 111
- Dupuy, T. J., Liu, M. C., Leggett, S. K., Ireland, M. J., Chiu, K., & Golimowski, D. A. 2015, *ApJ*, 805, 56
- Esposito, S., et al. 2013, *A&A*, 549, A52
- Faherty, J. K., Burgasser, A. J., Bochanski, J. J.,Looper, D. L., West, A. A., & van der Bliek, N. S. 2011, *AJ*, 141, 71
- Faherty, J. K., Burgasser, A. J., Cruz, K. L., Shara, M. M., Walter, F. M., & Gelino, C. R. 2009, *AJ*, 137, 1
- Faherty, J. K., et al. 2012, *ApJ*, 752, 56
- Faherty, J. K., Rice, E. L., Cruz, K. L., Mamajek, E. E., & Núñez, A. 2013, *AJ*, 145, 2
- Filippazzo, J. C., Rice, E. L., Faherty, J., Cruz, K. L., Van Gordon, M. M., & Looper, D. L. 2015, *ApJ*, 810, 158
- Gagné, J., Burgasser, A. J., Faherty, J. K., Lafrenière, D., Doyon, R., Filippazzo, J. C., Bowsher, E., & Nicholls, C. P. 2015, *ApJ*, 808, L20
- Gagné, J., et al. 2015a, *ApJS*, 219, 33
- Gagné, J., Lafrenière, D., Doyon, R., Artigau, É., Malo, L., Robert, J., & Nadeau, D. 2014a, *ApJ*, 792, L17
- Gagné, J., Lafrenière, D., Doyon, R., Malo, L., & Artigau, É. 2014b, *ApJ*, 783, 121
- Gagné, J., Lafrenière, D., Doyon, R., Malo, L., & Artigau, É. 2015b, *ApJ*, 798, 73
- Gálvez-Ortiz, M. C., et al. 2014, *MNRAS*, 439, 3890
- Gatewood, G., & Coban, L. 2009, *AJ*, 137, 402
- Gauza, B., Béjar, V. J. S., Pérez-Garrido, A., Rosa Zapatero Osorio, M., Lodieu, N., Rebolo, R., Pallé, E., & Nowak, G. 2015, *ApJ*, 804, 96
- Gizis, J. E. 2002, *ApJ*, 575, 484
- Gizis, J. E., Allers, K. N., Liu, M. C., Harris, H. C., Faherty, J. K., Burgasser, A. J., & Kirkpatrick, J. D. 2015, *ApJ*, 799, 203

- Gizis, J. E., et al. 2012, *AJ*, 144, 94
- Gizis, J. E., Jao, W.-C., Subasavage, J. P., & Henry, T. J. 2007, *ApJ*, 669, L45
- Gizis, J. E., Monet, D. G., Reid, I. N., Kirkpatrick, J. D., Liebert, J., & Williams, R. J. 2000, *AJ*, 120, 1085
- Gizis, J. E., Reid, I. N., Knapp, G. R., Liebert, J., Kirkpatrick, J. D., Koerner, D. W., & Burgasser, A. J. 2003, *AJ*, 125, 3302
- Goldman, B., Marsat, S., Henning, T., Clemens, C., & Greiner, J. 2010, *MNRAS*, 405, 1140
- Golimowski, D. A., et al. 2004, *AJ*, 127, 3516
- Guenther, E. W., Neuhäuser, R., Huélamo, N., Brandner, W., & Alves, J. 2001, *A&A*, 365, 514
- Hall, P. B. 2002a, *ApJ*, 580, L77
- . 2002b, *ApJ*, 564, L89
- Hanel, R., Conrath, B., Herath, L., Kunde, V., & Pirraglia, J. 1981, *J. Geophys. Res.*, 86, 8705
- Hawley, S. L., et al. 2002, *AJ*, 123, 3409
- Henry, T. J., Jao, W., Subasavage, J. P., Beaulieu, T. D., Ianna, P. A., Costa, E., & Méndez, R. A. 2006, *AJ*, 132, 2360
- Henry, T. J., Subasavage, J. P., Brown, M. A., Beaulieu, T. D., Jao, W.-C., & Hambly, N. C. 2004, *AJ*, 128, 2460
- Hinkley, S., et al. 2015, *ApJ*, 805, L10
- Hinkley, S., et al. 2013, *ApJ*, 779, 153
- Hinz, P. M., Rodigas, T. J., Kenworthy, M. A., Sivanandam, S., Heinze, A. N., Mamajek, E. E., & Meyer, M. R. 2010, *ApJ*, 716, 417
- Hodgkin, S. T., Irwin, M. J., Hewett, P. C., & Warren, S. J. 2009, *MNRAS*, 394, 675
- Huélamo, N., et al. 2010, *A&A*, 521, L54
- Ireland, M. J., Kraus, A., Martinache, F., Law, N., & Hillenbrand, L. A. 2011, *ApJ*, 726, 113
- Jameson, R. F., Casewell, S. L., Bannister, N. P., Lodieu, N., Keresztes, K., Dobbie, P. D., & Hodgkin, S. T. 2008, *MNRAS*, 384, 1399
- Janson, M., Jayawardhana, R., Girard, J. H., Lafrenière, D., Bonavita, M., Gizis, J., & Brandeker, A. 2012, *ApJ*, 758, L2

- Jones, J., et al. 2015, *ApJ*, 813, 58
- King, J. R., & Schuler, S. C. 2005, *PASP*, 117, 911
- King, J. R., Villarreal, A. R., Soderblom, D. R., Gulliver, A. F., & Adelman, S. J. 2003, *AJ*, 125, 1980
- Kirkpatrick, J. D. 2005, *ARA&A*, 43, 195
- Kirkpatrick, J. D., et al. 2008, *ApJ*, 689, 1295
- . 2011, *ApJS*, 197, 19
- Kirkpatrick, J. D., Dahn, C. C., Monet, D. G., Reid, I. N., Gizis, J. E., Liebert, J., & Burgasser, A. J. 2001, *AJ*, 121, 3235
- Kirkpatrick, J. D., Henry, T. J., & Simons, D. A. 1995, *AJ*, 109, 797
- Kirkpatrick, J. D., et al. 1999, *ApJ*, 519, 802
- . 2000, *AJ*, 120, 447
- . 2010, *ApJS*, 190, 100
- Klutsch, A., Freire Ferrero, R., Guillout, P., Frasca, A., Marilli, E., & Montes, D. 2014, *A&A*, 567, A52
- Knapp, G. R., et al. 2004, *AJ*, 127, 3553
- Kraus, A. L., & Hillenbrand, L. A. 2007, *AJ*, 134, 2340
- Kraus, A. L., Shkolnik, E. L., Allers, K. N., & Liu, M. C. 2014, *AJ*, 147, 146
- Kuzuhara, M., et al. 2013, *ApJ*, 774, 11
- Lafrenière, D., Jayawardhana, R., & van Kerkwijk, M. H. 2008, *ApJ*, 689, L153
- Lagrange, A., et al. 2010, *Science*, 329, 57
- Lagrange, A.-M., et al. 2009, *A&A*, 493, L21
- Law, N. M., Hodgkin, S. T., & Mackay, C. D. 2006, *MNRAS*, 368, 1917
- Lawrence, A., et al. 2007, *MNRAS*, 379, 1599
- Lee, J.-M., Heng, K., & Irwin, P. G. J. 2013, *ApJ*, 778, 97
- Leggett, S. K., Allard, F., & Hauschildt, P. H. 1998, *ApJ*, 509, 836
- Leggett, S. K., et al. 2002, *ApJ*, 564, 452



- Lépine, S., Thorstensen, J. R., Shara, M. M., & Rich, R. M. 2009, *AJ*, 137, 4109
- Liljestrom, T. 1991, *A&A*, 244, 483
- Liu, M. C., et al. 2011a, *ApJ*, 740, 108
- Liu, M. C., Dupuy, T. J., & Allers, K. N. 2013a, *Astronomische Nachrichten*, 334, 85
- Liu, M. C., Dupuy, T. J., Bowler, B. P., Leggett, S. K., & Best, W. M. J. 2012, *ApJ*, 758, 57
- Liu, M. C., Dupuy, T. J., & Ireland, M. J. 2008, *ApJ*, 689, 436
- Liu, M. C., Dupuy, T. J., & Leggett, S. K. 2010, *ApJ*, 722, 311
- Liu, M. C., Leggett, S. K., & Chiu, K. 2007, *ApJ*, 660, 1507
- Liu, M. C., Leggett, S. K., Golimowski, D. A., Chiu, K., Fan, X., Geballe, T. R., Schneider, D. P., & Brinkmann, J. 2006, *ApJ*, 647, 1393
- Liu, M. C., et al. 2013b, *ApJ*, 777, L20
- . 2011b, *ApJ*, 740, L32
- Lodieu, N., Hambly, N. C., Jameson, R. F., & Hodgkin, S. T. 2008, *MNRAS*, 383, 1385
- Looper, D. L., Burgasser, A. J., Kirkpatrick, J. D., & Swift, B. J. 2007a, *ApJ*, 669, L97
- Looper, D. L., Gelino, C. R., Burgasser, A. J., & Kirkpatrick, J. D. 2008a, *ApJ*, 685, 1183
- Looper, D. L., Kirkpatrick, J. D., & Burgasser, A. J. 2007b, *AJ*, 134, 1162
- Looper, D. L., et al. 2008b, *ApJ*, 686, 528
- Lowrance, P. J., et al. 1999, *ApJ*, 512, L69
- . 2000, *ApJ*, 541, 390
- Lucas, P. W., Roche, P. F., Allard, F., & Hauschildt, P. H. 2001, *MNRAS*, 326, 695
- Luhman, K. L. 2014, *ApJ*, 786, L18
- Luhman, K. L., Briceño, C., Stauffer, J. R., Hartmann, L., Barrado y Navascués, D., & Caldwell, N. 2003, *ApJ*, 590, 348
- Luhman, K. L., et al. 2006, *ApJ*, 649, 894
- . 2007, *ApJ*, 654, 570
- . 2012, *ApJ*, 744, 135

- Lurie, J. C., et al. 2014, *AJ*, 148, 91
- Mace, G. N., et al. 2013, *ApJS*, 205, 6
- Macintosh, B., et al. 2015, *Science*, 350, 64
- Madhusudhan, N., Burrows, A., & Currie, T. 2011, *ApJ*, 737, 34
- Mainzer, A., et al. 2011, *ApJ*, 731, 53
- Maire, A.-L., et al. 2016, *A&A*, 587, A56
- Males, J. R., et al. 2014, *ApJ*, 786, 32
- Malinen, J., et al. 2014, *A&A*, 563, A125
- Malo, L., Doyon, R., Lafrenière, D., Artigau, É., Gagné, J., Baron, F., & Riedel, A. 2013, *ApJ*, 762, 88
- Mamajek, E. E. 2005, *ApJ*, 634, 1385
- Mamajek, E. E., & Bell, C. P. M. 2014, *MNRAS*, 445, 2169
- Manjavacas, E., Goldman, B., Reffert, S., & Henning, T. 2013, *A&A*, 560, A52
- Marley, M. S., Saumon, D., Cushing, M., Ackerman, A. S., Fortney, J. J., & Freedman, R. 2012, *ApJ*, 754, 135
- Marocco, F., et al. 2013, *AJ*, 146, 161
- Marocco, F., et al. 2014, *MNRAS*, 439, 372
- Marois, C., Macintosh, B., Barman, T., Zuckerman, B., Song, I., Patience, J., Lafrenière, D., & Doyon, R. 2008, *Science*, 322, 1348
- Marois, C., Zuckerman, B., Konopacky, Q. M., Macintosh, B., & Barman, T. 2010, *Nature*, 468, 1080
- Martín, E. L., Basri, G., & Zapatero Osorio, M. R. 1999a, *AJ*, 118, 1005
- Martín, E. L., Delfosse, X., Basri, G., Goldman, B., Forveille, T., & Zapatero Osorio, M. R. 1999b, *AJ*, 118, 2466
- Martín, E. L., et al. 2010, *A&A*, 517, A53
- McCarthy, K., & Wilhelm, R. J. 2014, *AJ*, 148, 70
- McGovern, M. R., Kirkpatrick, J. D., McLean, I. S., Burgasser, A. J., Prato, L., & Lowrance, P. J. 2004, *ApJ*, 600, 1020

- McLean, I. S., McGovern, M. R., Burgasser, A. J., Kirkpatrick, J. D., Prato, L., & Kim, S. S. 2003, *ApJ*, 596, 561
- McLean, I. S., Prato, L., McGovern, M. R., Burgasser, A. J., Kirkpatrick, J. D., Rice, E. L., & Kim, S. S. 2007, *ApJ*, 658, 1217
- Meshkat, T., et al. 2015, *MNRAS*, 453, 2378
- Metchev, S. A., & Hillenbrand, L. A. 2004, *ApJ*, 617, 1330
- . 2006, *ApJ*, 651, 1166
- Metchev, S. A., Kirkpatrick, J. D., Berriman, G. B., &Looper, D. 2008, *ApJ*, 676, 1281
- Mohanty, S., Jayawardhana, R., & Barrado y Navascués, D. 2003, *ApJ*, 593, L109
- Mohanty, S., Jayawardhana, R., Huélamo, N., & Mamajek, E. 2007, *ApJ*, 657, 1064
- Monet, D. G., Dahn, C. C., Vrba, F. J., Harris, H. C., Pier, J. R., Luginbuhl, C. B., & Ables, H. D. 1992, *AJ*, 103, 638
- Montes, D., López-Santiago, J., Gálvez, M. C., Fernández-Figueroa, M. J., De Castro, E., & Cornide, M. 2001, *MNRAS*, 328, 45
- Nakajima, T., Oppenheimer, B. R., Kulkarni, S. R., Golimowski, D. A., Matthews, K., & Durrance, S. T. 1995, *Nature*, 378, 463
- Nakajima, T., Tsuji, T., & Yanagisawa, K. 2004, *ApJ*, 607, 499
- Naud, M.-E., et al. 2014, *ApJ*, 787, 5
- Neuhäuser, R., & Forbrich, J. 2008, *The Corona Australis Star Forming Region*, ed. B. Reipurth, 735
- Neuhäuser, R., Ginski, C., Schmidt, T. O. B., & Mugrauer, M. 2011, *MNRAS*, 416, 1430
- Neuhäuser, R., & Guenther, E. W. 2004, *A&A*, 420, 647
- Neuhäuser, R., et al. 2000, *A&AS*, 146, 323
- Nielsen, E. L., et al. 2012, *ApJ*, 750, 53
- . 2013, *ApJ*, 776, 4
- Nieva, M.-F., & Przybilla, N. 2012, *A&A*, 539, A143
- Oppenheimer, B. R., et al. 2013, *ApJ*, 768, 24
- Oppenheimer, B. R., Kulkarni, S. R., Matthews, K., & Nakajima, T. 1995, *Science*, 270, 1478

- Patience, J., King, R. R., de Rosa, R. J., & Marois, C. 2010, *A&A*, 517, A76
- Perryman, M. A. C., et al. 1998, *A&A*, 331, 81
- Pinfield, D. J., Dobbie, P. D., Jameson, R. F., Steele, I. A., Jones, H. R. A., & Katsiyannis, A. C. 2003, *MNRAS*, 342, 1241
- Puget, P., et al. 2004, in *Society of Photo-Optical Instrumentation Engineers (SPIE) Conference Series*, Vol. 5492, *Society of Photo-Optical Instrumentation Engineers (SPIE) Conference Series*, ed. A. F. M. Moorwood & M. Iye, 978–987
- Rameau, J., et al. 2013, *ApJ*, 772, L15
- Rayner, J. T., Toomey, D. W., Onaka, P. M., Denault, A. J., Stahlberger, W. E., Vacca, W. D., Cushing, M. C., & Wang, S. 2003, *PASP*, 115, 362
- Rebolo, R., Zapatero Osorio, M. R., Madrugá, S., Bejar, V. J. S., Arribas, S., & Licandro, J. 1998, *Science*, 282, 1309
- Reid, I. N., et al. 2003a, *AJ*, 126, 3007
- Reid, I. N., Cruz, K. L., Kirkpatrick, J. D., Allen, P. R., Mungall, F., Liebert, J., Lowrance, P., & Sweet, A. 2008, *AJ*, 136, 1290
- Reid, I. N., et al. 2003b, *AJ*, 125, 354
- Reid, I. N., Kirkpatrick, J. D., Liebert, J., Gizis, J. E., Dahn, C. C., & Monet, D. G. 2002, *AJ*, 124, 519
- Reid, I. N., Lewitus, E., Allen, P. R., Cruz, K. L., & Burgasser, A. J. 2006, *AJ*, 132, 891
- Reid, I. N., & Walkowicz, L. M. 2006, *PASP*, 118, 671
- Reid, N. 2003, *MNRAS*, 342, 837
- Reiners, A., & Basri, G. 2009, *ApJ*, 705, 1416
- Reipurth, B., & Clarke, C. 2001, *AJ*, 122, 432
- Reylé, C., et al. 2010, *A&A*, 522, A112
- Riaz, B., & Gizis, J. E. 2008, *ApJ*, 681, 1584
- Rice, E. L., Barman, T., Mclean, I. S., Prato, L., & Kirkpatrick, J. D. 2010a, *ApJS*, 186, 63
- Rice, E. L., Faherty, J. K., & Cruz, K. L. 2010b, *ApJ*, 715, L165
- Riedel, A. R., et al. 2014, *AJ*, 147, 85

- Robin, A. C., Reylé, C., Derrière, S., & Picaud, S. 2003, *A&A*, 409, 523
- Rodriguez, D. R., Bessell, M. S., Zuckerman, B., & Kastner, J. H. 2011, *ApJ*, 727, 62
- Roeser, S., Demleitner, M., & Schilbach, E. 2010, *AJ*, 139, 2440
- Russeil, D., Juvela, M., Lehtinen, K., Mattila, K., & Paatero, P. 2003, *A&A*, 409, 135
- Sahlmann, J., Lazorenko, P. F., Ségransan, D., Martín, E. L., Mayor, M., Queloz, D., & Udry, S. 2014, *A&A*, 565, A20
- Salim, S., Lépine, S., Rich, R. M., & Shara, M. M. 2003, *ApJ*, 586, L149
- Sandell, G., Reipurth, B., & Gahm, G. 1987, *A&A*, 181, 283
- Saumon, D., & Marley, M. S. 2008, *ApJ*, 689, 1327
- Schilbach, E., Röser, S., & Scholz, R.-D. 2009, *A&A*, 493, L27
- Schlafly, E. F., et al. 2014, *ApJ*, 786, 29
- Schlieder, J. E., et al. 2014, *ApJ*, 783, 27
- Schlieder, J. E., Lépine, S., & Simon, M. 2012, *AJ*, 143, 80
- Schmidt, S. J., Cruz, K. L., Bongiorno, B. J., Liebert, J., & Reid, I. N. 2007, *AJ*, 133, 2258
- Schmidt, S. J., Hawley, S. L., West, A. A., Bochanski, J. J., Davenport, J. R. A., Ge, J., & Schneider, D. P. 2015, *AJ*, 149, 158
- Schmidt, S. J., West, A. A., Hawley, S. L., & Pineda, J. S. 2010, *AJ*, 139, 1808
- Schneider, A. C., Cushing, M. C., Kirkpatrick, J. D., Mace, G. N., Gelino, C. R., Faherty, J. K., Fajardo-Acosta, S., & Sheppard, S. S. 2014, *AJ*, 147, 34
- Scholz, A., Kostov, V., Jayawardhana, R., & Mužić, K. 2015, *ApJ*, 809, L29
- Scholz, R.-D., McCaughrean, M. J., Zinnecker, H., & Lodieu, N. 2005, *A&A*, 430, L49
- Schönrich, R., Binney, J., & Dehnen, W. 2010, *MNRAS*, 403, 1829
- Seifahrt, A., Guenther, E., & Neuhäuser, R. 2005, *A&A*, 440, 967
- Seifahrt, A., Reiners, A., Almaghrbi, K. A. M., & Basri, G. 2010, *A&A*, 512, A37
- Shkolnik, E., Liu, M. C., & Reid, I. N. 2009, *ApJ*, 699, 649
- Shkolnik, E. L., Anglada-Escudé, G., Liu, M. C., Bowler, B. P., Weinberger, A. J., Boss, A. P., Reid, I. N., & Tamura, M. 2012, *ApJ*, 758, 56

- Shkolnik, E. L., Liu, M. C., Reid, I. N., Dupuy, T., & Weinberger, A. J. 2011, *ApJ*, 727, 6
- Simons, D. A., & Tokunaga, A. 2002, *PASP*, 114, 169
- Skemer, A. J., et al. 2012, *ApJ*, 753, 14
- . 2014, *ApJ*, 792, 17
- Smart, R. L., et al. 2013, *MNRAS*, 433, 2054
- Smith, L. C., et al. 2015, *MNRAS*, 454, 4476
- Stassun, K. G., Mathieu, R. D., & Valenti, J. A. 2006, *Nature*, 440, 311
- Stephens, D. C., et al. 2009, *ApJ*, 702, 154
- Stone, J. M., et al. 2016, *ApJ*, 818, L12
- Tabernero, H. M., Montes, D., & González Hernández, J. I. 2012, *A&A*, 547, A13
- Tanner, A., White, R., Bailey, J., Blake, C., Blake, G., Cruz, K., Burgasser, A. J., & Kraus, A. 2012, *ApJS*, 203, 10
- Teixeira, R., Ducourant, C., Chauvin, G., Krone-Martins, A., Song, I., & Zuckerman, B. 2008, *A&A*, 489, 825
- Thompson, M. A., et al. 2013, *PASP*, 125, 809
- Tinney, C. G., Burgasser, A. J., & Kirkpatrick, J. D. 2003, *AJ*, 126, 975
- Tinney, C. G., Faherty, J. K., Kirkpatrick, J. D., Cushing, M., Morley, C. V., & Wright, E. L. 2014, *ApJ*, 796, 39
- Tinney, C. G., Reid, I. N., Gizis, J., & Mould, J. R. 1995, *AJ*, 110, 3014
- Tokunaga, A. T., Simons, D. A., & Vacca, W. D. 2002, *PASP*, 114, 180
- Torres, C. A. O., Quast, G. R., Melo, C. H. F., & Sterzik, M. F. 2008, *Young Nearby Loose Associations*, ed. Reipurth, B., 757
- Torres, G., Guenther, E. W., Marschall, L. A., Neuhäuser, R., Latham, D. W., & Stefanik, R. P. 2003, *AJ*, 125, 825
- Torres, R. M., Loinard, L., Mioduszewski, A. J., & Rodríguez, L. F. 2009, *ApJ*, 698, 242
- Vacca, W. D., Cushing, M. C., & Rayner, J. T. 2003, *PASP*, 115, 389
- van Altena, W. F. 1969, *AJ*, 74, 2
- van Dam, M. A., et al. 2006, *PASP*, 118, 310

- van Leeuwen, F. 2007, *A&A*, 474, 653
- Vrba, F. J., et al. 2004, *AJ*, 127, 2948
- Wahhaj, Z., et al. 2011, *ApJ*, 729, 139
- Weinberger, A. J., Anglada-Escudé, G., & Boss, A. P. 2013, *ApJ*, 762, 118
- West, A. A., Hawley, S. L., Bochanski, J. J., Covey, K. R., Reid, I. N., Dhital, S., Hilton, E. J., & Masuda, M. 2008, *AJ*, 135, 785
- Wizinowich, P. L., et al. 2006, *PASP*, 118, 297
- Wright, E. L., et al. 2010, *AJ*, 140, 1868
- Zacharias, N., Finch, C. T., Girard, T. M., Henden, A., Bartlett, J. L., Monet, D. G., & Zacharias, M. I. 2013, *AJ*, 145, 44
- Zahnle, K. J., & Marley, M. S. 2014, *ApJ*, 797, 41
- Zapatero Osorio, M. R., Béjar, V. J. S., Miles-Páez, P. A., Peña Ramírez, K., Rebolo, R., & Pallé, E. 2014, *A&A*, 568, A6
- Zapatero Osorio, M. R., Rebolo, R., Bihain, G., Béjar, V. J. S., Caballero, J. A., & Álvarez, C. 2010, *ApJ*, 715, 1408
- Zuckerman, B., & Song, I. 2004, *ARA&A*, 42, 685
- Zuckerman, B., Song, I., Bessell, M. S., & Webb, R. A. 2001, *ApJ*, 562, L87

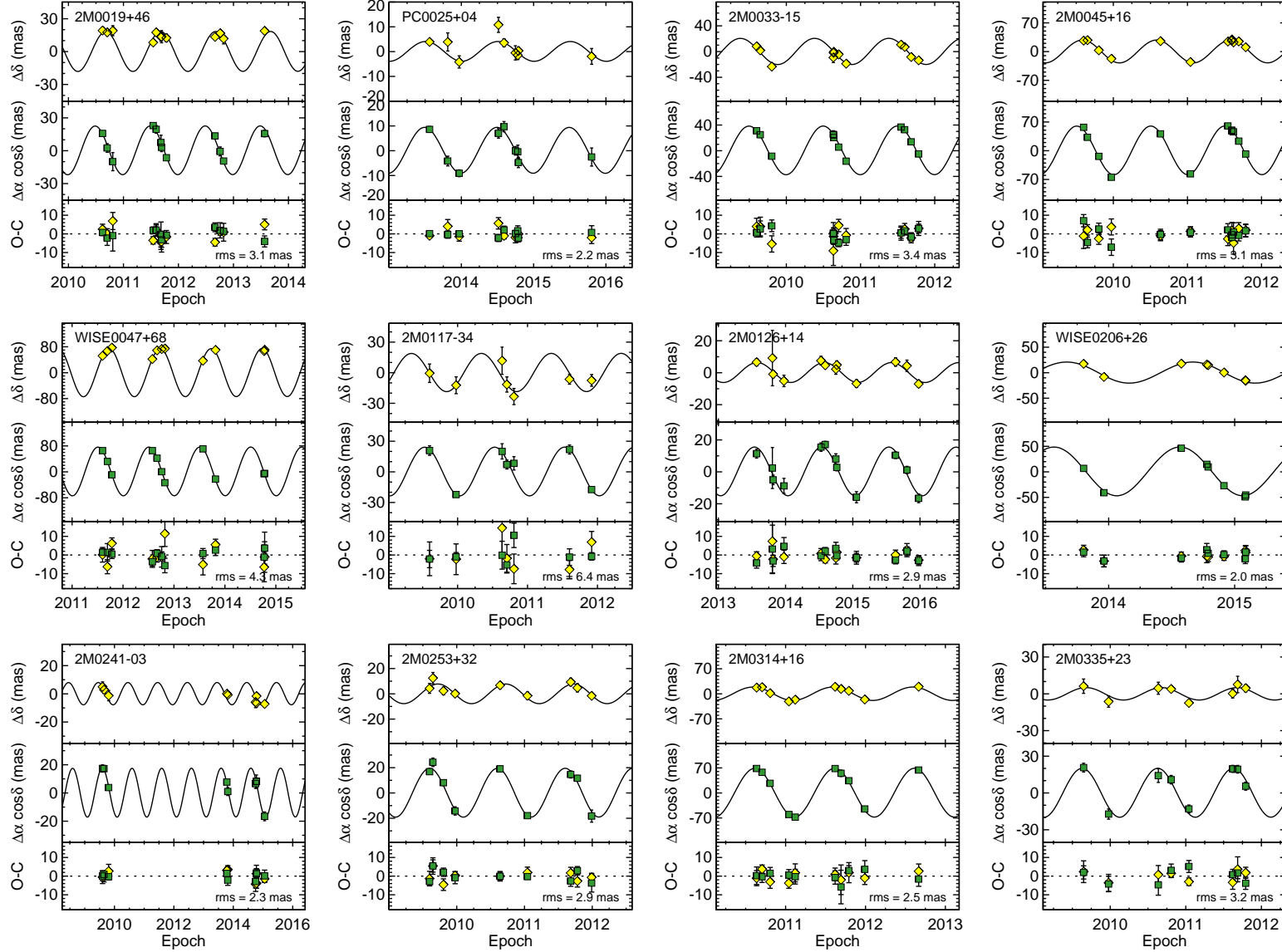


Fig. 1.— For each object, the top and middle panels show relative astrometry in  $\delta$  and  $\alpha$ , respectively, as a function of Julian year after subtracting the best-fit proper motion. (This is for display purposes only; in our analysis we fit for both the proper motion and parallax simultaneously.) The bottom panels show the residuals after subtracting both the parallax and proper motion.



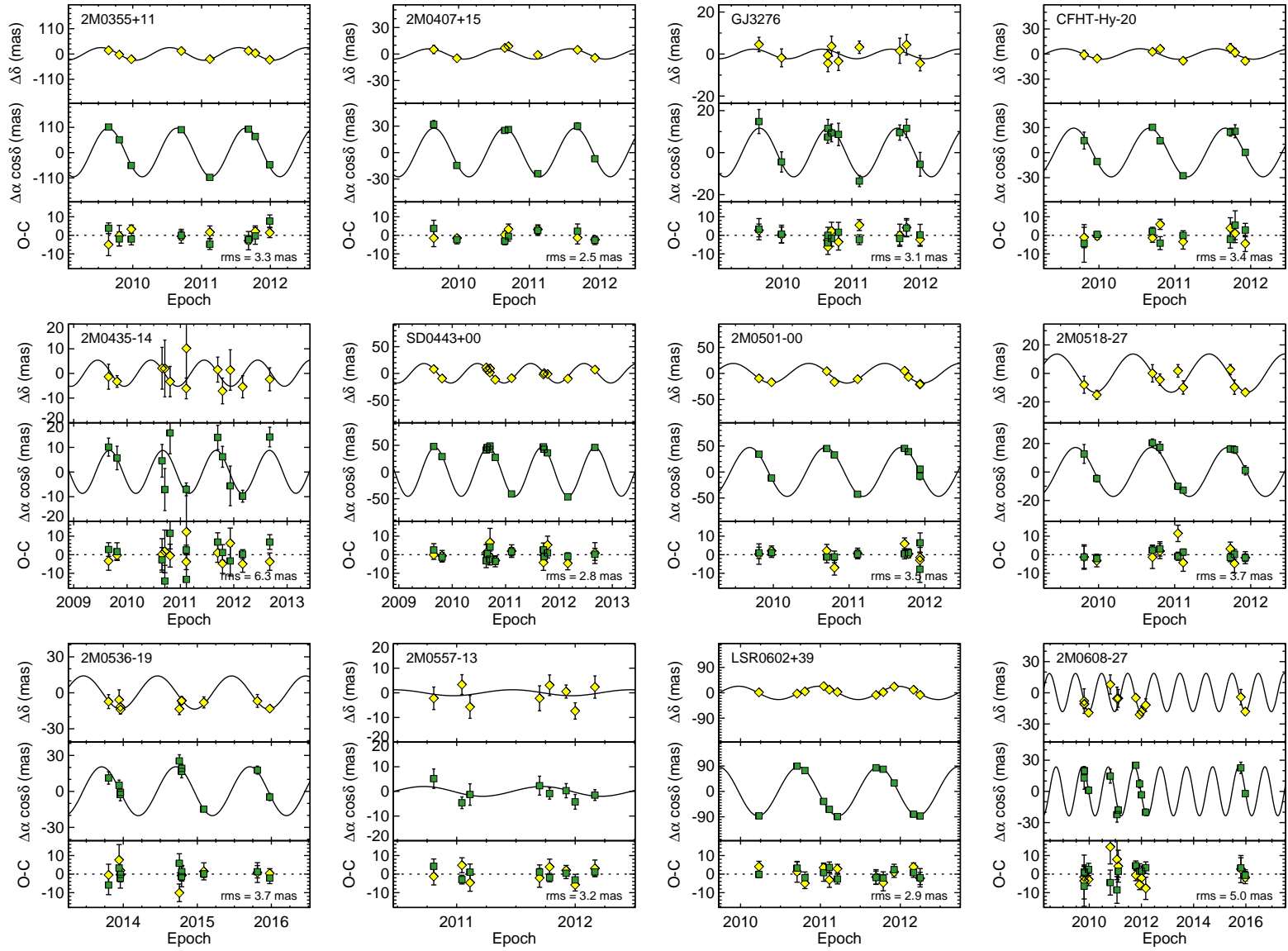


Fig. 1.— (Continued)

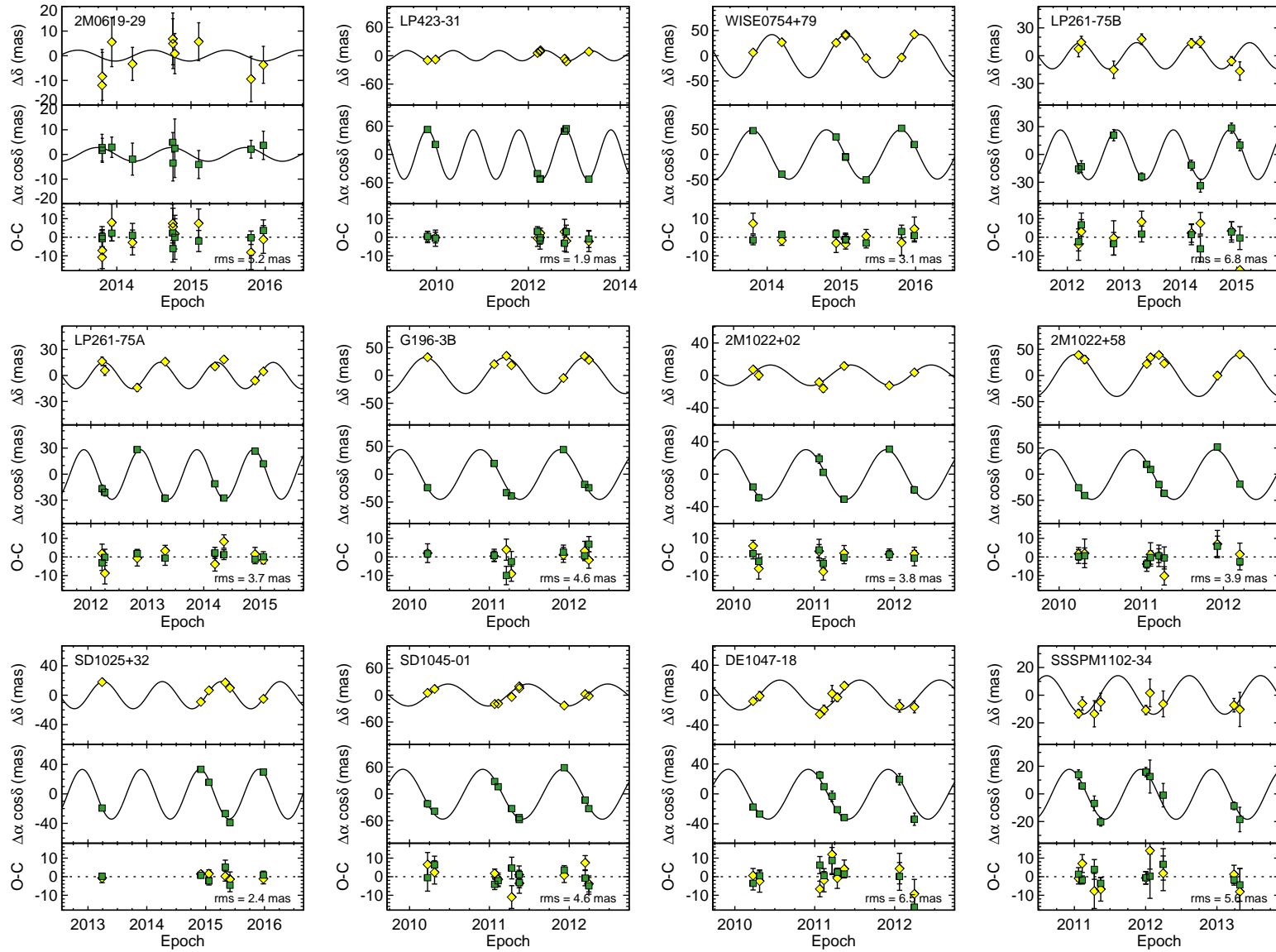


Fig. 1.— (Continued)

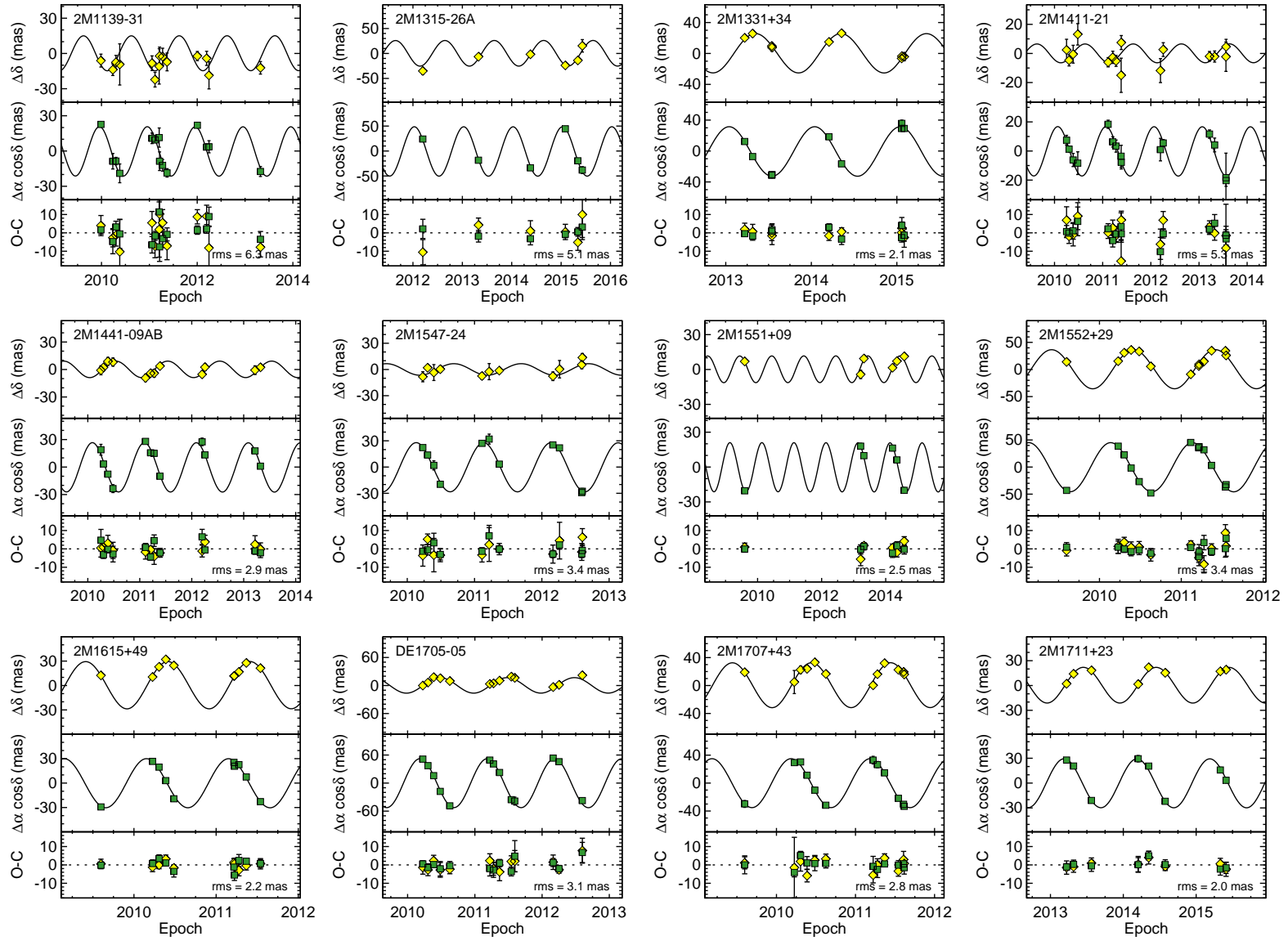


Fig. 1.— (Continued)

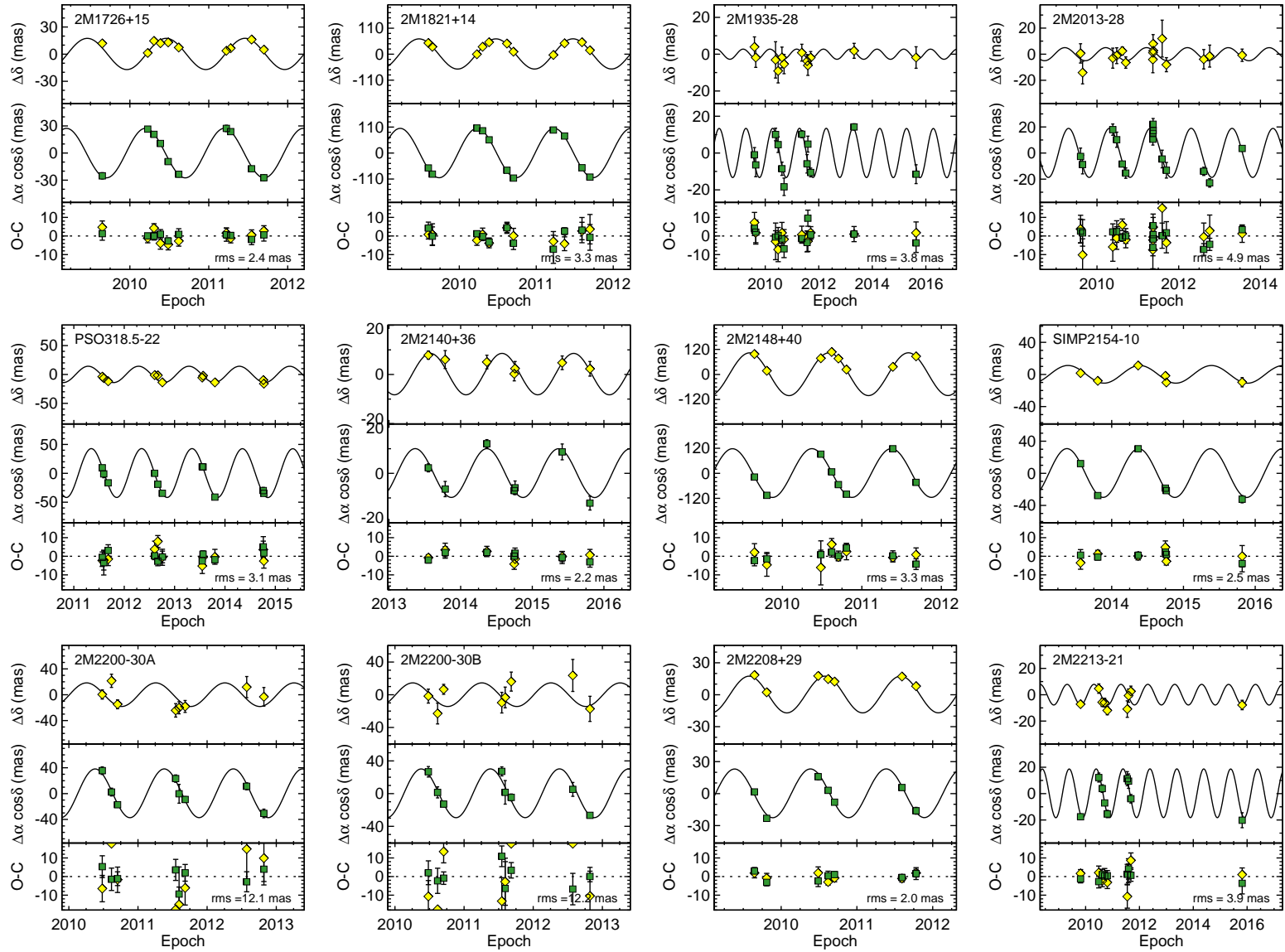


Fig. 1.— (Continued)

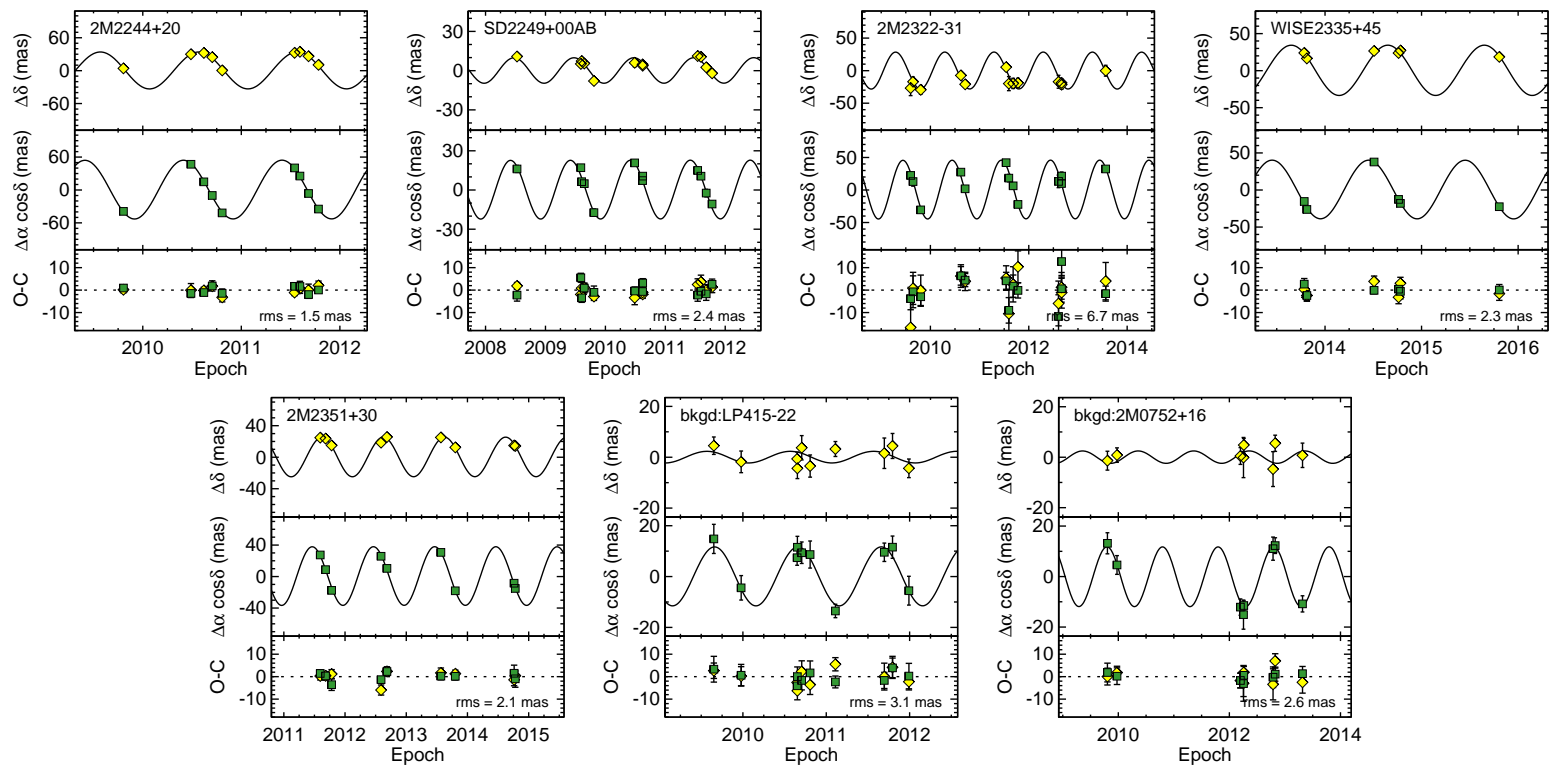


Fig. 1.— (Continued)

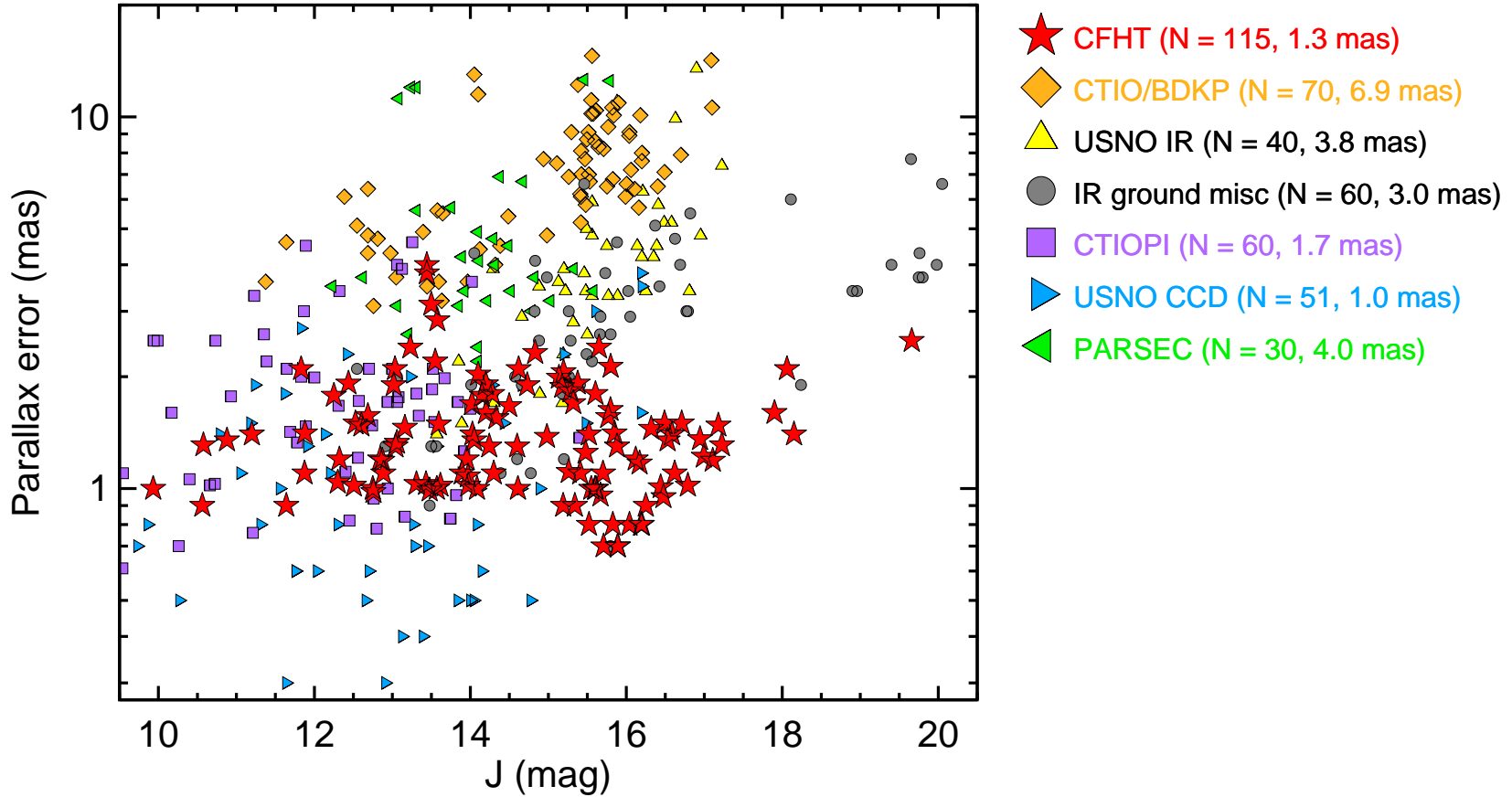


Fig. 2.— Our CFHT/WIRCam parallax errors plotted as a function of  $J$ -band magnitude alongside the results of other infrared parallax programs and larger optical programs that target ultracool dwarfs. Plotted CFHT results include the parallaxes published here as well as our previous work (Dupuy & Liu 2012; Dupuy et al. 2015), in total 115 parallax measurements with a median precision of 1.3 mas. Other plotted parallaxes are from the Brown Dwarf Kinematics Project at CTIO (Faherty et al. 2011; Faherty et al. 2012, 2013); the USNO IR program (Vrba et al. 2004; Burgasser et al. 2008); the optical CTIO Parallax Investigation program (Costa et al. 2005, 2006; Henry et al. 2006; Gizis et al. 2007; Riedel et al. 2014; Dieterich et al. 2014; Lurie et al. 2014); the optical USNO CCD program (Monet et al. 1992; Dahn et al. 2002; Dahn et al. 2008; Reid et al. 2003b; Gizis et al. 2015); and the optical PARSEC program (Andrei et al. 2011; Marocco et al. 2013). Other smaller individual samples of ground-based infrared parallaxes are plotted as a group, including results from NTT/SOFI (Tinney et al. 2003), Calar Alto 3.5-m/Omega-2000 (Schilbach et al. 2009; Manjavacas et al. 2013; Zapatero Osorio et al. 2014), UKIRT/WFCAM (Smart et al. 2013), and Magellan/FourStar (Tinney et al. 2014). Note that the extremely high-precision VLT optical parallaxes from Sahlmann et al. (2014), with  $\sigma_{\pi} = 0.06\text{--}0.14$  mas at  $J = 11.1\text{--}12.7$  mag, lie outside the plotted area.

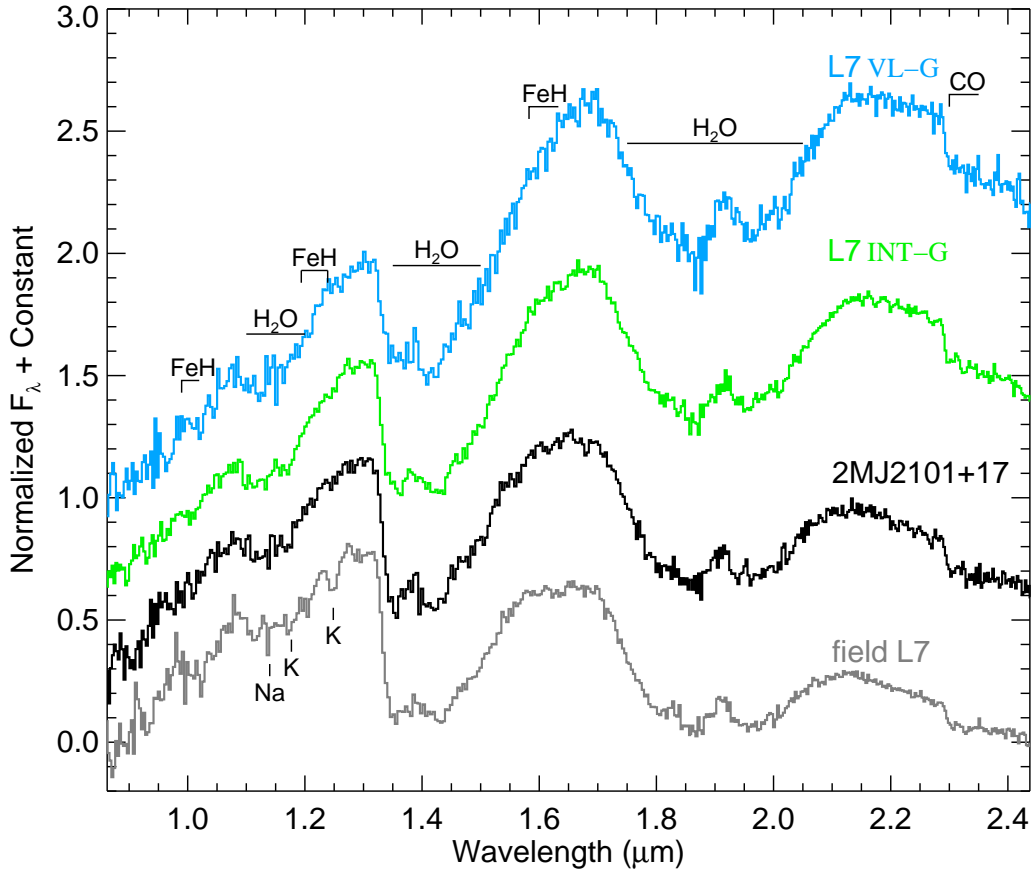


Fig. 3.— Comparison of the spectrum of 2MASS J2101+1756 to L7 dwarfs with a range of gravity classifications from Allers & Liu (2013a) and listed in the caption of Figure 31. We assign a spectral type of L7 and do not find any strong indication of youth.

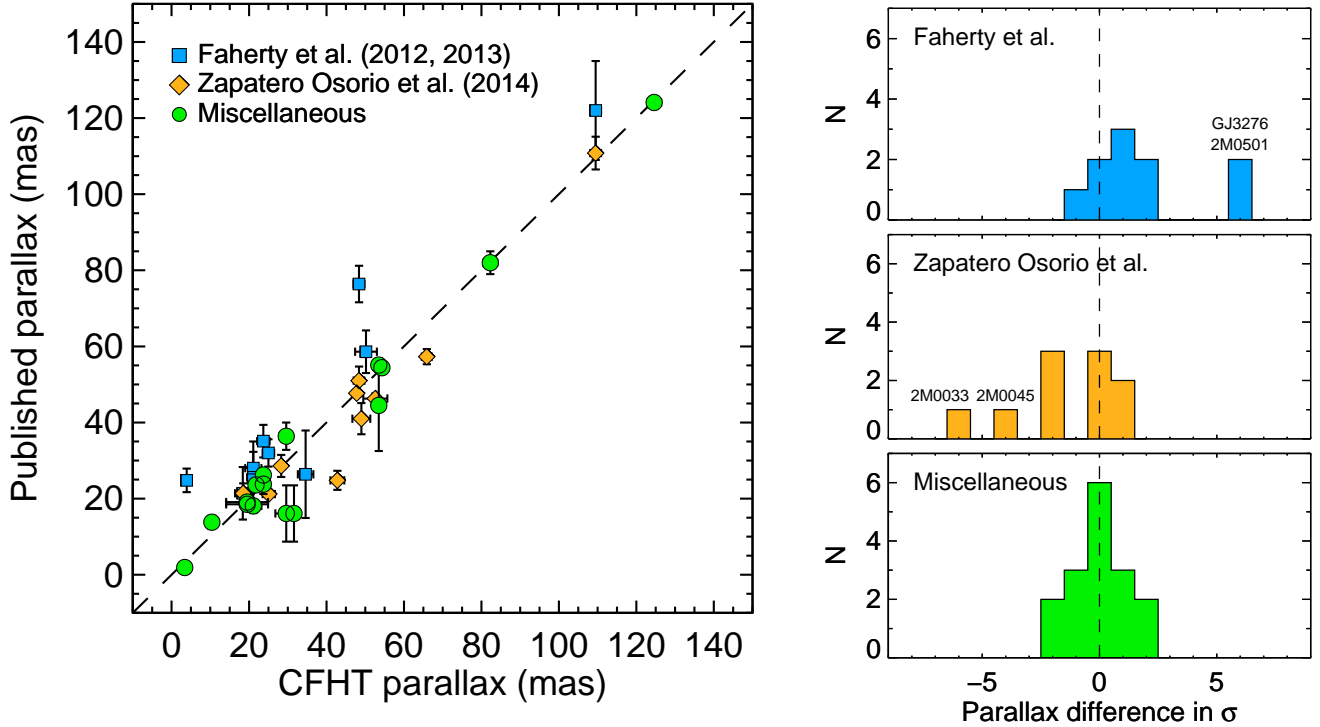


Fig. 4.— *Left*: Comparison of our CFHT parallaxes with other results in the literature. The published parallaxes are primarily from Faherty et al. (2012) and Zapatero Osorio et al. (2014), with some measurements coming from other miscellaneous sources (Dahn et al. 2002; Vrba et al. 2004; Costa et al. 2006; Teixeira et al. 2008; Gatewood & Coban 2009; Andrei et al. 2011; Shkolnik et al. 2012; Weinberger et al. 2013; Ducourant et al. 2014; Gizis et al. 2015). Data points without visible error bars have uncertainties smaller than the plotting symbols. Most of our parallaxes are consistent at  $1\sigma$  or less with previous results, and 90% are consistent at  $2.5\sigma$ . However, there are a number of more extreme  $\approx 4\text{--}6\sigma$  outliers. *Right*: The histograms show differences in parallaxes computed as  $(\pi_{\text{other}} - \pi_{\text{CFHT}})$ . The largest outliers come from the samples of Faherty et al. (2012) and Zapatero Osorio et al. (2014). The histograms suggest that parallaxes from Faherty et al. (2012) are systematically larger than our CFHT values and parallaxes from Zapatero Osorio et al. (2014) are systematically lower, while no systematic offset is apparent for other literature results.



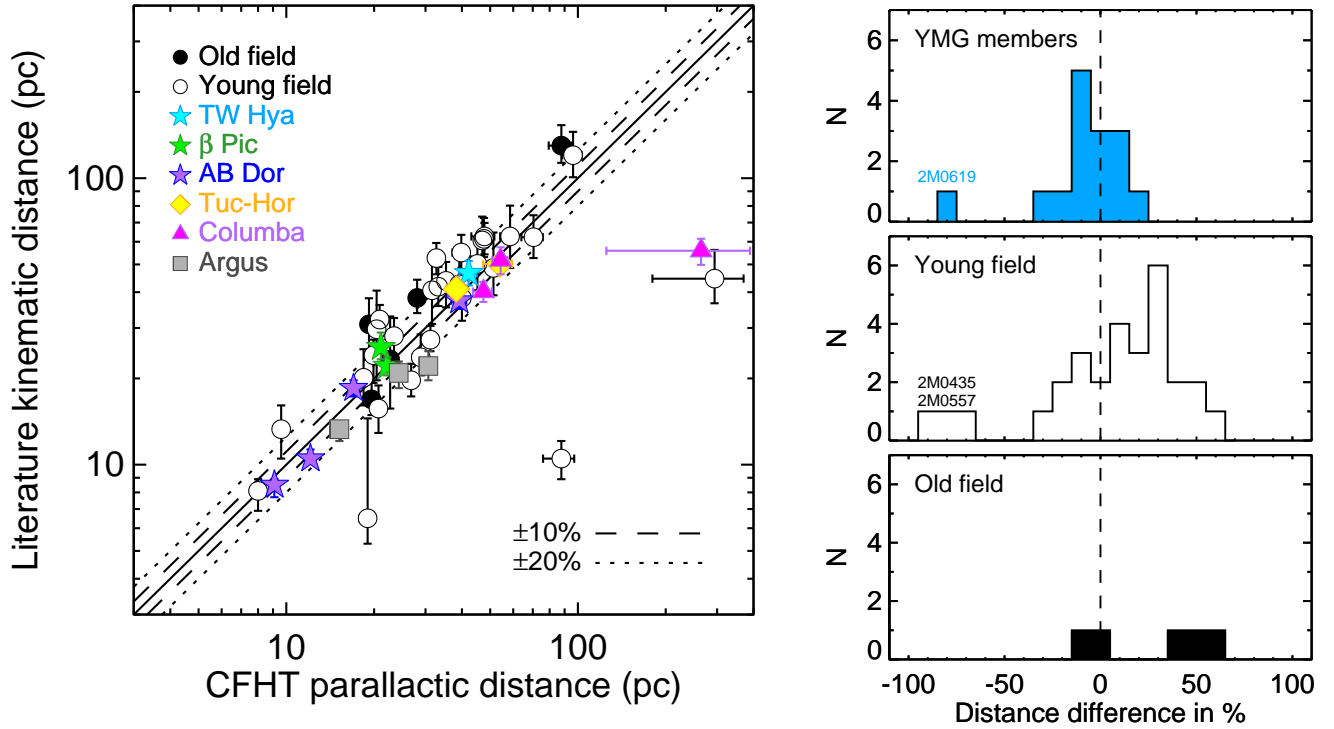


Fig. 5.— Comparison of our CFHT parallactic distances to kinematic distance estimates from BANYAN II (Gagné et al. 2014b) and Mamajek (2005). Most objects have distances that agree to within 20%, which is dominated by the uncertainty in the kinematic distances since the parallax errors are typically  $<6\%$ . Although the most visible outliers are those with CFHT parallaxes placing them at much larger distances, overall the kinematic distances for the “young field” population show a slight preference for being systematically 11% larger than our parallax distances. Data points without obvious error bars have uncertainties smaller than the plotting symbol. The histograms in the righthand panels show percentages computed as  $(d_{\text{kin}} - d_{\text{CFHT}})/d_{\text{CFHT}}$ .

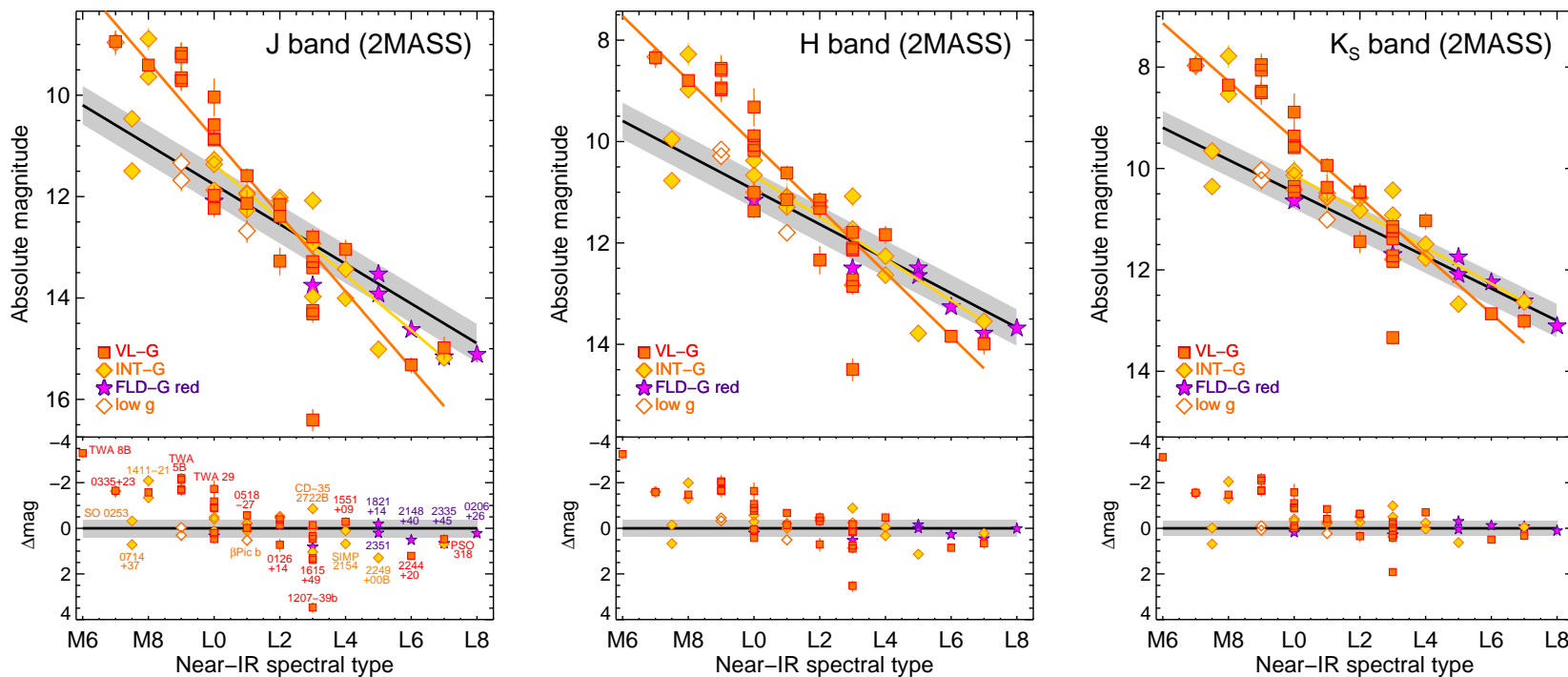


Fig. 6.— 2MASS  $JHK_S$  absolute magnitudes for all known field late-M and L dwarfs with parallaxes, near-IR spectral types, and spectroscopic evidence of youth. (About 80% of the objects are from this paper’s CFHT parallaxes.) Spectral types and gravity classifications are mostly based on the Allers & Liu (2013a) system (see Table 1). Objects labeled as “low g” (HR 6037 Ba and Bb [both M9] and  $\beta$  Pic b [L1]) appear young spectroscopically, but their spectra have insufficient wavelength coverage for a formal gravity classification. Objects labeled as “FLD-G red” have field gravities but unusually red colors highlighted in the literature. The errors on the absolute magnitudes are typically smaller than the plotting symbol. The thick black line shows our fit for field (old) ultracool dwarfs, and the grey swath shows the  $1\sigma$  scatter about that fit. The colored lines show the linear fits for the VL-G and INT-G samples (Table 10); the anomalously faint L3 object 2MASS J1207–3932b has been excluded from the line fits. Four low-gravity objects in our sample are not plotted here and not used for the line fits: three have low-S/N parallaxes due to their large distances ( $S/N < 4$ ,  $d \gtrsim 250$  pc; GJ 3276, 2MASS J0557–1359, and 2MASSI J0619–2903), and the fourth object (2MASSI J0435–1414, M7 VL-G) appears to have a circumstellar disk and its high luminosity places it off the plots (see Appendix). The lower panels show difference with respect to the field sequence. Note that the extent of the  $y$  axis is the same for all our plots of absolute magnitude versus spectral type (Figures 6, 7, 8, 9, and 10).

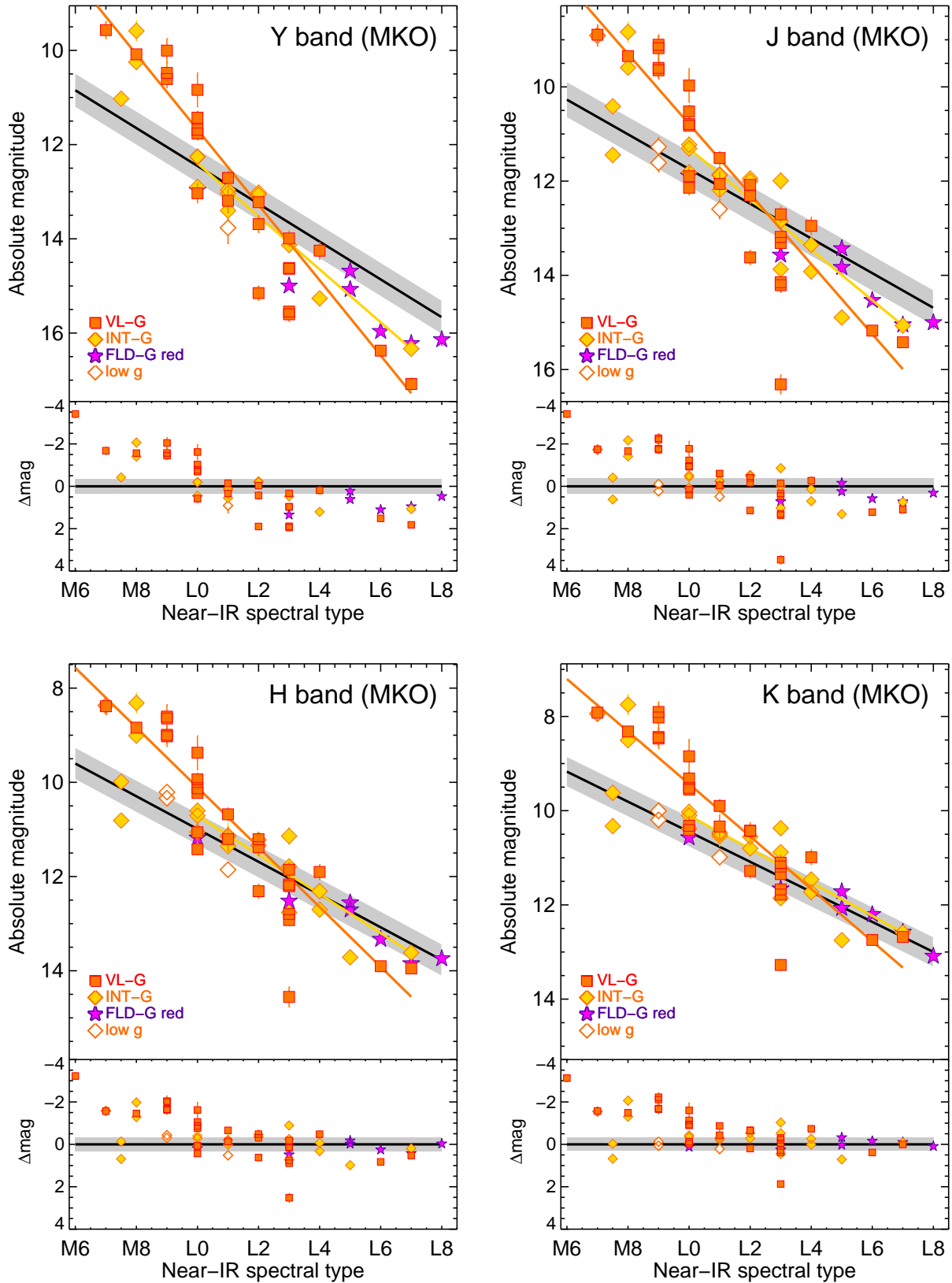


Fig. 7.— Absolute magnitudes in the MKO  $YJHK$  filters as a function of near-IR spectral type for our young sample. See Figure 6 caption for further details.

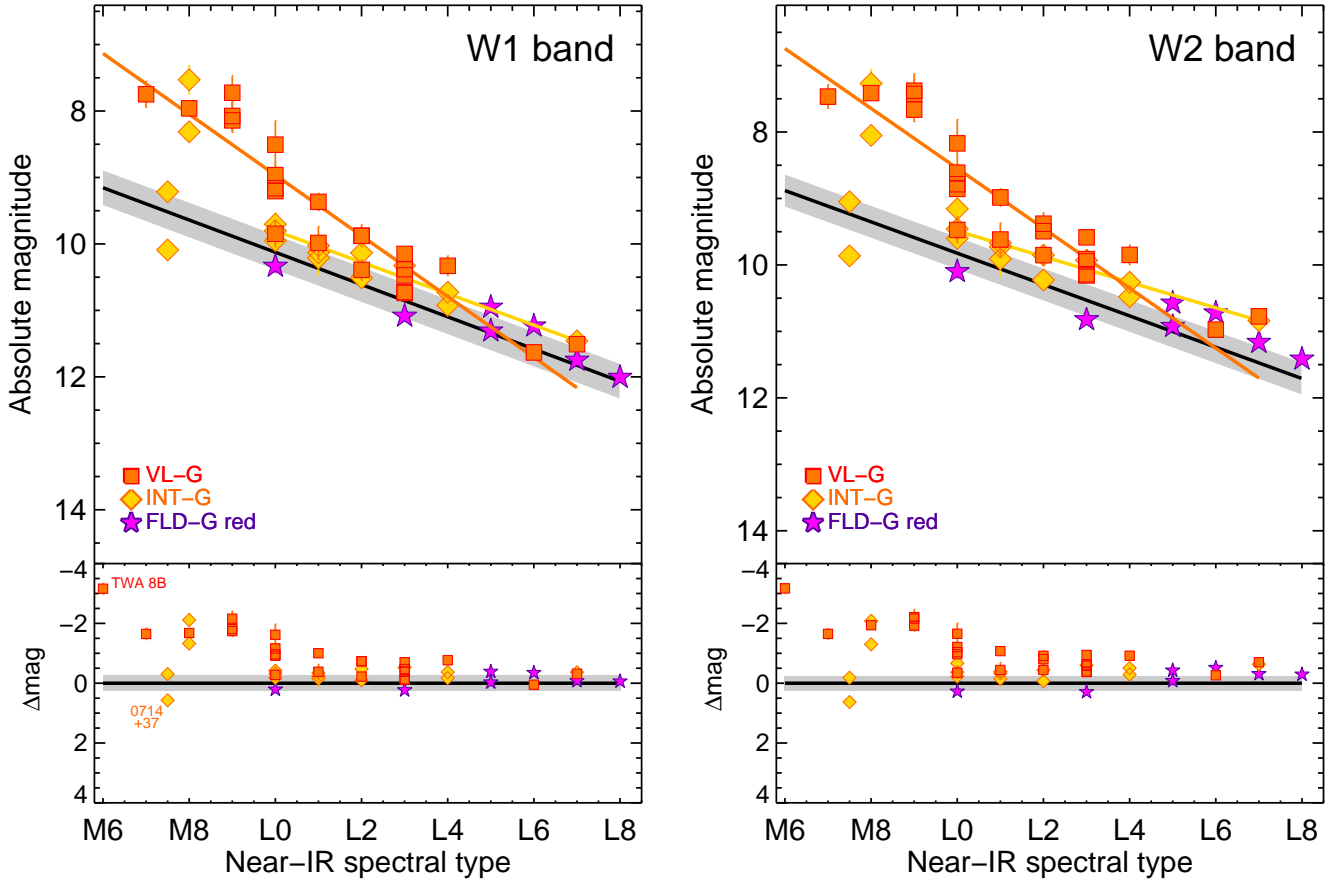


Fig. 8.— Absolute magnitudes in the *WISE* W1 and W2 filters as a function of spectral type for our young sample. See Figure 6 caption for further details.

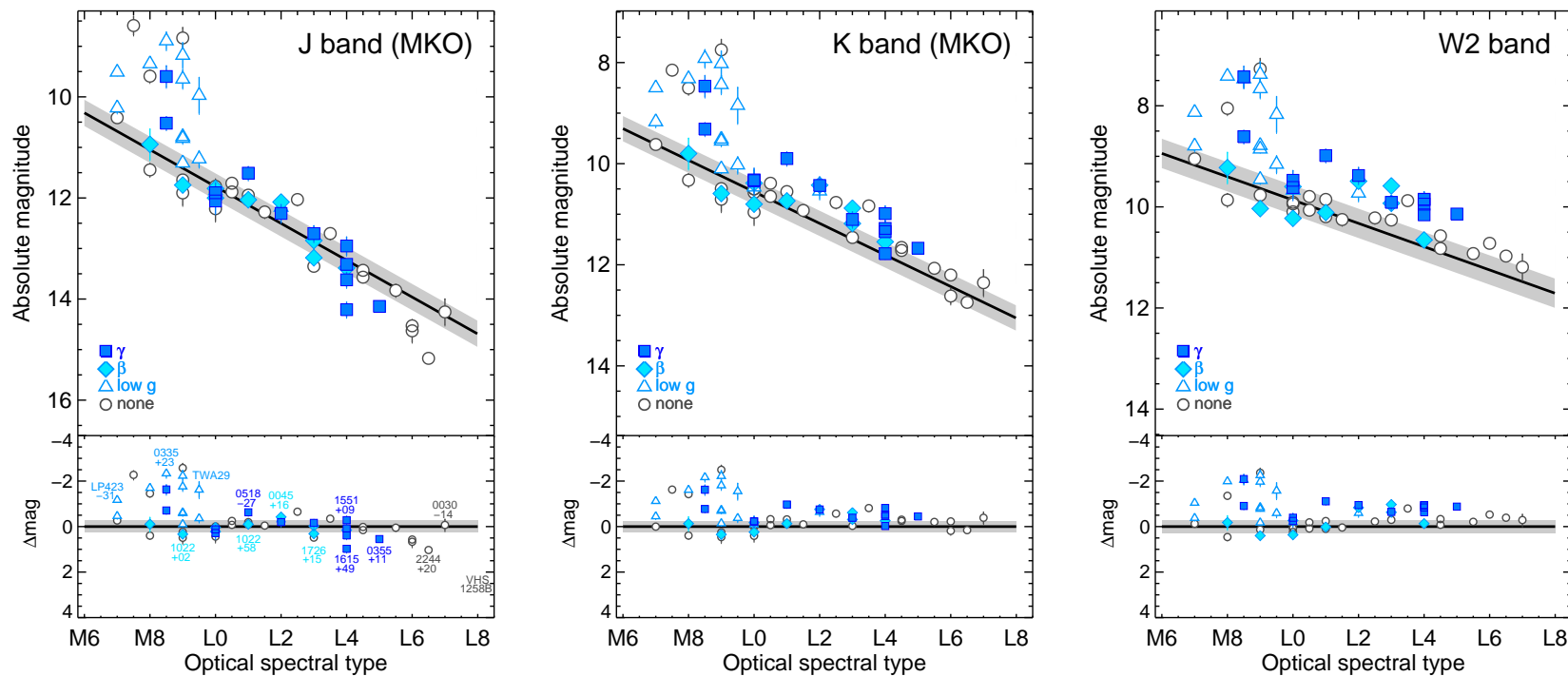


Fig. 9.— Absolute magnitudes in the  $J_{MKO}$ ,  $K_{MKO}$ , and  $W2$  bandpasses, as a function of optical spectral type and gravity classifications, with the latter following the system of Cruz et al. (2009). Objects labeled as “low g” are reported in the literature as being low gravity but do not have a formal gravity classification. Objects labeled as “none” have optical spectral types but no gravity classification. See Figure 6 caption for further details.

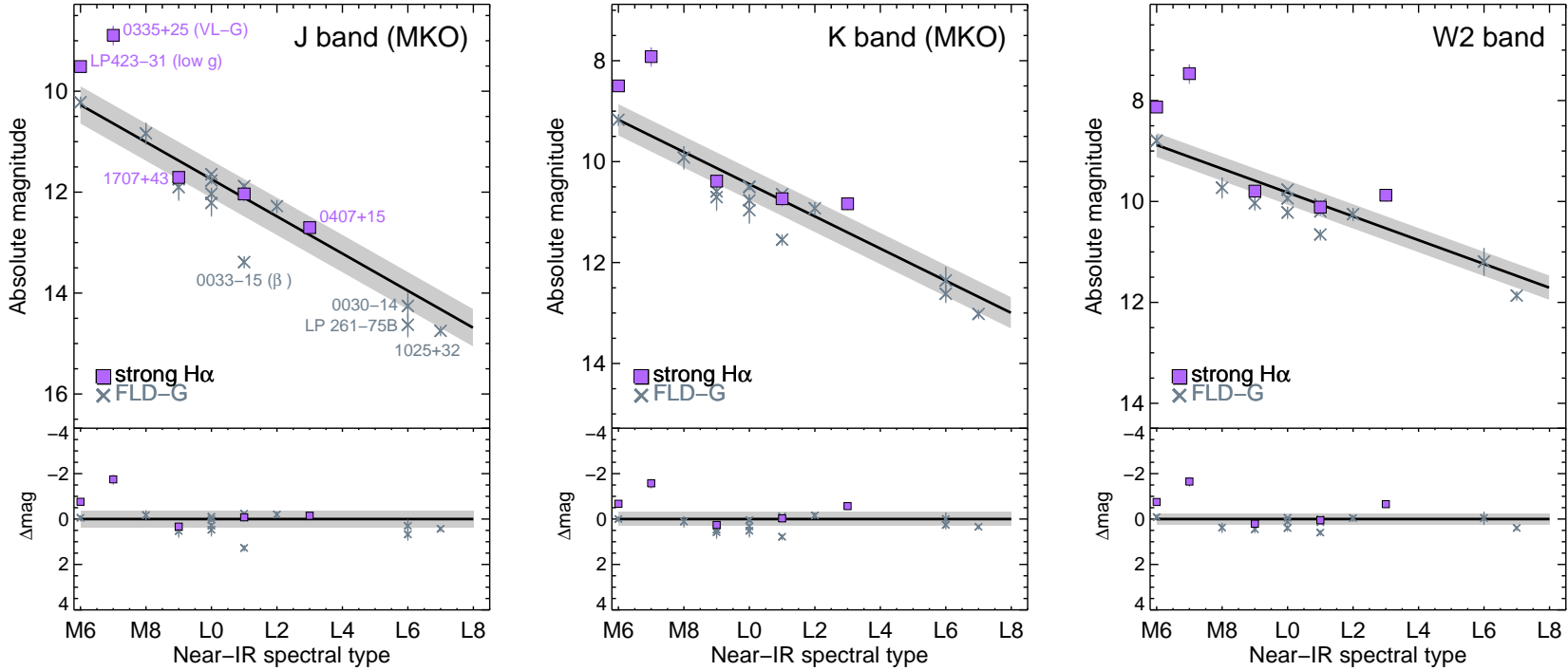


Fig. 10.— Absolute magnitudes in the  $J_{MKO}$ ,  $K_{MKO}$ , and  $W2$  bandpasses for our CFHT targets with FLD-G gravity classifications or with strong H $\alpha$  emission. Note that 2MASS J0033–1521 is classified as L1 FLD-G in the near-IR but L4 $\beta$  in the optical. See Figure 6 caption for further details. (The H $\alpha$  emitting L dwarf 2MASS J1315–2649 is not shown here as it does not have component spectral types on the Allers & Liu 2013a system.)

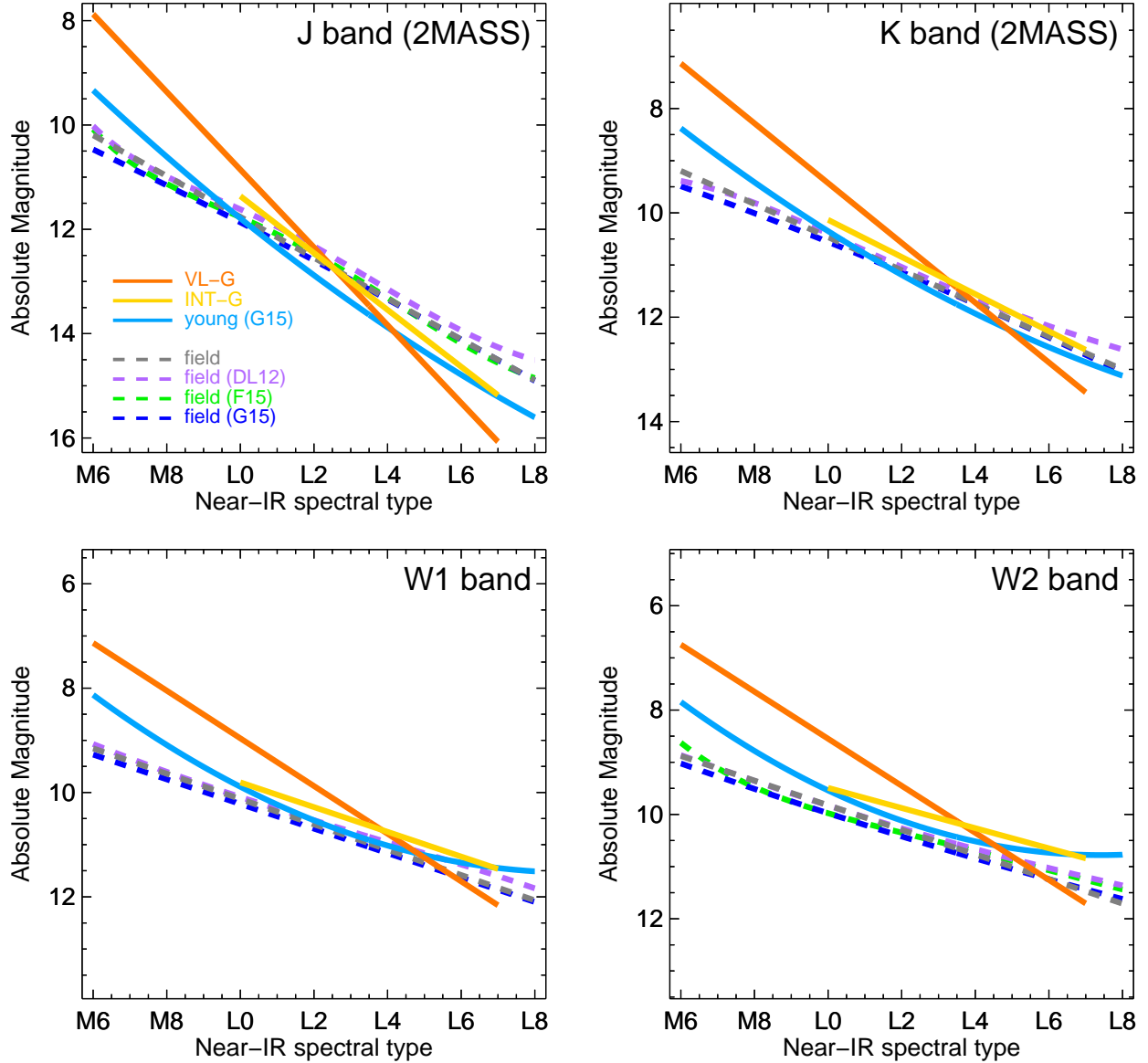


Fig. 11.— Comparison of polynomial fits for absolute magnitude as a function of near-IR spectral type. Fits for low-gravity objects are plotted as solid lines, with the VL-G (solid orange) and INT-G (solid yellow) relations from this work and the young relation from Gagné et al. (2015a) also plotted (solid medium blue). Fits for field objects are plotted as dashed lines, showing the ones for late-M and L dwarfs from this work (dashed grey) and Gagné et al. (2015a, dashed dark blue), and the ones for all ultracool dwarfs from Dupuy & Liu (2012, dashed purple) and Filippazzo et al. (2015, dashed green). The field dwarf relations are all in good agreement, while the low-gravity relations differ.

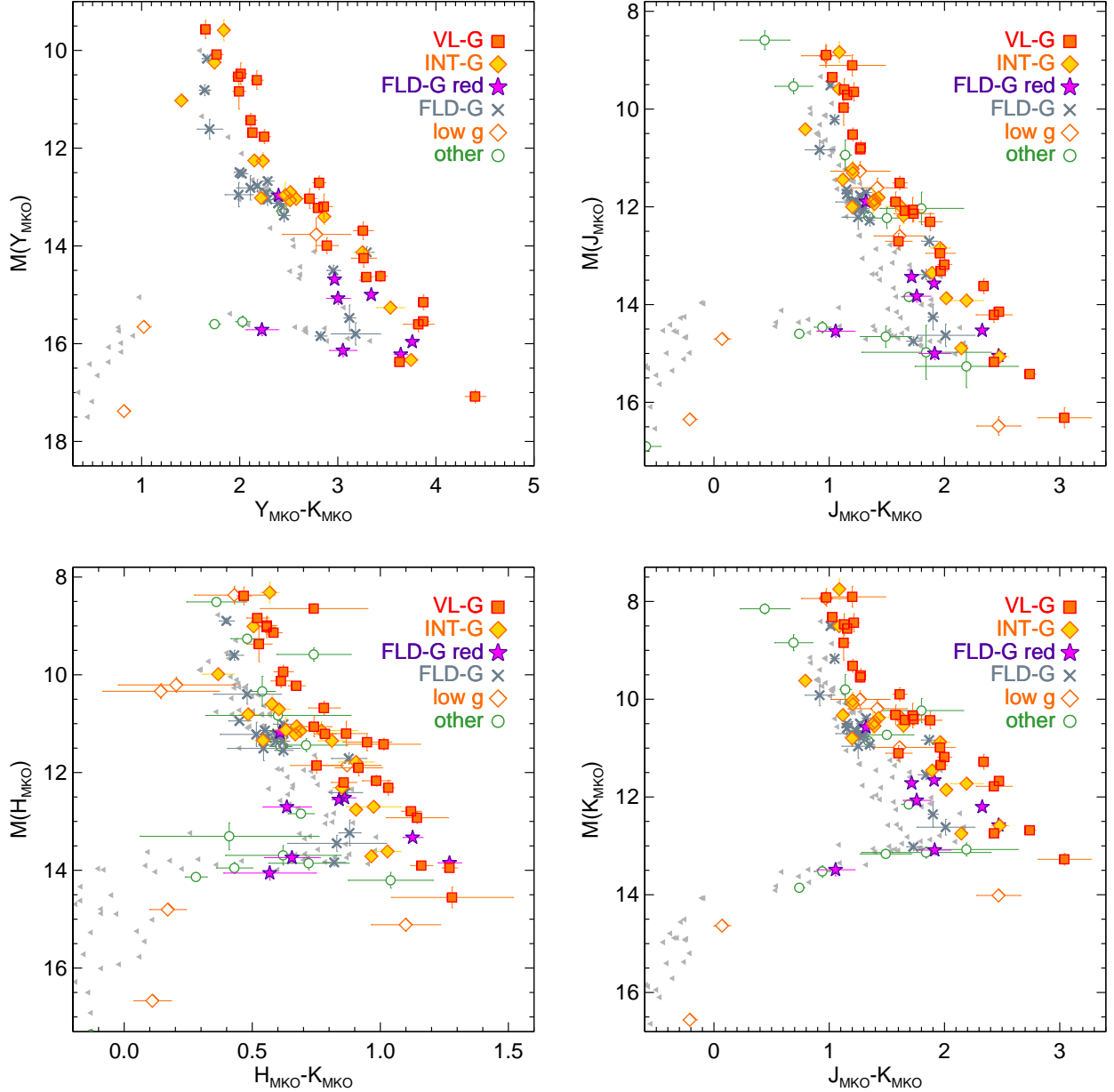


Fig. 12.— Color–magnitude diagrams showing our full sample of potentially young ultracool ( $\geq M6$ ) dwarfs with parallaxes from CFHT or the literature. All CMD plots span 9.5 mag in absolute magnitude. Objects are plotted according to their Allers & Liu (2013a) gravity classification (VL-G, INT-G and FLD-G) when available. Objects having low-gravity IR spectra but without a formal classification are labeled “low g.” Field-gravity objects noted as being unusually red in the near-IR are labeled “FLD-G red.” Open circles represent objects without any spectral gravity information (“other”); these are mostly companions and objects outside the M6–L7 spectral type range covered by the Allers & Liu (2013a) gravity system. For comparison, normal field objects (as described in Section 4.1) are shown as small gray triangles (from Dupuy & Liu 2012, updated at <http://www.as.utexas.edu/~tdupuy/plx>). We only plot (old) field objects with apparent magnitude errors  $< 0.10$  mag in the two bands used to compute the color and absolute magnitude errors  $< 0.10$  mag, and for clarity we do not plot error bars. For all the CMD plots, we exclude the young objects with  $S/N < 5$  parallaxes (GJ 3276, 2MASS J0557–1359, and 2MASS J0619–2903; all likely to be very young, as discussed in the Appendix) and also LP 261-75A (M4.5), given its earlier spectral type. Two very bright objects are off all the CMD plots (2MASS J0435–1414 [M7 VL-G] and TWA 8B [M6 VL-G]), and likewise the companion Gl 504b is too faint to appear.



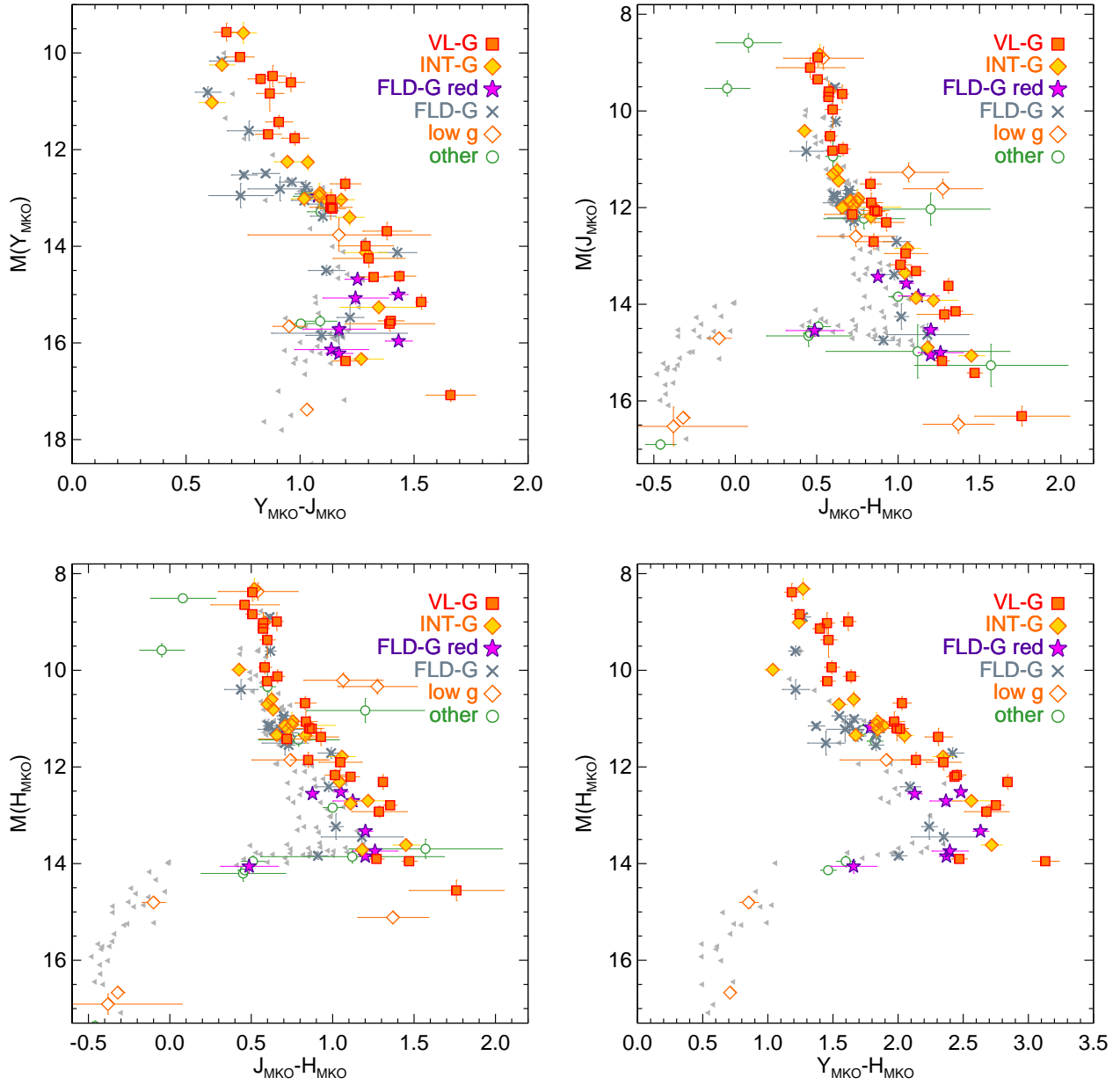


Fig. 12.— (continued) The faintest, bluest objects on the CMD plots involving  $J-H$  are Ross 458C and 51 Eri b (the one with the larger color uncertainties).

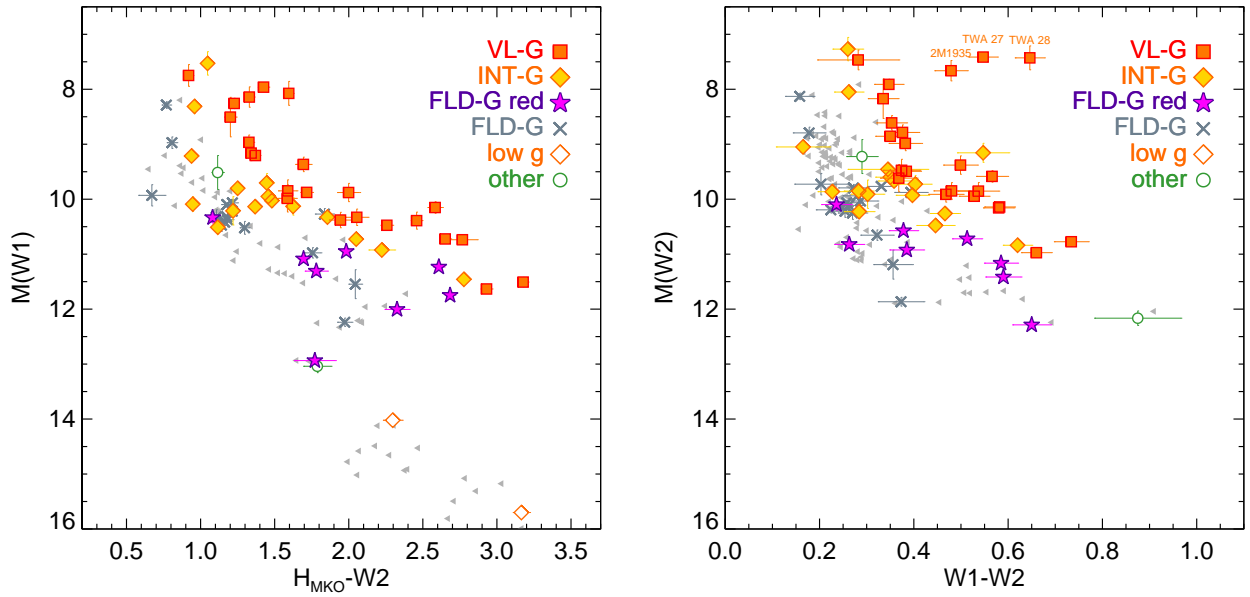


Fig. 13.— Same as Figure 12 but for *WISE* magnitudes. In order to more clearly show the gravity sequence, we restricted the  $W1 - W2$  color range, which causes the T dwarfs SDSS J1110+0116 and Ross 458C be off the right plot. Likewise, the right plot labels the three young objects with evidence for a mid-IR excess (TWA 27 [2MASS J1207–3932], TWA 28 [SSSPM J1102–3431], 2MASS J1935–2846), likely due to circumstellar material (see Appendix).

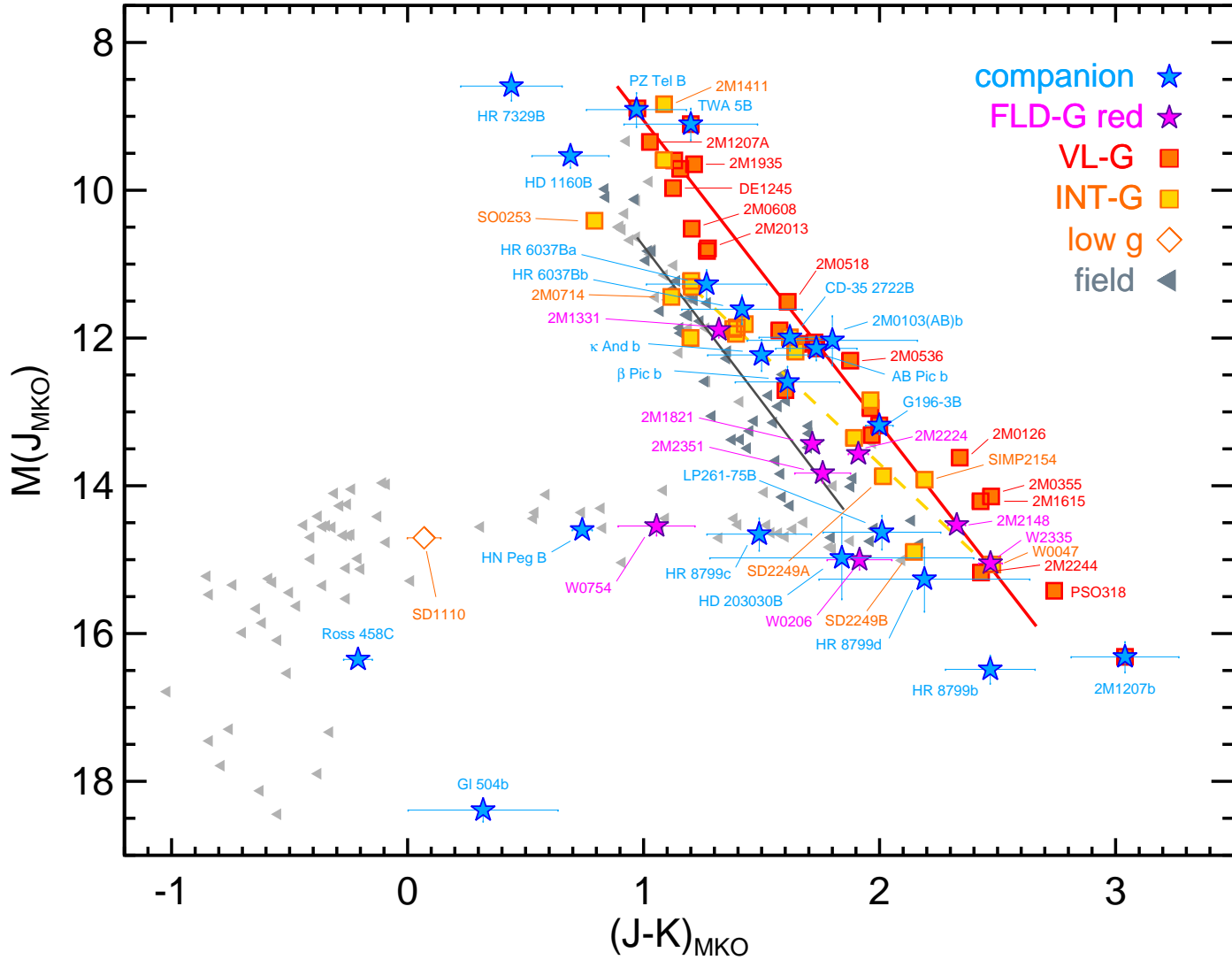


Fig. 14.— Color-magnitude diagram showing young ultracool companions with parallaxes in comparison to our low-gravity parallax sample (VL-G and INT-G). Normal field objects (gray triangles) are the same as in Figure 12. (The young companions GSC 08047–00232 B ( $M_{9.5 \pm 1}$ ; Chauvin et al. 2003; Neuhäuser & Guenther 2004; Chauvin et al. 2005a), 1RXS J235133.3+312720 ( $L_{0.1}^{+2}$ ; Bowler et al. 2012), 2MASS J01225093–2439505 B ( $L_{3.7 \pm 1.0}$ ; Bowler et al. 2013; Hinkley et al. 2015), and GU Psc b ( $T_{3.5 \pm 1}$ ; Naud et al. 2014) are not plotted, as they do not have parallactic distances.)

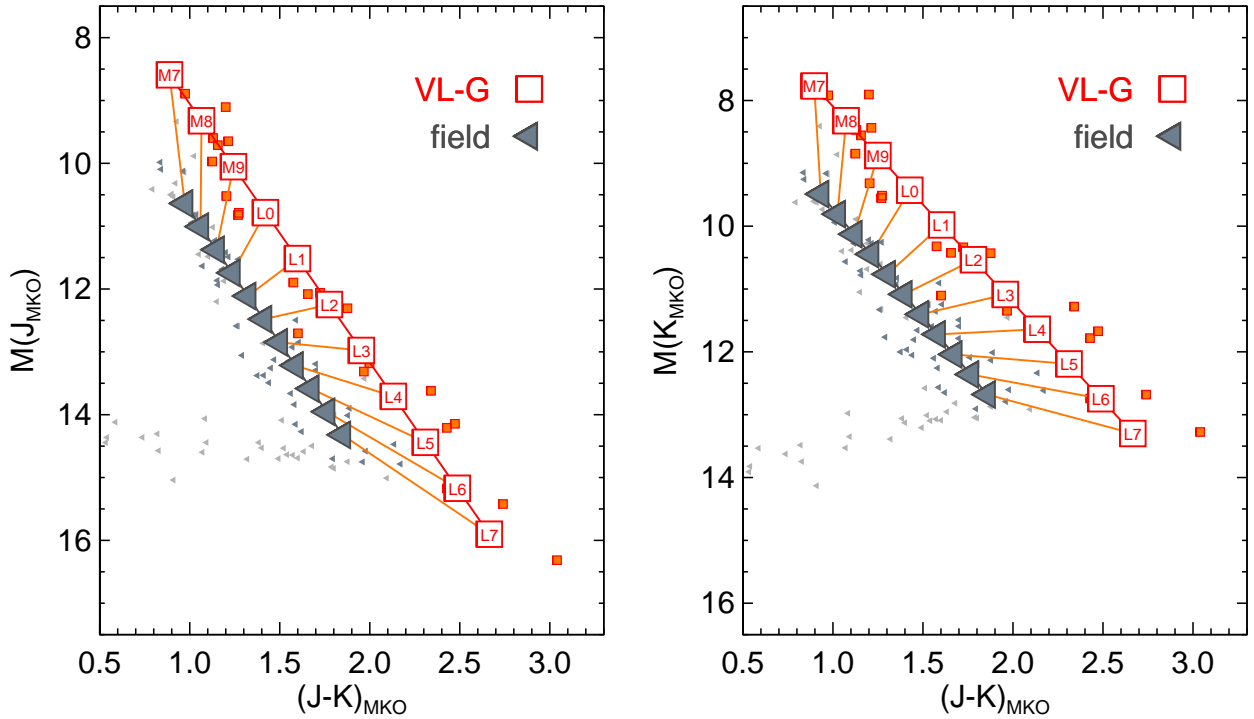


Fig. 15.— Color–magnitude diagram showing our lowest-gravity parallax sample (VL-G; small orange squares) alongside normal field objects (small gray triangles, same as in Figure 12). For each population we fitted a line to absolute magnitude as a function of color for objects with spectral types M7–L7. Combining these fits with the linear spectral type to absolute magnitude relations from Table 10 allows us to plot the mean location of each spectral type for each population on the color–magnitude diagram. Mean colors and magnitudes for low-gravity objects are marked by large, labeled open squares with orange lines connecting them to the mean field population location of the same spectral type. On average, the low-gravity sequence is brighter in both  $J$  and  $K$  at roughly the same  $J - K$  color as the field for early spectral types. Then, going to later spectral types, the low-gravity sequence gradually becomes redder in  $J - K$  as it becomes much fainter in  $J$  and somewhat fainter in  $K$ . (Only field objects with near-IR spectral types were used in that fit, indicated by darker gray triangles.)

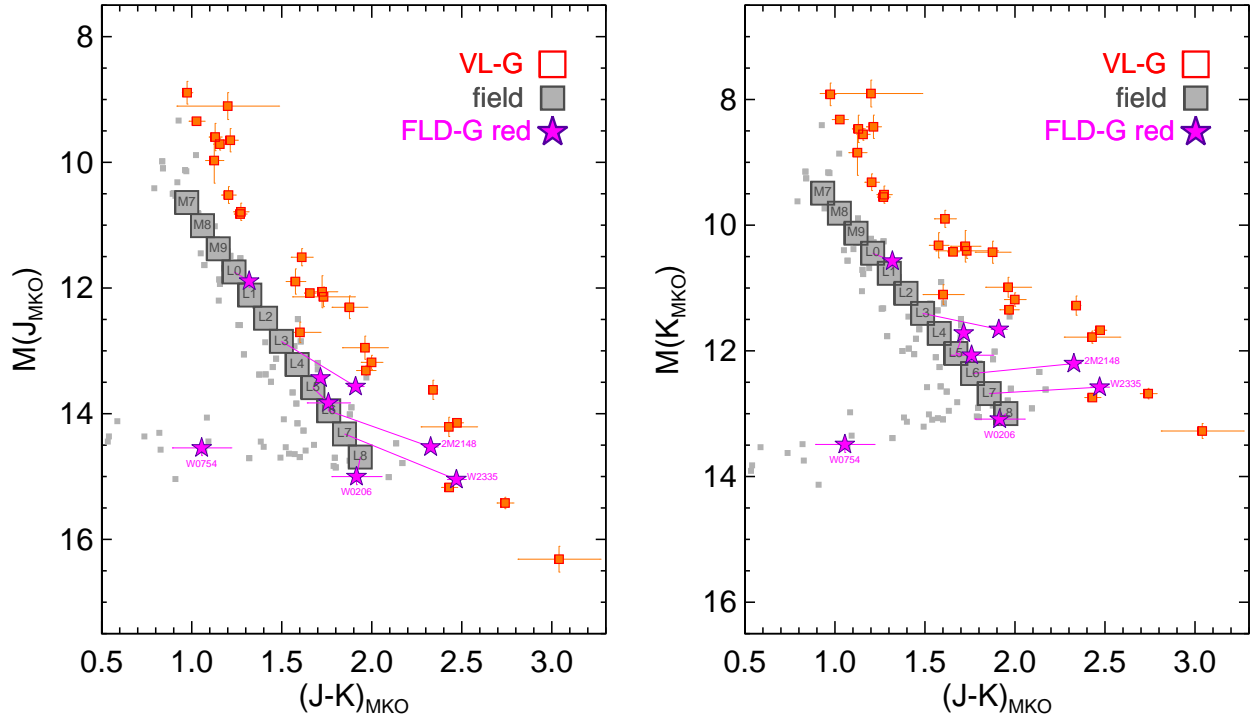


Fig. 16.— Color–magnitude diagram showing the CMD location of our unusually red field-gravity objects compared to our lowest-gravity parallax sample (VL-G; small orange squares) and normal field objects (small gray triangles, same as in Figure 12). Similar to Figure 15, the mean field sequence as a function of near-IR spectral type is shown with labeled gray squares. For each red object, a line connects its CMD position with the corresponding field value for the same near-IR spectral type.

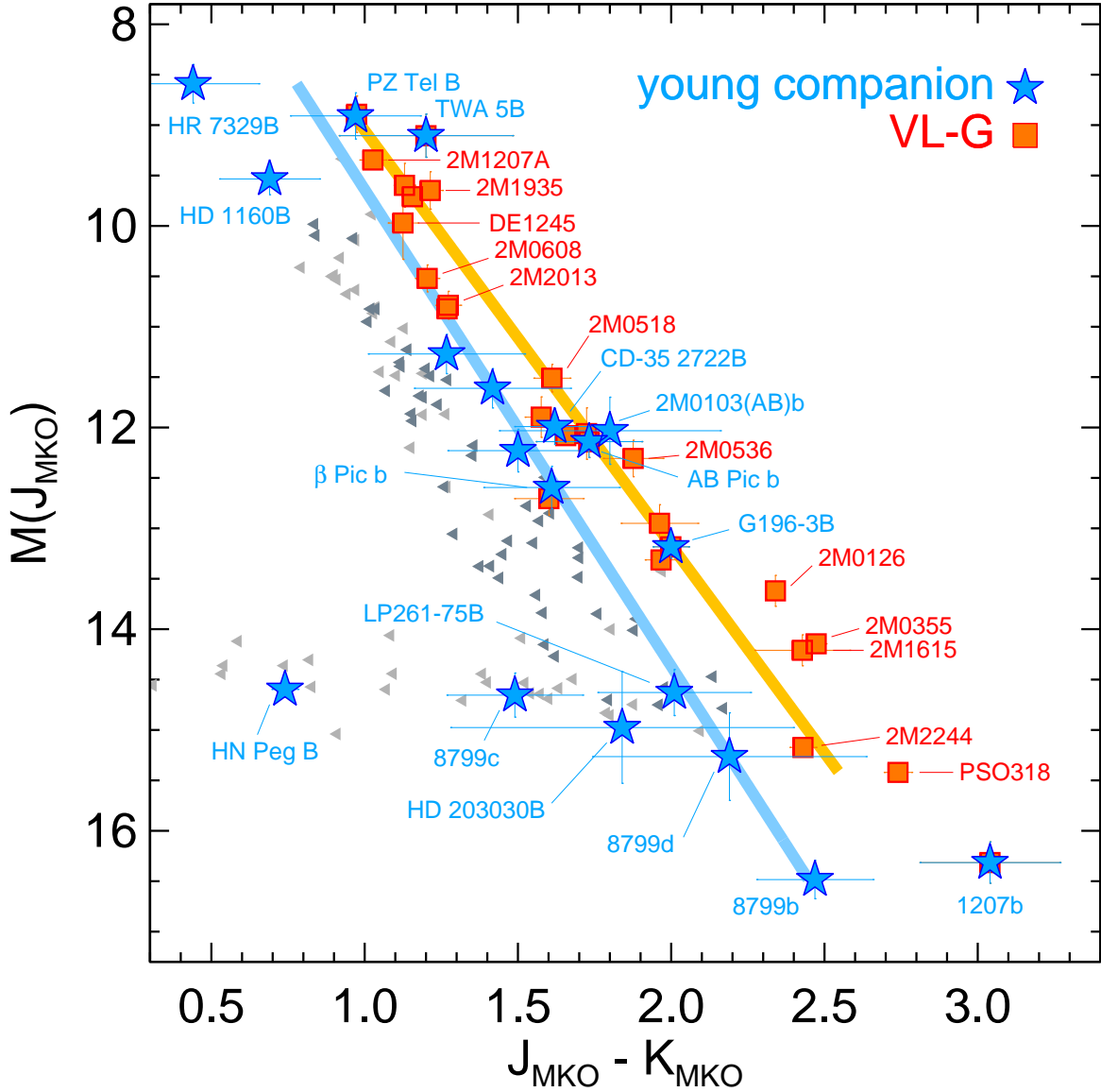


Fig. 17.— Color–magnitude diagram highlighting the late-M to late-L VL-G sequence compared to young ultracool companions with parallaxes, using the same data as in Figure 14. The solid lines show robust linear fits through the two datasets. (Given its extreme nature, 2MASS J1207–3932b is excluded from the fitting, as is the T2.5 companion HN Peg B given its spectral type is later than the VL-G sample here.) Note that three companions have VL-G classifications so they are plotted as a blue star overlaid on a red square: TWA 5B, AB Pic b, and G 196-3B.

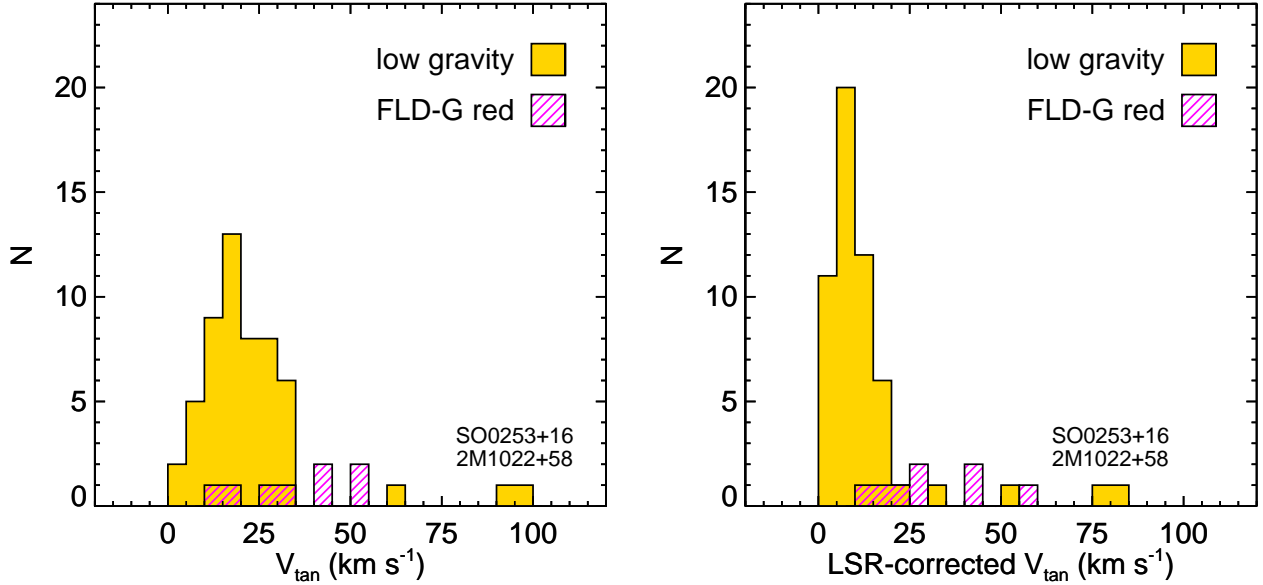


Fig. 18.— Tangential velocities are shown for all objects with some spectral signatures of low gravity (orange) and for unusually red field objects (hatched magenta). The two plots show the observed tangential velocity (*left*) and the LSR-corrected tangential velocity (*right*). Two low-gravity objects 2MASS J1022+5825 (optical L1 $\beta$ , near-IR L1 FLD-G) and SO J0253+1652 (near-IR M7.5 INT-G; a.k.a. Teegarden’s Star) have observed tangential velocities of  $\approx 100 \text{ km s}^{-1}$  in contrast to almost all other low-gravity objects, which have  $V_{\text{tan}} \lesssim 35 \text{ km s}^{-1}$ . This suggests either truly young objects acquire large space motions soon after birth or cases of old objects that somehow display spectral signatures of youth. The red FLD-G objects with  $V_{\text{tan}} > 35 \text{ km s}^{-1}$  are either at the earliest spectral types (2MASS J1331+3407) or latest (WISE J0206+2640, WISE J0754+7909).

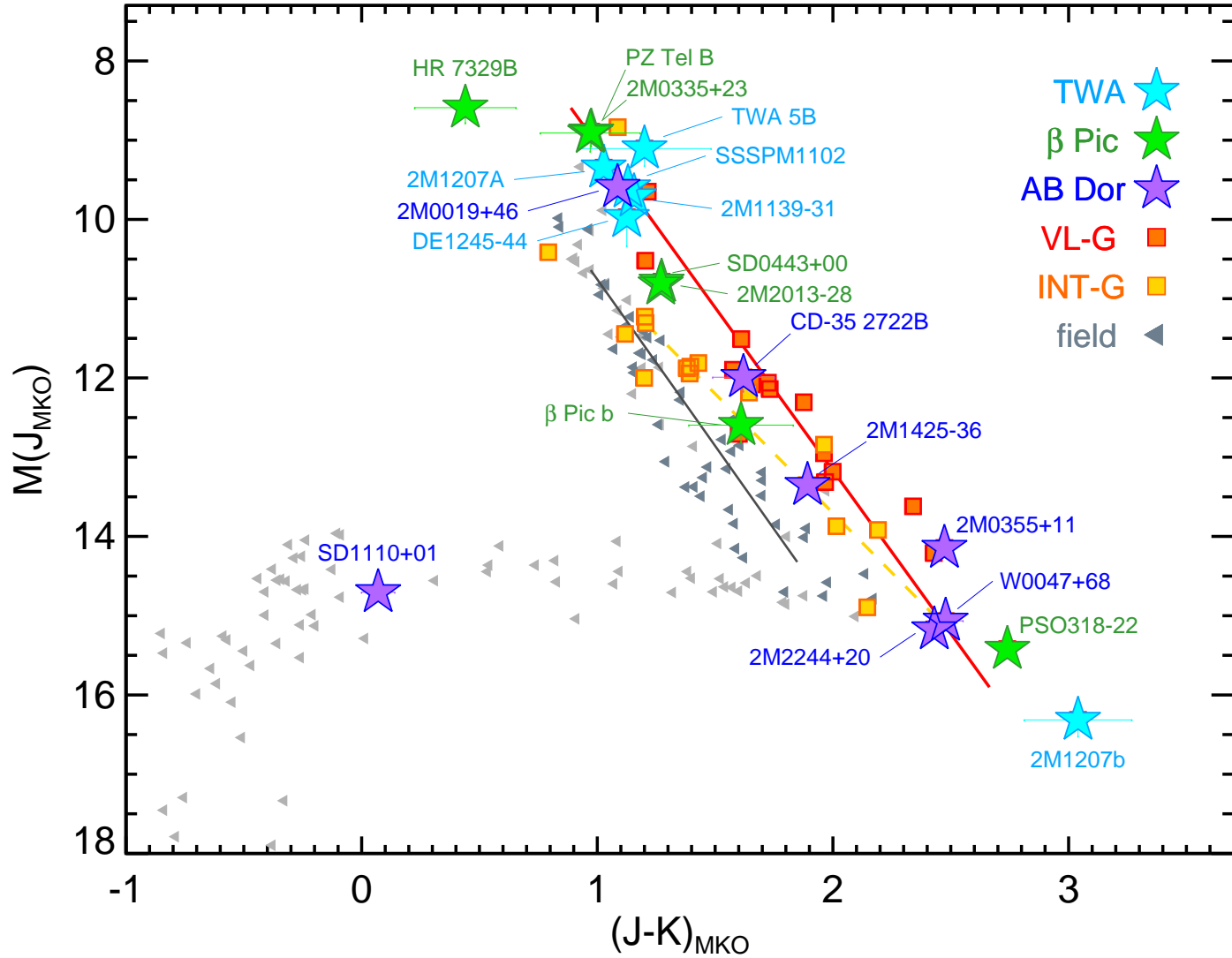


Fig. 19.— Color-magnitude diagram showing members of the three young moving groups with the most ultracool dwarfs identified to date: TWA ( $\approx 10$  Myr),  $\beta$  Pic ( $\approx 25$  Myr), and AB Dor ( $\approx 150$  Myr). Our low-gravity parallax sample (VL-G and INT-G) and the field population are shown for comparison, along with their linear fits (Section 4.2). The darker triangles show the subset of field objects used for the new M7–L7 linear fit (Section 4.1).



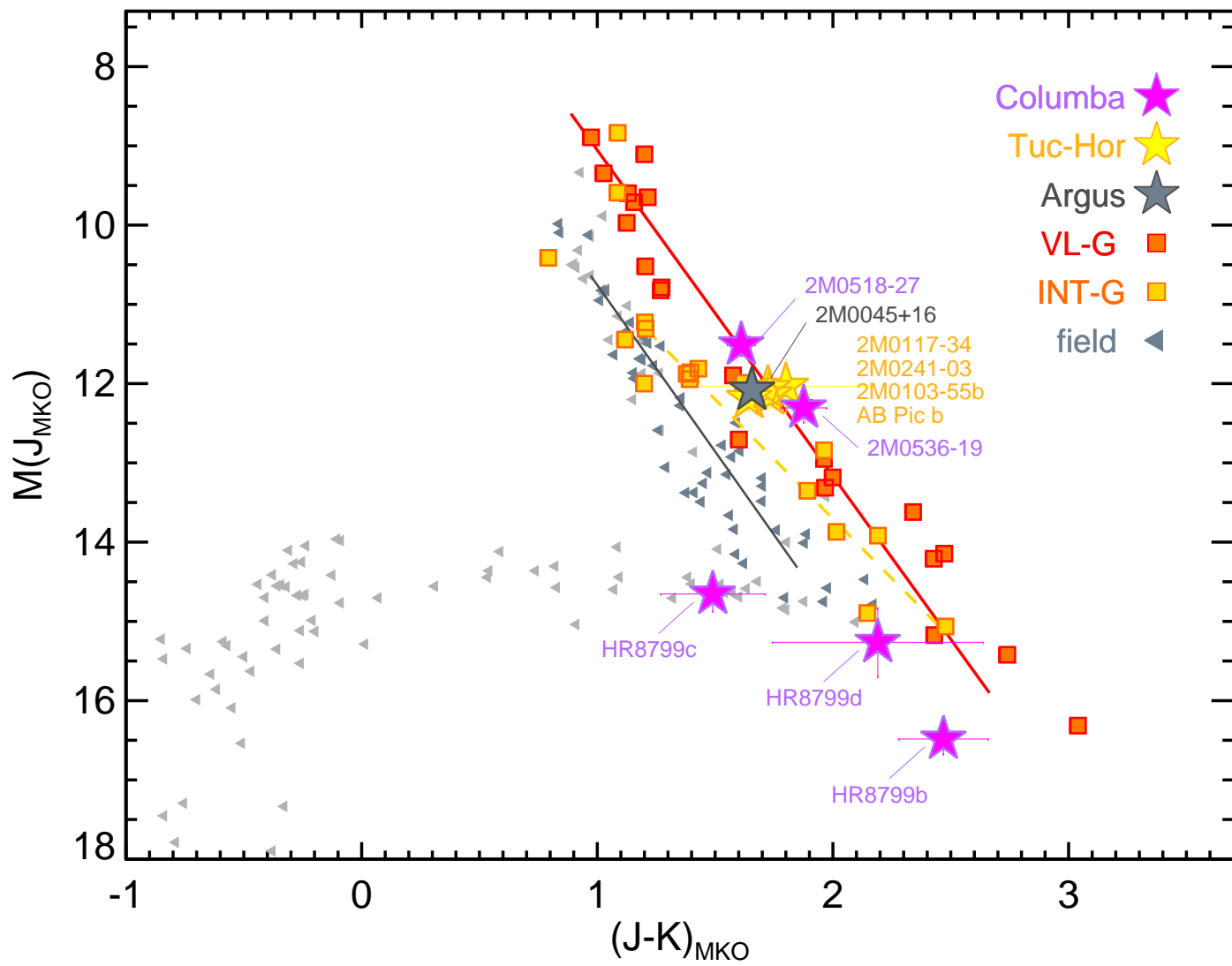


Fig. 20.— Same as Figure 19, for the more sparsely populated Columba ( $\approx 40$  Myr), Tuc-Hor ( $\approx 50$  Myr), and Argus (uncertain age) groups, with ages from Bell et al. (2015).

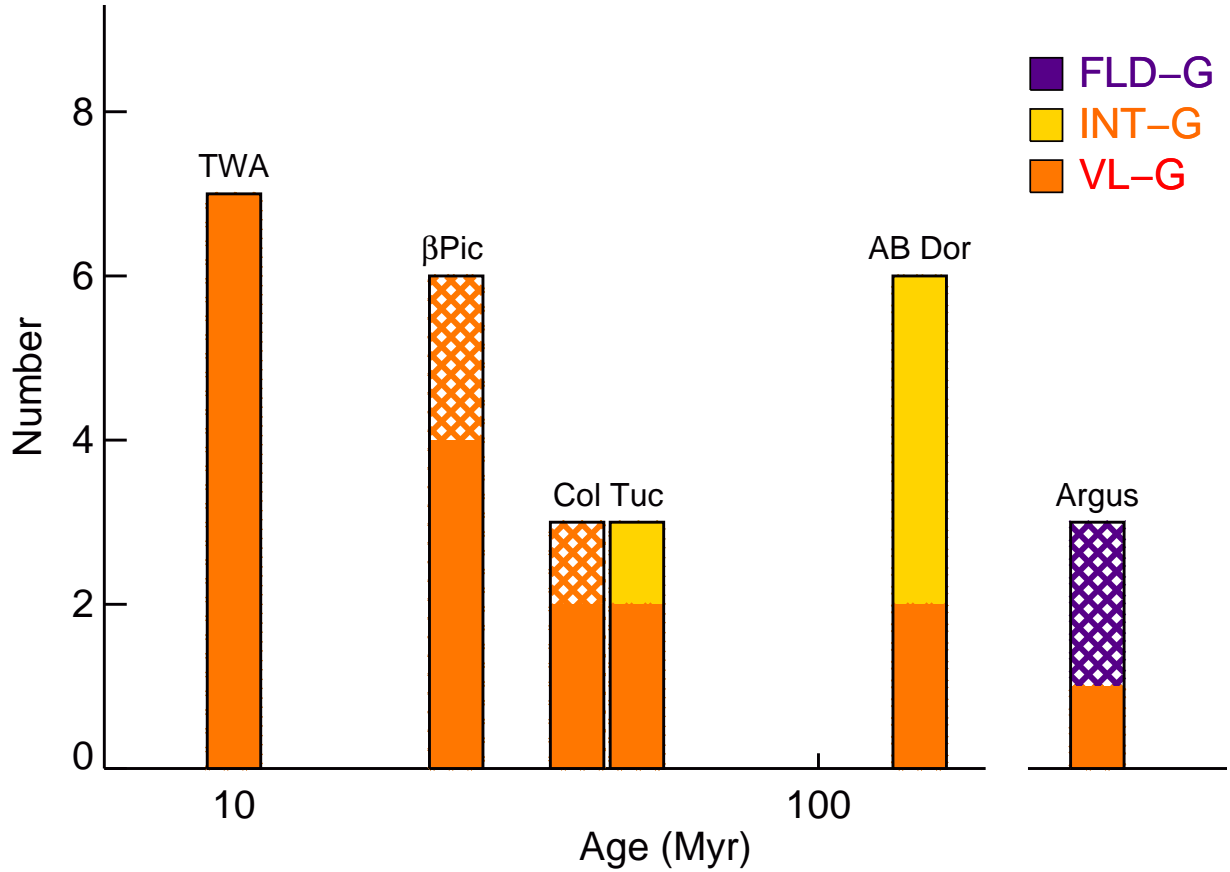


Fig. 21.— Distribution of near-IR gravity classifications for different moving groups. The x-axis is logarithmically spaced, with assumed ages of 10, 24, 42, 45, and 149 Myr for the TWA,  $\beta$  Pic, Columba, Tuc-Hor, and AB Dor groups (Bell et al. 2016) and with an indeterminate age for Argus. (The ages of Columba and Tuc-Hor have been nudged by 8% to avoid overlapping bars.) Objects with uncertain group membership are represented by hatched regions. (We have excluded 2MASS J0058–0651 [L1 INT-G] from this plot, given its possible membership in both the  $\beta$  Pic and AB Dor groups.) The VL-G objects dominate the younger groups but are a minority by the age of AB Dor. The groups with intermediate ages may have an intermediate fraction of VL-G objects but larger samples of group members are needed for an assessment.

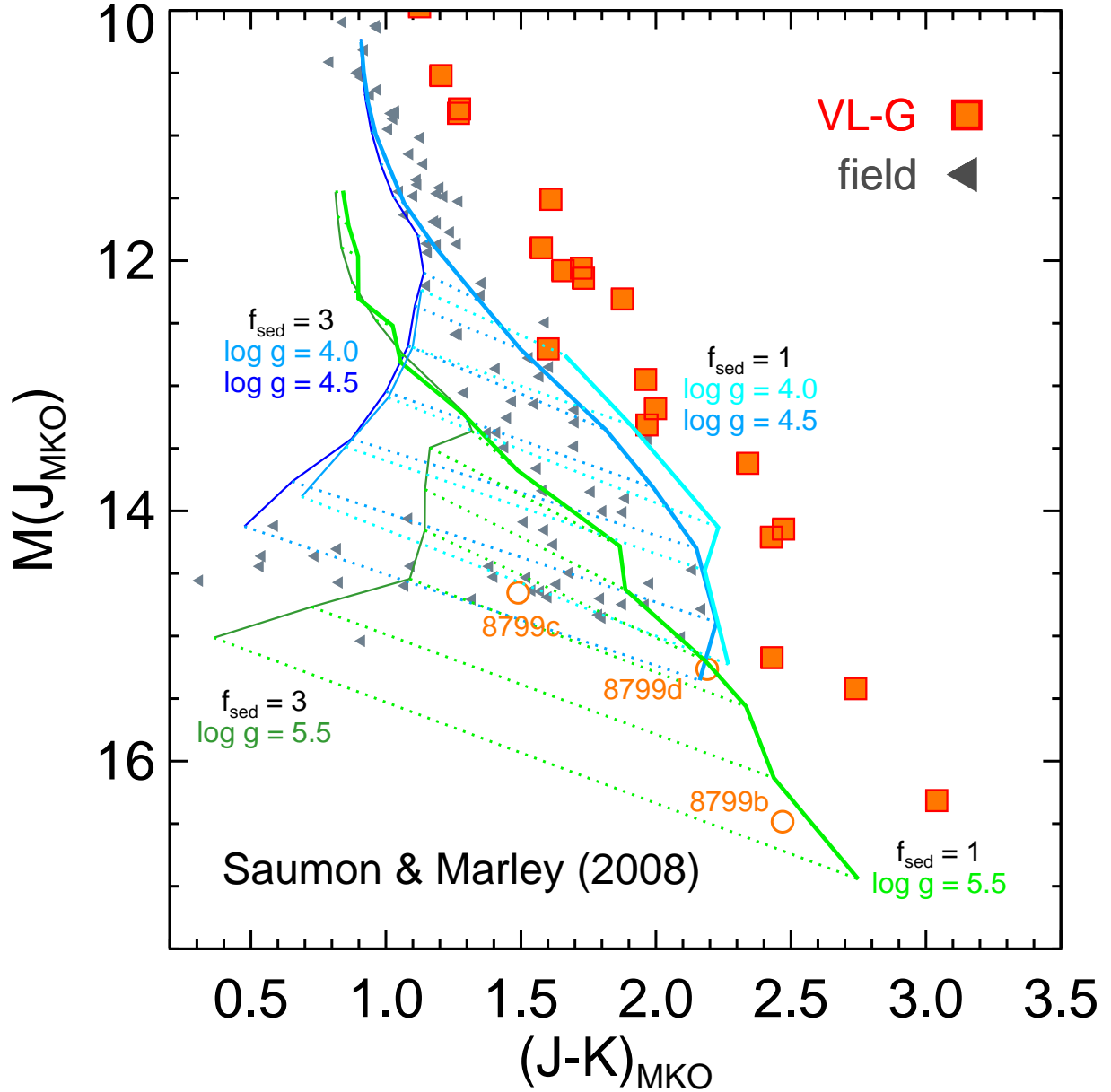


Fig. 22.— Color–magnitude diagram showing model-atmosphere grids from Saumon & Marley (2008) alongside our low-gravity parallax sample (VL-G) and the field population. We plot model sequences having thick clouds and redder near-IR colors ( $f_{\text{sed}} = 1$ ) as well as thin clouds and bluer near-IR colors ( $f_{\text{sed}} = 3$ ). Dotted lines connect models of the same  $T_{\text{eff}}$  and  $\log(g)$  but different  $f_{\text{sed}}$ , showing the effect of cloud thickness. We plot the highest gravity models ( $\log(g) = 5.5$  dex in green) for comparison to lower gravities ( $\log(g) = 4.0, 4.5$  dex in blue), where the lowest gravities are only complete for  $T_{\text{eff}} = 1100\text{--}1500$  K. Although these models successfully reproduce planetary-mass objects such as HR 8799b, they do not accurately follow the low-gravity sequence defined by our sample.

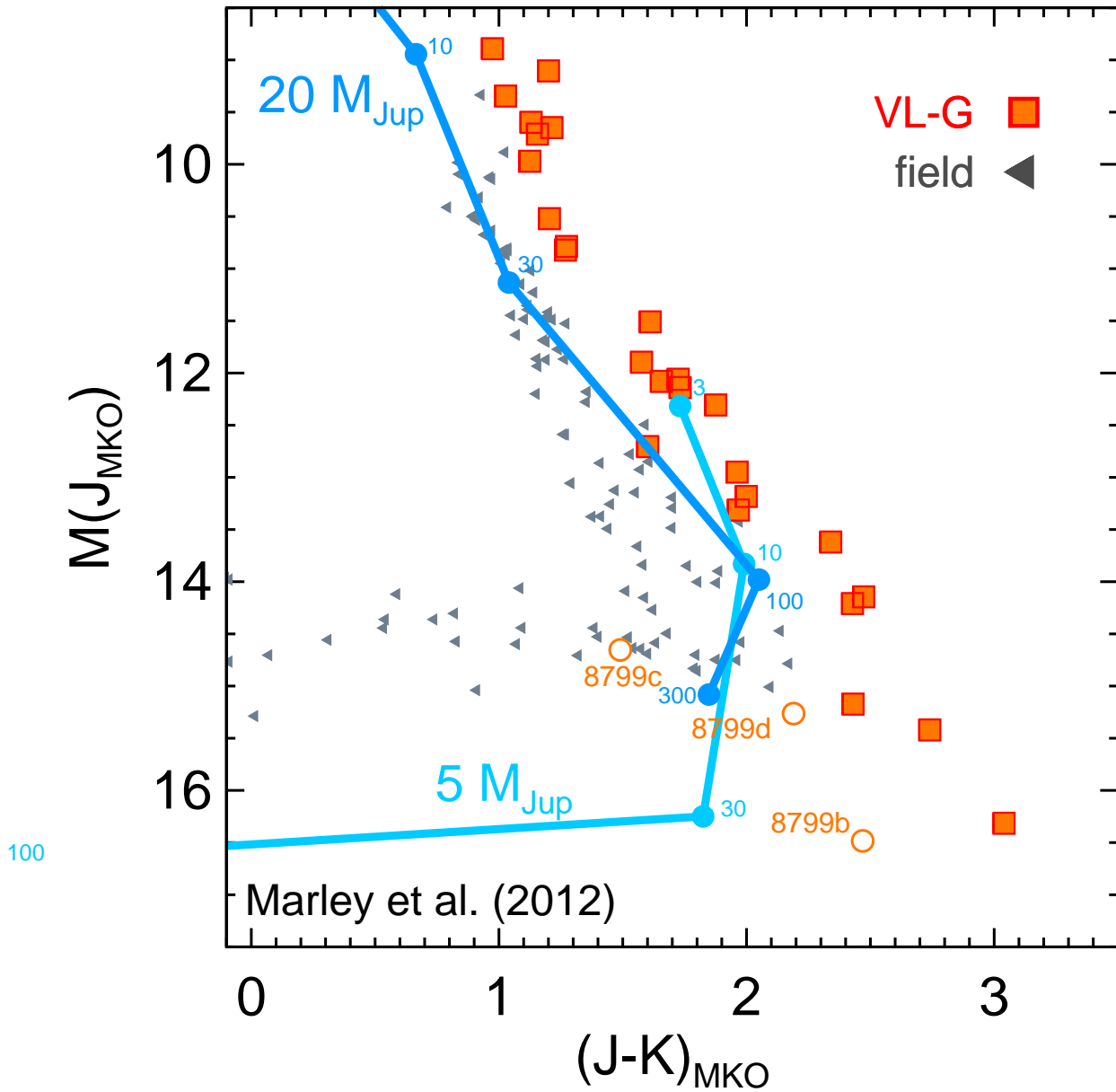


Fig. 23.— Color–magnitude diagram showing Marley et al. (2012) evolutionary models for  $5 M_{\text{Jup}}$  and  $20 M_{\text{Jup}}$  objects. The models use a simple prescription for the gravity-dependence of the L/T transition. Beads plotted along each track demarcate ages in Myr, as young as 3 Myr. Even these models intended for comparison to young planetary-mass objects such as HR 8799b do not accurately follow the low-gravity (VL-G) sequence defined by our sample. (Note that our VL-G sample is expected to include objects above  $20 M_{\text{Jup}}$ . Plotting of these iso-mass model tracks is meant to illustrate the current theoretical locus relative to the data, not to assign actual masses to the VL-G sample using the models.)

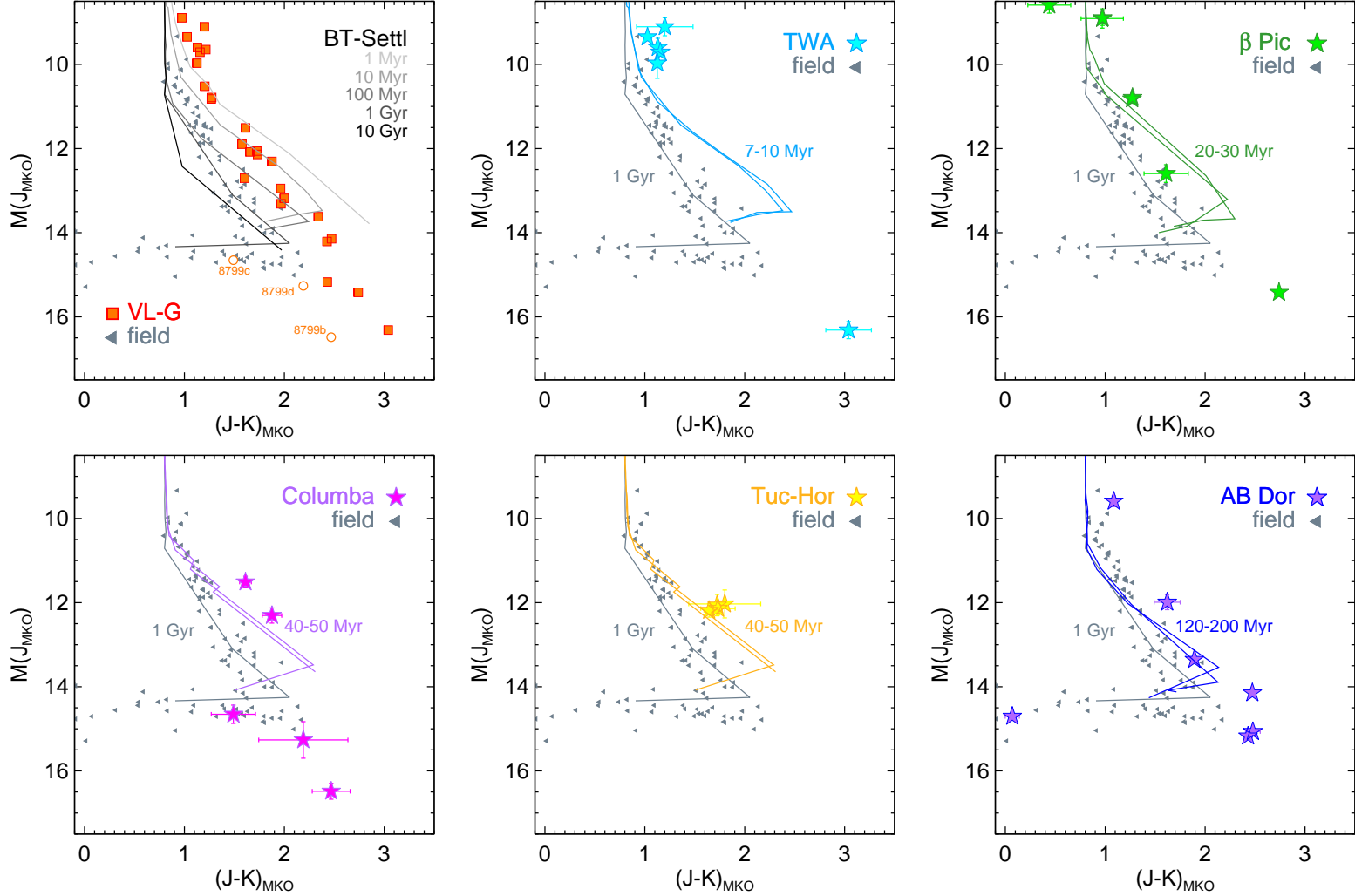


Fig. 24.— BT-Settl evolutionary model isochrones (Baraffe et al. 2015; Allard et al. 2015, in preparation) shown alongside our sample. *Top left:* Our empirical VL-G sequence, the field sequence from Dupuy & Liu (2012), and BT-Settl isochrones ranging from 1 Myr to 10 Gyr. Although older isochrones provide a reasonable match to the field sequence, our VL-G sequence tends to be redder than the models. No model isochrones match the faint ( $M_J \lesssim 14$  mag), red portion of the sequence. *Top middle to bottom right:* Subsets of our sample that belong to young moving groups (10–200 Myr) shown alongside isochrones encompassing each group’s age (Bell et al. 2015). Overall, model isochrones do not tend to match the locus of the observations at any age.

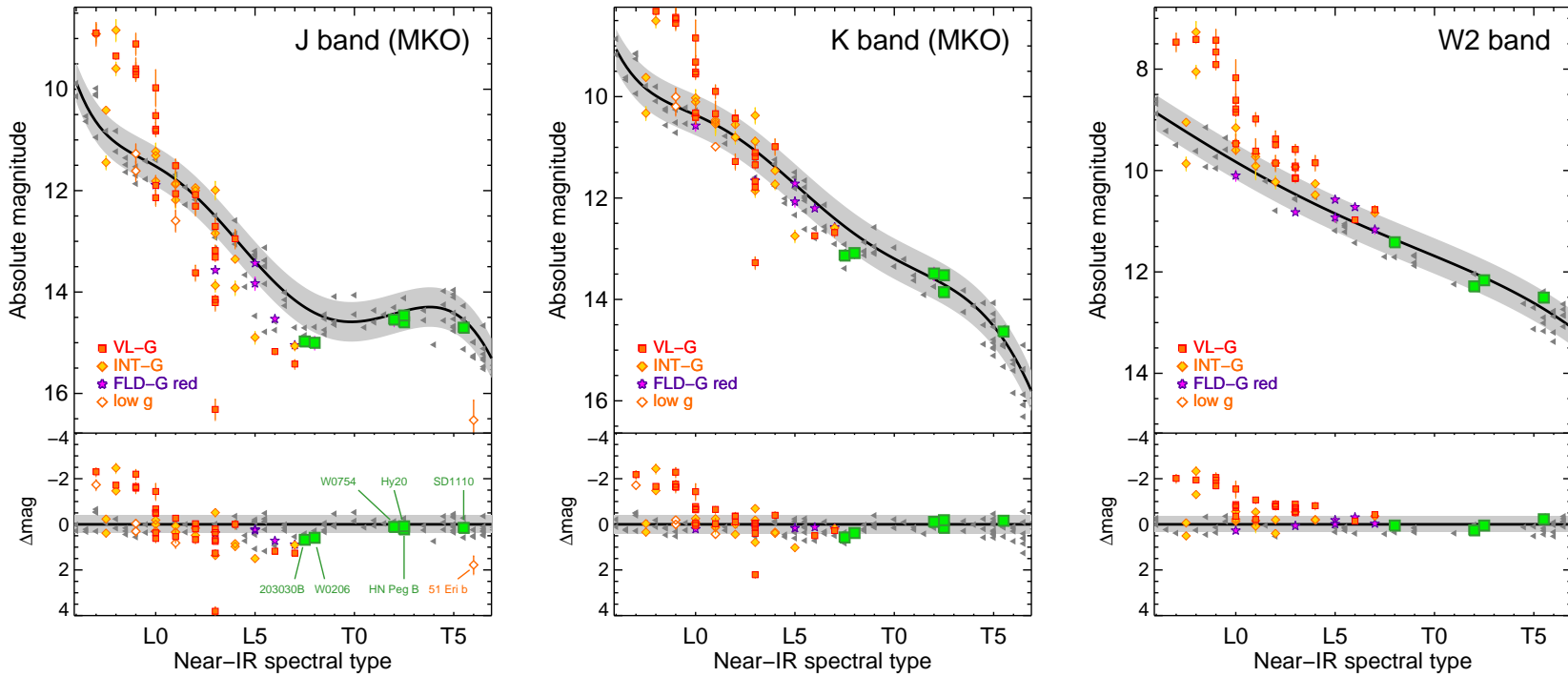


Fig. 25.— Absolute magnitudes versus spectral type for our sample with an expanded range of spectral types, in order to highlight the latest-type objects. The L/T objects are shown as green squares, with the measurement errors comparable to the symbol size. Normal field objects (small grey triangles) are the same as in Figure 12. The heavy black lines are the polynomial fits from Dupuy & Liu (2012), and the grey region shows the RMS about the fits. See Figure 6 caption for further details.

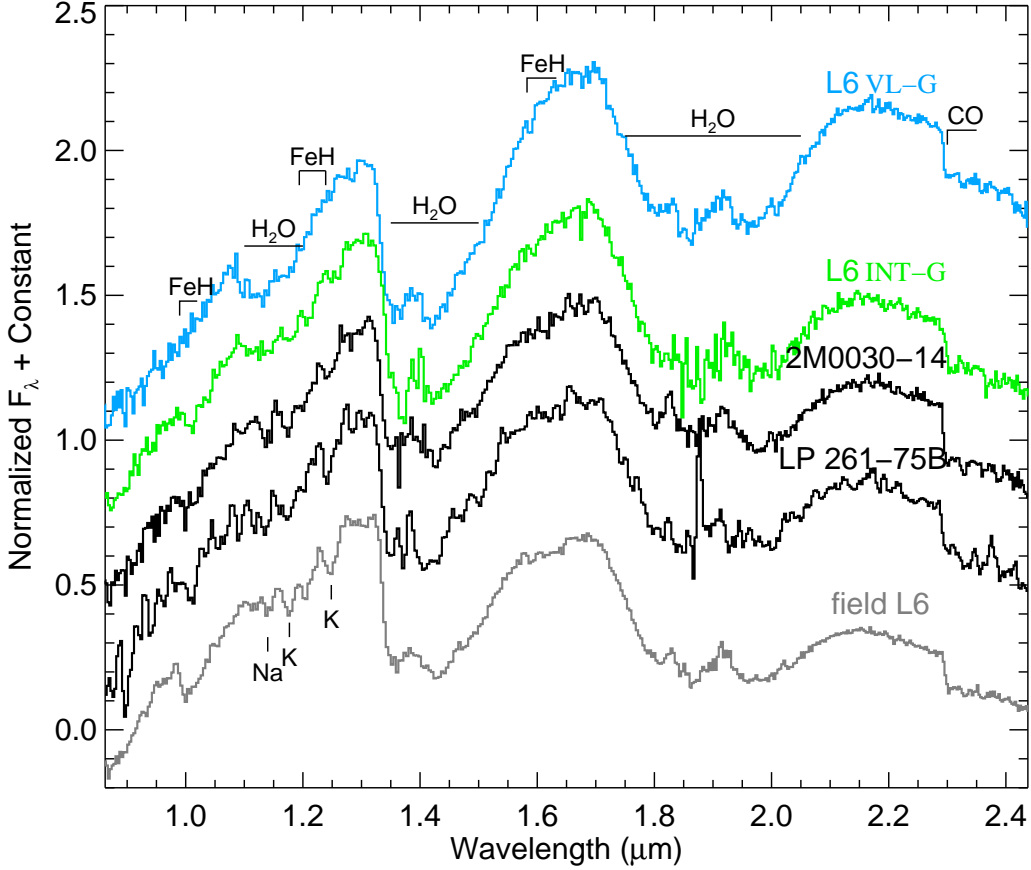


Fig. 26.— Comparison of the spectra of 2MASS J0030–1450 (Burgasser et al. 2010) and LP 261–75B (Bowler et al. 2013) to L6 dwarfs with a range of gravity classifications from Allers & Liu (2013a). The L6 VL-G, INT-G, and FLD-G spectra are 2MASS J2244+2043 (Looper et al. 2008b), 2MASS J0103+1935 (Allers & Liu 2013a), and 2MASS J1010–0406 (Kirkpatrick et al. 2010), respectively. Gagné et al. (2015a) type 2MASS 0030–1450 as L4–L6  $\beta$ , while we assign a spectral type of L6 FLD-G. Bowler et al. (2013) classify LP 261–75B as L4.5 FLD-G, while we assign L6 FLD-G (see Appendix).

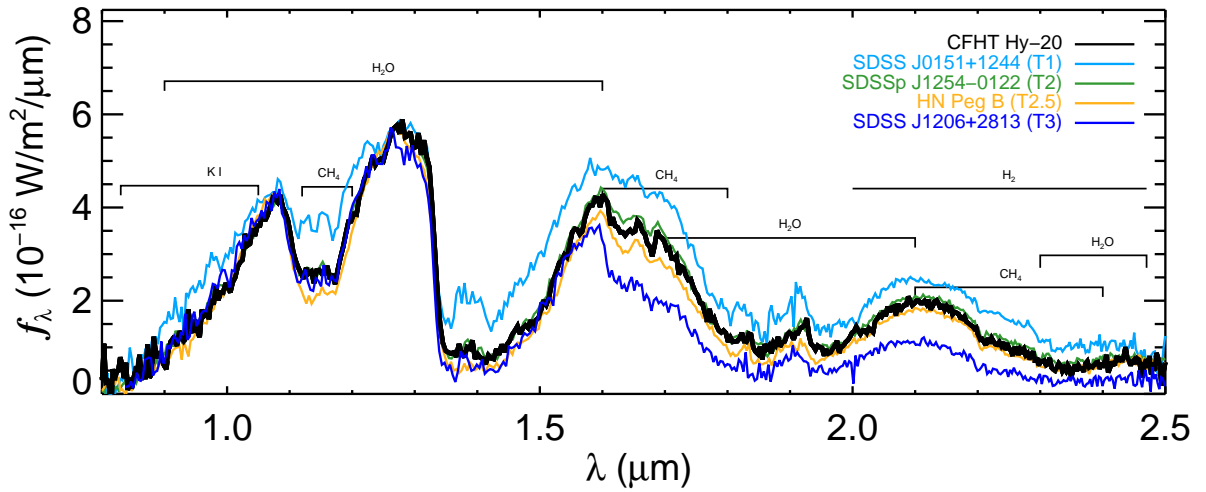


Fig. 27.— Near-IR spectrum of the Hyades member CFHT-Hy-20 compared to the T dwarf spectral standards SDSS J015141.69+124429.6 (T1), SDSSpJ125453.90–012247.4 (T2), and SDSS J120602.51+281328.7 (T3), along with the T2.5 companion HN Peg B.



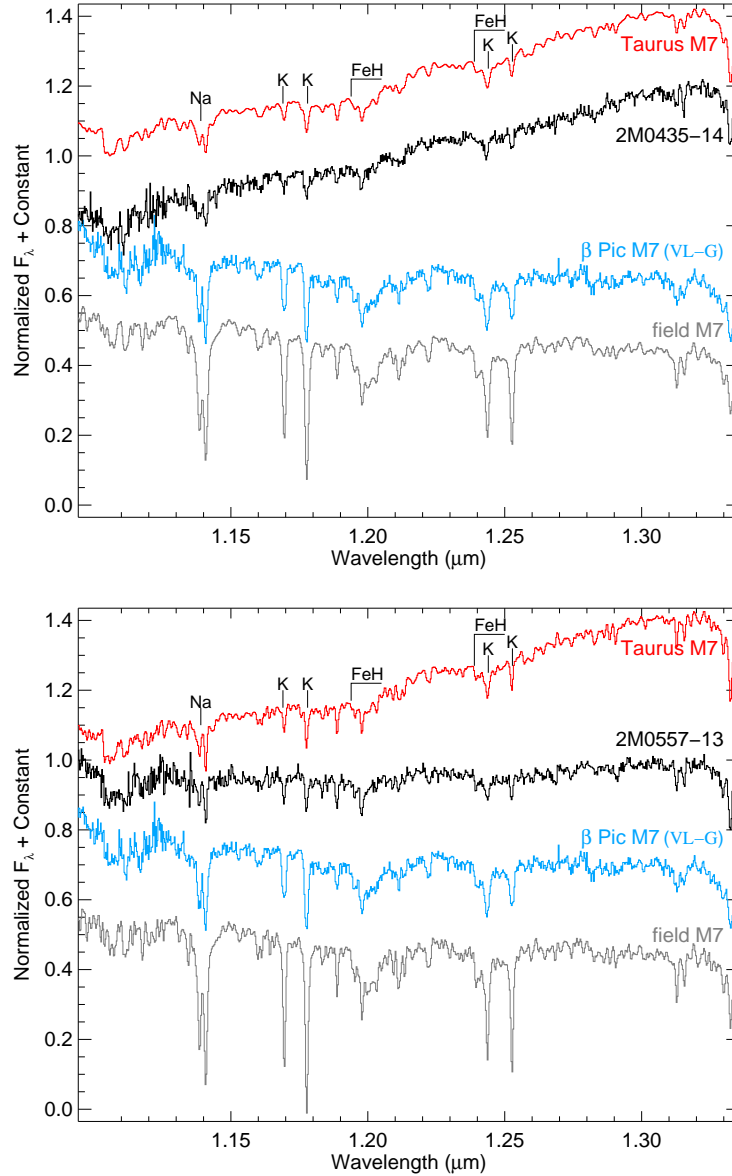


Fig. 28.— Gravity-sensitive features in the Allers & Liu (2013a) spectra of 2MASS J0435–1414 (top;  $R = 750$ ) and 2MASS J0557–1359 (bottom;  $R = 1200$ ) compared to a Taurus M7 dwarf (CFHT-BD-Tau 4; Allers et al. 2009), a  $\beta$  Pic moving group M7 dwarf (2MASS J0335+2342; Allers & Liu 2013a), and a field M7 dwarf (GJ 644C; Cushing et al. 2005). For each panel, all the plotted spectra have been smoothed to a common spectral resolution. The Taurus M7 spectrum shows slightly deeper K I, Na I, and FeH absorption, indicating that 2MASS J0435–1414 and 2MASS J0557–1359 are likely very young ( $\lesssim 3$  Myr old). (The difference in the overall continuum slopes of 2MASS J0435–14 and CFHT-BD-Tau 4 compared to the older objects can be minimize for assumed extinctions of  $A_V = 4.5$  and  $3.0$ , respectively, though we do not attempt to robustly determine the extinction here.)

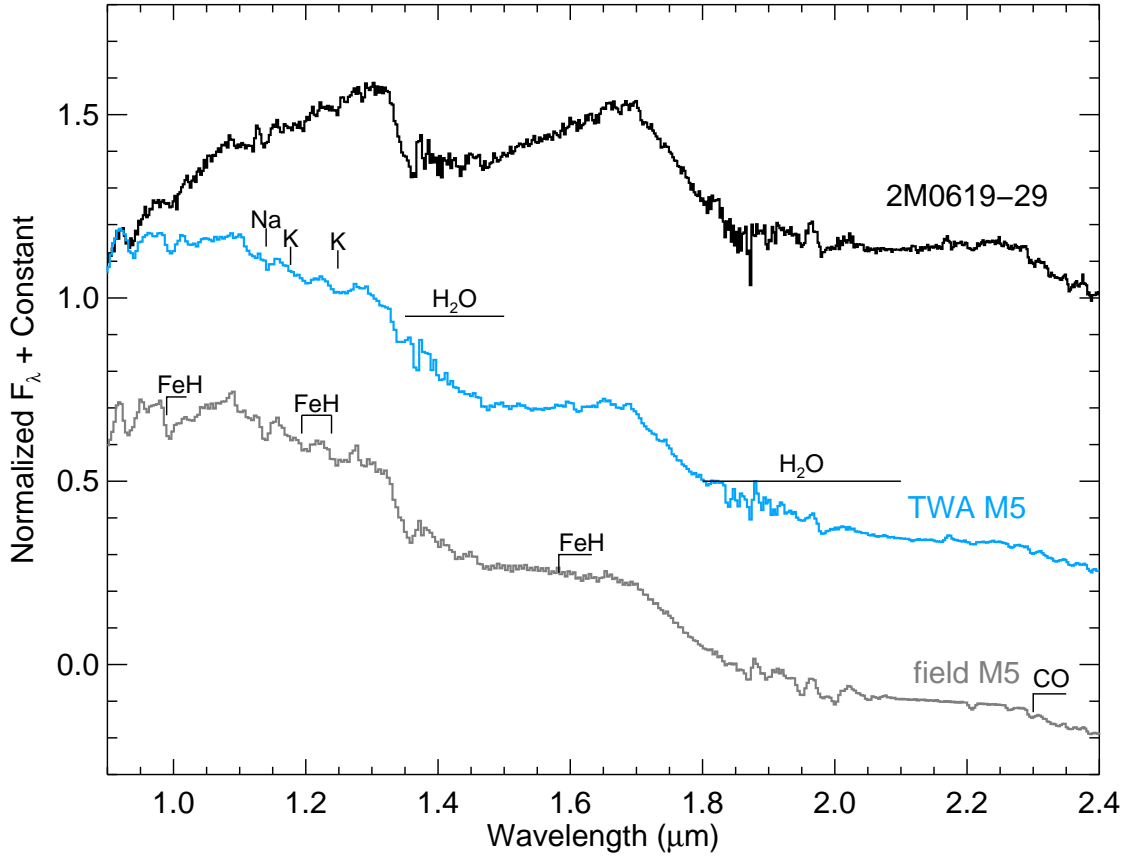


Fig. 29.— The spectrum of 2MASS J0619–2903 (Allers & Liu 2013a) compared to the TWA member, 2MASS J1235–3950 (M5 VL-G; Allers & Liu 2013a), and a field M5 (Gl 51; Kirkpatrick et al. 2010). The spectrum of 2MASS J0619–2903 is significantly reddened and has the triangular  $H$ -band shape and weak FeH absorption features typical of low gravity objects.

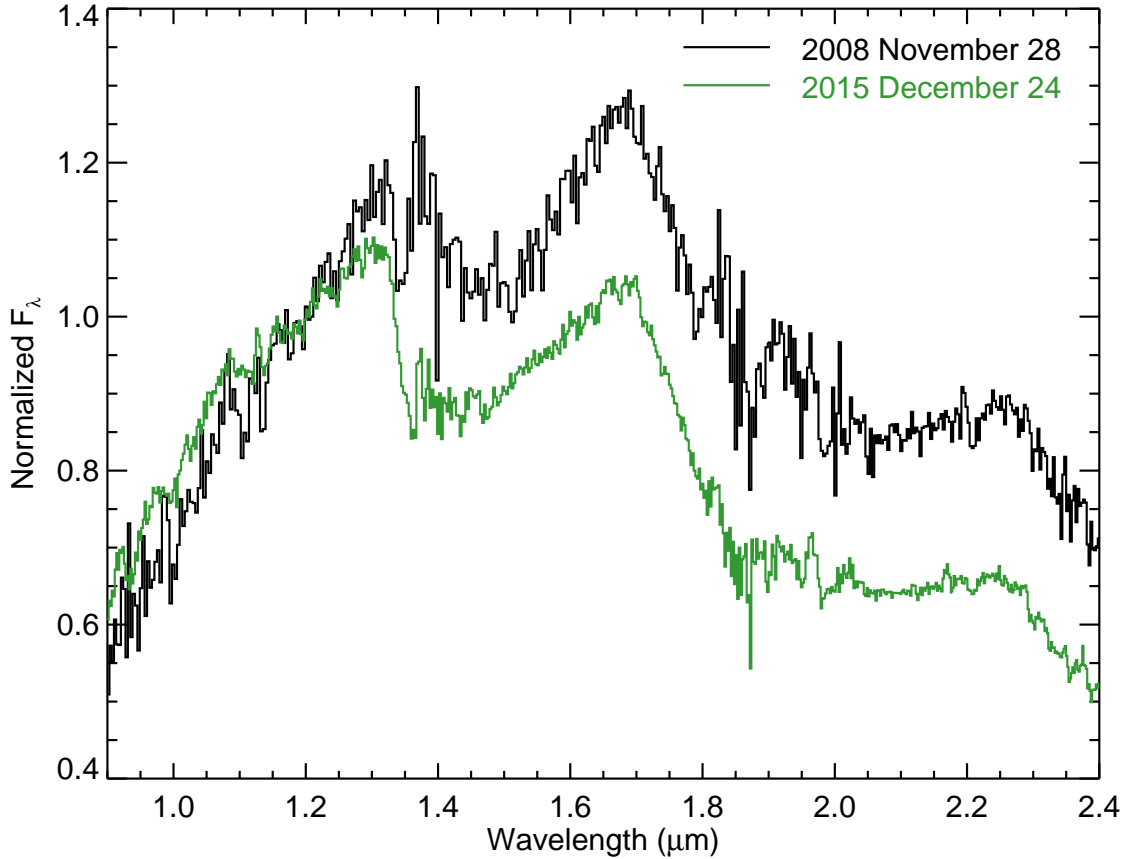


Fig. 30.— Comparison of our two epochs of near-IR prism spectra of 2MASS J0619–2903. The green-colored spectra was obtained by us in 2015, while the black spectra was obtained in 2008 (Allers & Liu 2013a). Spectra are normalized to the median flux from 1.1–1.3  $\mu\text{m}$ . The two epochs show significant differences in overall spectral shape, suggesting that 2MASS J0619-2903 may be variable.

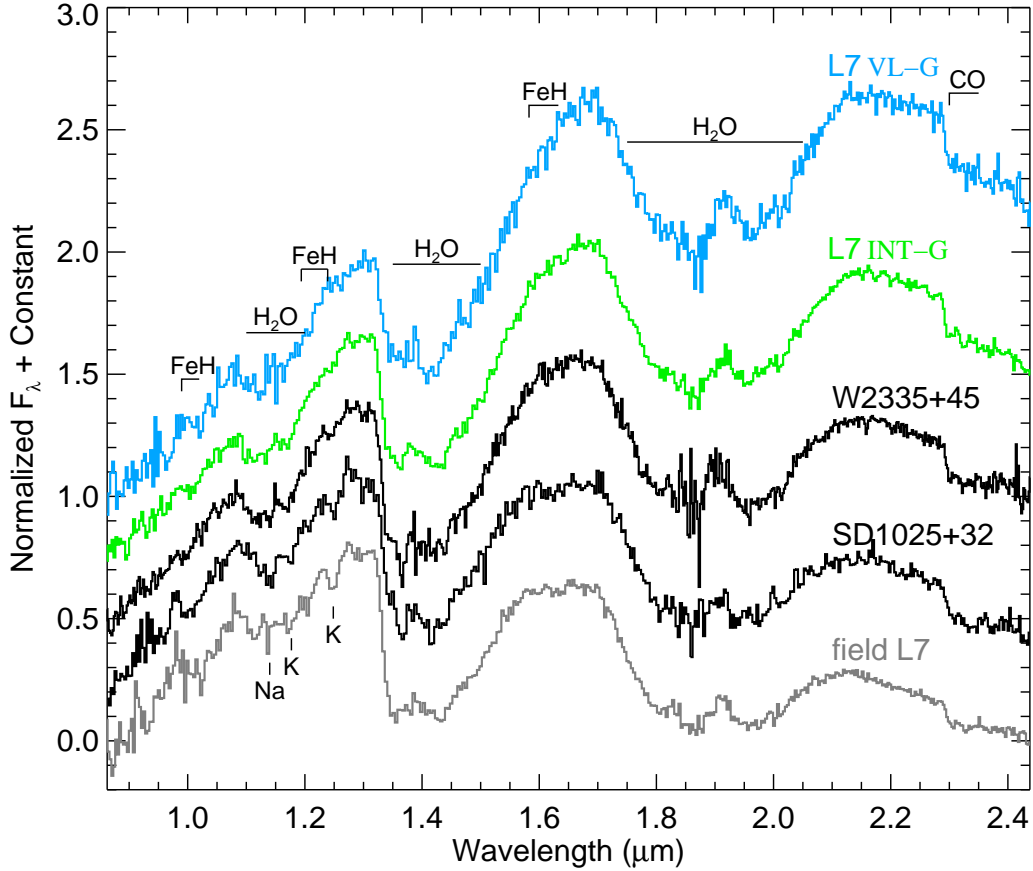


Fig. 31.— Near-IR spectra of SDSS J1025+3212 Chiu et al. (2006) and WISE J2335+4511 (this work) compared to L7 dwarfs with a range of gravity classifications (Allers & Liu 2013a). The L7 VL-G, INT-G, and FLD-G spectra are PSO J318.5-22 (Liu et al. 2013b), WISE J0047+6803 (Gizis et al. 2012), and DENIS J0205–1159 (Burgasser et al. 2010), respectively. The gravity classifications of PSO J318.5-22 and WISE 0047+6803 are consistent with their membership in the  $\beta$  Pictoris ( $\approx 25$  Myr; Bell et al. 2015) and AB Doradus ( $\approx 150$  Myr; Bell et al. 2015) moving groups, respectively. Based on visual comparison, we assign gravity designations of FLD-G to both SDSS J1025+3212 and WISE 2335+4511, but note that higher-resolution spectroscopy would allow for a more thorough analysis.

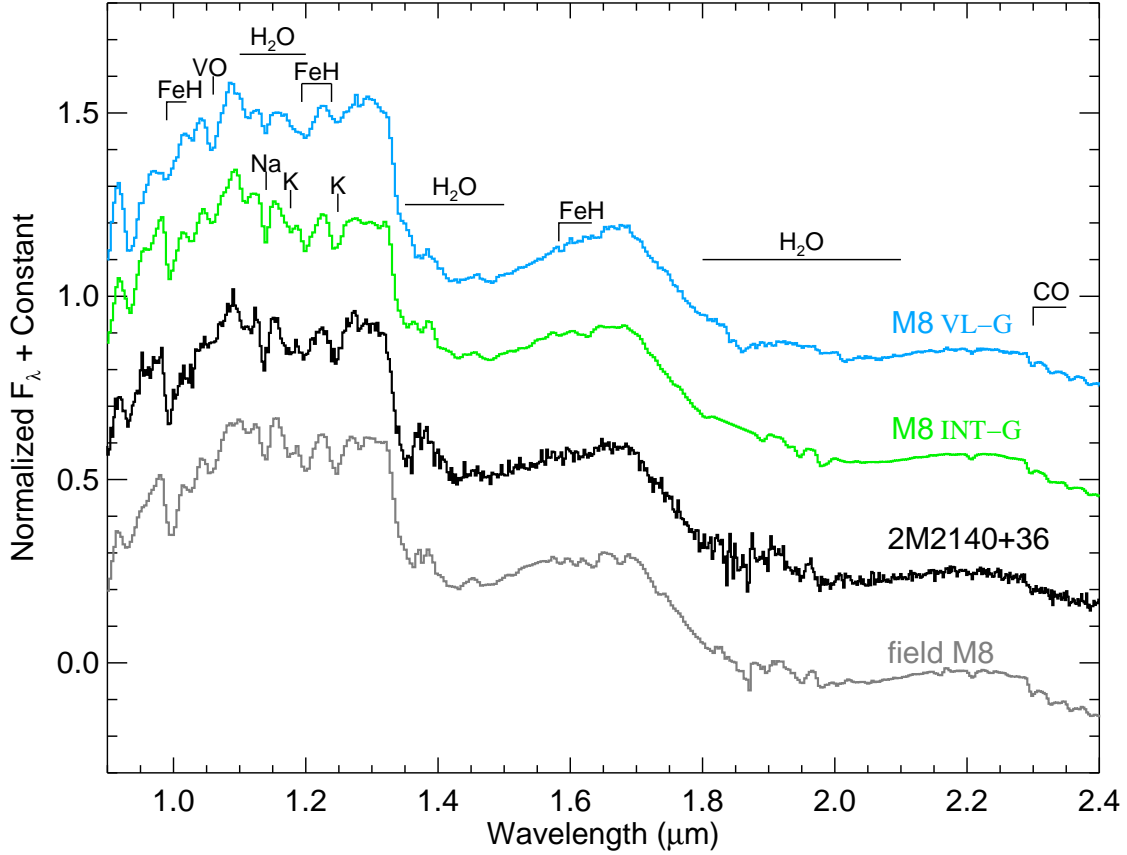


Fig. 32.— Our IRTF/SpEx near-IR spectrum of 2MASS J2140+3655 (July 2015 epoch) compared to objects spanning a range of gravity classifications from Allers & Liu (2013a). The M8 VL-G, INT-G, and FLD-G spectra are 2MASS J1207–3932 (Looper et al. 2007a), 2MASS J0019+4614 (Allers & Liu 2013a), and vB 10 (Burgasser et al. 2004), respectively. From this comparison, we type 2MASS J2140+3655 as M8p FLD-G. Its triangular *H*-band continuum is peculiar given the lack of other low-gravity indicators in its spectrum.

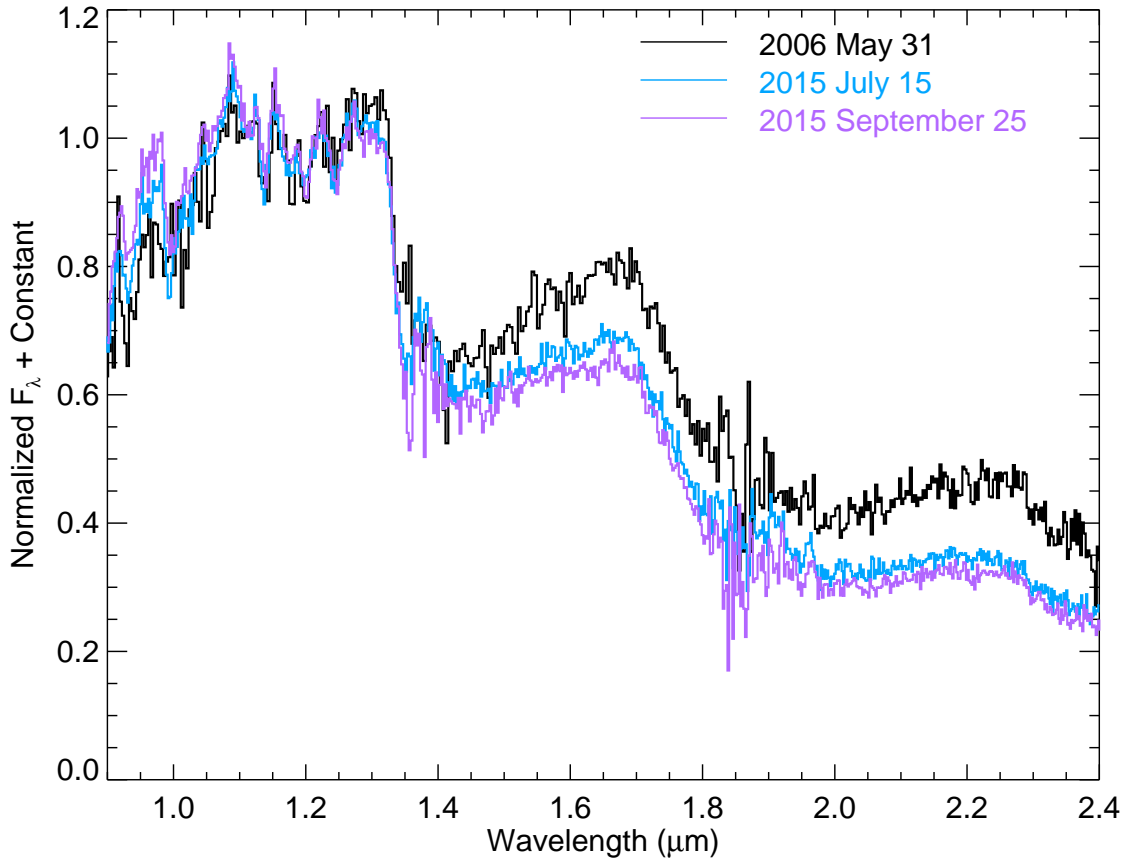


Fig. 33.— Three epochs of near-IR prism spectra for 2MASS J2140+3655. The two colored spectra were obtained by us in 2015 (Table 3), while the black one was obtained in 2006 by Kirkpatrick et al. (2010). Spectra are normalized to the median flux from 1.1–1.3  $\mu\text{m}$ .

Table 1. Summary of CFHT/WIRCcam Observed Sample

Target	Spec. Type Optical/NIR	Filter	FWHM ( $''$ )	$\Delta AM_{\max}$	$N_{fr}$	$N_{ep}$	$\Delta t$ (yr)	$N_{ref}$	$N_{cal}$	$\pi_{\text{abs}} - \pi_{\text{rel}}$ (mas)	Ref. for attributes (youth, etc.)
<b>Objects with spectroscopic signatures of youth (low gravity, lithium)</b>											
2MASS J0019262+461407	M8/M8 INT-G	$K_{H2}$	$0.53 \pm 0.09$	0.040	242	12	2.95	63	61	$1.17 \pm 0.11$	3, 41
PC 0025+0447	M9.5 $\ddagger$ /L0 INT-G	$J$	$0.63 \pm 0.10$	0.043	179	9	2.24	65	61	$0.23 \pm 0.02$	3, 29
2MASSW J0033239-152131	L4 $\beta$ /L1 FLD-G	$J$	$0.58 \pm 0.15$	0.046	186	12	2.18	29	14	$1.6 \pm 0.2$	3, 8, 40
2MASSW J0045214+163445	L2 $\beta$ /L2 VL-G	$K_{H2}$	$0.71 \pm 0.12$	0.053	130	12	2.19	32	29	$1.56 \pm 0.20$	3, 8, 40
WISEP J004701.06+680352.1	$\dots$ /L7 INT-G	$J$	$0.61 \pm 0.09$	0.046	96	11	3.18	1192	248	$0.99 \pm 0.03$	16, 24
2MASS J0117474-340325	L27 $\ddagger$ /L1 INT-G	$J$	$0.69 \pm 0.08$	0.015	106	7	2.32	48	16	$1.42 \pm 0.17$	3, 9
2MASS J01262109+1428057	L4 $\gamma$ /L2 VL-G	$J$	$0.64 \pm 0.22$	0.062	133	12	2.41	66	63	$0.43 \pm 0.05$	3, 11, 34
2MASS J0241115-032658	L0 $\gamma$ /L1 VL-G	$J$	$0.73 \pm 0.15$	0.034	72	9	5.45	39	35	$0.30 \pm 0.04$	3, 7, 8
2MASS J0253597+320637	M7 $\ddagger$ /M6 FLD-G	$J$	$0.55 \pm 0.18$	0.020	191	9	2.39	174	165	$1.10 \pm 0.07$	3, 6
2MASS J0335020+234235	M8.5 $\ddagger$ /M7 VL-G	$K_{H2}$	$0.54 \pm 0.08$	0.103	210	8	2.14	37	36	$1.38 \pm 0.17$	3, 38, 48
2MASS J03552337+1133437	L5 $\gamma$ /L3 VL-G	$J$	$0.56 \pm 0.10$	0.027	136	8	2.34	123	114	$1.22 \pm 0.09$	3, 8, 10, 40
GJ 3276 <sup>a</sup>	M6 $\gamma$ /M6 VL-G	$K_{H2}$	$0.52 \pm 0.07$	0.050	233	10	2.34	55	48	$1.39 \pm 0.16$	3, 10, 40
2MASS J0435145-141446	M7 $\delta$ /M7 VL-G	$K_{H2}$	$0.61 \pm 0.06$	0.179	197	12	3.02	32	27	$1.6 \pm 0.2$	3, 6
SDSS J044337.60+000205.2	M9 $\ddagger$ /L0 VL-G	$K_{H2}$	$0.61 \pm 0.12$	0.121	299	13	3.02	56	48	$1.39 \pm 0.15$	3, 7, 21, 30, 41
2MASS J05012406-0010452	L4 $\gamma$ /L3 VL-G	$J$	$0.66 \pm 0.16$	0.031	87	9	2.13	155	59	$1.11 \pm 0.08$	3, 8, 40
2MASS J0518461-275645	L1 $\gamma$ /L1 VL-G	$J$	$0.78 \pm 0.11$	0.032	175	9	2.12	108	40	$1.16 \pm 0.09$	3, 9, 11
2MASS J0536199-192039	L2 $\gamma$ /L2 VL-G	$J$	$0.85 \pm 0.21$	0.056	206	10	2.18	61	30	$0.79 \pm 0.07$	1, 3, 10, 11, 12
2MASS J05575096-1359503	M7 $\ddagger$ /M7 VL-G	$K_{H2}$	$0.69 \pm 0.09$	0.110	188	8	1.36	52	49	$1.15 \pm 0.12$	3, 48
2MASS J0608528-275358	M8.5 $\gamma$ /L0 VL-G	$J$	$0.79 \pm 0.17$	0.022	273	13	6.17	93	72	$0.94 \pm 0.07$	1, 3, 6, 14, 21, 42, 43
2MASS J0619526-290359	M6 $\ddagger$ /M5 $\ddagger$	$J$	$0.82 \pm 0.07$	0.091	214	10	2.17	132	96	$1.07 \pm 0.06$	3, 7
LP 423-31	M7 $\ddagger$ /M6 FLD-G	$K_{H2}$	$0.58 \pm 0.16$	0.077	171	8	3.51	64	57	$0.99 \pm 0.09$	3, 6, 48
2MASS J10220489+0200477	M9 $\beta$ /M9 FLD-G	$J$	$0.66 \pm 0.06$	0.044	76	7	2.01	54	52	$1.25 \pm 0.14$	3, 10, 21, 40
2MASS J10224821+5825453	L1 $\beta$ /L1 FLD-G	$J$	$0.64 \pm 0.15$	0.047	139	8	1.96	28	25	$1.30 \pm 0.20$	3, 8, 40
SDSS J102552.43+321234.0	$\dots$ /L7 FLD-G	$J$	$0.64 \pm 0.08$	0.080	115	6	2.74	88	85	$0.99 \pm 0.07$	1, 21
2MASS J14112131-2119503	M9/M8 INT-G	$K_{H2}$	$0.65 \pm 0.19$	0.118	212	15	3.31	34	30	$1.29 \pm 0.19$	3, 41
2MASS J15474719-2423493	M9 $\ddagger$ /L0 INT-G	$J$	$0.73 \pm 0.16$	0.019	195	11	2.37	122	112	$0.79 \pm 0.07$	3, 40
2MASS J15515237+0941148	L4 $\gamma$ /L4 VL-G	$J$	$0.57 \pm 0.12$	0.028	125	6	4.98	135	132	$0.63 \pm 0.05$	3, 11
2MASS J15525906+2948485	L0 $\beta$ /L0 INT-G	$J$	$0.60 \pm 0.12$	0.040	250	13	1.95	69	65	$1.24 \pm 0.13$	3, 8, 40
2MASS J1615425+495321	L4 $\gamma$ /L3 VL-G	$J$	$0.70 \pm 0.12$	0.032	162	10	1.94	73	67	$1.14 \pm 0.12$	3, 7, 11, 21, 40
2MASS J1711135+232633	L0 $\ddagger$ /L1 INT-G	$J$	$0.63 \pm 0.11$	0.027	110	8	2.19	166	158	$0.84 \pm 0.05$	3, 50
2MASSW J1726000+153819	L3 $\beta$ /L3 INT-G	$J$	$0.51 \pm 0.15$	0.025	144	10	2.05	354	89	$0.70 \pm 0.04$	3, 8, 19
2MASS J19355595-2846343	M9 $\ddagger$ /M9 VL-G	$J$	$0.64 \pm 0.11$	0.037	276	12	6.04	93	90	$0.77 \pm 0.07$	3, 30, 40
2MASS J20135152-2806020	M9 $\ddagger$ /L0 VL-G	$J$	$0.64 \pm 0.15$	0.026	308	15	3.95	48	45	$1.02 \pm 0.14$	3, 40
PSO J318.5338-22.8603	$\dots$ /L7 VL-G	$J$	$0.60 \pm 0.21$	0.037	261	12	3.21	68	37	$0.72 \pm 0.08$	24
SIMP J215434.5-105530.8	$\dots$ /L4 INT-G	$J$	$0.58 \pm 0.12$	0.149	94	6	2.25	95	27	$0.44 \pm 0.03$	13
2MASSW J2208136+292121	L3 $\gamma$ /L3 VL-G	$J$	$0.54 \pm 0.10$	0.018	142	7	2.13	341	96	$0.85 \pm 0.04$	3, 8, 19
2MASS J22134491-2136079	L0 $\gamma$ /L0 VL-G	$J$	$0.60 \pm 0.07$	0.013	180	9	6.00	82	22	$1.04 \pm 0.09$	3, 7, 8, 21
2MASSW J2244316+204343	L6.5/L6 VL-G	$J$	$0.61 \pm 0.09$	0.031	158	9	1.98	245	44	$1.01 \pm 0.06$	3, 21, 26, 32
SDSS J224953.46+004404.6AB	L3/L3 INT-G <sup>b</sup>	$J$	$0.67 \pm 0.06$	0.028	272	12	3.26	37	33	$1.15 \pm 0.16$	3, 36
2MASS J23224684-3133231	L0 $\beta$ /L2 INT-G	$J$	$0.67 \pm 0.08$	0.106	275	13	3.96	26	18	$1.4 \pm 0.2$	3, 9, 10
<b>Young stars with companions</b>											
LP 261-75A	M4.5/ $\dots$	$K_{H2}$	$0.62 \pm 0.09$	0.135	138	8	2.86	32	26	$1.28 \pm 0.16$	39, 48
LP 261-75B	L6/L6 FLD-G	$K_{H2}$	$0.78 \pm 0.12$	0.135	138	8	2.86	32	26	$1.28 \pm 0.16$	1, 39
G 196-3B	L3 $\beta$ /L3 VL-G	$J$	$0.63 \pm 0.09$	0.028	106	7	2.02	43	37	$1.24 \pm 0.16$	2, 3, 4, 8, 20, 21, 28, 31, 33, 37, 51
<b>Candidate stellar association members</b>											
2MASS J03140344+1603056	L0/L0 FLD-G	$K_{H2}$	$0.50 \pm 0.07$	0.089	211	10	2.03	47	33	$1.31 \pm 0.13$	3, 47
CFHT-Hy-20	$\dots$ /T2.5	$J$	$0.62 \pm 0.22$	0.017	56	8	2.12	205	38	$1.04 \pm 0.06$	5
LSR J0602+3910	L1/L2 INT-G	$K_{H2}$	$0.64 \pm 0.12$	0.072	168	11	2.02	160	154	$0.90 \pm 0.06$	3, 44, 47
SDSS J104523.98-014957.7	L1/L1 FLD-G	$K_{H2}$	$0.65 \pm 0.10$	0.050	200	10	2.02	20	18	$1.5 \pm 0.2$	3, 18, 47
DENIS-P J1047.5-1815	L2.5/L0 FLD-G	$J$	$0.74 \pm 0.09$	0.027	154	9	2.02	58	37	$1.06 \pm 0.11$	3, 18, 47
SSSPM J1102-3431 <sup>c</sup>	M8.5p $\gamma$ /M9 VL-G	$K_{H2}$	$0.70 \pm 0.12$	0.106	194	9	2.26	107	75	$1.37 \pm 0.09$	3, 10, 45
2MASSW J1139511-315921 <sup>d</sup>	M9 $\ddagger$ /M9 VL-G	$K_{H2}$	$0.71 \pm 0.10$	0.133	271	14	3.33	77	62	$1.15 \pm 0.11$	3, 15, 25, 35
DENIS-P J1441.6-0945AB	L0.5/L1 FLD-G <sup>b</sup>	$J$	$0.68 \pm 0.08$	0.045	183	12	3.07	93	37	$0.99 \pm 0.10$	1, 46, 47
DENIS-P J170548.3-051645	L0.5/L1 FLD-G	$J$	$0.58 \pm 0.12$	0.026	239	13	2.37	165	127	$0.67 \pm 0.05$	3, 47
DENIS-P J220002.0-303832A	M9/M9 FLD-G	$J$	$0.62 \pm 0.14$	0.030	77	8	2.34	80	28	$0.91 \pm 0.10$	3, 47
DENIS-P J220002.0-303832B	L0/L0 FLD-G	$J$	$0.67 \pm 0.14$	0.030	77	8	2.34	80	28	$0.90 \pm 0.10$	3, 47
<b>Unusually red and/or peculiar ultracool dwarfs</b>											
WISEP J020625.26+264023.6	$\dots$ /L8	$J$	$0.76 \pm 0.15$	0.054	125	8	1.29	142	46	$0.58 \pm 0.05$	23
WISE J075430.95+790957.8	$\dots$ /T2p(red)	$J$	$0.83 \pm 0.12$	0.085	224	8	2.17	104	41	$1.13 \pm 0.08$	1, 27
2MASS J13313310+3407583	L0/L0 FLD-G	$J$	$0.75 \pm 0.14$	0.135	164	9	1.87	26	20	$1.12 \pm 0.20$	1, 22, 40

Table 1—Continued

Target	Spec. Type Optical/NIR	Filter	FWHM (")	$\Delta AM_{\max}$	$N_{\text{fr}}$	$N_{\text{ep}}$	$\Delta t$ (yr)	$N_{\text{ref}}$	$N_{\text{cal}}$	$\pi_{\text{abs}} - \pi_{\text{rel}}$ (mas)	Ref. for attributes (youth, etc.)
2MASS J18212815+1414010	L4.5/L5 FLD-G	<i>J</i>	$0.62 \pm 0.19$	0.030	225	11	2.10	879	246	$0.52 \pm 0.02$	1, 26
2MASS J21403907+3655563 <sup>c</sup>	... /M8p FLD-G	<i>J</i>	$0.60 \pm 0.11$	0.095	166	7	2.26	169	101	$0.88 \pm 0.05$	1, 22
2MASS J21481633+4003594	L6/L6 FLD-G	<i>J</i>	$0.64 \pm 0.10$	0.035	149	8	2.03	709	234	$0.62 \pm 0.02$	3, 24, 26
WISE J233527.07+451140.9	... /L7p FLD-G	<i>J</i>	$0.63 \pm 0.11$	0.010	39	6	2.02	325	126	$0.83 \pm 0.04$	1, 49
2MASS J23512200+3010540	L5.5/L5 FLD-G	<i>J</i>	$0.53 \pm 0.04$	0.011	149	9	3.19	60	34	$0.75 \pm 0.09$	1, 22
<b>Strong H<math>\alpha</math> emitters</b>											
2MASS J04070752+1546457	L3.5/L3 FLD-G	<i>J</i>	$0.60 \pm 0.11$	0.040	125	7	2.28	165	158	$1.11 \pm 0.07$	3, 40
2MASS J13153094–2649513AB	L5.5/L6 FLD-G <sup>b</sup>	<i>J</i>	$0.62 \pm 0.12$	0.019	110	6	3.23	166	68	$0.98 \pm 0.07$	15, 17
2MASSI J1707333+430130	L0.5/M9 FLD-G	<i>J</i>	$0.58 \pm 0.15$	0.020	284	12	2.02	118	107	$1.10 \pm 0.09$	3, 6
<b>Serendipitous parallaxes</b>											
LP 415-22	... / ...	$K_{\text{H}2}$	$0.52 \pm 0.08$	0.050	233	10	2.34	55	48	$1.36 \pm 0.15$	...
2MASS J07521548+1614237	... / ...	$K_{\text{H}2}$	$0.63 \pm 0.19$	0.077	171	8	3.51	64	57	$1.02 \pm 0.10$	...

<sup>a</sup>A.k.a. 2MASS J04221413+1530525.

<sup>b</sup>Integrated-light spectral types are listed for these unresolved binary targets.

<sup>c</sup>A.k.a. TWA 28.

<sup>d</sup>A.k.a. TWA 26.

<sup>e</sup>Subsequent re-observation of this source by us indicates that the source may not be systematically red for its spectral type (see Appendix).

Note. — Opt./IR Spec. Type: Spectrally peculiar objects are denoted by “p” and types uncertain by  $\pm 1$ ,  $\pm 1.5$ , and  $\pm 2$  subclasses are denoted by “:”, “.:”, and “::”, respectively. For the M5–L7 objects, all the near-IR spectral types are based on the Allers & Liu (2013a) system, which has an intrinsic uncertainty of  $\pm 1$  subclass. Objects that have been noted in the literature to have spectral signatures of youth but lacking a formal gravity classification are denoted by †. FWHM: The median and rms of the FWHM measured for the science target over all epochs.  $\Delta AM_{\max}$ : Maximum difference in airmass over all epochs.  $N_{\text{fr}}$ : Total number of frames obtained (typically  $\approx 20$  per epoch).  $N_{\text{ep}}$ : Number of distinct observing epochs (i.e., nights).  $N_{\text{ref}}$ : Number of reference stars used.  $N_{\text{cal}}$ : Subset of reference stars used in the absolute astrometric calibration (i.e., those available in 2MASS or SDSS).  $\pi_{\text{abs}} - \pi_{\text{rel}}$ : Offset from relative to absolute parallax computed for each field using the Besançon model of the Galaxy (Robin et al. 2003) as described in Section 2.2.

References. — (1) This work; (2) Allers et al. (2007); (3) Allers & Liu (2013a); (4) Basri et al. (2000); (5) Bouvier et al. (2008); (6) Cruz et al. (2003); (7) Cruz et al. (2007); (8) Cruz et al. (2009); (9) Faherty et al. (2009); (10) Faherty et al. (2012); (11) Faherty et al. (2013); (12) Gagné et al. (2014b); (13) Gagné et al. (2014a); (14) Gagné et al. (2015a); (15) Gizis (2002); (16) Gizis et al. (2012); (17) Hall (2002a); (18) Jameson et al. (2008); (19) Kirkpatrick et al. (2000); (20) Kirkpatrick et al. (2001); (21) Kirkpatrick et al. (2008); (22) Kirkpatrick et al. (2010); (23) Kirkpatrick et al. (2011); (24) Liu et al. (2013b); (25)Looper et al. (2007a); (26) Looper et al. (2008b); (27) Mace et al. (2013); (28) Martín et al. (1999b); (29) Martín et al. (1999a); (30) Martín et al. (2010); (31) McGovern et al. (2004); (32) McLean et al. (2003); (33) McLean et al. (2007); (34) Metchev et al. (2008); (35) Mohanty et al. (2003); (36) Nakajima et al. (2004); (37) Rebolo et al. (1998); (38) Reid et al. (2002); (39) Reid & Walkowicz (2006); (40) Reid et al. (2008); (41) Reiners & Basri (2009); (42) Rice et al. (2010a); (43) Rice et al. (2010b); (44) Salim et al. (2003); (45) Scholz et al. (2005); (46) Seifahrt et al. (2005); (47) Seifahrt et al. (2010); (48) Shkolnik et al. (2009); (49) Thompson et al. (2013); (50) West et al. (2008); (51) Zapatero Osorio et al. (2010).



Table 2. CFHT/WIRCam Parallax and Proper Motion Results

Target	$\alpha_{J2000}$ (deg)	$\delta_{J2000}$ (deg)	Epoch (MJD)	Relative			Absolute			$\chi^2/\text{dof}$
				$\pi_{\text{rel}}$ (")	$\mu_{\alpha, \text{rel}} \cos \delta$ (" yr <sup>-1</sup> )	$\mu_{\delta, \text{rel}}$ (" yr <sup>-1</sup> )	$\pi_{\text{abs}}$ (")	$\mu_{\alpha, \text{abs}} \cos \delta$ (" yr <sup>-1</sup> )	$\mu_{\delta, \text{abs}}$ (" yr <sup>-1</sup> )	
2MASS J0019262+461407	004.8602716	+46.2353705	55423.55	0.0243(15)	0.1194(9)	-0.0754(9)	0.0255(15)	0.1193(13)	-0.0777(11)	24.8/19
PC 0025+0447	006.9251141	+05.0617997	56497.62	0.0102(8)	0.0166(11)	-0.0014(11)	0.0104(8)	0.0161(11)	-0.0033(12)	12.6/13
2MASSW J0033239-152131	008.3501667	-15.3585656	55050.54	0.0412(18)	0.3025(10)	0.0360(15)	0.0428(18)	0.3061(24)	0.0324(26)	22.1/19
2MASSW J0045214+163445	011.3387503	+16.5794601	55050.55	0.0644(13)	0.3513(11)	-0.0475(12)	0.0659(13)	0.3544(22)	-0.0511(20)	16.9/19
WISEP J004701.06+680352.1	011.7555865	+68.0645252	55780.58	0.0816(19)	0.3846(11)	-0.2005(14)	0.0823(18)	0.3807(11)	-0.2042(14)	22.4/17
2MASS J0117474-340325	019.4479413	-34.0572078	55050.59	0.0247(19)	0.1060(14)	-0.0498(35)	0.0261(19)	0.1115(21)	-0.0524(38)	11.0/9
2MASS J01262109+1428057	021.5883123	+14.4682530	56500.62	0.0167(12)	0.0760(11)	-0.0362(10)	0.0171(12)	0.0749(12)	-0.0394(12)	17.1/19
WISEP J020625.26+264023.6	031.6058917	+26.6733413	56585.42	0.0514(14)	0.4439(19)	-0.0377(23)	0.0521(14)	0.4427(21)	-0.0419(23)	9.7/11
2MASS J0241115-032658	040.2983859	-03.4495775	55050.63	0.0182(20)	0.0716(4)	-0.0208(4)	0.0185(21)	0.0696(5)	-0.0251(6)	15.1/13
2MASS J0253597+320637	043.4998002	+32.1102750	55050.64	0.0202(10)	0.0942(10)	-0.0942(11)	0.0213(10)	0.0959(11)	-0.0969(11)	14.2/13
2MASS J03140344+1603056	048.5136973	+16.0514971	55429.58	0.0708(15)	-0.2454(19)	-0.0464(18)	0.0721(15)	-0.2427(22)	-0.0498(21)	9.4/15
2MASS J0335020+234235	053.7588666	+23.7102603	55068.63	0.0204(18)	0.0466(17)	-0.0565(21)	0.0218(18)	0.0489(20)	-0.0598(23)	12.2/11
2MASS J03552337+1133437	058.8480801	+11.5603551	55068.64	0.1083(13)	0.2210(13)	-0.6228(14)	0.1095(14)	0.2236(14)	-0.6256(15)	16.3/11
2MASS J04070752+1546457	061.7817636	+15.7793595	55068.64	0.0278(13)	0.0727(14)	-0.0616(10)	0.0289(13)	0.0749(15)	-0.0643(11)	13.8/9
LP 415-22	065.4936486	+15.5392209	55069.63	0.0116(15)	-0.0266(21)	-0.1093(17)	0.0130(16)	-0.0244(22)	-0.1125(19)	13.8/15
GJ 3276	065.5591963	+15.5145277	55069.63	0.0026(10)	0.0014(15)	0.0018(14)	0.0039(10)	0.0036(16)	-0.0014(16)	15.5/15
CFHT-Hy-20	067.6618228	+13.1657846	55125.57	0.0298(15)	0.1408(16)	-0.0140(17)	0.0308(15)	0.1426(16)	-0.0165(17)	11.4/11
2MASS J0435145-141446	068.8106905	-14.2462535	55070.65	0.0099(14)	-0.0040(14)	0.0093(13)	0.0114(14)	-0.0006(19)	0.0093(20)	16.8/19
SDSS J044337.60+000205.2	070.9069339	+00.0345669	55070.64	0.0459(10)	0.0512(10)	-0.1029(11)	0.0473(10)	0.0536(13)	-0.1046(15)	14.4/21
2MASS J05012406-0010452	075.3512321	-00.1792290	55127.55	0.0472(14)	0.1881(13)	-0.1424(15)	0.0484(14)	0.1897(14)	-0.1439(16)	11.8/13
2MASS J0518461-275645	079.6923698	-27.9459520	55127.57	0.0173(11)	0.0331(15)	-0.0067(16)	0.0184(11)	0.0349(15)	-0.0049(18)	15.2/13
2MASS J0536199-192039	084.0834569	-19.3442093	56585.57	0.0204(16)	0.0274(14)	-0.0226(16)	0.0211(16)	0.0255(16)	-0.0264(17)	10.0/15
2MASS J05575096-1359503	089.4625451	-13.9971490	55491.55	0.0022(12)	0.0057(23)	0.0010(31)	0.0034(12)	0.0062(23)	0.0019(32)	12.7/11
LSR J0602+3910	090.6279861	+39.1816078	55281.22	0.0869(10)	0.1581(13)	-0.5026(14)	0.0878(10)	0.1583(13)	-0.5049(15)	19.9/17
2MASS J0608528-275358	092.2203780	-27.8994700	55125.59	0.0241(15)	0.0121(5)	0.0049(6)	0.0250(15)	0.0124(6)	0.0073(8)	20.4/21
2MASS J0619526-290359	094.9691731	-29.0663405	56585.59	0.0031(20)	0.0052(20)	-0.0047(38)	0.0036(20)	0.0045(21)	-0.0081(39)	6.4/15
2MASS J07521548+1614237	118.0644352	+16.2401206	55125.64	0.0121(14)	-0.0583(12)	-0.0298(10)	0.0132(14)	-0.0591(14)	-0.0298(11)	7.8/11
LP 423-31	118.1003410	+16.2035099	55125.64	0.0533(14)	0.1830(11)	-0.3478(11)	0.0543(14)	0.1821(14)	-0.3478(11)	4.2/11
WISE J075430.95+790957.8	118.6314624	+79.1665794	56588.65	0.0500(12)	0.2895(14)	0.3349(24)	0.0511(12)	0.2857(18)	0.3310(24)	9.6/11
LP 261-75A	147.7687911	+35.9689334	56000.28	0.0303(13)	-0.0934(10)	-0.1609(12)	0.0316(13)	-0.0935(17)	-0.1641(19)	13.2/11
LP 261-75B	147.7726011	+35.9668078	56000.28	0.0283(28)	-0.0938(20)	-0.1610(23)	0.0296(28)	-0.0940(24)	-0.1643(27)	12.0/11
G 196-3B	151.0862151	+50.3828611	55279.34	0.0477(23)	-0.1290(14)	-0.1958(26)	0.0490(23)	-0.1314(19)	-0.2005(29)	14.6/9
2MASS J10220489+0200477	155.5201822	+02.0122656	55285.38	0.0333(20)	-0.1730(20)	-0.4163(18)	0.0346(20)	-0.1783(25)	-0.4185(21)	13.3/9
2MASS J10224821+5825453	155.6975496	+58.4273889	55283.35	0.0513(31)	-0.7945(27)	-0.7252(29)	0.0526(31)	-0.7963(32)	-0.7298(34)	11.2/11
SDSS J102552.43+321234.0	156.4695667	+32.2089577	56380.36	0.0363(13)	0.3132(11)	-0.2296(13)	0.0373(12)	0.3134(11)	-0.2331(16)	7.1/7
SDSS J104523.98-014957.7	161.3488079	-01.8325992	55279.39	0.0603(14)	-0.4819(22)	-0.0045(23)	0.0618(15)	-0.4875(34)	-0.0073(33)	20.4/15
DENIS-P J1047.5-1815	161.8787980	-18.2655001	55280.38	0.0368(19)	-0.3546(22)	0.0469(31)	0.0379(19)	-0.3607(25)	0.0470(32)	16.9/13
SSSPM J1102-3431	165.5407191	-34.5096781	55583.54	0.0197(21)	-0.0571(15)	-0.0164(23)	0.0211(21)	-0.0543(18)	-0.0196(24)	10.6/13
2MASSW J1139511-315921	174.9630550	-31.9891060	55192.67	0.0225(16)	-0.0801(10)	-0.0276(17)	0.0237(16)	-0.0869(14)	-0.0275(18)	29.6/23
2MASS J13153094-2649513AB	198.8760311	-26.8319686	56000.52	0.0537(19)	-0.6800(14)	-0.2863(20)	0.0550(21)	-0.6781(17)	-0.2877(19)	7.6/7
2MASS J13313310+3407583	202.8857472	+34.1315245	56373.55	0.0345(15)	-0.3507(13)	-0.1807(17)	0.0356(16)	-0.3527(18)	-0.1843(22)	8.6/13
2MASS J14112131-2119503	212.8386621	-21.3307619	55288.48	0.0182(19)	-0.0807(8)	-0.0701(11)	0.0195(19)	-0.0859(19)	-0.0727(16)	18.9/25
DENIS-P J1441.6-0945AB	220.4041413	-09.7661398	55289.52	0.0286(16)	-0.2022(7)	-0.0153(10)	0.0296(17)	-0.2061(10)	-0.0178(11)	21.1/19
2MASS J15474719-2423493	236.9464492	-24.3972545	55281.58	0.0293(11)	-0.1372(8)	-0.1299(16)	0.0301(11)	-0.1401(10)	-0.1322(16)	17.4/17
2MASS J15515237+0941148	237.9682027	+09.6874780	55050.25	0.0215(15)	-0.0596(6)	-0.0593(5)	0.0221(15)	-0.0621(6)	-0.0577(6)	9.2/7
2MASS J15525906+2948485	238.2457305	+29.8131565	55050.25	0.0465(10)	-0.1539(14)	-0.0639(16)	0.0478(10)	-0.1563(16)	-0.0675(19)	19.8/21
2MASS J1615425+495321	243.9271293	+49.8893975	55050.28	0.0309(10)	-0.0909(10)	0.0180(13)	0.0320(10)	-0.0928(12)	0.0152(18)	16.2/15
DENIS-P J170548.3-051645	256.4518928	-05.2797053	55279.63	0.0529(10)	0.1181(8)	-0.1169(12)	0.0535(10)	0.1170(9)	-0.1198(12)	16.1/21
2MASS J1707333+430130	256.8881664	+43.0251813	55050.28	0.0350(10)	-0.2083(13)	-0.0270(15)	0.0361(10)	-0.2098(14)	-0.0303(17)	21.6/19

Table 2—Continued

Target	$\alpha_{J2000}$ (deg)	$\delta_{J2000}$ (deg)	Epoch (MJD)	Relative			Absolute			$\chi^2/\text{dof}$
				$\pi_{\text{rel}}$ ( $''$ )	$\mu_{\alpha,\text{rel}} \cos \delta$ ( $'' \text{ yr}^{-1}$ )	$\mu_{\delta,\text{rel}}$ ( $'' \text{ yr}^{-1}$ )	$\pi_{\text{abs}}$ ( $''$ )	$\mu_{\alpha,\text{abs}} \cos \delta$ ( $'' \text{ yr}^{-1}$ )	$\mu_{\delta,\text{abs}}$ ( $'' \text{ yr}^{-1}$ )	
2MASSI J1711135+232633	257.8062976	+23.4425953	56373.61	0.0297(15)	-0.0636(13)	-0.0428(14)	0.0306(17)	-0.0685(13)	-0.0412(15)	7.8/11
2MASSW J1726000+153819	261.5003777	+15.6385206	55069.25	0.0276(10)	-0.0475(13)	-0.0592(14)	0.0283(10)	-0.0488(13)	-0.0632(15)	15.7/15
2MASS J18212815+1414010	275.3680641	+14.2330443	55050.31	0.1041(10)	0.2274(15)	-0.2411(18)	0.1046(10)	0.2261(15)	-0.2454(18)	19.9/17
2MASS J19355595-2846343	293.9833277	-28.7761413	55050.37	0.0135(13)	0.0276(7)	-0.0584(10)	0.0142(12)	0.0273(9)	-0.0616(11)	14.6/19
2MASS J20135152-2806020	303.4649304	-28.1006069	55050.37	0.0199(13)	0.0413(8)	-0.0627(14)	0.0210(13)	0.0415(12)	-0.0661(17)	24.2/25
PSO J318.5338-22.8603	318.5341407	-22.8603323	55768.45	0.0444(17)	0.1369(10)	-0.1389(10)	0.0451(17)	0.1363(10)	-0.1443(13)	16.8/17
2MASS J21403907+3655563	325.1625120	+36.9322937	56493.50	0.0106(11)	-0.1242(13)	-0.0600(12)	0.0114(10)	-0.1292(15)	-0.0623(13)	9.5/9
2MASS J21481633+4003594	327.0706996	+40.0679073	55068.40	0.1240(18)	0.7777(17)	0.4604(22)	0.1246(18)	0.7753(17)	0.4571(22)	12.8/11
SIMP J215434.5-105530.8	328.6445086	-10.9252593	56499.49	0.0322(10)	0.1689(16)	0.0062(20)	0.0326(10)	0.1668(17)	0.0022(22)	8.4/7
DENIS-P J220002.0-303832A	330.0093130	-30.6423076	55373.60	0.0400(40)	0.2420(24)	-0.0488(48)	0.0410(40)	0.2432(26)	-0.0529(49)	21.2/11
DENIS-P J220002.0-303832B	330.0093321	-30.6420370	55373.60	0.0333(39)	0.2420(22)	-0.0755(54)	0.0348(38)	0.2435(23)	-0.0792(53)	21.2/11
2MASSW J2208136+292121	332.0571016	+29.3560502	55068.43	0.0243(16)	0.0905(11)	-0.0222(11)	0.0251(16)	0.0889(11)	-0.0258(12)	11.8/9
2MASS J22134491-2136079	333.4375653	-21.6018641	55128.27	0.0199(19)	0.0500(9)	-0.0663(7)	0.0209(19)	0.0515(13)	-0.0706(10)	12.7/13
2MASSW J2244316+204343	341.1330783	+20.7280859	55125.30	0.0577(10)	0.2308(8)	-0.2310(9)	0.0587(10)	0.2303(9)	-0.2348(10)	11.9/13
SDSS J224953.46+004404.6AB	342.4730584	+00.7347146	54658.58	0.0243(14)	0.0819(7)	0.0131(6)	0.0255(14)	0.0826(16)	0.0086(15)	27.6/19
2MASS J23224684-3133231	350.6946631	-31.5577239	55050.52	0.0487(28)	-0.2105(11)	-0.5315(17)	0.0502(28)	-0.2062(27)	-0.5359(26)	24.8/21
WISE J233527.07+451140.9	353.8627169	+45.1946592	56579.36	0.0432(15)	-0.0888(15)	-0.0769(18)	0.0440(14)	-0.0927(16)	-0.0799(16)	8.7/7
2MASS J23512200+3010540	357.8428500	+30.1818517	55779.57	0.0405(14)	0.2547(7)	0.0125(6)	0.0412(14)	0.2525(10)	0.0104(9)	16.0/13

Note. — This table gives all the astrometric parameters derived from our Markov Chain Monte Carlo (MCMC) analysis for each target. For parameters in units of arcseconds, errors are given in parentheses in units of  $10^{-4}$  arcsec. ( $\alpha$ ,  $\delta$ , MJD): Coordinates that correspond to the epoch listed, which is the first epoch of our observations for that target. ( $\pi$ ,  $\mu_{\alpha} \cos \delta$ ,  $\mu_{\delta}$ ): Parallax and proper motion parameters are listed as both as relative and absolute values. Relative values are our directly fitted results. Absolute values include a correction for the mean parallax and proper motion of our reference stars, which includes an additional uncertainty added in quadrature to our direct fitting results (see Section 2.2).  $\chi^2/\text{dof}$ : The lowest  $\chi^2$  in each set of MCMC chains along with the degrees of freedom (dof).

Table 3. IRTF/SpeX Prism Near-IR Spectroscopy

Object	UT Date	Slit (")	sec $z$	$N_{exp} \times t$ (s)	$T_{int}$ (s)	$\langle S/N \rangle$ ( $YJHK$ )
CFHT-Hy-20	2009-11-03	$0.5 \times 15$	1.21	$26 \times 120$	3120.0	20, 54, 34, 20
2MASS J0619–2903	2015-12-24	$0.5 \times 15$	1.52	$12 \times 119.5$	1434.5	70, 98, 98, 102
DENIS-P J1441–0945AB	2015-01-28	$0.5 \times 15$	1.19	$9 \times 9.7$	87.6	40, 65, 56, 46
2MASS J2140+3655	2015-07-15	$0.5 \times 15$	1.06	$9 \times 59.8$	537.9	59, 67, 49, 36
	2015-09-25	$0.5 \times 15$	1.05	$9 \times 119.5$	1075.9	58, 65, 45, 35
WISE J2335+4511	2015-07-23	$0.5 \times 15$	1.21	$9 \times 179.8$	1618.0	20, 35, 38, 50

Note. — The last column gives the median S/N of the spectrum within the standard near-IR bandpasses.

Table 4. Near-IR Spectral Classification of Late-M and L Dwarfs

Object	Published SpT		SpT (Visual)		SpT (Index)				Gravity	SpT
	Opt./NIR	Refs	<i>J</i> -band <sup>a</sup>	<i>K</i> -band <sup>a</sup>	H <sub>2</sub> O	H <sub>2</sub> OD	H <sub>2</sub> O-1	H <sub>2</sub> O-2	Scores <sup>a</sup>	Adopted
2MASS J0030300–145033	L7/L4-L6 $\beta$	3, 4, 5	L6 $\pm$ 1	L7 $\pm$ 1	...	L4.6 $\pm$ 0.9	...	...	nnn1	L6 FLD-G <sup>b</sup>
2MASS J0619526–290359	M6/M5	14, 1	M6 $\pm$ 1	M6 $\pm$ 1	M7.0 $\pm$ 0.5	...	M3.8 $\pm$ 1.1	M5.9 $\pm$ 0.5	2n22	M6 VL-G <sup>b</sup>
LP 261-75B	L6/L4.5	1, 5	L7 $\pm$ 1	L6 $\pm$ 1	...	L4.5 $\pm$ 0.9	...	...	nnn1	L6 FLD-G <sup>b</sup>
2MASS J13153094–2649513AB	L5.5/L5	6, 13	L7 $\pm$ 1	L5 $\pm$ 1	...	L5.9 $\pm$ 0.8	...	...	nnn0	L6 FLD-G
2MASS J13313310+3407583	L0/L1p	7	M9 $\pm$ 1	L0 $\pm$ 1	L0.1 $\pm$ 0.5	...	M7.0 $\pm$ 1.1	M9.7 $\pm$ 0.6	0000	L0 FLD-G
DENIS J144137.2–094558AB	L0.5/ ...	6	L1 $\pm$ 1	L1 $\pm$ 1	L1.3 $\pm$ 0.5	L1.1 $\pm$ 0.9	L0.0 $\pm$ 1.1	L1.0 $\pm$ 0.6	00?0	L1 FLD-G
2MASS J18212815+1414010	L4.5/L5p	7, 8	L4 $\pm$ 1	L5 $\pm$ 1	...	L5.3 $\pm$ 0.9	L4.6 $\pm$ 1.1	...	0n0?	L5 FLD-G
2MASS J21403907+3655563	... /M8p	7	M7.5 $\pm$ 1	M8.5 $\pm$ 1	M7.2 $\pm$ 0.6	...	M9.7 $\pm$ 1.1	M7.8 $\pm$ 0.8	?n01	M8p FLD-G
DENIS J220002.0–303832B	... /L0	2	L1 $\pm$ 1	L0 $\pm$ 1	M9.6 $\pm$ 0.5	...	M9.3 $\pm$ 1.1	M9.1 $\pm$ 0.7	0000	L0 FLD-G
2MASSW J2224438–015852	L4.5/L3.5	5, 10	L4 $\pm$ 1	L3 $\pm$ 1	L2.9 $\pm$ 0.2	L3.9 $\pm$ 0.8	M9.3 $\pm$ 1.2	...	1010	L3 FLD-G
WISE J233527.07+451140.9	... /L9p	9	L9 $\pm$ 2	L7 $\pm$ 1	...	L6.9 $\pm$ 0.9	...	...	nnn0	L7p FLD-G <sup>b</sup>
2MASS J23512200+3010540	L5.5/L5p	7	L6 $\pm$ 1	L5 $\pm$ 1	...	L4.6 $\pm$ 0.9	...	...	0n01	L5 FLD-G

<sup>a</sup>Gravity scores are listed in the following order: FeH, VO, alkali lines, and *H*-band continuum shape. See Allers & Liu (2013a) for details.

<sup>b</sup>Gravity classification based on visual inspection.

References. — (1) Bowler et al. (2013); (2) Burgasser & McElwain (2006); (3) Burgasser et al. (2010); (4) Gagné et al. (2015b); (5) Kirkpatrick et al. (2000); (6) Kirkpatrick et al. (2008); (7) Kirkpatrick et al. (2010); (8)Looper et al. (2008b); (9) Thompson et al. (2013); (10) Knapp et al. (2004); (11) Cruz et al. (2003); (12) Schneider et al. (2014); (13) Burgasser et al. (2011); (14) Cruz et al. (2007)

Table 5. Near-IR Spectral Classification of Late-L and T Dwarfs

Object	H <sub>2</sub> O- <i>J</i>	CH <sub>4</sub> - <i>J</i>	H <sub>2</sub> O- <i>H</i>	CH <sub>4</sub> - <i>H</i>	CH <sub>4</sub> - <i>K</i>	H <sub>2</sub> O- <i>K</i>	SpT: Index	SpT: Visual	SpT: Final
WISE J0206+2640	0.675 (L8.0)	0.806 (<T0)	0.695 (L6.7)	1.075 (<T1)	0.922 (L6.9)	0.726 (–)	L7.2±0.7	L8 (red)	L8 (red)
CFHT-Hy-20	0.461 (T2.9)	0.670 (<T0)	0.459 (T3.3)	0.896 (T1.6)	0.544 (T2.3)	0.539 (–)	T2.5±0.7	T2	T2.5
WISE J0754+7909	0.471 (T2.7)	0.652 (T0.1)	0.465 (T3.2)	1.072 (<T1)	0.715 (T0.7)	0.478 (–)	T1.7±1.5	T2p (red)	T2p (red)

Table 6. Photometry for Our Sample and Other Potentially Young Objects

Object	Parallax (mas)	Ref.	MKO				2MASS			ALLWISE		Refs.
			Y (mag)	J (mag)	H (mag)	K (mag)	J (mag)	H (mag)	K <sub>S</sub> (mag)	W1 (mag)	W2 (mag)	
HD 984B	21.2 ± 0.6	52	...	...	{12.63 ± 0.05}	{12.15 ± 0.04}	...	12.58 ± 0.05	12.19 ± 0.04	...	...	1, 44
HD 1160B	9.7 ± 0.5	52	...	...	14.60 ± 0.11	14.65 ± 0.08	{13.91 ± 0.12}	{14.66 ± 0.11}	{14.60 ± 0.08}	13.95 ± 0.12	...	1, 38, 47
2MASSJ0019262+461407	25.5 ± 1.5	1	[13.22 ± 0.05]	[12.56 ± 0.02]	[11.98 ± 0.02]	[11.47 ± 0.01]	12.60 ± 0.02	11.94 ± 0.02	11.50 ± 0.01	11.28 ± 0.02	11.02 ± 0.02	1, 2
PC 0025+0447	10.4 ± 0.8	1	17.18 ± 0.02	16.14 ± 0.02	15.52 ± 0.02	14.94 ± 0.02	16.19 ± 0.09	15.29 ± 0.10	14.96 ± 0.12	14.62 ± 0.03	14.07 ± 0.05	1, 2, 3
2MASSWJ0030300−145033	37 ± 5	53	[17.61 ± 0.05]	16.39 ± 0.03	15.37 ± 0.03	14.49 ± 0.03	16.28 ± 0.11	15.27 ± 0.10	14.48 ± 0.10	13.68 ± 0.03	13.33 ± 0.03	1, 2, 29
2MASSWJ0033239−152131	42.8 ± 1.8	1	[16.34 ± 0.06]	[15.23 ± 0.06]	[14.25 ± 0.05]	[13.39 ± 0.04]	15.29 ± 0.06	14.21 ± 0.05	13.41 ± 0.04	12.82 ± 0.02	12.50 ± 0.03	1, 2
2MASSWJ0045214+163445	65.9 ± 1.3	1	[14.13 ± 0.05]	[12.99 ± 0.02]	[12.11 ± 0.04]	[11.33 ± 0.02]	13.06 ± 0.02	12.06 ± 0.04	11.37 ± 0.02	10.78 ± 0.02	10.40 ± 0.02	1, 2
WISEPJ004701.06+680352.1	82.3 ± 1.8	1	[16.76 ± 0.07]	[15.49 ± 0.07]	[14.04 ± 0.04]	[13.01 ± 0.03]	15.60 ± 0.07	13.97 ± 0.04	13.05 ± 0.03	11.88 ± 0.02	11.26 ± 0.02	1, 2
2MASSWJ0058425−065123	34 ± 4	42	[15.32 ± 0.05]	[14.23 ± 0.03]	[13.48 ± 0.03]	[12.85 ± 0.03]	14.31 ± 0.03	13.44 ± 0.03	12.90 ± 0.03	12.57 ± 0.02	12.27 ± 0.03	1, 2
2MASSJ01033563−5515561b	21.2 ± 1.4	51	...	15.40 ± 0.30	14.20 ± 0.20	13.60 ± 0.20	15.40 ± 0.30	14.20 ± 0.20	13.60 ± 0.20	...	...	18
2MASSJ0117474−340325	26.1 ± 1.9	1	[16.32 ± 0.05]	[15.10 ± 0.04]	[14.27 ± 0.04]	[13.46 ± 0.04]	15.18 ± 0.04	14.21 ± 0.04	13.49 ± 0.04	13.05 ± 0.02	12.64 ± 0.02	1, 2
2MASSJ01262109+1428057	17.1 ± 1.2	1	18.99 ± 0.08	17.46 ± 0.04	16.15 ± 0.02	15.11 ± 0.02	17.11 ± 0.21	16.17 ± 0.22	15.28 ± 0.15	14.23 ± 0.03	13.69 ± 0.03	1, 2, 3
WISEPJ020625.26+264023.6	52.1 ± 1.4	1	[17.55 ± 0.11]	[16.42 ± 0.11]	[15.16 ± 0.08]	[14.50 ± 0.08]	16.53 ± 0.11	15.10 ± 0.08	14.52 ± 0.08	13.42 ± 0.03	12.83 ± 0.03	1, 2
2MASSJ02212859−6831400	25.4 ± 3.6	26	...	{13.91 ± 0.03}	{13.31 ± 0.03}	{12.78 ± 0.04}	13.97 ± 0.03	13.27 ± 0.03	12.81 ± 0.04	12.49 ± 0.02	12.20 ± 0.02	1, 2
2MASSJ0241115−032658	18.5 ± 2.1	1	[16.86 ± 0.06]	[15.72 ± 0.06]	[14.87 ± 0.05]	[14.00 ± 0.05]	15.80 ± 0.06	14.81 ± 0.05	14.03 ± 0.05	13.65 ± 0.03	13.28 ± 0.03	1, 2
SOJ025300.5+165258 <sup>†</sup>	259.3 ± 0.9	27	[8.96 ± 0.05]	[8.34 ± 0.03]	[7.92 ± 0.04]	[7.55 ± 0.05]	8.39 ± 0.03	7.88 ± 0.04	7.59 ± 0.05	7.14 ± 0.05	6.98 ± 0.02	1, 2
2MASSJ0253597+320637	21.3 ± 1.0	1	[14.17 ± 0.05]	[13.58 ± 0.02]	[12.96 ± 0.02]	[12.53 ± 0.03]	13.62 ± 0.02	12.93 ± 0.02	12.55 ± 0.03	12.33 ± 0.02	12.15 ± 0.03	1, 2
2MASSJ03140344+1603056	72.1 ± 1.5	1	[13.23 ± 0.05]	[12.48 ± 0.02]	[11.86 ± 0.04]	[11.21 ± 0.02]	12.53 ± 0.02	11.82 ± 0.04	11.24 ± 0.02	10.93 ± 0.02	10.65 ± 0.02	1, 2
2MASSJ0335020+234235	21.8 ± 1.8	1	[12.88 ± 0.05]	[12.20 ± 0.02]	[11.69 ± 0.02]	[11.23 ± 0.02]	12.25 ± 0.02	11.65 ± 0.02	11.26 ± 0.02	11.06 ± 0.08	10.77 ± 0.02	1, 2
LP 944-20	155.9 ± 1.0	19	[11.53 ± 0.05]	10.68 ± 0.03	9.98 ± 0.03	9.53 ± 0.03	10.73 ± 0.02	10.02 ± 0.02	9.55 ± 0.02	9.13 ± 0.02	8.80 ± 0.02	1, 2, 31 <sup>1</sup>
2MASSJ03552337+1133437	109.5 ± 1.4	1	[15.35 ± 0.05]	[13.95 ± 0.02]	[12.60 ± 0.03]	[11.48 ± 0.02]	14.05 ± 0.02	12.53 ± 0.03	11.53 ± 0.02	10.53 ± 0.02	9.94 ± 0.02	1, 2
2MASSJ04070752+1546457	28.9 ± 1.3	1	[16.83 ± 0.06]	[15.40 ± 0.06]	[14.41 ± 0.06]	[13.53 ± 0.04]	15.48 ± 0.06	14.35 ± 0.06	13.56 ± 0.04	12.97 ± 0.02	12.57 ± 0.03	1, 2
GJ 3276 <sup>†</sup>	3.9 ± 1.0	1	[13.60 ± 0.05]	[12.70 ± 0.02]	[11.81 ± 0.02]	[11.24 ± 0.02]	12.76 ± 0.02	11.77 ± 0.02	11.28 ± 0.02	11.04 ± 0.02	10.71 ± 0.02	1, 2
CFHT-Hy-20	30.8 ± 1.5	1	[18.11 ± 0.05]	17.02 ± 0.05	16.51 ± 0.05	16.08 ± 0.05	17.18 ± 0.05	16.44 ± 0.05	16.02 ± 0.05	15.60 ± 0.05	14.72 ± 0.08	1, 11
2MASSJ0435145−141446	11.4 ± 1.4	1	[13.00 ± 0.05]	[11.81 ± 0.03]	[10.68 ± 0.03]	[9.90 ± 0.02]	11.88 ± 0.03	10.62 ± 0.03	9.95 ± 0.02	9.73 ± 0.02	9.27 ± 0.02	1, 2
51 Eri b	33.98 ± 0.34	52	...	{18.87 ± 0.40}	{19.25 ± 0.21}	...	19.09 ± 0.40	19.20 ± 0.21	...	...	...	1, 37
SDSSJ044337.60+000205.2	47.3 ± 1.0	1	[13.31 ± 0.05]	[12.45 ± 0.03]	[11.85 ± 0.02]	[11.18 ± 0.02]	12.51 ± 0.03	11.80 ± 0.02	11.22 ± 0.02	10.83 ± 0.02	10.48 ± 0.02	1, 2
2MASSJ05012406−0010452	48.4 ± 1.4	1	[16.21 ± 0.05]	[14.89 ± 0.04]	[13.78 ± 0.03]	[12.92 ± 0.04]	14.98 ± 0.04	13.71 ± 0.03	12.96 ± 0.04	12.05 ± 0.02	11.52 ± 0.02	1, 2
2MASSJ0518461−275645	18.4 ± 1.1	1	[16.38 ± 0.05]	[15.19 ± 0.04]	[14.35 ± 0.05]	[13.57 ± 0.04]	15.26 ± 0.04	14.30 ± 0.05	13.61 ± 0.04	13.04 ± 0.02	12.66 ± 0.03	1, 2
2MASSJ0536199−192039	21.1 ± 1.6	1	[17.07 ± 0.08]	[15.69 ± 0.08]	[14.76 ± 0.07]	[13.81 ± 0.06]	15.77 ± 0.08	14.69 ± 0.07	13.85 ± 0.06	13.26 ± 0.03	12.76 ± 0.03	1, 2
β Pic b	51.44 ± 0.12	52	15.21 ± 0.34	14.04 ± 0.21	13.30 ± 0.11	12.43 ± 0.07	14.12 ± 0.21	13.24 ± 0.11	12.45 ± 0.07	...	...	8, 10, 17, 39
2MASSJ05575096−1359503	3.4 ± 1.2	1	[13.56 ± 0.05]	[12.82 ± 0.02]	[12.19 ± 0.03]	[11.69 ± 0.02]	12.87 ± 0.02	12.15 ± 0.03	11.73 ± 0.02	11.24 ± 0.02	10.60 ± 0.02	1, 2
LSRJ0602+3910	87.8 ± 1.0	1	[13.35 ± 0.05]	[12.23 ± 0.02]	[11.50 ± 0.02]	[10.84 ± 0.02]	12.30 ± 0.02	11.45 ± 0.02	10.86 ± 0.02	10.42 ± 0.02	10.14 ± 0.02	1, 2
2MASSJ0608528−275358	25.0 ± 1.5	1	[14.44 ± 0.05]	[13.53 ± 0.03]	[12.95 ± 0.03]	[12.33 ± 0.03]	13.60 ± 0.03	12.90 ± 0.03	12.37 ± 0.03	11.98 ± 0.02	11.62 ± 0.02	1, 2
CD-35 2722 B	47.0 ± 3.0	54	...	13.63 ± 0.11	12.78 ± 0.12	12.01 ± 0.07	{13.72 ± 0.11}	{12.72 ± 0.12}	{12.07 ± 0.07}	...	...	1, 54
AB Pic b	21.7 ± 0.7	52	...	15.46 ± 0.14	14.74 ± 0.10	13.73 ± 0.10	15.55 ± 0.14	14.69 ± 0.10	13.77 ± 0.10	...	...	6, 7, 15
2MASSJ0619526−290359	3.6 ± 2.0	1	[16.09 ± 0.05]	[15.08 ± 0.04]	[14.24 ± 0.04]	[13.40 ± 0.05]	15.14 ± 0.04	14.19 ± 0.04	13.45 ± 0.05	13.03 ± 0.02	12.60 ± 0.02	1, 2
2MASSJ07140394+3702459	80 ± 5	20	...	{11.93 ± 0.02}	{11.29 ± 0.03}	{10.81 ± 0.02}	11.98 ± 0.02	11.25 ± 0.03	10.84 ± 0.02	10.57 ± 0.02	10.35 ± 0.02	1, 2
LP 423-31	54.3 ± 1.4	1	[11.49 ± 0.05]	[10.84 ± 0.02]	[10.22 ± 0.02]	[9.82 ± 0.02]	10.88 ± 0.02	10.20 ± 0.02	9.85 ± 0.02	9.61 ± 0.02	9.45 ± 0.02	1, 2
WISEJ075430.95+790957.8	51.1 ± 1.2	1	[17.17 ± 0.11]	[16.00 ± 0.11]	[15.52 ± 0.14]	[14.95 ± 0.12]	16.17 ± 0.11	15.44 ± 0.14	14.93 ± 0.12	14.39 ± 0.03	13.74 ± 0.03	1, 2
LP 261-75B	31.6 ± 1.3	1	[18.30 ± 0.21]	[17.13 ± 0.21]	[15.95 ± 0.14]	[15.12 ± 0.13]	17.23 ± 0.21	15.90 ± 0.14	15.14 ± 0.13	...	...	1, 2
G 196-3B	49.0 ± 2.3	1	[16.17 ± 0.05]	[14.73 ± 0.05]	[13.72 ± 0.04]	[12.73 ± 0.03]	14.83 ± 0.05	13.65 ± 0.04	12.78 ± 0.03	11.70 ± 0.02	11.13 ± 0.02	1, 2
2MASSJ10220489+0200477	34.6 ± 2.0	1	15.07 ± 0.02	14.05 ± 0.02	13.44 ± 0.02	12.90 ± 0.02	14.10 ± 0.03	13.40 ± 0.03	12.90 ± 0.03	12.62 ± 0.02	12.34 ± 0.03	1, 2, 3
2MASSJ10224821+5825453	52.6 ± 3.1	1	[14.52 ± 0.05]	[13.43 ± 0.03]	[12.69 ± 0.03]	[12.13 ± 0.03]	13.50 ± 0.03	12.64 ± 0.03	12.16 ± 0.03	11.77 ± 0.02	11.51 ± 0.02	1, 2
SDSSJ102552.43+321234.0	37.3 ± 1.2	1	[17.99 ± 0.05]	16.89 ± 0.05	15.98 ± 0.03	15.16 ± 0.03	[16.99 ± 0.05]	15.59 ± 0.17	15.07 ± 0.18	14.38 ± 0.03	14.01 ± 0.04	1, 2, 16
SDSSJ104523.98−014957.7	61.8 ± 1.5	1	14.23 ± 0.02	13.08 ± 0.02	12.40 ± 0.02	11.78 ± 0.02	13.16 ± 0.02	12.35 ± 0.03	11.78 ± 0.02	11.46 ± 0.02	11.24 ± 0.02	1, 2, 3
DENISJ1047.5−1815	37.9 ± 1.9	1	[15.16 ± 0.05]	[14.14 ± 0.03]	[13.47 ± 0.03]	[12.87 ± 0.03]	14.20 ± 0.03	13.42 ± 0.03	12.89 ± 0.03	12.58 ± 0.02	12.32 ± 0.02	1, 2
SSSPMJ1102−3431 <sup>†</sup>	21.1 ± 2.1	1	[13.86 ± 0.05]	[12.98 ± 0.02]	[12.40 ± 0.02]	[11.85 ± 0.02]	13.03 ± 0.02	12.36 ± 0.02	11.89 ± 0.02	11.45 ± 0.02	10.81 ± 0.02	1, 2

118

Table 6—Continued

Object	Parallax (mas)	Ref.	MKO				2MASS			ALLWISE		Refs.
			<i>Y</i> (mag)	<i>J</i> (mag)	<i>H</i> (mag)	<i>K</i> (mag)	<i>J</i> (mag)	<i>H</i> (mag)	<i>K<sub>S</sub></i> (mag)	W1 (mag)	W2 (mag)	
SDSSJ111010.01+011613.1	52.1 ± 1.2	23	[17.07 ± 0.05]	16.12 ± 0.05	16.22 ± 0.05	16.05 ± 0.05	16.34 ± 0.12	15.92 ± 0.14	[15.93 ± 0.05]	15.44 ± 0.04	13.92 ± 0.04	1, 2, 32
TWA 5B	20.0 ± 0.7	55	...	12.60 ± 0.20	12.14 ± 0.06	11.40 ± 0.20	[12.67 ± 0.20]	[12.09 ± 0.06]	[11.45 ± 0.20]	...	...	1, 34
TWA 8B	25.9 ± 2.0	22	[10.37 ± 0.05]	[9.80 ± 0.02]	[9.31 ± 0.02]	[8.98 ± 0.03]	9.84 ± 0.02	9.28 ± 0.02	9.01 ± 0.03	8.93 ± 0.08	8.65 ± 0.05	1, 2
2MASSWJ1139511−315921 <sup>†</sup>	26.2 ± 1.1	22	[13.45 ± 0.05]	[12.62 ± 0.03]	[12.05 ± 0.02]	[11.46 ± 0.02]	12.69 ± 0.03	12.00 ± 0.02	11.50 ± 0.02	11.17 ± 0.02	10.82 ± 0.02	1, 2
2MASSWJ1207334−393254 <sup>†</sup>	19.1 ± 0.4	21	[13.68 ± 0.05]	[12.94 ± 0.03]	[12.43 ± 0.03]	[11.91 ± 0.03]	13.00 ± 0.03	12.39 ± 0.03	11.95 ± 0.03	11.56 ± 0.02	11.01 ± 0.02	1, 14, 45
2MASSWJ1207334−393254b	19.1 ± 0.4	21	...	[19.91 ± 0.20]	[18.15 ± 0.21]	[16.87 ± 0.11]	20.00 ± 0.20	18.09 ± 0.21	16.93 ± 0.11	...	...	1, 14, 23, 45, 50
DENISJ124514.1−442907 <sup>†</sup>	12.7 ± 2.1	55	[15.32 ± 0.05]	[14.45 ± 0.03]	[13.85 ± 0.03]	[13.33 ± 0.04]	14.52 ± 0.03	13.80 ± 0.03	13.37 ± 0.04	12.99 ± 0.02	12.65 ± 0.02	1, 2
Ross 458C	85.5 ± 1.5	52	17.72 ± 0.02	16.69 ± 0.01	17.01 ± 0.04	16.90 ± 0.06	[16.98 ± 0.01]	[16.96 ± 0.04]	[16.79 ± 0.06]	16.04 ± 0.06	13.85 ± 0.04	1, 28
LSPMJ1314+1320A	57.98 ± 0.05	24	...	10.43 ± 0.03	9.94 ± 0.04	9.48 ± 0.02	10.47 ± 0.03	9.91 ± 0.04	9.51 ± 0.02	...	...	2, 24
LSPMJ1314+1320B	57.98 ± 0.05	24	...	10.51 ± 0.03	9.97 ± 0.04	9.56 ± 0.02	10.51 ± 0.03	9.94 ± 0.04	9.59 ± 0.02	...	...	2, 24
2MASSJ13153094−2649513A	55.0 ± 2.1	1	...	15.14 ± 0.05	14.14 ± 0.03	13.45 ± 0.04	{15.23 ± 0.05}	{14.08 ± 0.03}	{13.47 ± 0.04}	...	...	1, 13
2MASSJ13153094−2649513B	55.0 ± 2.1	1	...	18.20 ± 0.06	18.66 ± 0.07	18.79 ± 0.11	{18.46 ± 0.06}	{18.61 ± 0.07}	{18.66 ± 0.11}	...	...	1, 13
Gl 504b	56.95 ± 0.26	52	...	{19.61 ± 0.15}	{20.21 ± 0.14}	{19.29 ± 0.28}	19.91 ± 0.15	20.14 ± 0.14	19.19 ± 0.28	...	...	1, 30
2MASSJ13313310+3407583	35.6 ± 1.6	1	15.21 ± 0.02	14.13 ± 0.02	13.42 ± 0.02	12.81 ± 0.02	14.33 ± 0.03	13.40 ± 0.03	12.89 ± 0.02	12.58 ± 0.02	12.34 ± 0.02	1, 2, 3
2MASSJ14112131−2119503	19.5 ± 1.9	1	[13.14 ± 0.05]	[12.39 ± 0.02]	[11.87 ± 0.03]	[11.30 ± 0.02]	12.44 ± 0.02	11.83 ± 0.03	11.33 ± 0.02	11.08 ± 0.02	10.82 ± 0.02	1, 2
DENISJ142527.9−365023	86.4 ± 0.8	19	...	{13.67 ± 0.03}	{12.62 ± 0.02}	{11.77 ± 0.03}	13.75 ± 0.03	12.57 ± 0.02	11.81 ± 0.03	11.04 ± 0.02	10.57 ± 0.02	1, 2
DENISJ1441.6−0945A	29.6 ± 1.7	1	[15.61 ± 0.05]	[14.59 ± 0.03]	[13.88 ± 0.03]	[13.30 ± 0.03]	14.65 ± 0.03	13.83 ± 0.03	13.32 ± 0.03	...	...	1, 2
DENISJ1441.6−0945B	29.6 ± 1.7	1	[15.93 ± 0.05]	[14.84 ± 0.03]	[14.11 ± 0.03]	[13.50 ± 0.03]	14.90 ± 0.03	14.06 ± 0.03	13.52 ± 0.03	...	...	1, 2
2MASSJ15474719−2423493	30.1 ± 1.1	1	[14.86 ± 0.05]	[13.91 ± 0.03]	[13.31 ± 0.03]	[12.71 ± 0.03]	13.97 ± 0.03	13.27 ± 0.03	12.74 ± 0.03	12.41 ± 0.08	12.06 ± 0.03	1, 2
2MASSJ15515237+0941148	22.1 ± 1.5	1	[17.53 ± 0.11]	[16.23 ± 0.11]	[15.18 ± 0.07]	[14.27 ± 0.06]	16.32 ± 0.11	15.11 ± 0.07	14.31 ± 0.06	13.61 ± 0.02	13.13 ± 0.03	1, 2
2MASSJ15525906+2948485	47.8 ± 1.0	1	[14.50 ± 0.05]	[13.41 ± 0.03]	[12.66 ± 0.03]	[11.99 ± 0.03]	13.48 ± 0.03	12.61 ± 0.03	12.02 ± 0.03	11.55 ± 0.02	11.20 ± 0.02	1, 2
2MASSJ1615425+495321	32.0 ± 1.0	1	[18.08 ± 0.14]	[16.68 ± 0.14]	[15.40 ± 0.10]	[14.26 ± 0.07]	16.79 ± 0.14	15.33 ± 0.10	14.31 ± 0.07	13.21 ± 0.02	12.63 ± 0.02	1, 2
HR 6037Ba	19.2 ± 0.4	52	...	[14.85 ± 0.19]	[13.79 ± 0.15]	[13.59 ± 0.17]	14.92 ± 0.19	13.74 ± 0.15	13.62 ± 0.17	...	...	1, 39, 48
HR 6037Bb	19.2 ± 0.4	52	...	[15.19 ± 0.19]	[13.92 ± 0.15]	[13.78 ± 0.17]	15.26 ± 0.19	13.87 ± 0.15	13.81 ± 0.17	...	...	1, 39, 48
DENISJ170548.3−051645	53.5 ± 1.0	1	[14.27 ± 0.05]	[13.24 ± 0.03]	[12.60 ± 0.02]	[12.01 ± 0.02]	13.31 ± 0.03	12.55 ± 0.02	12.03 ± 0.02	11.68 ± 0.02	11.42 ± 0.02	1, 2
2MASSJ1707333+430130	36.1 ± 1.0	1	[14.89 ± 0.05]	[13.92 ± 0.03]	[13.22 ± 0.03]	[12.60 ± 0.03]	13.97 ± 0.03	13.18 ± 0.03	12.62 ± 0.03	12.28 ± 0.02	12.01 ± 0.02	1, 2
2MASSJ17111135+232633	30.6 ± 1.7	1	[15.61 ± 0.05]	[14.43 ± 0.03]	[13.72 ± 0.03]	[13.03 ± 0.03]	14.50 ± 0.03	13.67 ± 0.03	13.06 ± 0.03	12.60 ± 0.02	12.24 ± 0.02	1, 2
2MASSWJ1726000+153819	28.3 ± 1.0	1	[16.87 ± 0.06]	[15.58 ± 0.06]	[14.53 ± 0.05]	[13.62 ± 0.05]	15.67 ± 0.06	14.47 ± 0.05	13.66 ± 0.05	13.07 ± 0.02	12.67 ± 0.03	1, 2
2MASSJ18212815+1414010	104.6 ± 1.0	1	[14.59 ± 0.05]	[13.33 ± 0.02]	[12.46 ± 0.02]	[11.62 ± 0.02]	13.43 ± 0.02	12.40 ± 0.02	11.65 ± 0.02	10.85 ± 0.02	10.48 ± 0.02	1, 2
PZ Tel B	19.4 ± 1.0	52	...	12.47 ± 0.20	11.93 ± 0.14	{11.50 ± 0.07}	{12.52 ± 0.20}	{11.89 ± 0.14}	11.53 ± 0.07	...	...	1, 38
HR 7329B	20.74 ± 0.21	52	...	{12.01 ± 0.19}	11.93 ± 0.06	{11.57 ± 0.10}	12.06 ± 0.19	11.75 ± 0.10	11.60 ± 0.10	...	...	1, 35, 46
2MASSJ19355595−2846343	14.2 ± 1.2	1	[14.85 ± 0.05]	[13.89 ± 0.03]	[13.23 ± 0.02]	[12.67 ± 0.03]	13.95 ± 0.03	13.18 ± 0.02	12.71 ± 0.03	12.38 ± 0.02	11.90 ± 0.03	1, 2
2MASSJ20135152−2806020	21.0 ± 1.3	1	[15.15 ± 0.05]	[14.18 ± 0.03]	[13.52 ± 0.03]	[12.90 ± 0.03]	14.24 ± 0.03	13.46 ± 0.03	12.94 ± 0.03	12.55 ± 0.02	12.17 ± 0.03	1, 2
DENISJ205754.1−025229	70.1 ± 3.7	26	[14.15 ± 0.05]	[13.05 ± 0.02]	[12.32 ± 0.02]	[11.70 ± 0.03]	13.12 ± 0.02	12.27 ± 0.02	11.72 ± 0.03	11.29 ± 0.02	11.02 ± 0.02	1, 2
PSOJ318.5338−22.8603	45.1 ± 1.7	1	18.81 ± 0.10	17.15 ± 0.04	15.68 ± 0.02	14.41 ± 0.02	16.71 ± 0.20	15.72 ± 0.17	14.74 ± 0.12	13.24 ± 0.02	12.50 ± 0.03	33
HD 203030B	24.5 ± 0.7	52	...	{18.03 ± 0.55}	{16.91 ± 0.12}	{16.19 ± 0.10}	18.13 ± 0.55	16.85 ± 0.12	16.21 ± 0.10	...	...	1, 43
2MASSJ21043907+3655563	11.4 ± 1.0	1	[16.33 ± 0.07]	[15.55 ± 0.07]	[15.11 ± 0.08]	[14.63 ± 0.11]	15.61 ± 0.07	15.07 ± 0.08	14.68 ± 0.11	14.65 ± 0.03	14.44 ± 0.05	1, 2
HN Peg B	55.9 ± 0.5	52	[16.86 ± 0.05]	15.86 ± 0.03	15.40 ± 0.03	15.12 ± 0.03	16.70 ± 0.16	15.55 ± 0.11	15.63 ± 0.25	...	...	1, 2, 36
2MASSJ21481633+4003594	101.0 ± 1.8	1	[15.48 ± 0.05]	[14.05 ± 0.03]	[12.85 ± 0.03]	[11.73 ± 0.02]	14.15 ± 0.03	12.78 ± 0.03	11.77 ± 0.02	10.76 ± 0.02	10.24 ± 0.02	1, 2
SIMPJ215434.5−105530.8	32.6 ± 1.0	1	[17.70 ± 0.12]	[16.35 ± 0.12]	[15.14 ± 0.08]	[14.16 ± 0.07]	16.44 ± 0.12	15.07 ± 0.08	14.20 ± 0.07	13.36 ± 0.03	12.91 ± 0.03	1, 2
DENISJ220002.0−303832A	38 ± 4	1	[14.91 ± 0.10]	[14.00 ± 0.10]	[13.32 ± 0.10]	[12.81 ± 0.10]	14.05 ± 0.10	13.28 ± 0.10	12.83 ± 0.10	...	...	1, 12
DENISJ220002.0−303832B	38 ± 4	1	[15.05 ± 0.10]	[14.31 ± 0.10]	[13.61 ± 0.10]	[13.06 ± 0.10]	14.36 ± 0.10	13.57 ± 0.10	13.09 ± 0.10	...	...	1, 12
2MASSWJ2208136+292121	25.1 ± 1.6	1	[16.99 ± 0.09]	[15.71 ± 0.09]	[14.86 ± 0.07]	[14.11 ± 0.07]	15.80 ± 0.09	14.79 ± 0.07	14.15 ± 0.07	13.38 ± 0.03	12.91 ± 0.03	1, 2
2MASSJ22134491−2136079	20.9 ± 1.9	1	[16.43 ± 0.05]	[15.30 ± 0.04]	[14.46 ± 0.06]	[13.72 ± 0.04]	15.38 ± 0.04	14.40 ± 0.06	13.76 ± 0.04	13.25 ± 0.03	12.87 ± 0.03	1, 2
2MASSWJ2224438−015852	86.2 ± 1.1	23	[15.32 ± 0.05]	13.89 ± 0.03	12.84 ± 0.03	11.98 ± 0.03	14.07 ± 0.03	12.82 ± 0.03	12.02 ± 0.02	11.41 ± 0.02	11.15 ± 0.02	1, 2, 29
2MASSWJ2244316+204343	58.7 ± 1.0	1	[17.53 ± 0.05]	16.33 ± 0.03	15.06 ± 0.03	13.90 ± 0.03	16.48 ± 0.14	15.00 ± 0.07	14.02 ± 0.07	12.79 ± 0.02	12.13 ± 0.02	1, 2, 29
SDSSJ224953.46+004404.6A	25.5 ± 1.4	1	...	16.84 ± 0.01	15.73 ± 0.01	14.82 ± 0.01	16.94 ± 0.13	15.80 ± 0.11	14.76 ± 0.07	...	...	1, 2, 3, 4
SDSSJ224953.46+004404.6B	25.5 ± 1.4	1	...	17.86 ± 0.02	16.68 ± 0.01	15.72 ± 0.01	17.98 ± 0.13	16.75 ± 0.11	15.64 ± 0.07	...	...	1, 2, 3, 4
HR 8799b	25.4 ± 0.7	52	...	19.46 ± 0.18	18.09 ± 0.12	{16.99 ± 0.06}	{19.59 ± 0.18}	{18.03 ± 0.12}	16.96 ± 0.06	...	...	1, 25, 49

Table 6—Continued

Object	Parallax (mas)	Ref.	MKO				2MASS			AllWISE		Refs.
			<i>Y</i> (mag)	<i>J</i> (mag)	<i>H</i> (mag)	<i>K</i> (mag)	<i>J</i> (mag)	<i>H</i> (mag)	<i>K<sub>S</sub></i> (mag)	W1 (mag)	W2 (mag)	
HR 8799c	$25.4 \pm 0.7$	52	...	$17.63 \pm 0.21$	$17.18 \pm 0.15$	$\{16.14 \pm 0.07\}$	$\{17.74 \pm 0.21\}$	$\{17.11 \pm 0.15\}$	$16.18 \pm 0.07$	...	...	1, 25, 49
HR 8799d	$25.4 \pm 0.7$	52	...	$18.24 \pm 0.43$	$16.67 \pm 0.19$	$\{16.05 \pm 0.12\}$	$\{18.35 \pm 0.43\}$	$\{16.60 \pm 0.19\}$	$16.09 \pm 0.12$	...	...	1, 40, 49
HR 8799e	$25.4 \pm 0.7$	52	...	...	$16.28 \pm 0.27$	$\{15.87 \pm 0.22\}$	...	$\{16.21 \pm 0.27\}$	$15.91 \pm 0.22$	...	...	1, 41, 49
2MASSJ23224684–3133231	$50.2 \pm 2.8$	1	$[14.51 \pm 0.05]$	$[13.50 \pm 0.03]$	$[12.84 \pm 0.02]$	$[12.30 \pm 0.02]$	$13.58 \pm 0.03$	$12.79 \pm 0.02$	$12.32 \pm 0.02$	$12.01 \pm 0.02$	$11.72 \pm 0.02$	1, 2
WISEJ233527.07+451140.9	$44.0 \pm 1.4$	1	$[18.00 \pm 0.05]$	$16.83 \pm 0.03$	$15.63 \pm 0.02$	$14.36 \pm 0.04$	$[16.94 \pm 0.03]$	$[15.56 \pm 0.02]$	$[14.40 \pm 0.04]$	$13.53 \pm 0.02$	$12.95 \pm 0.03$	1, 5
$\kappa$ And b	$19.37 \pm 0.19$	52	...	$\{15.79 \pm 0.21\}$	$\{15.00 \pm 0.13\}$	$\{14.29 \pm 0.09\}$	$15.86 \pm 0.21$	$14.95 \pm 0.13$	$14.32 \pm 0.09$	...	...	1, 9
2MASSJ23512200+3010540	$41.2 \pm 1.4$	1	$[17.00 \pm 0.10]$	$[15.75 \pm 0.10]$	$[14.63 \pm 0.07]$	$[13.99 \pm 0.06]$	$15.85 \pm 0.10$	$14.57 \pm 0.07$	$14.02 \pm 0.06$	$13.23 \pm 0.02$	$12.85 \pm 0.03$	1, 2

Note. — Published photometry for our parallax sample, as well as other young objects from the literature, supplemented by synthetic photometry calculated here. For objects with near-infrared spectra and some published *JHK* photometry, we calculate 2MASS–MKO conversions and *Y* – *J* colors directly from that object’s spectrum. We denote these synthesized values with brackets [...]. For objects without spectra, we estimate 2MASS–MKO conversions based on the values for other objects expected to be of similar spectral type. We denote these estimated values with braces {...}. Our synthesized *Y* – *J* colors have uncertainties of 0.05 mag, and UKIDSS DR10 photometry have systematic errors of  $\approx 0.02$  mag in *Y* and  $\approx 0.015$  mag in *JHK* (Hodgkin et al. 2009). *WISE* photometry is from the AllWISE Source Catalog that merges the cryogenic *WISE* mission survey data (Wright et al. 2010) with the post-cryogenic NEOWISE survey (Mainzer et al. 2011).

<sup>†</sup>Alternate names: SO J025300.5+165258 (Teegarden’s star), GJ 3276 (2MASS J04221413+1530525), SSSPM J1102–3431 (TWA 28), 2MASSW J1139511–315921 (TWA 26), 2MASSW J1207334–393254 (TWA 27), DENIS J124514.1–442907 (TWA 29).

References. — (1) This work; (2) 2MASS Point Source Catalog (Cutri et al. 2003); (3) UKIDSS DR10; (4) Allers et al. (2010); (5) Best et al. (2015); (6) Biller et al. (2013); (7) Bonnefoy et al. (2010); (8) Bonnefoy et al. (2011); (9) Bonnefoy et al. (2014a); (10) Bonnefoy et al. (2014b); (11) Bouvier et al. (2008); (12) Burgasser & McElwain (2006); (13) Burgasser et al. (2011); (14) Chauvin et al. (2004); (15) Chauvin et al. (2005b); (16) Chiu et al. (2006); (17) Currie et al. (2013); (18) Delorme et al. (2013); (19) Dieterich et al. (2014); (20) Dittmann et al. (2014); (21) Ducourant et al. (2008); (22) Ducourant et al. (2014); (23) Dupuy & Liu (2012); (24) Dupuy et al. (2016b); (25) Esposito et al. (2013); (26) Faherty et al. (2012); (27) Gatewood & Coban (2009); (28) Goldman et al. (2010); (29) Knapp et al. (2004); (30) Kuzuhara et al. (2013); (31) Leggett et al. (1998); (32) Leggett et al. (2002); (33) Liu et al. (2013b); (34) Lowrance et al. (1999); (35) Lowrance et al. (2000); (36) Luhman et al. (2007); (37) Macintosh et al. (2015); (38) Maire et al. (2016); (39) Males et al. (2014); (40) Marois et al. (2008); (41) Marois et al. (2010); (42) Marocco et al. (2013); (43) Metchev & Hillenbrand (2006); (44) Meshkat et al. (2015); (45) Mohanty et al. (2007); (46) Neuhäuser et al. (2011); (47) Nielsen et al. (2012); (48) Nielsen et al. (2013); (49) Oppenheimer et al. (2013); (50) Patience et al. (2010); (51) Riedel et al. (2014); (52) van Leeuwen (2007); (53) Vrba et al. (2004); (54) Wahhaj et al. (2011); (55) Weinberger et al. (2013).



Table 7. Absolute Magnitudes for Our Sample and Other Potentially Young Objects

Object	Spec. Type Optical/NIR	Ref.	MKO				2MASS			ALLWISE		Notes
			$M_Y$ (mag)	$M_J$ (mag)	$M_H$ (mag)	$M_K$ (mag)	$M_J$ (mag)	$M_H$ (mag)	$M_{K_S}$ (mag)	$M_{W1}$ (mag)	$M_{W2}$ (mag)	
<b>Very low gravity objects (VL-G)</b>												
2MASSJ0045+1634	L2 $\beta$ /L2 VL-G	5, 22, 73	[13.22 $\pm$ 0.07]	[12.08 $\pm$ 0.05]	[11.21 $\pm$ 0.06]	[10.43 $\pm$ 0.05]	12.15 $\pm$ 0.05	11.15 $\pm$ 0.06	10.46 $\pm$ 0.05	9.88 $\pm$ 0.05	9.49 $\pm$ 0.05	Argus
2MASSJ0126+1428	L4 $\gamma$ /L2 VL-G	5, 30	15.15 $\pm$ 0.17	13.62 $\pm$ 0.16	12.31 $\pm$ 0.15	11.27 $\pm$ 0.15	13.27 $\pm$ 0.26	12.33 $\pm$ 0.27	11.44 $\pm$ 0.21	10.38 $\pm$ 0.15	9.85 $\pm$ 0.16	...
2MASSJ0241-0326	L0 $\gamma$ /L1 VL-G	5, 22	[13.19 $\pm$ 0.26]	[12.06 $\pm$ 0.26]	[11.20 $\pm$ 0.26]	[10.33 $\pm$ 0.26]	12.13 $\pm$ 0.26	11.15 $\pm$ 0.26	10.37 $\pm$ 0.26	9.98 $\pm$ 0.25	9.62 $\pm$ 0.25	(Tuc-Hor)
2MASSJ0335+2342	M8.5/M7 VL-G	5, 33, 71, 79	[9.57 $\pm$ 0.18]	[8.89 $\pm$ 0.18]	[8.38 $\pm$ 0.18]	[7.92 $\pm$ 0.18]	8.94 $\pm$ 0.18	8.35 $\pm$ 0.18	7.95 $\pm$ 0.18	7.75 $\pm$ 0.20	7.47 $\pm$ 0.18	$\beta$ Pic, strong H $\alpha$
2MASSJ0355+1133	L5 $\gamma$ /L3 VL-G	5, 22, 73	[15.54 $\pm$ 0.06]	[14.15 $\pm$ 0.04]	[12.79 $\pm$ 0.04]	[11.67 $\pm$ 0.03]	14.25 $\pm$ 0.04	12.73 $\pm$ 0.04	11.72 $\pm$ 0.03	10.72 $\pm$ 0.04	10.14 $\pm$ 0.03	AB Dor
GJ3276 $\dagger$	M6 $\gamma$ /M6 VL-G	5, 73	[6.58 $\pm$ 0.54]	[5.68 $\pm$ 0.54]	[4.79 $\pm$ 0.54]	[4.22 $\pm$ 0.54]	5.73 $\pm$ 0.54	4.74 $\pm$ 0.54	4.25 $\pm$ 0.54	4.02 $\pm$ 0.54	3.69 $\pm$ 0.54	...
2MASSJ0435-1414	M6 $\delta$ /M7 VL-G	5, 18	[8.30 $\pm$ 0.27]	[7.10 $\pm$ 0.27]	[5.97 $\pm$ 0.27]	[5.20 $\pm$ 0.27]	7.17 $\pm$ 0.27	5.91 $\pm$ 0.27	5.24 $\pm$ 0.27	5.02 $\pm$ 0.27	4.56 $\pm$ 0.27	MBM20,disk?
SDSSJ0443+0002	M9/L0 VL-G	5, 21, 37, 43	[11.68 $\pm$ 0.07]	[10.82 $\pm$ 0.05]	[10.23 $\pm$ 0.05]	[9.55 $\pm$ 0.05]	10.88 $\pm$ 0.05	10.18 $\pm$ 0.05	9.59 $\pm$ 0.05	9.21 $\pm$ 0.05	8.86 $\pm$ 0.05	$\beta$ Pic
2MASSJ0501-0010	L4 $\gamma$ /L3 VL-G	5, 22, 73	[14.63 $\pm$ 0.08]	[13.31 $\pm$ 0.07]	[12.20 $\pm$ 0.07]	[11.34 $\pm$ 0.07]	13.40 $\pm$ 0.07	12.13 $\pm$ 0.07	11.38 $\pm$ 0.07	10.47 $\pm$ 0.07	9.94 $\pm$ 0.07	...
2MASSJ0518-2756	L1 $\gamma$ /L1 VL-G	5, 30	[12.71 $\pm$ 0.14]	[11.51 $\pm$ 0.14]	[10.68 $\pm$ 0.14]	[9.90 $\pm$ 0.14]	11.59 $\pm$ 0.14	10.62 $\pm$ 0.14	9.94 $\pm$ 0.14	9.37 $\pm$ 0.13	8.99 $\pm$ 0.13	(Columba)
2MASSJ0536-1920	L2 $\gamma$ /L2 VL-G	5, 30	[13.69 $\pm$ 0.18]	[12.31 $\pm$ 0.18]	[11.38 $\pm$ 0.18]	[10.43 $\pm$ 0.17]	12.39 $\pm$ 0.18	11.32 $\pm$ 0.18	10.48 $\pm$ 0.17	9.88 $\pm$ 0.16	9.38 $\pm$ 0.16	(Columba)
2MASSJ0557-1359	M7/M7 VL-G	5, 79	[6.22 $\pm$ 0.76]	[5.47 $\pm$ 0.76]	[4.84 $\pm$ 0.76]	[4.35 $\pm$ 0.76]	5.52 $\pm$ 0.76	4.80 $\pm$ 0.76	4.38 $\pm$ 0.76	3.89 $\pm$ 0.76	3.25 $\pm$ 0.76	...
2MASSJ0608-2753	M8.5 $\gamma$ /L0 VL-G	5, 43, 75	[11.43 $\pm$ 0.14]	[10.52 $\pm$ 0.13]	[9.94 $\pm$ 0.13]	[9.31 $\pm$ 0.13]	10.58 $\pm$ 0.13	9.88 $\pm$ 0.13	9.36 $\pm$ 0.13	8.96 $\pm$ 0.13	8.61 $\pm$ 0.13	(Columba)
AB Pic b	... /L0 VL-G	5	...	12.14 $\pm$ 0.16	11.42 $\pm$ 0.12	10.41 $\pm$ 0.12	12.23 $\pm$ 0.16	11.37 $\pm$ 0.12	10.45 $\pm$ 0.12	...	...	Tuc-Hor
G196-3B	L3 $\beta$ /L3 VL-G	5, 22, 82	[14.62 $\pm$ 0.11]	[13.18 $\pm$ 0.11]	[12.17 $\pm$ 0.11]	[11.18 $\pm$ 0.11]	13.28 $\pm$ 0.11	12.10 $\pm$ 0.11	11.23 $\pm$ 0.11	10.15 $\pm$ 0.11	9.58 $\pm$ 0.11	...
SSSPMJ1102-3431 $\dagger$	M8.5p $\gamma$ /M9 VL-G	5, 43, 78	[10.48 $\pm$ 0.22]	[9.60 $\pm$ 0.22]	[9.02 $\pm$ 0.22]	[8.47 $\pm$ 0.22]	9.65 $\pm$ 0.22	8.98 $\pm$ 0.22	8.51 $\pm$ 0.22	8.07 $\pm$ 0.22	7.43 $\pm$ 0.22	(TWA 28)
TWA5B	... /M9 VL-G	5	...	9.10 $\pm$ 0.21	8.64 $\pm$ 0.10	7.90 $\pm$ 0.21	[9.17 $\pm$ 0.21]	[8.59 $\pm$ 0.10]	[7.95 $\pm$ 0.21]	...	...	TWA
TWA8B	M5/M6 VL-G	5, 80	[7.44 $\pm$ 0.18]	[6.86 $\pm$ 0.17]	[6.38 $\pm$ 0.17]	[6.05 $\pm$ 0.17]	6.90 $\pm$ 0.17	6.34 $\pm$ 0.17	6.08 $\pm$ 0.17	5.99 $\pm$ 0.19	5.71 $\pm$ 0.18	TWA
2MASSJ1139-3159 $\dagger$	M9/M9 VL-G	5, 51, 73	[10.54 $\pm$ 0.10]	[9.71 $\pm$ 0.09]	[9.14 $\pm$ 0.09]	[8.55 $\pm$ 0.09]	9.78 $\pm$ 0.09	9.09 $\pm$ 0.09	8.59 $\pm$ 0.09	8.26 $\pm$ 0.09	7.91 $\pm$ 0.09	TWA 26
2MASSJ1207-3932 $\dagger$	M8/M8 VL-G	5, 34	[10.08 $\pm$ 0.07]	[9.35 $\pm$ 0.05]	[8.84 $\pm$ 0.05]	[8.32 $\pm$ 0.05]	9.41 $\pm$ 0.05	8.80 $\pm$ 0.05	8.36 $\pm$ 0.05	7.96 $\pm$ 0.05	7.41 $\pm$ 0.05	TWA 27
2MASSJ1207-3932b	... /L3 VL-G	5	...	[16.32 $\pm$ 0.21]	[14.56 $\pm$ 0.21]	[13.28 $\pm$ 0.12]	16.41 $\pm$ 0.21	14.50 $\pm$ 0.21	13.34 $\pm$ 0.12	...	...	TWA 27b
DENISJ1245-4429 $\dagger$	M9.5/L0 VL-G	5, 50	[10.83 $\pm$ 0.36]	[9.96 $\pm$ 0.36]	[9.37 $\pm$ 0.36]	[8.84 $\pm$ 0.36]	10.03 $\pm$ 0.36	9.31 $\pm$ 0.36	8.88 $\pm$ 0.36	8.50 $\pm$ 0.36	8.16 $\pm$ 0.36	(TWA 29)
2MASSJ1551+0941	L4 $\gamma$ /L4 VL-G	5, 30	[14.25 $\pm$ 0.18]	[12.95 $\pm$ 0.18]	[11.91 $\pm$ 0.16]	[10.99 $\pm$ 0.15]	13.04 $\pm$ 0.18	11.84 $\pm$ 0.16	11.04 $\pm$ 0.15	10.33 $\pm$ 0.14	9.85 $\pm$ 0.15	...
2MASSJ1615+4953	L4 $\gamma$ /L3 VL-G	5, 21, 30, 73	[15.60 $\pm$ 0.15]	[14.21 $\pm$ 0.15]	[12.92 $\pm$ 0.12]	[11.78 $\pm$ 0.10]	14.31 $\pm$ 0.15	12.86 $\pm$ 0.12	11.83 $\pm$ 0.10	10.74 $\pm$ 0.07	10.16 $\pm$ 0.07	...
2MASSJ1935-2846	M9/M9 VL-G	5, 73	[10.61 $\pm$ 0.19]	[9.65 $\pm$ 0.19]	[9.00 $\pm$ 0.18]	[8.44 $\pm$ 0.19]	9.72 $\pm$ 0.19	8.95 $\pm$ 0.18	8.48 $\pm$ 0.19	8.15 $\pm$ 0.18	7.67 $\pm$ 0.18	( $\beta$ Pic)
2MASSJ2013-2806	M9/L0 VL-G	5, 73	[11.76 $\pm$ 0.14]	[10.78 $\pm$ 0.14]	[10.12 $\pm$ 0.14]	[9.51 $\pm$ 0.14]	10.85 $\pm$ 0.14	10.07 $\pm$ 0.14	9.55 $\pm$ 0.14	9.16 $\pm$ 0.14	8.78 $\pm$ 0.14	( $\beta$ Pic)
PSOJ318.5-22	... /L7 VL-G	49	17.08 $\pm$ 0.13	15.42 $\pm$ 0.09	13.95 $\pm$ 0.09	12.68 $\pm$ 0.09	14.98 $\pm$ 0.22	13.99 $\pm$ 0.19	13.01 $\pm$ 0.15	11.51 $\pm$ 0.09	10.78 $\pm$ 0.09	$\beta$ Pic
2MASSJ2208+2921	L3 $\gamma$ /L3 VL-G	5, 22	[13.99 $\pm$ 0.16]	[12.71 $\pm$ 0.16]	[11.86 $\pm$ 0.16]	[11.10 $\pm$ 0.16]	12.80 $\pm$ 0.16	11.79 $\pm$ 0.16	11.15 $\pm$ 0.16	10.38 $\pm$ 0.14	9.91 $\pm$ 0.14	$\beta$ Pic?
2MASSJ2213-2136	L0 $\gamma$ /L0 VL-G	5, 22, 43	[13.03 $\pm$ 0.21]	[11.89 $\pm$ 0.20]	[11.06 $\pm$ 0.21]	[10.32 $\pm$ 0.20]	11.97 $\pm$ 0.20	11.00 $\pm$ 0.21	10.35 $\pm$ 0.20	9.84 $\pm$ 0.20	9.47 $\pm$ 0.20	...
2MASSJ2244+2043	L6.5/L6 VL-G	5, 43	[16.37 $\pm$ 0.06]	15.17 $\pm$ 0.05	13.90 $\pm$ 0.05	12.74 $\pm$ 0.05	15.32 $\pm$ 0.14	13.84 $\pm$ 0.07	12.87 $\pm$ 0.08	11.63 $\pm$ 0.04	10.97 $\pm$ 0.04	(AB Dor)
<b>Intermediate gravity objects (INT-G)</b>												
2MASSJ0019+4614	M8/M8 INT-G	5, 20	[10.25 $\pm$ 0.14]	[9.59 $\pm$ 0.13]	[9.01 $\pm$ 0.13]	[8.50 $\pm$ 0.13]	9.63 $\pm$ 0.13	8.97 $\pm$ 0.13	8.53 $\pm$ 0.13	8.31 $\pm$ 0.13	8.05 $\pm$ 0.13	AB Dor
PC0025+0447	M9.5/L0 INT-G	5, 41	12.25 $\pm$ 0.17	11.22 $\pm$ 0.17	10.59 $\pm$ 0.17	10.01 $\pm$ 0.17	11.26 $\pm$ 0.19	10.36 $\pm$ 0.19	10.04 $\pm$ 0.20	9.69 $\pm$ 0.17	9.15 $\pm$ 0.17	...
WISEP J0047+6803	... /L7 INT-G	5	[16.33 $\pm$ 0.08]	[15.07 $\pm$ 0.08]	[13.62 $\pm$ 0.06]	[12.59 $\pm$ 0.06]	15.18 $\pm$ 0.08	13.55 $\pm$ 0.06	12.63 $\pm$ 0.06	11.46 $\pm$ 0.05	10.84 $\pm$ 0.05	AB Dor
2MASSJ0058-0651	L0/L1 INT-G	32, 42, 61	[12.96 $\pm$ 0.26]	[11.88 $\pm$ 0.26]	[11.13 $\pm$ 0.26]	[10.50 $\pm$ 0.26]	11.96 $\pm$ 0.26	11.09 $\pm$ 0.26	10.55 $\pm$ 0.26	10.21 $\pm$ 0.26	9.91 $\pm$ 0.26	(AB Dor)/( $\beta$ Pic)
2MASSJ0117-3403	L2 $\gamma$ /L1 INT-G	5, 20	[13.40 $\pm$ 0.16]	[12.19 $\pm$ 0.16]	[11.35 $\pm$ 0.16]	[10.54 $\pm$ 0.16]	12.26 $\pm$ 0.16	11.29 $\pm$ 0.16	10.57 $\pm$ 0.16	10.13 $\pm$ 0.16	9.73 $\pm$ 0.16	(Tuc-Hor)
SOJ0253+1652 $\dagger$	M7/M7.5 INT-G	32, 38	[11.03 $\pm$ 0.05]	[10.41 $\pm$ 0.03]	[9.99 $\pm$ 0.04]	[9.62 $\pm$ 0.05]	10.46 $\pm$ 0.03	9.95 $\pm$ 0.04	9.65 $\pm$ 0.05	9.21 $\pm$ 0.05	9.05 $\pm$ 0.02	...
LSR J0602+3910	L1/L2 INT-G	5, 76	[13.07 $\pm$ 0.06]	[11.95 $\pm$ 0.03]	[11.22 $\pm$ 0.03]	[10.55 $\pm$ 0.03]	12.02 $\pm$ 0.03	11.17 $\pm$ 0.03	10.58 $\pm$ 0.03	10.14 $\pm$ 0.03	9.85 $\pm$ 0.03	Pleiades MG
CD-35 2722B	... /L3 INT-G	5	...	11.99 $\pm$ 0.18	11.14 $\pm$ 0.18	10.37 $\pm$ 0.16	{12.08 $\pm$ 0.18}	{11.08 $\pm$ 0.18}	{10.43 $\pm$ 0.16}	...	...	AB Dor
2MASSJ0714+3702	M8/M7.5 INT-G	32, 73, 77	...	{11.44 $\pm$ 0.13}	{10.81 $\pm$ 0.13}	{10.33 $\pm$ 0.13}	11.49 $\pm$ 0.13	10.77 $\pm$ 0.13	10.36 $\pm$ 0.13	10.09 $\pm$ 0.13	9.86 $\pm$ 0.13	...
2MASSJ1411-2119	M9/M8 INT-G	5, 20	[9.59 $\pm$ 0.22]	[8.83 $\pm$ 0.22]	[8.32 $\pm$ 0.22]	[7.75 $\pm$ 0.21]	8.89 $\pm$ 0.22	8.28 $\pm$ 0.22	7.78 $\pm$ 0.21	7.53 $\pm$ 0.22	7.27 $\pm$ 0.22	...
DENISJ1425-3650	L3/L4 INT-G	32, 73	...	{13.35 $\pm$ 0.03}	{12.31 $\pm$ 0.03}	{11.46 $\pm$ 0.03}	13.43 $\pm$ 0.03	12.26 $\pm$ 0.03	11.49 $\pm$ 0.03	10.72 $\pm$ 0.03	10.26 $\pm$ 0.03	AB Dor
2MASSJ1547-2423	M9/L0 INT-G	5, 73	[12.25 $\pm$ 0.09]	[11.30 $\pm$ 0.08]	[10.70 $\pm$ 0.09]	[10.10 $\pm$ 0.08]	11.36 $\pm$ 0.08	10.66 $\pm$ 0.09	10.13 $\pm$ 0.08	9.80 $\pm$ 0.11	9.45 $\pm$ 0.08	...
2MASSJ1552+2948	L0 $\beta$ /L0 INT-G	5, 22, 73	[12.90 $\pm$ 0.07]	[11.81 $\pm$ 0.05]	[11.05 $\pm$ 0.05]	[10.38 $\pm$ 0.05]	11.87 $\pm$ 0.05	11.00 $\pm$ 0.05	10.42 $\pm$ 0.05	9.95 $\pm$ 0.05	9.60 $\pm$ 0.05	...
2MASSJ1711+2326	L0/L1 INT-G	5, 21	[13.03 $\pm$ 0.13]	[11.85 $\pm$ 0.12]	[11.15 $\pm$ 0.12]	[10.46 $\pm$ 0.12]	11.93 $\pm$ 0.12	11.09 $\pm$ 0.12	10.48 $\pm$ 0.12	10.02 $\pm$ 0.12	9.67 $\pm$ 0.12	...
2MASSJ1726+1538	L3 $\beta$ /L3 INT-G	5, 22	[14.13 $\pm$ 0.10]	[12.84 $\pm$ 0.10]	[11.78 $\pm$ 0.09]	[10.88 $\pm$ 0.09]	12.93 $\pm$ 0.10	11.72 $\pm$ 0.09	10.92 $\pm$ 0.09	10.33 $\pm$ 0.08	9.93 $\pm$ 0.08	...
SIMP J2154-1055	... /L4 INT-G	31	[15.26 $\pm$ 0.14]	[13.92 $\pm$ 0.14]	[12.70 $\pm$ 0.11]	[11.73 $\pm$ 0.10]	14.01 $\pm$ 0.14	12.64 $\pm$ 0.11	11.77 $\pm$ 0.10	10.93 $\pm$ 0.07	10.48 $\pm$ 0.07	...

Table 7—Continued

Object	Spec. Type Optical/NIR	Ref.	MKO				2MASS			AllWISE		Notes
			$M_Y$ (mag)	$M_J$ (mag)	$M_H$ (mag)	$M_K$ (mag)	$M_J$ (mag)	$M_H$ (mag)	$M_{K_S}$ (mag)	$M_{W1}$ (mag)	$M_{W2}$ (mag)	
SDSSJ2249+0044A	... /L3 INT-G	4, 5	...	$13.87 \pm 0.12$	$12.76 \pm 0.12$	$11.85 \pm 0.12$	$13.97 \pm 0.18$	$12.83 \pm 0.16$	$11.79 \pm 0.14$	...	...	...
SDSSJ2249+0044B	... /L5 INT-G	4, 5	...	$14.89 \pm 0.12$	$13.71 \pm 0.12$	$12.74 \pm 0.12$	$15.01 \pm 0.18$	$13.78 \pm 0.16$	$12.67 \pm 0.14$	...	...	...
2MASSJ2322-3133	L0 $\beta$ /L2 INT-G	5, 29, 73	$[13.02 \pm 0.13]$	$[12.00 \pm 0.13]$	$[11.34 \pm 0.13]$	$[10.80 \pm 0.13]$	$12.08 \pm 0.13$	$11.29 \pm 0.13$	$10.83 \pm 0.13$	$10.51 \pm 0.13$	$10.22 \pm 0.12$	...
<b>Other low gravity objects</b>												
2MASSJ0033-1521	L4 $\beta$ /L1 FLD-G	5, 22, 73	$[14.50 \pm 0.11]$	$[13.39 \pm 0.11]$	$[12.41 \pm 0.11]$	$[11.55 \pm 0.10]$	$13.44 \pm 0.11$	$12.36 \pm 0.11$	$11.57 \pm 0.10$	$10.98 \pm 0.10$	$10.65 \pm 0.10$	...
2MASSJ0221-6831	M8 $\beta$ /...	73	...	$\{10.94 \pm 0.31\}$	$\{10.34 \pm 0.31\}$	$\{9.80 \pm 0.31\}$	$10.99 \pm 0.31$	$10.30 \pm 0.31$	$9.83 \pm 0.31$	$9.51 \pm 0.31$	$9.22 \pm 0.31$	...
2MASSJ0253+3206	M7/M6 FLD-G	5, 20	$[10.81 \pm 0.12]$	$[10.21 \pm 0.11]$	$[9.60 \pm 0.11]$	$[9.17 \pm 0.11]$	$10.25 \pm 0.11$	$9.57 \pm 0.11$	$9.19 \pm 0.11$	$8.97 \pm 0.11$	$8.79 \pm 0.11$	...
51 Eri b	... /T6	56	...	$\{16.53 \pm 0.40\}$	$\{16.91 \pm 0.21\}$	...	$16.75 \pm 0.40$	$16.86 \pm 0.21$	...	...	...	$\beta$ Pic
$\beta$ Pic b	... /L1	11	$13.77 \pm 0.34$	$12.60 \pm 0.21$	$11.86 \pm 0.11$	$10.99 \pm 0.07$	$12.68 \pm 0.21$	$11.80 \pm 0.11$	$11.01 \pm 0.07$	...	...	$\beta$ Pic
2MASSJ0619-2903	M6/M5	5, 20	$[8.89 \pm 1.19]$	$[7.88 \pm 1.19]$	$[7.04 \pm 1.19]$	$[6.20 \pm 1.19]$	$7.94 \pm 1.19$	$6.99 \pm 1.19$	$6.25 \pm 1.19$	$5.83 \pm 1.19$	$5.40 \pm 1.19$	disk?
2MASSJ1022+0200	M9 $\beta$ /M9 FLD-G	5, 73	$12.77 \pm 0.13$	$11.74 \pm 0.13$	$11.14 \pm 0.13$	$10.59 \pm 0.13$	$11.79 \pm 0.13$	$11.09 \pm 0.13$	$10.59 \pm 0.13$	$10.32 \pm 0.13$	$10.03 \pm 0.13$	...
2MASSJ1022+5825	L1 $\beta$ /L1 FLD-G	5, 22, 73	$[13.13 \pm 0.14]$	$[12.04 \pm 0.13]$	$[11.29 \pm 0.13]$	$[10.74 \pm 0.13]$	$12.10 \pm 0.13$	$11.25 \pm 0.13$	$10.77 \pm 0.13$	$10.37 \pm 0.13$	$10.11 \pm 0.13$	strong H $\alpha$
SDSSJ1110+0116	... /T5.5	13	$[15.66 \pm 0.07]$	$14.70 \pm 0.07$	$14.80 \pm 0.07$	$14.63 \pm 0.07$	$14.93 \pm 0.13$	$14.51 \pm 0.15$	$[14.52 \pm 0.07]$	$14.02 \pm 0.07$	$12.51 \pm 0.06$	AB Dor
Ross458C	... /T8	24	$17.38 \pm 0.04$	$16.35 \pm 0.04$	$16.67 \pm 0.06$	$16.56 \pm 0.07$	$[16.64 \pm 0.04]$	$[16.62 \pm 0.06]$	$[16.45 \pm 0.07]$	$15.70 \pm 0.07$	$13.51 \pm 0.06$	...
LSPMJ1314+1320A	... /...	...	...	$9.25 \pm 0.03$	$8.76 \pm 0.04$	$8.30 \pm 0.02$	$9.28 \pm 0.03$	$8.73 \pm 0.04$	$8.32 \pm 0.02$	...	...	...
LSPMJ1314+1320B	... /...	...	...	$9.33 \pm 0.03$	$8.79 \pm 0.04$	$8.38 \pm 0.02$	$9.33 \pm 0.03$	$8.76 \pm 0.04$	$8.40 \pm 0.02$	...	...	...
HR6037Ba	... /M9:	40, 68	...	$[11.26 \pm 0.20]$	$[10.20 \pm 0.16]$	$[10.00 \pm 0.18]$	$11.33 \pm 0.20$	$10.15 \pm 0.16$	$10.03 \pm 0.18$	...	...	...
HR6037Bb	... /M9:	40, 68	...	$[11.60 \pm 0.20]$	$[10.33 \pm 0.16]$	$[10.19 \pm 0.18]$	$11.67 \pm 0.20$	$10.28 \pm 0.16$	$10.22 \pm 0.18$	...	...	...
HR8799b	... /...	...	...	$16.48 \pm 0.19$	$15.11 \pm 0.13$	$\{14.01 \pm 0.08\}$	$\{16.61 \pm 0.19\}$	$\{15.05 \pm 0.13\}$	$13.98 \pm 0.08$	...	...	Columba
HR8799c	... /...	...	...	$14.65 \pm 0.22$	$14.20 \pm 0.16$	$\{13.16 \pm 0.09\}$	$\{14.76 \pm 0.22\}$	$\{14.13 \pm 0.16\}$	$13.20 \pm 0.09$	...	...	Columba
HR8799d	... /...	...	...	$15.26 \pm 0.43$	$13.69 \pm 0.20$	$\{13.07 \pm 0.13\}$	$\{15.37 \pm 0.43\}$	$\{13.62 \pm 0.20\}$	$13.11 \pm 0.13$	...	...	Columba
HR8799e	... /...	...	...	...	$13.30 \pm 0.28$	$\{12.89 \pm 0.23\}$	...	$\{13.23 \pm 0.28\}$	$12.93 \pm 0.23$	...	...	Columba
<b>Unusually red FLD-G objects</b>												
WISEJ0206+2640	... /L8(red)	1	$[16.14 \pm 0.13]$	$[15.00 \pm 0.13]$	$[13.74 \pm 0.10]$	$[13.08 \pm 0.09]$	$15.11 \pm 0.13$	$13.68 \pm 0.10$	$13.11 \pm 0.09$	$12.00 \pm 0.06$	$11.41 \pm 0.06$	...
WISEJ0754+7909	... /T2p(red)	1	$[15.72 \pm 0.12]$	$[14.55 \pm 0.12]$	$[14.06 \pm 0.14]$	$[13.49 \pm 0.13]$	$14.71 \pm 0.12$	$13.98 \pm 0.14$	$13.48 \pm 0.13$	$12.94 \pm 0.06$	$12.29 \pm 0.06$	...
2MASSJ1331+3407	L0/L0 FLD-G	1, 73	$12.97 \pm 0.10$	$11.89 \pm 0.10$	$11.18 \pm 0.10$	$10.57 \pm 0.10$	$12.09 \pm 0.10$	$11.16 \pm 0.10$	$10.64 \pm 0.10$	$10.33 \pm 0.10$	$10.10 \pm 0.10$	...
2MASSJ1821+1414	L4.5/L5p FLD-G	1, 52	$[14.68 \pm 0.05]$	$[13.43 \pm 0.03]$	$[12.56 \pm 0.03]$	$[11.72 \pm 0.03]$	$13.53 \pm 0.03$	$12.49 \pm 0.03$	$11.75 \pm 0.03$	$10.95 \pm 0.03$	$10.57 \pm 0.03$	...
2MASSJ2148+4003	L6/L6 FLD-G	49, 52	$[15.51 \pm 0.06]$	$[14.07 \pm 0.05]$	$[12.87 \pm 0.05]$	$[11.75 \pm 0.04]$	$14.17 \pm 0.05$	$12.80 \pm 0.05$	$11.79 \pm 0.04$	$10.78 \pm 0.05$	$10.26 \pm 0.04$	...
2MASSJ2224-0158	L4.5/L3 FLD-G	1, 42	$[15.00 \pm 0.06]$	$13.57 \pm 0.04$	$12.52 \pm 0.04$	$11.66 \pm 0.04$	$13.75 \pm 0.04$	$12.50 \pm 0.04$	$11.70 \pm 0.04$	$11.09 \pm 0.04$	$10.82 \pm 0.03$	...
WISEJ2335+4511	... /L7p FLD-G	1	$[16.22 \pm 0.08]$	$15.05 \pm 0.07$	$13.85 \pm 0.07$	$12.58 \pm 0.08$	$[15.16 \pm 0.07]$	$[13.78 \pm 0.07]$	$[12.61 \pm 0.08]$	$11.75 \pm 0.07$	$11.16 \pm 0.07$	...
2MASSJ2351+3010	L5.5/L5 FLD-G	1, 44	$[15.07 \pm 0.13]$	$[13.83 \pm 0.13]$	$[12.71 \pm 0.10]$	$[12.07 \pm 0.10]$	$13.92 \pm 0.13$	$12.65 \pm 0.10$	$12.09 \pm 0.10$	$11.31 \pm 0.08$	$10.92 \pm 0.08$	Argus?
<b>Other young companions</b>												
HD984B	... /M6	64	...	...	$\{9.26 \pm 0.08\}$	$\{8.78 \pm 0.08\}$	...	$9.21 \pm 0.08$	$8.82 \pm 0.08$	...	...	...
HD1160B	... /M6	57	...	$9.52 \pm 0.15$	$9.57 \pm 0.13$	$\{8.83 \pm 0.16\}$	$\{9.58 \pm 0.15\}$	$\{9.52 \pm 0.13\}$	$8.87 \pm 0.16$	...	...	...
2MASSJ0103-55(AB)b	... /...	...	...	$12.03 \pm 0.33$	$10.83 \pm 0.24$	$10.23 \pm 0.24$	$12.03 \pm 0.33$	$10.83 \pm 0.24$	$10.23 \pm 0.24$	...	...	Tuc-Hor
LP261-75B	L6/L6 FLD-G	1, 42	$[15.80 \pm 0.23]$	$[14.63 \pm 0.23]$	$[13.45 \pm 0.16]$	$[12.62 \pm 0.16]$	$14.72 \pm 0.23$	$13.39 \pm 0.16$	$12.64 \pm 0.16$	...	...	...
Gl504b	... /...	...	...	$\{18.39 \pm 0.15\}$	$\{18.99 \pm 0.14\}$	$\{18.07 \pm 0.28\}$	$18.69 \pm 0.15$	$18.92 \pm 0.14$	$17.97 \pm 0.28$	...	...	...
PZ Tel B	... /M7	57	...	$8.91 \pm 0.23$	$8.37 \pm 0.18$	$\{7.94 \pm 0.13\}$	$\{8.96 \pm 0.23\}$	$\{8.33 \pm 0.18\}$	$7.97 \pm 0.13$	...	...	$\beta$ Pic
HR7329B	M7.5/M7.5	36, 54	...	$\{8.59 \pm 0.19\}$	$8.51 \pm 0.06$	$\{8.15 \pm 0.10\}$	$8.64 \pm 0.19$	$8.33 \pm 0.10$	$8.18 \pm 0.10$	...	...	$\beta$ Pic
HD203030B	... /L7.5	63	...	$\{14.97 \pm 0.55\}$	$\{13.85 \pm 0.14\}$	$\{13.13 \pm 0.12\}$	$15.07 \pm 0.55$	$13.79 \pm 0.14$	$13.15 \pm 0.12$	...	...	...
HN Peg B	... /T2.5	55	$[15.60 \pm 0.05]$	$14.60 \pm 0.03$	$14.14 \pm 0.03$	$13.86 \pm 0.03$	$15.44 \pm 0.16$	$14.29 \pm 0.11$	$14.37 \pm 0.25$	...	...	...
$\kappa$ And b	... /L1:	39	...	$\{12.23 \pm 0.21\}$	$\{11.44 \pm 0.13\}$	$\{10.73 \pm 0.09\}$	$12.30 \pm 0.21$	$11.39 \pm 0.13$	$10.76 \pm 0.09$	...	...	...
<b>Miscellaneous</b>												
2MASSJ0030-1450	L7/L6 FLD-G	1, 42	$[15.47 \pm 0.27]$	$14.26 \pm 0.26$	$13.24 \pm 0.26$	$12.36 \pm 0.26$	$14.14 \pm 0.28$	$13.14 \pm 0.28$	$12.35 \pm 0.28$	$11.55 \pm 0.26$	$11.19 \pm 0.26$	Argus?
2MASSJ0314+1603	L0/L0 FLD-G	5, 73	$[12.52 \pm 0.07]$	$[11.77 \pm 0.05]$	$[11.15 \pm 0.06]$	$[10.50 \pm 0.05]$	$11.81 \pm 0.05$	$11.11 \pm 0.06$	$10.53 \pm 0.05$	$10.22 \pm 0.05$	$9.94 \pm 0.05$	UMa MG

Table 7—Continued

Object	Spec. Type Optical/NIR	Ref.	MKO				2MASS			AllWISE		Notes
			$M_Y$ (mag)	$M_J$ (mag)	$M_H$ (mag)	$M_K$ (mag)	$M_J$ (mag)	$M_H$ (mag)	$M_{K_S}$ (mag)	$M_{W1}$ (mag)	$M_{W2}$ (mag)	
LP944-20	M9/L0 FLD-G	5, 74	[12.49 ± 0.05]	11.64 ± 0.03	10.94 ± 0.03	10.49 ± 0.03	11.69 ± 0.03	10.98 ± 0.03	10.51 ± 0.03	10.10 ± 0.03	9.77 ± 0.02	Castor, Li
2MASSJ0407+1546	L3.5/L3 FLD-G	5, 73	[14.13 ± 0.11]	[12.70 ± 0.11]	[11.71 ± 0.11]	[10.84 ± 0.10]	12.78 ± 0.11	11.66 ± 0.11	10.86 ± 0.10	10.27 ± 0.10	9.88 ± 0.10	strong H $\alpha$
CFHT-Hy-20	... /T2.5	1	[15.55 ± 0.12]	14.46 ± 0.12	13.95 ± 0.12	13.52 ± 0.12	14.62 ± 0.12	13.88 ± 0.12	13.47 ± 0.12	13.04 ± 0.11	12.16 ± 0.13	(Hyades)
LP423-31	M7/M6 FLD-G	5, 20, 72, 79	[10.17 ± 0.07]	[9.51 ± 0.06]	[8.90 ± 0.06]	[8.50 ± 0.06]	9.55 ± 0.06	8.87 ± 0.06	8.52 ± 0.06	8.29 ± 0.06	8.13 ± 0.06	strong H $\alpha$
SDSSJ1025+3212	... /L7 FLD-G	1, 5	[15.84 ± 0.09]	14.75 ± 0.09	13.84 ± 0.08	13.02 ± 0.08	[14.85 ± 0.09]	13.45 ± 0.18	12.93 ± 0.20	12.24 ± 0.08	11.86 ± 0.08	...
SDSSJ1045-0149	L1/L1 FLD-G	5, 20, 34, 37	13.19 ± 0.06	12.04 ± 0.05	11.36 ± 0.05	10.73 ± 0.05	12.11 ± 0.06	11.31 ± 0.06	10.73 ± 0.06	10.42 ± 0.06	10.19 ± 0.06	Hyades MG
DENISJ1047-1815	L2.5/L0 FLD-G	5, 20, 62	[13.05 ± 0.12]	[12.03 ± 0.11]	[11.36 ± 0.11]	[10.77 ± 0.11]	12.09 ± 0.11	11.32 ± 0.11	10.78 ± 0.11	10.47 ± 0.11	10.22 ± 0.11	Hyades MG
2MASSJ1315-2649A	... /L3.5:..	15	...	13.84 ± 0.10	12.84 ± 0.09	12.15 ± 0.09	{13.93 ± 0.10}	{12.78 ± 0.09}	{12.17 ± 0.09}	...	...	strong H $\alpha$
2MASSJ1315-2649B	... /T7	15	...	16.90 ± 0.10	17.36 ± 0.11	17.49 ± 0.14	{17.16 ± 0.10}	{17.31 ± 0.11}	{17.36 ± 0.14}	...	...	...
DENISJ1441-0945A	... / ...	...	[12.96 ± 0.13]	[11.94 ± 0.13]	[11.23 ± 0.13]	[10.65 ± 0.13]	12.00 ± 0.13	11.18 ± 0.13	10.67 ± 0.13	...	...	Hyades MG
DENISJ1441-0945B	... / ...	...	[13.28 ± 0.13]	[12.19 ± 0.13]	[11.46 ± 0.13]	[10.85 ± 0.13]	12.25 ± 0.13	11.41 ± 0.13	10.87 ± 0.13	...	...	Hyades MG
DENISJ1705-0516	L0.5/L1 FLD-G	5, 73	[12.92 ± 0.07]	[11.88 ± 0.05]	[11.24 ± 0.05]	[10.65 ± 0.05]	11.95 ± 0.05	11.19 ± 0.05	10.67 ± 0.05	10.32 ± 0.05	10.07 ± 0.05	UMa MG
2MASSJ1707+4301	L0.5/M9 FLD-G	5, 20	[12.67 ± 0.08]	[11.71 ± 0.07]	[11.01 ± 0.07]	[10.39 ± 0.07]	11.76 ± 0.07	10.97 ± 0.07	10.41 ± 0.07	10.07 ± 0.07	9.80 ± 0.07	strong H $\alpha$
DENISJ2057-0252	L1.5/L2 FLD-G	5, 20	[13.38 ± 0.13]	[12.28 ± 0.12]	[11.55 ± 0.12]	[10.93 ± 0.12]	12.35 ± 0.12	11.50 ± 0.12	10.95 ± 0.12	10.52 ± 0.12	10.25 ± 0.12	Li
2MASSJ2140+3655	... /M8p FLD-G	1, 44	[11.62 ± 0.20]	[10.84 ± 0.20]	[10.40 ± 0.21]	[9.92 ± 0.22]	10.90 ± 0.20	10.36 ± 0.21	9.97 ± 0.22	9.94 ± 0.19	9.73 ± 0.20	...
DENISJ2200-3038A	M9/M9 FLD-G	5, 14, 73	[12.81 ± 0.25]	[11.90 ± 0.25]	[11.22 ± 0.25]	[10.70 ± 0.25]	11.95 ± 0.25	11.18 ± 0.25	10.73 ± 0.25	...	...	Hyades MG
DENISJ2200-3038B	L0/L0 FLD-G	1, 14, 73	[12.95 ± 0.25]	[12.21 ± 0.25]	[11.51 ± 0.25]	[10.96 ± 0.25]	12.26 ± 0.25	11.47 ± 0.25	10.99 ± 0.25	...	...	Hyades MG

Note. — Absolute magnitudes computed from the photometry and parallaxes compiled in Table 6. Brackets [...] denote photometry based on synthesized 2MASS–MKO conversions or  $Y - J$  colors from that object’s spectrum. Braces {...} denote photometry based on estimated 2MASS–MKO conversions for objects expected to be of similar spectral type. Notes are given indicating young group membership status and other attributes. Question marks indicate unlikely but potentially viable candidate members, and parentheses indicate probable members lacking RV confirmation (see Table 13). Pleiades MG, Hyades MG, and UMa MG are looser associations proposed elsewhere in the literature that were not part of our kinematic analysis and do not correspond to the actual Pleiades, Hyades, or Ursa Majoris clusters. Spectrally peculiar objects are denoted by “p” and spectral types uncertain by  $\pm 1$ ,  $\pm 1.5$ , and  $\pm 2$  subclasses are denoted by “:”, “:..”, and “:..”, respectively. For the M5–L7 objects with Allers & Liu (2013a) gravity classifications, the intrinsic uncertainty in the spectral type is  $\pm 1$  subclass.

† Alternate names: SO J0253+1652 (Teegarden’s star), GJ3276 (2MASSJ0422+1530), SSSPMJ1102-3431 (TWA 28), 2MASSJ1139-3159 (TWA 26), 2MASSJ1207-3932 (TWA 27), DENISJ1245-4429 (TWA 29).

References. — (1) This work; (2) 2MASS Point Source Catalog (Cutri et al. 2003); (3) UKIDSS DR10; (4) Allers et al. (2010); (5) Allers & Liu (2013a); (6) Best et al. (2015); (7) Biller et al. (2013); (8) Bonnefoy et al. (2010); (9) Bonnefoy et al. (2011); (10) Bonnefoy et al. (2014a); (11) Bonnefoy et al. (2014b); (12) Bouvier et al. (2008); (13) Burgasser et al. (2006); (14) Burgasser & McElwain (2006); (15) Burgasser et al. (2011); (16) Chauvin et al. (2004); (17) Chauvin et al. (2005b); (18) Chauvin et al. (2012); (19) Chiu et al. (2006); (20) Cruz et al. (2003); (21) Cruz et al. (2007); (22) Cruz et al. (2009); (23) Currie et al. (2013); (24) Cushing et al. (2011); (25) Delorme et al. (2013); (26) Dupuy & Liu (2012); (27) Dupuy et al. (2016b); (28) Esposito et al. (2013); (29) Faherty et al. (2012); (30) Faherty et al. (2013); (31) Gagné et al. (2014a); (32) Gagné et al. (2015a); (33) Gizis et al. (2000); (34) Gizis (2002); (35) Goldman et al. (2010); (36) Guenther et al. (2001); (37) Hawley et al. (2002); (38) Henry et al. (2004); (39) Hinkley et al. (2013); (40) Huélamo et al. (2010); (41) Kirkpatrick et al. (1995); (42) Kirkpatrick et al. (2000); (43) Kirkpatrick et al. (2008); (44) Kirkpatrick et al. (2010); (45) Knapp et al. (2004); (46) Kuzuhara et al. (2013); (47) Leggett et al. (1998); (48) Leggett et al. (2002); (49) Liu et al. (2013b); (50)Looper et al. (2007b); (51) Looper et al. (2007a); (52) Looper et al. (2008b); (53) Lowrance et al. (1999); (54) Lowrance et al. (2000); (55) Luhman et al. (2007); (56) Macintosh et al. (2015); (57) Maire et al. (2016); (58) Males et al. (2014); (59) Marois et al. (2008); (60) Marois et al. (2010); (61) Marocco et al. (2013); (62) Martín et al. (1999b); (63) Metchev & Hillenbrand (2006); (64) Meshkat et al. (2015); (65) Mohanty et al. (2007); (66) Neuhäuser et al. (2011); (67) Nielsen et al. (2012); (68) Nielsen et al. (2013); (69) Oppenheimer et al. (2013); (70) Patience et al. (2010); (71) Reid et al. (2002); (72) Reid et al. (2003a); (73) Reid et al. (2008); (74) Reiners & Basri (2009); (75) Rice et al. (2010b); (76) Salim et al. (2003); (77) Schmidt et al. (2007); (78) Scholz et al. (2005); (79) Shkolnik et al. (2009); (80) Torres et al. (2003); (81) Wahhaj et al. (2011); (82) Zapatero Osorio et al. (2010).

Table 8. Comparison of CFHT Parallaxes to Literature Values

Object	Absolute Parallax (mas)				$\Delta$ Proper Motion (mas/yr) <sup>a</sup>		Ref.
	CFHT	Lit.	Difference		RA	Dec.	
Faherty et al. (2012, 2013)							
2MASS J03552337+1133437	109.5 ± 1.4	122.0 ± 13.0	1.0 $\sigma$	11%	5.6 ± 5.2	0.4 ± 5.2	1
GJ 3276	3.9 ± 1.0	24.8 ± 3.1	6.4 $\sigma$	536%	20.8 ± 3.1	−8.8 ± 3.1	2
2MASS J05012406−0010452	48.4 ± 1.4	76.4 ± 4.8	5.6 $\sigma$	58%	7.3 ± 4.5	−11.2 ± 4.5	2
2MASSI J0518461−275645	18.4 ± 1.1	21.4 ± 6.9	0.4 $\sigma$	16%	6.3 ± 4.5	11.1 ± 4.4	2
2MASSI J0536199−192039	21.1 ± 1.6	25.6 ± 9.4	0.5 $\sigma$	21%	0.9 ± 5.5	4.2 ± 5.3	2
2MASSI J0608528−275358	25.0 ± 1.5	32.0 ± 3.6	1.8 $\sigma$	28%	3.5 ± 3.6	−3.4 ± 3.6	2
2MASS J10220489+0200477	34.6 ± 2.0	26.4 ± 11.5	−0.7 $\sigma$	−24%	−22.1 ± 7.1	10.5 ± 7.1	2
SSSPM J1102−3431	21.1 ± 2.1	28.0 ± 4.3	1.4 $\sigma$	33%	1.4 ± 4.3	−12.2 ± 4.5	2
2MASSW J1139511−315921	23.7 ± 1.6	35.1 ± 4.3	2.5 $\sigma$	48%	−11.7 ± 4.6	−17.1 ± 4.8	2
2MASS J23224684−3133231	50.2 ± 2.8	58.6 ± 5.6	1.3 $\sigma$	17%	−11.4 ± 7.9	−8.6 ± 7.9	2
Zapatero Osorio et al. (2014)							
2MASSW J0033239−152131	42.8 ± 1.8	24.8 ± 2.5	−5.8 $\sigma$	−42%	−3.4 ± 10.7	3.5 ± 18.5	3
2MASSW J0045214+163445	65.9 ± 1.3	57.3 ± 2.0	−3.6 $\sigma$	−13%	−1.8 ± 13.9	−16.1 ± 11.1	3
2MASSI J0241115−032658	18.5 ± 2.1	21.4 ± 2.6	0.9 $\sigma$	16%	−14.4 ± 11.7	−2.7 ± 8.6	3
2MASS J03552337+1133437	109.5 ± 1.4	110.8 ± 4.3	0.3 $\sigma$	1%	−1.4 ± 13.3	4.4 ± 15.1	3
2MASS J05012406−0010452	48.4 ± 1.4	51.0 ± 3.7	0.7 $\sigma$	5%	−0.6 ± 9.6	−1.1 ± 12.6	3
G196-3B	49.0 ± 2.3	41.0 ± 4.1	−1.7 $\sigma$	−16%	0.9 ± 10.9	1.6 ± 14.0	3
2MASS J10224821+5825453	52.6 ± 3.1	46.3 ± 1.3	−1.9 $\sigma$	−12%	2.7 ± 7.2	14.0 ± 13.6	3
2MASS J15525906+2948485	47.8 ± 1.0	47.7 ± 0.9	−0.1 $\sigma$	0%	−2.2 ± 5.5	−5.3 ± 10.8	3
2MASSW J1726000+153819	28.3 ± 1.0	28.6 ± 2.9	0.1 $\sigma$	1%	−5.7 ± 7.2	−7.5 ± 5.4	3
2MASSW J2208136+292121	25.1 ± 1.6	21.2 ± 0.7	−2.2 $\sigma$	−16%	−1.8 ± 3.2	−9.6 ± 3.9	3
Miscellaneous							
PC 0025+0447	10.4 ± 0.8	13.8 ± 1.6	1.9 $\sigma$	33%	5.6 ± 1.2	−2.5 ± 1.2	4
WISEP J004701.06+680352.1	82.3 ± 1.8	82.0 ± 3.0	−0.1 $\sigma$	0%	−6.3 ± 3.2	−7.2 ± 4.2	5
2MASSI J0335020+234235	21.8 ± 1.8	23.6 ± 1.3	0.8 $\sigma$	8%	...	...	6
2MASS J05575096−1359503	3.4 ± 1.2	1.9 ± 1.0	−1.0 $\sigma$	−44%	...	...	6
LP 423-31	54.3 ± 1.4	54.4 ± 1.0	0.1 $\sigma$	0%	0.5	8.6	7
LP 261-75B	31.6 ± 1.3	16.1 ± 7.4	−2.1 $\sigma$	−49%	6.1 ± 7.5	−3.5 ± 9.9	8
SSSPM J1102−3431	21.1 ± 2.1	18.1 ± 0.5	−1.4 $\sigma$	−14%	12.9 ± 1.9	−5.6 ± 2.5	9
2MASSW J1139511−315921	23.7 ± 1.6	26.2 ± 1.1	1.3 $\sigma$	11%	6.4 ± 1.5	0.0 ± 1.9	10
2MASSW J1139511−315921	23.7 ± 1.6	23.8 ± 2.6	0.0 $\sigma$	0%	−5.7 ± 4.1	0.2 ± 2.8	11
2MASSW J1207334−393254	19.5 ± 5.4	19.1 ± 0.4	−0.1 $\sigma$	−2%	5.9 ± 3.0	−2.7 ± 2.7	12
2MASSW J1207334−393254	19.5 ± 5.4	18.5 ± 1.0	−0.2 $\sigma$	−5%	4.4 ± 3.4	−2.5 ± 3.8	13
DENIS J1441.6−0945	29.6 ± 1.7	36.4 ± 3.6	1.7 $\sigma$	23%	−8.0 ± 3.1	−2.2 ± 4.6	14
DENIS J170548.3−051645	53.5 ± 1.0	44.5 ± 12.0	−0.7 $\sigma$	−17%	6.1 ± 12.1	−4.3 ± 7.2	15
DENIS J170548.3−051645	53.5 ± 1.0	55.1 ± 1.8	0.8 $\sigma$	3%	−4.4 ± 1.9	−8.5 ± 2.2	16
2MASS J21481633+4003594	124.6 ± 1.8	124.1 ± 0.6	−0.3 $\sigma$	0%	1.4 ± 1.9	−6.1 ± 2.6	5

References. — (1) Faherty et al. (2013), (2) Faherty et al. (2012), (3) Zapatero Osorio et al. (2014), (4) Dahn et al. (2002), (5) Gizis et al. (2015), (6) Shkolnik et al. (2012), (7) Gatewood & Coban (2009), (8) Vrba et al. (2004), (9) Teixeira et al. (2008), (10) Ducourant et al. (2014), (11) Weinberger et al. (2013), (12) Ducourant et al. (2008), (13) Gizis et al. (2007), (14) Costa et al. (2006), (15) Andrei et al. (2011), (16) Dieterich et al. (2014).

<sup>a</sup>The difference between our absolute proper motions and literature values that are typically reported as relative.

Table 9. Comparison of CFHT Parallax Distances to Literature Kinematic Distances

Object	CFHT Distance (pc)	Kinematic Distance (pc)	Difference		Ref.
AB Dor					
2MASS J0019262+461407	$39.2^{+2.2}_{-2.4}$	$37.4^{+2.8}_{-2.4}$	$-0.5\sigma$	-5%	1
WISEP J004701.06+680352.1	$12.1 \pm 0.3$	$10.5^{+0.8}_{-0.4}$	$-2.0\sigma$	-14%	1
2MASS J03552337+1133437	$9.1 \pm 0.1$	$8.5^{+0.4}_{-0.8}$	$-1.5\sigma$	-7%	1
2MASSW J2244316+204343	$17.0^{+0.3}_{-0.3}$	$18.5 \pm 1.2$	$1.2\sigma$	9%	1
Argus					
2MASSW J0045214+163445	$15.2 \pm 0.3$	$13.3^{+0.8}_{-1.2}$	$-2.2\sigma$	-12%	1
SIMP J215434.5-105530.8†	$30.7 \pm 0.9$	$22.1^{+2.8}_{-2.4}$	$-2.9\sigma$	-28%	2
2MASS J23512200+3010540	$24.3^{+0.8}_{-0.9}$	$20.9^{+2.0}_{-2.4}$	$-1.6\sigma$	-14%	1
$\beta$ Pictoris					
SDSS J044337.60+000205.2	$21.1 \pm 0.4$	$25.7^{+3.2}_{-2.4}$	$1.9\sigma$	22%	1
PSO J318.5338-22.8603	$22.2^{+0.8}_{-0.9}$	$22.1 \pm 1.6$	$0.1\sigma$	0%	1
Columba					
2MASS J0518461-275645	$54.3^{+3.0}_{-3.4}$	$51.8 \pm 5.6$	$-0.4\sigma$	-5%	1
2MASS J0536199-192039	$47.4^{+3.3}_{-3.8}$	$40.2 \pm 3.2$	$-1.4\sigma$	-15%	1
2MASS J0619526-290359†	$278^{+112}_{-153}$	$55.8^{+5.6}_{-6.0}$	$-1.5\sigma$	-80%	1
Tucana-Horologium					
2MASS J0117474-340325	$38.3^{+2.6}_{-3.0}$	$41.0^{+2.4}_{-2.0}$	$0.8\sigma$	7%	1
2MASS J0241115-032658	$54.0^{+5.4}_{-6.7}$	$50.2 \pm 3.2$	$-0.5\sigma$	-7%	1
TW Hya					
SSSPM J1102-3431	$47.4^{+4.2}_{-5.1}$	$43.0 \pm 7.0$	$-0.5\sigma$	-9%	3
2MASSW J1139511-315921	$42.2^{+2.7}_{-3.0}$	$40.0 \pm 4.0$	$-0.4\sigma$	-5%	3
2MASSW J1139511-315921	$42.2^{+2.7}_{-3.0}$	$46.6^{+4.8}_{-4.4}$	$0.9\sigma$	10%	1
BANYAN “Young field”					
PC 0025+0447	$96.2^{+6.8}_{-7.9}$	$120.3^{+24.8}_{-19.6}$	$1.2\sigma$	25%	1
2MASSW J0033239-152131	$23.4^{+0.9}_{-1.0}$	$28.1^{+4.4}_{-4.8}$	$1.0\sigma$	20%	1
2MASS J01262109+1428057	$58.5^{+3.8}_{-4.4}$	$62.6^{+17.6}_{-14.0}$	$0.3\sigma$	7%	1
2MASS J0253597+320637	$47.0^{+2.1}_{-2.3}$	$60.6^{+12.8}_{-11.2}$	$1.2\sigma$	29%	1
2MASS J0435145-141446	$87.7^{+9.4}_{-11.8}$	$10.5 \pm 1.6$	$-6.5\sigma$	-88%	1
2MASS J05012406-0010452	$20.7^{+0.6}_{-0.6}$	$15.7^{+3.2}_{-2.8}$	$-1.5\sigma$	-24%	1
2MASS J05575096-1359503	$294^{+76}_{-114}$	$44.6^{+11.6}_{-8.0}$	$-2.2\sigma$	-85%	1
2MASS J0608528-275358	$40.0^{+2.2}_{-2.5}$	$38.2^{+8.0}_{-6.4}$	$-0.2\sigma$	-4%	1

Table 9—Continued

Object	CFHT Distance (pc)	Kinematic Distance (pc)	Difference	Ref.
LP 423-31	$18.4 \pm 0.5$	$20.1^{+5.2}_{-4.0}$	$0.4\sigma$ 9%	1
LP 261-75A	$31.6^{+1.2}_{-1.4}$	$40.6^{+10.4}_{-9.6}$	$0.9\sigma$ 28%	1
LP 261-75B	$33.8^{+2.9}_{-3.4}$	$40.6^{+10.4}_{-9.6}$	$0.7\sigma$ 20%	1
G 196-3B	$20.4^{+0.9}_{-1.0}$	$29.7^{+10.8}_{-10.0}$	$0.9\sigma$ 46%	1
2MASS J10220489+0200477	$28.9^{+1.6}_{-1.8}$	$23.7^{+4.8}_{-3.2}$	$-1.0\sigma$ -18%	1
2MASS J10224821+5825453	$19.0^{+1.0}_{-1.2}$	$6.5^{+8.0}_{-1.2}$	$-1.5\sigma$ -66%	1
SDSS J102552.43+321234.0	$26.8 \pm 0.8$	$19.7^{+2.8}_{-2.4}$	$-2.4\sigma$ -27%	1
2MASS J14112131-2119503	$51.3^{+4.5}_{-5.4}$	$48.6^{+16.0}_{-9.6}$	$-0.2\sigma$ -5%	1
2MASS J15474719-2423493	$33.2^{+1.2}_{-1.3}$	$41.8^{+7.2}_{-6.0}$	$1.4\sigma$ 26%	1
2MASS J15515237+0941148	$45.2^{+2.8}_{-3.3}$	$50.2^{+10.4}_{-9.6}$	$0.5\sigma$ 11%	1
2MASS J15525906+2948485	$20.9 \pm 0.4$	$32.1 \pm 4.0$	$2.8\sigma$ 53%	1
2MASSI J1615425+495321	$31.2^{+0.9}_{-1.0}$	$27.3^{+3.2}_{-2.4}$	$-1.2\sigma$ -13%	1
2MASSI J1711135+232633	$32.7^{+1.7}_{-1.9}$	$52.6^{+6.8}_{-6.4}$	$3.0\sigma$ 61%	1
2MASSW J1726000+153819	$35.3 \pm 1.2$	$43.8^{+7.2}_{-8.4}$	$1.0\sigma$ 24%	1
2MASS J18212815+1414010	$9.6 \pm 0.1$	$13.3 \pm 2.8$	$1.3\sigma$ 39%	1
2MASS J19355595-2846343†	$70.4^{+5.4}_{-6.4}$	$62.2^{+12.0}_{-9.6}$	$-0.6\sigma$ -12%	1
2MASS J20135152-2806020	$47.6^{+2.8}_{-3.1}$	$61.4^{+11.2}_{-8.4}$	$1.6\sigma$ 29%	1
2MASS J21481633+4003594	$8.0 \pm 0.1$	$8.1^{+0.8}_{-1.2}$	$0.1\sigma$ 1%	1
2MASSW J2208136+292121	$39.8^{+2.4}_{-2.7}$	$55.0^{+8.4}_{-9.6}$	$1.5\sigma$ 38%	1
2MASS J22134491-2136079	$47.8^{+3.9}_{-4.7}$	$62.6^{+7.2}_{-8.4}$	$1.6\sigma$ 31%	1
SDSS J224953.46+004404.6AB	$39.2^{+2.0}_{-2.3}$	$42.6^{+11.2}_{-7.6}$	$0.4\sigma$ 9%	1
2MASS J23224684-3133231	$19.9^{+1.0}_{-1.2}$	$24.1^{+3.2}_{-4.8}$	$0.9\sigma$ 21%	1
BANYAN “Old field”				
WISEP J020625.26+264023.6	$19.2 \pm 0.5$	$30.9 \pm 7.2$	$1.6\sigma$ 61%	1
WISE J075430.95+790957.8	$19.6 \pm 0.5$	$16.9^{+2.4}_{-2.0}$	$-1.1\sigma$ -14%	1
2MASS J13313310+3407583	$28.1^{+1.2}_{-1.3}$	$38.2^{+6.0}_{-4.4}$	$2.2\sigma$ 36%	1
2MASS J21403907+3655563	$87.7^{+7.0}_{-8.3}$	$129.9^{+23.2}_{-16.8}$	$2.3\sigma$ 48%	1
WISE J233527.07+451140.9	$22.7 \pm 0.7$	$23.3^{+9.6}_{-7.6}$	$0.1\sigma$ 3%	1

References. — (1) Gagné et al. (2014b), (2) Gagné et al. (2014a), (3) Mamajek (2005).

Note. — The group memberships listed here are those proposed in the literature. Objects with † have changes in their memberships, as summarized in Table 13.

Table 10. Coefficients of Linear Relations in the Paper

$x$	$y$	Field (IR types)			Field (Opt. types)			VL-G			INT-G <sup>a</sup>		
		$c_0$	$c_1$	rms	$c_0$	$c_1$	rms	$c_0$	$c_1$	rms	$c_0$	$c_1$	rms
SpT	$Y_{\text{MKO}}$	8.437	0.402	0.35	8.677	0.404	0.29	3.689	0.799	0.77	6.778	0.562	0.36
SpT	$J_{\text{MKO}}$	8.062	0.368	0.37	8.131	0.364	0.26	3.475	0.731	0.72	5.941	0.537	0.50
SpT	$H_{\text{MKO}}$	7.516	0.348	0.33	7.820	0.331	0.24	3.778	0.633	0.64	6.557	0.415	0.43
SpT	$K_{\text{MKO}}$	7.258	0.319	0.31	7.433	0.312	0.25	3.898	0.553	0.56	6.555	0.355	0.39
SpT	$J_{2\text{MASS}}$	7.848	0.391	0.38	8.021	0.380	0.30	3.406	0.745	0.72	5.914	0.545	0.50
SpT	$H_{2\text{MASS}}$	7.555	0.340	0.36	7.723	0.332	0.30	3.734	0.632	0.64	6.552	0.411	0.47
SpT	$K_{S,2\text{MASS}}$	7.292	0.317	0.33	7.491	0.308	0.29	3.699	0.573	0.55	6.573	0.356	0.36
SpT	W1	7.698	0.243	0.26	7.610	0.255	0.29	4.392	0.457	0.46	7.436	0.237	0.13
SpT	W2	7.466	0.236	0.24	7.559	0.231	0.29	4.039	0.451	0.48	7.561	0.193	0.18
$J_{\text{MKO}}$	$(J - K)_{\text{MKO}}$	-1.56	0.238	0.12	...	...	...	-1.20	0.243	0.30	-2.55	0.332	0.13
$K_{\text{MKO}}$	$(J - K)_{\text{MKO}}$	-1.82	0.290	0.16	...	...	...	-1.59	0.320	0.17	-3.62	0.481	0.20

Note. — These fits are defined as  $y = c_0 + c_1x$ , and the rms of the data about the fit is also given. Spectral type (SpT) is defined to be 10.0 for L0, 15.0 for L5, and so on. The field relations are valid for objects of spectral types M6 to L8. The VL-G relations are valid from M6 to L7. The INT-G relations are valid from L0 to L7. For the VL-G sample, 2MASS J1207–3932b was excluded from the fits. Its impact on the fitted coefficients is negligible, but its extreme outlying position would artificially inflate the resulting RMS values if it were included. Note that for some spectral type ranges for some filters, the linear fit is not a particularly good representation (e.g., *WISE* photometry for late-L dwarfs) and more accurate photometric distances may be obtained by averaging over the specific spectral subclasses of interest.

<sup>a</sup>For the INT-G sample, these line fits for the late-M dwarfs are not very good, given the small number of objects and large dispersion (e.g., see Figure 6).

Table 11. Tangential Velocities

Object	$V_{\text{tan}}$ (km s <sup>-1</sup> )	LSR Corrected		
		$\Delta\mu_{\alpha} \cos \delta$ (mas yr <sup>-1</sup> )	$\Delta\mu_{\delta}$ (mas yr <sup>-1</sup> )	$V'_{\text{tan}}$ (km s <sup>-1</sup> )
Low-gravity objects				
2MASSI J0019262+461407	26.5 ± 1.6	77.9 ± 4.6	-36.3 ± 2.1	10.9 ± 1.6
PC 0025+0447	7.5 ± 0.8	31.6 ± 2.4	-17.5 ± 1.3	9.6 ± 0.7
2MASSW J0030300-145033	31.3 ± 4.0	113.4 ± 13.6	-54.3 ± 6.5	17.0 ± 3.9
2MASSW J0033239-152131	34.1 ± 1.5	129.5 ± 5.4	-61.3 ± 2.6	22.2 ± 1.4
2MASSW J0045214+163445	25.8 ± 0.5	197.1 ± 3.9	-117.8 ± 2.3	12.3 ± 0.5
WISEP J004701.06+680352.1	24.9 ± 0.5	245.7 ± 5.4	-108.5 ± 2.4	9.5 ± 0.5
2MASSW J0058425-065123	25.8 ± 3.2	99.4 ± 11.8	-51.6 ± 6.1	11.3 ± 3.1
2MASSI J0117474-340325	22.4 ± 1.7	74.6 ± 5.4	-18.8 ± 1.4	9.1 ± 1.7
2MASS J01262109+1428057	23.5 ± 1.7	48.1 ± 3.4	-32.6 ± 2.3	7.7 ± 1.7
2MASS J02212859-6831400	10.4 ± 1.8	61.7 ± 8.8	29.4 ± 4.2	3.6 ± 1.1
2MASSI J0241115-032658	19.0 ± 2.3	41.8 ± 4.7	-28.1 ± 3.2	7.2 ± 2.1
SO J025300.5+165258	93.8 ± 0.6	557.0 ± 2.0	-574.4 ± 2.1	79.2 ± 0.6
2MASSI J0253597+320637	30.3 ± 1.5	45.6 ± 2.1	-54.8 ± 2.6	14.6 ± 1.5
2MASSI J0335020+234235	16.8 ± 1.5	37.3 ± 3.1	-55.3 ± 4.6	2.8 ± 1.3
LP 944-20	12.4 ± 0.1	258.6 ± 1.7	25.4 ± 0.2	7.6 ± 0.1
2MASS J03552337+1133437	28.8 ± 0.4	161.7 ± 2.1	-235.9 ± 3.0	17.1 ± 0.4
GJ 3276	5.1 ± 3.4	4.5 ± 1.2	-9.2 ± 2.3	9.8 ± 2.8
2MASSI J0435145-141446	4.0 ± 1.0	11.2 ± 1.4	-10.0 ± 1.2	9.5 ± 1.0
SDSS J044337.60+000205.2	11.8 ± 0.3	41.6 ± 0.9	-77.9 ± 1.6	2.9 ± 0.3
2MASS J05012406-0010452	23.3 ± 0.7	31.4 ± 0.9	-79.2 ± 2.3	16.8 ± 0.7
2MASSI J0518461-275645	9.1 ± 0.7	7.7 ± 0.5	-0.4 ± 0.0	7.1 ± 0.7
2MASSI J0536199-192039	8.3 ± 0.7	3.9 ± 0.3	-11.3 ± 0.9	5.9 ± 0.7
2MASS J05575096-1359503	10.0 ± 22.8	-0.4 ± 0.1	-2.9 ± 1.0	12.1 ± 22.7
LSR J0602+3910	28.6 ± 0.3	-14.8 ± 0.2	-282.6 ± 3.2	15.2 ± 0.3
2MASSI J0608528-275358	2.7 ± 0.2	-6.3 ± 0.4	-0.5 ± 0.0	3.8 ± 0.2
2MASSI J0619526-290359	12.7 ± 96.3	-1.4 ± 0.8	0.2 ± 0.1	13.9 ± 96.2
LP 423-31	34.3 ± 0.9	-85.1 ± 2.2	-126.0 ± 3.2	30.3 ± 0.8
G 196-3B	23.2 ± 1.1	-135.2 ± 6.3	-103.1 ± 4.8	9.4 ± 0.9
2MASS J10220489+0200477	62.3 ± 3.7	-98.8 ± 5.7	-58.3 ± 3.4	50.5 ± 3.6
2MASS J10224821+5825453	97.3 ± 5.8	-150.4 ± 8.9	-96.6 ± 5.7	81.5 ± 5.8
SSSPM J1102-3431	13.0 ± 1.4	-63.6 ± 6.3	-21.0 ± 2.1	2.2 ± 1.1
SDSS J111010.01+011613.1	32.3 ± 0.7	-158.0 ± 3.6	-86.3 ± 2.0	18.5 ± 0.7
TWA 5B	18.7 ± 0.8	-61.3 ± 2.1	-24.3 ± 0.9	3.7 ± 0.7
TWA 8B	17.8 ± 1.4	-79.5 ± 6.1	-35.3 ± 2.7	2.9 ± 1.0
2MASSW J1139511-315921	18.2 ± 1.3	-72.9 ± 4.9	-31.4 ± 2.1	2.9 ± 1.1
2MASSW J1207334-393254	16.9 ± 0.4	-58.6 ± 1.2	-27.1 ± 0.6	1.8 ± 0.2
DENIS J124514.1-442907	17.9 ± 5.9	-37.9 ± 6.2	-21.4 ± 3.5	6.8 ± 4.5
2MASS J14112131-2119503	27.4 ± 2.8	-49.0 ± 4.8	-42.5 ± 4.1	11.6 ± 2.8
DENIS J142527.9-365023	29.8 ± 0.3	-207.3 ± 2.0	-214.0 ± 2.1	14.3 ± 0.3



Table 11—Continued

Object	$V_{\text{tan}}$ (km s <sup>-1</sup> )	LSR Corrected		
		$\Delta\mu_{\alpha} \cos \delta$ (mas yr <sup>-1</sup> )	$\Delta\mu_{\delta}$ (mas yr <sup>-1</sup> )	$V'_{\text{tan}}$ (km s <sup>-1</sup> )
2MASS J15474719–2423493	30.3 ± 1.1	–47.1 ± 1.7	–78.1 ± 2.9	16.9 ± 1.1
2MASS J15515237+0941148	18.2 ± 1.3	–33.5 ± 2.3	–25.9 ± 1.8	9.2 ± 1.3
2MASS J15525906+2948485	16.9 ± 0.4	–71.9 ± 1.5	–4.4 ± 0.1	10.5 ± 0.4
2MASSI J1615425+495321	13.9 ± 0.5	–39.4 ± 1.2	35.2 ± 1.1	8.5 ± 0.4
2MASSI J1711135+232633	12.4 ± 0.7	–15.9 ± 0.9	–9.2 ± 0.5	9.5 ± 0.7
2MASSW J1726000+153819	13.4 ± 0.5	–9.1 ± 0.3	–21.5 ± 0.8	9.7 ± 0.5
2MASS J19355595–2846343	22.5 ± 2.0	19.5 ± 1.6	–39.3 ± 3.3	7.9 ± 2.0
2MASS J20135152–2806020	17.6 ± 1.2	38.0 ± 2.4	–55.1 ± 3.4	2.6 ± 1.1
DENIS J205754.1–025229	5.8 ± 0.4	157.8 ± 8.3	–122.6 ± 6.5	10.9 ± 0.3
PSO J318.5338–22.8603	20.9 ± 0.8	108.0 ± 4.1	–102.3 ± 3.9	5.3 ± 0.8
SIMP J215434.5–105530.8	24.3 ± 0.8	87.9 ± 2.7	–61.9 ± 1.9	14.8 ± 0.6
2MASSW J2208136+292121	17.5 ± 1.2	69.8 ± 4.4	–19.7 ± 1.3	3.8 ± 1.2
2MASS J22134491–2136079	19.8 ± 1.9	58.8 ± 5.3	–41.6 ± 3.8	6.8 ± 1.3
2MASSW J2244316+204343	26.6 ± 0.5	173.5 ± 3.0	–72.3 ± 1.2	13.9 ± 0.4
SDSS J224953.46+004404.6AB	15.4 ± 0.9	75.8 ± 4.2	–41.7 ± 2.3	9.5 ± 0.4
Unusually red field objects				
WISEP J020625.26+264023.6	40.5 ± 1.1	132.8 ± 3.6	–117.0 ± 3.1	29.0 ± 1.0
WISE J075430.95+790957.8	40.6 ± 1.0	–81.4 ± 1.9	–148.1 ± 3.5	56.0 ± 1.0
2MASS J13313310+3407583	53.0 ± 2.4	–99.0 ± 4.5	–22.1 ± 1.0	40.1 ± 2.4
2MASS J18212815+1414010	15.1 ± 0.2	44.1 ± 0.4	–88.4 ± 0.8	10.9 ± 0.2
2MASS J21481633+4003594	34.2 ± 0.5	330.9 ± 4.8	–31.8 ± 0.5	25.1 ± 0.5
2MASSW J2224438-015852	54.1 ± 0.7	247.3 ± 3.2	–145.1 ± 1.9	41.4 ± 0.7
WISE J233527.07+451140.9	13.2 ± 0.5	135.2 ± 4.3	–44.9 ± 1.4	24.8 ± 0.4
2MASS J23512200+3010540	29.1 ± 1.0	126.9 ± 4.3	–59.0 ± 2.0	16.5 ± 0.9
Other objects				
2MASS J03140344+1603056	16.3 ± 0.4	139.7 ± 2.9	–161.8 ± 3.4	26.2 ± 0.3
2MASS J04070752+1546457	16.2 ± 0.8	38.6 ± 1.7	–67.6 ± 3.0	6.0 ± 0.6
LP 415-22	42.0 ± 5.6	15.0 ± 1.8	–30.6 ± 3.8	33.2 ± 5.4
CFHT-Hy-20	22.1 ± 1.1	32.2 ± 1.6	–69.7 ± 3.4	18.9 ± 1.0
2MASS J07521548+1614237	23.8 ± 2.7	–20.7 ± 2.2	–30.6 ± 3.3	13.8 ± 2.4
LP 261-75A	28.3 ± 1.2	–84.5 ± 3.5	–70.4 ± 2.9	14.1 ± 1.1
LP 261-75B	30.3 ± 3.0	–79.2 ± 7.5	–66.0 ± 6.2	15.9 ± 2.8
SDSS J102552.43+321234.0	49.6 ± 1.6	–107.2 ± 3.4	–73.9 ± 2.4	57.2 ± 1.5
SDSS J104523.98–014957.7	37.4 ± 0.9	–182.8 ± 4.4	–100.0 ± 2.4	24.4 ± 0.9
DENIS-P J1047.5–1815	45.5 ± 2.3	–112.4 ± 5.6	–49.4 ± 2.5	33.3 ± 2.3
2MASS J13153094–2649513AB	63.5 ± 2.4	–157.7 ± 6.0	–108.6 ± 4.1	47.4 ± 2.4
DENIS-P J1441.6–0945AB	33.1 ± 1.9	–66.8 ± 3.8	–58.5 ± 3.4	23.2 ± 1.8
DENIS-P J170548.3–051645	14.8 ± 0.3	–31.6 ± 0.6	–102.5 ± 1.9	13.3 ± 0.2

Table 11—Continued

Object	$V_{\text{tan}}$ (km s <sup>-1</sup> )	LSR Corrected		
		$\Delta\mu_{\alpha} \cos \delta$ (mas yr <sup>-1</sup> )	$\Delta\mu_{\delta}$ (mas yr <sup>-1</sup> )	$V'_{\text{tan}}$ (km s <sup>-1</sup> )
2MASS J1707333+430130	$27.8 \pm 0.8$	$-20.5 \pm 0.6$	$31.1 \pm 0.9$	$26.1 \pm 0.8$
2MASS J21403907+3655563	$59.6 \pm 5.4$	$29.7 \pm 2.6$	$-3.7 \pm 0.3$	$70.4 \pm 5.4$
DENIS-P J220002.0–303832A	$28.8 \pm 2.9$	$112.0 \pm 10.9$	$-87.8 \pm 8.6$	$15.7 \pm 2.6$
DENIS-P J220002.0–303832B	$34.9 \pm 4.0$	$95.1 \pm 10.4$	$-74.5 \pm 8.1$	$20.2 \pm 3.9$
2MASS J23224684–3133231	$54.2 \pm 3.1$	$153.5 \pm 8.6$	$-80.0 \pm 4.5$	$54.8 \pm 2.9$

Table 12. *UVW* Determinations for Objects with Published Radial Velocities

Object	RV		<i>U</i> (km s <sup>-1</sup> )	<i>V</i> (km s <sup>-1</sup> )	<i>W</i> (km s <sup>-1</sup> )	<i>v</i> <sub>tot</sub> (km s <sup>-1</sup> )
	<i>v</i> (km s <sup>-1</sup> )	Ref				
2MASSI J0019262+461407	-19.5 ± 2.0	8	-7.2 ± 1.3	-30.1 ± 1.9	-11.0 ± 1.2	32.9 ± 1.7
2MASSW J0045214+163445	3.3 ± 0.2	1	-21.3 ± 0.4	-13.9 ± 0.4	-5.5 ± 0.2	26.0 ± 0.5
WISEP J004701.06+680352.1	-20.0 ± 1.4	5	-8.2 ± 0.9	-27.6 ± 1.2	-13.9 ± 0.3	31.9 ± 1.0
SO J025300.5+165258	68.3 ± 0.1 <sup>a</sup>	16	-69.5 ± 0.5	-71.9 ± 0.6	-58.8 ± 0.4	116.0 ± 0.5
2MASSI J0253597+320637	-36.3 ± 0.8	13	17.8 ± 0.8	-43.2 ± 1.4	7.3 ± 0.5	47.3 ± 1.1
2MASS J03140344+1603056	-8.0 ± 1.1	12	15.9 ± 0.9	6.6 ± 0.3	-5.8 ± 0.7	18.2 ± 0.6
2MASSI J0335020+234235	15.5 ± 1.7	15	-16.6 ± 1.5	-12.6 ± 1.5	-9.5 ± 0.9	22.9 ± 1.6
LP 944-20	7.6 ± 2.0	8	-13.5 ± 0.6	-5.3 ± 1.0	-0.7 ± 1.6	14.6 ± 1.0
2MASS J03552337+1133437	11.9 ± 0.2	1	-5.5 ± 0.2	-26.5 ± 0.3	-15.4 ± 0.2	31.1 ± 0.4
SDSS J044337.60+000205.2	19.5 ± 1.5 <sup>a</sup>	2,8	-12.6 ± 1.2	-16.2 ± 0.5	-9.9 ± 0.7	22.8 ± 1.3
2MASS J05575096-1359503	30.3 ± 2.8	15	-23.6 ± 8.8	-21.1 ± 11.7	-0.9 ± 25.3	32.5 ± 27.3
LSR J0602+3910	7.9 ± 0.1	1	-12.1 ± 0.1	-26.7 ± 0.3	-4.3 ± 0.1	29.7 ± 0.3
2MASSI J0608528-275358	24.0 ± 1.0	10	-14.0 ± 0.6	-18.7 ± 0.8	-6.1 ± 0.4	24.2 ± 1.0
2MASS J07140394+3702459	40.0 ± 0.1	3	-40.6 ± 0.6	-8.0 ± 1.1	5.3 ± 1.5	41.8 ± 0.4
LP 423-31	-14.7 ± 0.2	15	27.6 ± 0.4	-24.9 ± 0.8	-2.8 ± 0.1	37.3 ± 0.8
LP 261-75A	10.2 ± 0.2	15	-13.6 ± 0.4	-26.9 ± 1.1	-0.9 ± 0.4	30.1 ± 1.1
LP 261-75B	10.2 ± 0.2 <sup>b</sup>	15	-14.1 ± 0.8	-28.7 ± 2.8	-1.6 ± 1.0	32.0 ± 2.9
G 196-3B	-0.7 ± 1.2 <sup>b</sup>	15	-9.3 ± 0.9	-20.9 ± 1.0	-3.8 ± 0.9	23.2 ± 1.1
2MASS J10220489+0200477	-8.4 ± 5.0	17	9.9 ± 1.7	-43.9 ± 4.2	-44.0 ± 4.2	63.1 ± 3.7
2MASS J10224821+5825453	19.3 ± 0.1	1	-70.5 ± 3.6	-69.8 ± 4.6	0.1 ± 0.9	99.2 ± 5.7
SDSS J104523.98-014957.7	6.3 ± 0.1	1	-32.7 ± 0.8	-14.3 ± 0.3	-13.0 ± 0.5	37.9 ± 0.9
DENIS-P J1047.5-1815	6.0 ± 1.1	12	-41.7 ± 2.1	-14.0 ± 1.0	-13.3 ± 1.1	45.9 ± 2.3
SDSS J111010.01+011613.1	7.5 ± 3.8	4	-5.9 ± 0.6	-30.1 ± 2.2	-12.6 ± 3.1	33.3 ± 1.1
TWA 5B	11.6 ± 1.4	6, 9	-10.9 ± 0.8	-18.5 ± 1.3	-4.7 ± 1.1	22.0 ± 1.0
TWA 8B	8.9 ± 0.3	14	-11.1 ± 1.0	-16.0 ± 0.7	-4.3 ± 0.8	19.9 ± 1.3
2MASSW J1139511-315921	9.1 ± 1.2 <sup>a</sup>	6, 7, 9	-10.7 ± 1.0	-16.6 ± 1.2	-5.0 ± 0.9	20.4 ± 1.3
2MASSW J1207334-393254AB	9.1 ± 1.2 <sup>a</sup>	6, 7, 9	-8.7 ± 0.5	-16.6 ± 1.0	-4.3 ± 0.5	19.2 ± 0.6
2MASS J13313310+3407583	15.4 ± 7.8	11	-20.8 ± 1.1	-44.5 ± 2.6	25.2 ± 7.5	55.6 ± 3.2
2MASS J14112131-2119503	-0.8 ± 2.0	8	-10.7 ± 1.7	-24.2 ± 2.7	-7.1 ± 1.4	27.5 ± 2.8
DENIS J142527.9-365023	5.4 ± 0.2	1	-5.2 ± 0.2	-26.3 ± 0.3	-14.1 ± 0.2	30.3 ± 0.3
DENIS-P J1441.6-0945AB	-28.3 ± 1.1	12	-39.0 ± 1.4	-17.8 ± 1.4	-7.9 ± 1.0	43.6 ± 1.6
2MASS J15525906+2948485	-18.4 ± 0.1	1	-8.9 ± 0.2	-22.8 ± 0.3	-4.9 ± 0.2	25.0 ± 0.3
DENIS-P J170548.3-051645	12.2 ± 0.1	1	16.8 ± 0.2	0.9 ± 0.1	-9.2 ± 0.3	19.2 ± 0.2
2MASSI J1707333+430130	-10.8 ± 0.7	15	-3.5 ± 0.3	-25.4 ± 0.7	15.3 ± 0.8	29.9 ± 0.8
2MASSI J1711135+232633	-20.9 ± 8.6	11	-8.9 ± 5.1	-22.2 ± 5.1	-4.1 ± 4.5	24.3 ± 6.9
2MASS J18212815+1414010	9.8 ± 0.2	1	13.2 ± 0.1	4.3 ± 0.1	-11.4 ± 0.2	18.0 ± 0.2
DENIS-P J205754.1-025229	-24.7 ± 0.4	1	-12.4 ± 0.3	-20.0 ± 0.4	9.5 ± 0.3	25.4 ± 0.4
DENIS-P J220002.0-303832A	-25.3 ± 1.0	11	-35.5 ± 2.2	-14.4 ± 1.2	2.7 ± 2.0	38.4 ± 2.3
DENIS-P J220002.0-303832AB	-25.3 ± 1.0	11	-36.7 ± 2.5	-16.7 ± 1.5	1.2 ± 2.2	40.4 ± 2.8
DENIS-P J220002.0-303832B	-25.3 ± 1.0	11	-38.4 ± 2.8	-19.6 ± 1.9	-0.7 ± 2.5	43.2 ± 3.4

Table 12—Continued

Object	RV		$U$ (km s <sup>-1</sup> )	$V$ (km s <sup>-1</sup> )	$W$ (km s <sup>-1</sup> )	$v_{\text{tot}}$ (km s <sup>-1</sup> )
	$v$ (km s <sup>-1</sup> )	Ref				
2MASSW J2224438-015852	$-37.5 \pm 0.1$	1	$-10.6 \pm 0.1$	$-64.6 \pm 0.5$	$-6.8 \pm 0.4$	$65.9 \pm 0.6$
SDSS J224953.46+004404.6AB	$-2.9 \pm 0.7^{\text{b}}$	13	$-14.4 \pm 0.8$	$-4.8 \pm 0.5$	$-4.0 \pm 0.7$	$15.7 \pm 0.9$

<sup>a</sup>Adopted radial velocity is the weighted mean of published values.

<sup>b</sup>Radial velocity measurements are for the comoving M dwarf companions to these objects (Rebolo et al. 1998; Allers et al. 2010).

References. — (1) Blake et al. 2010; (2) Deshpande et al. 2012; (3) Deshpande et al. 2013; (4) Gagné et al. 2015; (5) Gizis et al. 2015; (6) Mohanty et al. 2003; (7) Reid 2003; (8) Reiners & Basri 2009; (9) Rice et al. 2010a; (10) Rice et al. 2010b; (11) Schmidt et al. 2010; (12) Seifahrt et al. 2010; (13) E. Shkolnik, priv. comm.; (14) Shkolnik et al. 2011; (15) Shkolnik et al. 2012; (16) Tanner et al. 2012; (17) West et al. 2008;

Table 13. Membership Summary for Young Field Ultracool Dwarfs

Object	Spec. Type Optical/NIR	BANYAN II: Kinematics + SEDs (Gagné et al. 2014b; Gagné et al. 2015a)		BANYAN II: Kinematics only (This work)		$\bar{\chi}^2(UVW, XYZ)$	Membership
		RV $\pi$ yng	YMG	RV $\pi$ yng	YMG		
<i>AB Dor</i>							
2MASS J0019262+461407	M8/M8 INT-G	y - y	ABDMG(92.1%)	y y y	ABDMG(96%)	ABDMG[2.6/0.6]	ABDMG
WISEP J004701.06+680352.1	.../L7 INT-G	- - y	ABDMG(98.2%)	y y y	ABDMG(100%)	ABDMG[0.4/0.5]	ABDMG
2MASSW J0058425-065123	L0/L1 INT-G	- y y	ABDMG(63.7%)/BPMG(31.8%)	- y y	ABDMG(75%)/BPMG(22%)	ABDMG[>1.9/0.2], BPMG[>2.3/1.0]	(ABDMG)/(BPMG)
2MASS J03552337+1133437	L5 $\gamma$ /L3 VL-G	y y y	ABDMG(99.5%)	y y y	ABDMG(99.7%)	ABDMG[1.4/0.3]	ABDMG
SDSS J111010.01+011613.1	.../T5.5	y y y	ABDMG(97%) <sup>1</sup>	y y y	ABDMG(97%)	ABDMG(1.2/1.2)	ABDMG
DENIS J142527.9-365023	L3:/L4 INT-G	y y y	ABDMG(99.9%)	y y y	ABDMG(99.9%)	ABDMG[1.9/0.6]	ABDMG
2MASSW J2244316+204343	L6.5/L6 VL-G	- - y	ABDMG(99.1%)	- y y	ABDMG(99.9%)	ABDMG[>1.0/0.3]	(ABDMG)
<i>Argus</i>							
2MASSW J0030300-145033	L7/L6 FLD-G	- y y	ARG(26.5%)	- y -	O.FLD(64%)/Y.FLD(20%)/ARG(16%)	ARG[>1.0/4.1]	ARG?
2MASSW J0045214+163445	L2 $\beta$ /L2 VL-G	y - y	ARG(99.9%)	y y y	ARG(99.9%)	ARG[0.8/4.3]	ARG
2MASS J23512200+3010540	L5.5/L5 FLD-G	- - -	Field(92.8%)	- y -	ARG(89%)	...	ARG?
<i><math>\beta</math> Pic</i>							
2MASS J0335020+234235	M8.5/M7 VL-G	y y y	BPic(84.2%)	y y y	BPMG(83%)/Y.FLD(17%)	BPMG[3.3/1.2]	BPMG <sup>9</sup>
SDSS J044337.60+000205.2	M9/L0 VL-G	y - y	BPic(99.8%)	y y y	BPMG(99.9%)	BPMG[0.3/0.4]	BPMG
2MASS J19355595-2846343	M9/M9 VL-G	- - y	BPMG(9%)/Y.FLD(90%)	- y y	Y.FLD(99.0%)	BPMG[>0.8/2.0]	BPMG?
2MASS J20135152-2806020	M9/L0 VL-G	- - y	BPMG(43%)/Y.FLD(57%)	- y y	BPMG(70%)/Y.FLD(30%)	BPMG[>0.5/1.0]	(BPMG)
PSO J318.5338-22.8603	.../L7 VL-G	- y y	BPMG(99.7%)	y y y	BPMG(99.9%)	BPMG[>0.1/0.2]	BPMG
2MASSW J2208136+292121	L3 $\gamma$ /L3 VL-G	- - y	BPMG(10%)/Y.FLD(90%)	- y y	Y.FLD(78%)/BPMG(18%)	BPMG[>0.1/2.4]	BPMG?
<i>Columba</i>							
2MASS J0518461-275645	L1 $\gamma$ /L1 VL-G	- y y	COL(96%)	- y y	COL(99.6%)	COL[>0.0/0.4], THA[>1.3/2.1]	(COL)
2MASS J0536199-192039	L2 $\gamma$ /L2 VL-G	- y y	COL(97.6%)	- y y	COL(99.1%)	COL[>0.8/0.8], BPMG[>2.9/1.5]	(COL)
2MASS J0608528-275358	M8.5 $\gamma$ /L0 VL-G	y y y	COL(3%)/Y.FLD(96%)	y y y	COL(33%)/Y.FLD(67%)	COL[2.7/1.1], BPMG[3.2/1.2]	COL?
<i>Tuc-Hor</i>							
2MASS J0117474-340325	L2 $\gamma$ /L1 INT-G	- - y	THA(99.3%)	- y y	THA(99.4%)	COL[>0.8/1.7], ABDMG[>3.6/0.3], BPMG[>2.2/2.5], THA[>0.1/1.4]	(THA)
2MASS J0241115-032658	L0 $\gamma$ /L1 VL-G	- - y	THA(79.1%)	- y y	THA(82%)/Y.FLD(18%)	COL[>2.8/1.1], BPMG[>3.2/3.7]	(THA)
<i>TWA</i>							
SSSPM J1102-3431 <sup>4</sup>	M8.5p $\gamma$ /M9 VL-G	- y y	TWA(99.3%) <sup>2</sup>	- y y	TWA(99.6%)	...	(TWA)
TWA 5B	.../M9 VL-G	...	...	y y y	TWA(100%)	TWA[0.1/0.1]	TWA
TWA 8B	M5/M6 VL-G	...	...	y y y	TWA(99.9%)	TWA[1.7/0.6]	TWA
2MASSW J1139511-315921 <sup>5</sup>	M9/M9 VL-G	- y y	TWA(99.3%)	y y y	TWA(100%)	TWA[0.4/0.4]	TWA
2MASSW J1207334-393254Ab <sup>6</sup>	M8/M8 VL-G + .../L3 VL-G	- y y	TWA(99.9%)	y y y	TWA(100%)	TWA[2.6/0.1]	TWA
2MASS J12451416-4429077 <sup>7</sup>	M9.5/L0 VL-G	- y y	TWA(93.3%)	- y y	TWA(92%)	TWA[>0.3/0.7]	(TWA)
<i>Young Field</i>							

Table 13—Continued

Object	Spec. Type Optical/NIR	BANYAN II: Kinematics + SEDs (Gagné et al. 2014b; Gagné et al. 2015a)		BANYAN II: Kinematics only (This work)		$\chi^2(UVW, XYZ)$	Membership
		RV	$\pi$ yng	RV	$\pi$ yng		
		YMG		YMG			
PC 0025+0447	M9.5/L0 INT-G	- y y	Y.FLD(100%)	- y y	Y.FLD(100%)	...	Y.FLD
2MASSW J0033239-152131	L4 $\beta$ /L1 FLD-G	- - y	ARG(32%)/Y.FLD(68%)	- y y	Y.FLD(99%)	...	Y.FLD
2MASS J01262109+1428057	L4 $\gamma$ /L2 VL-G	- - y	BPMG(3%)/Y.FLD(97%)	- y y	Y.FLD(97%)	COL[>1.2/2.2]	Y.FLD
2MASS J02212859-6831400	M8 $\beta$ /...	- y y	Y.FLD(98.4%)	- y y	Y.FLD(98%)	BPMG[>2.6/1.3]	Y.FLD
Teegarden's Star <sup>8</sup>	M7/M7.5 INT-G	- y y	Y.FLD	y y y	Y.FLD(100%)	...	Y.FLD
2MASSI J0253597+320637	M7/M6 FLD-G	- - y	BPMG(21%)/Y.FLD(75%)	y y y	Y.FLD(100%)	...	Y.FLD
2MASS J05012406-0010452	L4 $\gamma$ /L3 VL-G	- y y	COL(49%)/CAR(17%)	- y y	Y.FLD(100%)	...	Y.FLD
2MASS J07140394+3702459	M8/M7.5 INT-G	- y y	ARG(88.9%)	y y y	Y.FLD(100%)	...	Y.FLD
LP 423-31	M7/M6 FLD-G	y y y	Y.FLD(100%)	y y y	Y.FLD(100%)	...	Y.FLD
LP 261-75B	L6/L6 FLD-G	y y -	ABDMG(18.9%)	y y y	Y.FLD(100%)	...	Y.FLD
G 196-3B	L3 $\beta$ /L3 VL-G	- - y	ABDMG(32%)/CAR(97%)	y y y	Y.FLD(88%)/CAR(11%)	...	(Y.FLD)
2MASS J10220489+0200477	M9 $\beta$ /M9 FLD-G	y y y	ABDMG(3%)/Y.FLD(97%)	y y y	Y.FLD(100%)	...	Y.FLD
2MASS J10224821+5825453	L1 $\beta$ /L1 FLD-G	y - y	Y.FLD(100%)	y y y	Y.FLD(100%)	...	Y.FLD
2MASS J13153094-2649513AB	.../L3.5:: + .../T7	...	...	- y -	O.FLD(96%)	...	O.FLD
2MASS J14112131-2119503	M9/M8 INT-G	y - y	Field	y y y	Y.FLD(100%)	TWA[2.0/2.0]	Y.FLD
2MASS J15474719-2423493	M9/L0 INT-G	- - y	ARG(0.1%)/Y.FLD(99.9%)	- y y	Y.FLD(100%)	...	Y.FLD
2MASS J15515237+0941148	L4 $\gamma$ /L4 VL-G	- - y	Y.FLD(100%)	- y y	Y.FLD(100%)	...	Y.FLD
2MASS J15525906+2948485	L0 $\beta$ /L0 INT-G	y - y	Y.FLD(100%)	y y y	Y.FLD(100%)	...	Y.FLD
2MASSI J1615425+495321	L4 $\gamma$ /L3 VL-G	- - y	ABDMG(3%)/Y.FLD(97%)	- y y	Y.FLD(99.6%)	...	Y.FLD
2MASSI J1711135+232633	L0/L1 INT-G	y - y	Y.FLD(100%)	y y y	Y.FLD(99.0%)	...	Y.FLD
2MASSW J1726000+153819	L3 $\beta$ /L3 INT-G	- - y	Y.FLD(100%)	- y y	Y.FLD(100%)	...	Y.FLD
DENIS-P J205754.1-025229	L1.5/L2 FLD-G	- y y	Y.FLD(100%)	y y y	Y.FLD(100%)	...	Y.FLD
SIMP J215434.5-105530.8	.../L4 INT-G	- - y	ARG(59%) <sup>3</sup>	- y y	Y.FLD(77%)/ARG(23%)	...	(Y.FLD)
2MASS J22134491-2136079	L0 $\gamma$ /L0 VL-G	- - y	BPMG(3%)/Y.FLD(97%)	- y y	Y.FLD(88%)	...	Y.FLD
SDSS J224953.46+004404.6AB	.../L3 INT-G + .../L5 INT-G	- - y	Y.FLD(99.8%)	y y y	Y.FLD(100%)	...	Y.FLD
2MASS J23224684-3133231	L0 $\beta$ /L2 INT-G	- y y	Y.FLD(100%)	- y y	Y.FLD(100%)	...	Y.FLD
<i>Old Field</i>							
WISEP J020625.26+264023.6	.../L8(red)	- - -	Y.FLD(3%)/O.FLD(97%)	- y -	Y.FLD(9%)/O.FLD(91%)	...	O.FLD
WISE J075430.95+790957.8	.../T2p(red)	- - -	O.FLD(99.8%)	- y -	O.FLD(99.9%)	...	O.FLD
SDSSJ 102552.43+321234.0	.../L7 FLD-G	- - y	Y.FLD(100%)	- y -	O.FLD(99.8%)	...	O.FLD
2MASS J13313310+3407583	L0/L0 FLD-G	y - -	O.FLD(100%)	y y -	O.FLD(99.8%)	...	O.FLD
2MASSI J1707333+430130	L0.5/M9 FLD-G	...	...	y y -	O.FLD(98%)	...	O.FLD
2MASS J18212815+1414010	L4.5/L5p FLD-G	y - y	Y.FLD(100%)	y y -	O.FLD(82%)/Y.FLD(18%)	...	O.FLD
2MASS J21403907+3655563	.../M8p FLD-G	- - -	O.FLD(99.9%)	- y -	O.FLD(100%)	...	O.FLD
2MASSW J2224438-015852	L4.5/L3 FLD-G	- y -	O.FLD(96.2%)	y y -	O.FLD(99.8%)	...	O.FLD
<i>Other Field</i>							
2MASS J03140344+1603056	L0/L0 FLD-G	y - -	...	y y -	O.FLD(85%)/Y.FLD(15%)	...	Field (Uma MG)
2MASS J04070752+1546457	L3.5/L3 FLD-G	- - -	Field	- y -	Y.FLD(49%)/O.FLD(40%)	...	Field
LSR J0602+3910	L1/L2 INT-G	...	...	y y y	Y.FLD(100%)	...	Field (Pleiades MG)
SDSS J104523.98-014957.7	L1/L1 FLD-G	...	...	y y -	O.FLD(80%)/Y.FLD(20%)	...	Field (Hyades MG)
DENIS-P J1047.5-1815	L2.5/L0 FLD-G	...	...	y y -	O.FLD(82%)/Y.FLD(18%)	...	Field (Hyades MG)
DENIS-P J1441.6-0945AB	L0.5/L1 FLD-G	...	...	y y -	O.FLD(84%)/Y.FLD(16%)	...	Field (Hyades MG)
DENIS-P J170548.3-051645	L0.5/L1 FLD-G	...	...	y y -	O.FLD(76%)/Y.FLD(24%)	...	Field (Uma MG)
2MASS J21481633+4003594	L6/L6 FLD-G	- - y	ARG(48%)/Y.FLD(52%)	- y -	Y.FLD(67%)/O.FLD(33%)	...	Field
DENIS-P J220002.0-303832AB	M9/M9 FLD-G + L0/L0 FLD-G	...	...	y y -	O.FLD(83%)/Y.FLD(17%)	...	Field (Hyades MG)

Table 13—Continued

Object	Spec. Type Optical/NIR	BANYAN II: Kinematics + SEDs (Gagné et al. 2014b; Gagné et al. 2015a)			BANYAN II: Kinematics only (This work)			$\tilde{\chi}^2(UVW, XYZ)$	Membership		
		RV $\pi$ yng		YMG	RV $\pi$ yng		YMG				
		-	-	-	-	-	-				
WISE J233527.07+451140.9	.../L7p FLD-G	-	-	-	Y.FLD(3%)/O.FLD(97%)	-	y	-	O.FLD(73%)/Y.FLD(27%)	...	Field
<i>Miscellaneous</i>											
LP 944-20	M9/L0 FLD-G	y	y	y	CAS(99.7%)/ARG(17.5%)	y	y	y	ARG(69%)/Y.FLD(31%)	...	CAS
CFHT-Hy-20	.../T2.5	...	...	...	...	-	y	-	O.FLD(86%)/Y.FLD(14%)	...	(Hyades)
2MASS J0435145-141446	M6 $\delta$ /M7 VL-G	-	-	y	Y.FLD(100%)	-	y	y	Y.FLD(100%)	...	MBM20
<i>Too distant for BANYAN</i>											
GJ 3276 (2MASS J0422+1530)	M6 $\gamma$ /M6 VL-G	...	...	...	...	-	y	y	Y.FLD(100%)	...	n/a
2MASS J05575096-1359503	M7/M7 VL-G	y	-	y	Y.FLD(99.7%)	y	y	y	Y.FLD(100%)	...	n/a
2MASS J0619526-290359	M6/M5	-	-	y	COL(80.7%)	-	y	y	Y.FLD(100%)	...	n/a

Note. — Summary of our membership assessment for candidate young ultracool dwarfs with parallaxes, from our CFHT sample and from the literature. The first two blocks of columns give the results from the published BANYAN II analysis (using kinematics and SEDs) and from our use of the online BANYAN II (using kinematics only). For the published results from Gagné et al. (2014b), for objects with YMG memberships <50%, we list the most likely membership (typically in the Young Field) when available. (Comparable information is not available for Gagné et al. 2015a.) For our kinematics-only calculations, we list all groups with >10% membership probabilities. The “RV  $\pi$  yng” columns shows the inputs to the membership analysis, namely if a radial velocity was used, if a parallax was used, and if BANYAN II’s “Young Field” option was used. *Reduced chi squared values* ( $\tilde{\chi}^2$ ): These are computed by comparing each object’s position to the young moving groups in Table 14, with the first tabulated value being for *UVW* and the second for *XYZ*. For objects with radial velocities, the listed  $\tilde{\chi}^2_{UVW}$  is the minimum possible value, i.e., the velocity that brings the object closest to the group’s *UVW* position. We require  $\tilde{\chi}^2 < 4$  for both *UVW* and *XYZ* for a group to be mentioned, except in the case of the possible ARG members where slightly larger values are listed to account for the uncertain membership of this group. *Membership*: Group assignments listed in normal font are secure. Those in parenthesis (...) are probable given the available data but need to be fully verified, typically with radial velocity measurements. Memberships with a “?” designation are uncertain. See Section 4.4 for additional details.

<sup>1</sup>Membership analysis from Gagné et al. (2015).

<sup>2</sup>Membership analysis from Gagné et al. (2015b).

<sup>3</sup>Membership analysis from Gagné et al. (2014a).

<sup>4</sup>TWA 28

<sup>5</sup>TWA 26

<sup>6</sup>TWA 27

<sup>7</sup>TWA 29

<sup>8</sup>A.k.a. SO J0253+1652.

<sup>9</sup>Identified as a  $\beta$  Pic member by Shkolnik et al. (2012).

Table 14. Stellar Moving Groups

Group	$U$	$V$	$W$	$X$	$Y$	$Z$	Ref
Young ( $\lesssim 100$ Myr) Groups							
AB Dor <sup>b</sup>	$-7.6 \pm 1.1$	$-27.3 \pm 1.5$	$-14.9 \pm 1.0$	$-6.0 \pm 32.3$	$-14.1 \pm 38.5$	$-20.5 \pm 19.5$	1, 2
Argus <sup>a</sup>	$-22.0 \pm 0.3$	$-14.4 \pm 1.3$	$-5.0 \pm 1.3$	$5.2 \pm 19.7$	$-115.1 \pm 35.5$	$-17.5 \pm 12.5$	2
$\beta$ Pic <sup>a</sup>	$-10.9 \pm 1.5$	$-16.0 \pm 1.4$	$-9.2 \pm 1.8$	$8.4 \pm 31.9$	$-5.0 \pm 15.4$	$-15.0 \pm 8.0$	3
Columba <sup>a</sup>	$-13.2 \pm 1.3$	$-21.8 \pm 0.8$	$-5.9 \pm 1.2$	$-42.6 \pm 25.7$	$-56.5 \pm 33.6$	$-48.0 \pm 23.2$	2
Tuc-Hor <sup>b</sup>	$-10.6 \pm 1.1$	$-21.0 \pm 1.1$	$-2.1 \pm 1.1$	$2.6 \pm 24.3$	$-24.3 \pm 9.3$	$-35.3 \pm 3.5$	2, 4
TWA <sup>b</sup>	$-10.9 \pm 0.8$	$-18.2 \pm 0.8$	$-5.3 \pm 0.8$	$18.3 \pm 14.7$	$-52.2 \pm 18.5$	$21.9 \pm 5.6$	5, 6
Older ( $\gtrsim 100$ Myr) Groups							
Castor Stream <sup>a</sup>	$-10.7 \pm 6.5$	$-7.5 \pm 4.4$	$-8.8 \pm 4.2$	...	...	...	7
IC2391 Stream <sup>a</sup>	$-23.9 \pm 3.8$	$-18.9 \pm 4.9$	$-8.0 \pm 5.6$	...	...	...	7
Hyades Stream <sup>a</sup>	$-38.0 \pm 6.6$	$-16.9 \pm 4.2$	$-4.7 \pm 7.1$	...	...	...	7
Pleiades Stream <sup>a</sup>	$-9.8 \pm 5.1$	$-22.9 \pm 6.0$	$-9.2 \pm 6.2$	...	...	...	7
Ursa Major Nucleus	$15.0 \pm 1.2$	$2.8 \pm 1.3$	$-8.1 \pm 1.5$	$-7.8 \pm 2.8$	$9.6 \pm 1.5$	$21.8 \pm 1.3$	3, 8
Ursa Major Stream <sup>a</sup>	$14.4 \pm 3.1$	$2.1 \pm 3.3$	$-9.6 \pm 3.6$	...	...	...	7

<sup>a</sup>Uncertainties on  $UVW$  are the observed dispersion in measured  $UVW$  of group members.

<sup>b</sup>Uncertainties on  $UVW$  includes uncertainties on the  $UVW$  of the group as well as the groups' internal dispersion.

References. — (1) Barenfeld et al. (2013); (2) Torres et al. (2008); (3) Mamajek & Bell (2014); (4) Kraus et al. (2014); (5) Weinberger et al. (2013); (6) Ducourant et al. (2014); (7) Klutsch et al. (2014); (8) King et al. (2003)



Table 15. Summary of Membership Changes Relative to BANYAN II Results

Object	Previous	This Work
Changed Memberships		
2MASSW J0030300–145033	ARG(26.5%)	ARG?
2MASSW J0033239–152131	ARG(32%)/Y.FLD(68%)	Y.FLD
2MASS J01262109+1428057	BPMG(3%)/Y.FLD(97%)	Y.FLD
2MASSI J0253597+320637	BPMG(21%)/Y.FLD(75%)	Y.FLD
2MASSI J0435145–141446	Y.FLD(100%)	MBM20
2MASS J05012406–0010452	COL(49%)/CAR(17%)	Y.FLD
2MASS J05575096–1359503	Y.FLD(99.7%)	n/a (too far)
2MASSI J0608528–275358	COL(3%)/Y.FLD(96%)	COL?
2MASSI J0619526–290359	COL(80.7%)	n/a (too far)
2MASS J07140394+3702459	ARG(88.9%)	Y.FLD
LP 261-75AB	ABD(18.9%)	Y.FLD
G 196-3B	ABD(32%)/CAR(97%)	(Y.FLD)
2MASS J10220489+0200477	ABD(3%)/Y.FLD(97%)	Y.FLD
SDSSJ 102552.43+321234.0	Y.FLD(100%)	O.FLD
2MASSI J1615425+495321	ABD(3%)/Y.FLD(97%)	Y.FLD
2MASS J18212815+1414010	Y.FLD(100%)	O.FLD
2MASS J19355595–2846343	BPMG(9%)/Y.FLD(90%)	BPMG?
2MASS J21481633+4003594	ARG(48.1%)/Y.FLD(52.0%)	Field
SIMP J215434.5–105530.8	ARG(59%) <sup>2</sup>	(Y.FLD)
2MASSW J2208136+292121	BPMG(10%)/Y.FLD(90%)	BPMG?
2MASS J22134491–2136079	BPMG(3%)/Y.FLD(97%)	Y.FLD
WISE J233527.07+451140.9	Y.FLD(3%)/O.FLD(97%)	Field
2MASS J23512200+3010540	Field(92.8%)	ARG?
Improved Memberships		
2MASSI J0019262+461407	ABD(92.1%)	ABD
2MASSW J0045214+163445	ARG(99.9%)	ARG
WISEP J020625.26+264023.6	Y.FLD(3%)/O.FLD(97%)	O.FLD
2MASSI J0117474–340325	THA(99.3%)	(THA)
2MASSI J0241115–032658	THA(79.1%)	(THA)
2MASS J04070752+1546457	Field	Field
SDSS J044337.60+000205.2	BPic(99.8%)	BPMG
2MASSI J0518461–275645	COL(96%)	(COL)
2MASSI J0536199–192039	COL(97.6%)	(COL)

Table 15—Continued

Object	Previous	This Work
WISE J075430.95+790957.8	O.FLD(99.8%)	O.FLD
2MASSJ 10224821+5825453	Y.FLD(100%)	Y.FLD
SSSPM J1102–3431 (TWA 28)	TWA(99.3%) <sup>1</sup>	(TWA)
2MASSW J1139511–315921 (TWA 26)	TWA(99.3%)	TWA
2MASSW J1207334–393254 (TWA 27)	TWA(99.9%)	TWA
2MASS J13313310+3407583	O.FLD(100%)	O.FLD
2MASS J14112131–2119503	Field	Y.FLD
2MASS J15474719–2423493	ARG(0.1%)/Y.FLD(99.9%)	Y.FLD
2MASS J15515237+0941148	Y.FLD(100%)	Y.FLD
2MASS J15525906+2948485	Y.FLD(100%)	Y.FLD
2MASSI J1711135+232633	Y.FLD(100%)	Y.FLD
2MASSW J1726000+153819	Y.FLD(100%)	Y.FLD
2MASS J20135152–2806020	BPMG(43%)/Y.FLD(57%)	(BPMG)
DENIS-P J205754.1–025229	Y.FLD(100%)	Y.FLD
PSO J318.5338–22.8603	BPMG(99.7%)	BPMG
2MASS J21403907+3655563	O.FLD(99.9%)	O.FLD
2MASSW J2244316+204343	ABD(99.1%)	(ABD)
SDSS J224953.46+004404.6AB	Y.FLD(99.8%)	Y.FLD
2MASS J23224684–3133231	Y.FLD(100%)	Y.FLD

Note. — See Section 4.4 and the notes of Table 13 for an explanation of results and the adopted notation. Objects designated as "Improved Membership" are mostly previously identified candidates (based on analyses without parallaxes) whose membership is now corroborated by our new parallax measurements. See Appendix for details of individual objects.

<sup>1</sup>Gagné et al. (2015b)

<sup>2</sup>Gagné et al. (2014a)